Arctic Report Card 2020

The sustained transformation to a warmer, less frozen and biologically changed Arctic remains clear

DOI: 10.25923/MN5P-T549X

R.L. Thoman, J. Richter-Menge,
and M.L. Druckenmiller; Eds.

December 2020

Richard L. Thoman, Jacqueline Richter-Menge, and Matthew L. Druckenmiller; Editors
Benjamin J. DeAngelo; NOAA Executive Editor
Kelley A. Uhlig; NOAA Coordinating Editor

www.arctic.noaa.gov/Report-Card

How to Cite Arctic Report Card 2020

Citing the complete report or Executive Summary:

Thoman, R. L., J. Richter-Menge, and M. L. Druckenmiller, Eds., 2020: *Arctic Report Card 2020*, https://doi.org/10.25923/mn5p-t549.

Citing an essay (example):

Frey, K. E., J. C. Comiso, L. W. Cooper, J. M. Grebmeier, and L. V. Stock, 2020: Arctic Ocean primary productivity: The response of marine algae to climate warming and sea ice decline. *Arctic Report Card 2020*, R. L. Thoman, J. Richter-Menge, and M. L. Druckenmiller, Eds., https://doi.org/10.25923/vtdn-2198.

(Note: Each essay has a unique DOI assigned)

Front cover photo credits

Center: Yamal Peninsula wildland fire, Siberia, 2017 – Jeffrey T. Kerby, National Geographic Society, Aarhus Institute of Advanced Studies, Aarhus University, Aarhus, Denmark

Top Left: Large blocks of ice-rich permafrost fall onto the beach along the Laptev Sea coast, Siberia, 2017 – Pier Paul Overduin, Alfred Wegner Institute for Polar and Marine Research, Potsdam, Germany

Top Right: *R/V Polarstern* during polar night, MOSAiC Expedition, 2019 – Matthew Shupe, Cooperative Institute for Research in Environmental Sciences, University of Colorado and NOAA Physical Sciences Laboratory, Boulder, Colorado, USA

Table of Contents

2020 Headlines

The sustained transformation to a warmer, less frozen and biologically changed Arctic remains clear

Extreme warm air temperatures in the Eurasian Arctic illustrate significant region-wide effects of year-to-year variability and connections across the Arctic environment.

Highlights

- The average annual land **surface air temperature** north of 60° N for October 2019-September 2020 was the second highest on record since at least 1900. Record warm temperatures in the Eurasian Arctic were associated with extreme conditions in the ocean and on the land.

In the oceans

- **Sea ice** loss in spring 2020 was particularly early in the East Siberian Sea and Laptev Sea regions, setting new record lows in the Laptev Sea for June. The end of summer sea ice extent in 2020 was the second lowest in the 42-year satellite record, with 2012 being the record minimum year.
- August mean **sea surface temperatures** in 2020 were ~1-3°C warmer than the 1982-2010 August mean over most of the Arctic Ocean, with exceptionally warm temperatures in the Laptev and Kara seas that coincided with the early loss of sea ice in this region.
- During July and August 2020, regional **ocean primary productivity** in the Laptev Sea was ~2 times higher for July and ~6 times higher for August compared to their respective monthly averages.
- **Bowhead whales** have been a staple resource for coastal Indigenous peoples for millennia and are uniquely adapted for the arctic marine ecosystem. The Pacific Arctic population size has increased in the past 30 years likely due to increases in ocean primary production and northward transport of the zooplankton they feed on.
- Shifts in air temperatures, storminess, sea ice and ocean conditions have combined to increase **coastal permafrost erosion** rates, in regions where a high proportion of Arctic residents live and industrial, commercial, tourist and military activities are expanding.

On the land

- The exceptional warm spring air temperatures across Siberia resulted in record low June **snow cover** extent across the Eurasian Arctic, as observed in the past 54 years.
- Extreme **wildfires** in 2020 in the Sakha Republic of northern Russia coincided with unparalleled warm air temperatures and record snow loss in the region.
- Since 2016, **tundra greenness** trends have diverged strongly by continent, declining sharply in North America but remaining above the long-term average in Eurasia.
- From September 2019 to August 2020, the **Greenland Ice Sheet** experienced higher ice loss than the 1981-2010 average but substantially lower than the record 2018/19 loss.
- **Glaciers and ice sheets** outside of Greenland have continued a trend of significant ice loss, dominated largely by ice loss from Alaska and Arctic Canada.

Observing Arctic change

- Advancements in the **integration of models and observations** have increased the skill and utility of Arctic sea ice predictions on seasonal to decadal to century timescales.
- Important additions to the Arctic Observing Network (**AON**) systems and data products and advancements in process-level understanding have improved the quality and accessibility of information used to produce the Arctic Report Card.
- The unique Multidisciplinary drifting Observatory for the Study of Arctic Climate (**MOSAiC**) project concluded a historic, international, yearlong expedition into the Arctic ice pack in September 2020, collecting a legacy dataset that aims to advance the understanding, modeling and predicting of Arctic environmental change.
- Opening of the new **NOAA Barrow Observatory**, near Utqiaġvik, Alaska, enables the continuation of nearly half a century of atmosphere and terrestrial in situ observations.

Executive Summary

DOI: 10.25923/mn5p-t549

R. L. Thoman[1,2], J. Richter-Menge[3], and M. L. Druckenmiller[4]

[1]Alaska Center for Climate Assessment and Policy, University of Alaska Fairbanks, Fairbanks, AK, USA
[2]International Arctic Research Center, University of Alaska Fairbanks, Fairbanks, AK, USA
[3]Institute of Northern Engineering, University of Alaska Fairbanks, Fairbanks, AK, USA
[4]National Snow and Ice Data Center, University of Colorado Boulder, Boulder, CO, USA

The Arctic Report Card (ARC) provides an annual update on the state of the Arctic's climate and environment as well as highlights of Arctic science news of the past year. ARC2020 features 16 essays, 11 of which provide updates on a wide range of Arctic science topics, from the past year's air temperatures and sea ice conditions to the latest in bowhead whale research. Taken as a whole, across a variety of disciplines and viewpoints, the story is unambiguous: the transformation of the Arctic to a warmer, less frozen, and biologically changed region is well underway. Extreme high temperatures in the Eurasian Arctic in spring and summer 2020 provide a clear demonstration of the strong connections within the Arctic environment that characterize this region. Three closely connected essays examine the acquisition of observational data and their use in modeling to understand physical systems in the Arctic. ARC2020 also marks the publication's 15th anniversary. Two essays reflect back across the evolution of the ARC itself and the tools utilized to help understand the changes in progress. We must report that, like so much else, ARC2020 was altered by the COVID-19 pandemic. A planned essay on the impacts of the changing Arctic on food security from the viewpoints of Indigenous marine mammal hunters from two northwest Alaska communities had to be postponed to a future ARC due to travel and community-related exposure restrictions.

Changes in air temperature and sea ice (extent, volume, and seasonality) are at the root of changes across the Arctic environment. In a year of many extremes, the annual (October to September) SAT anomaly poleward of 60° N was 1.9°C above the 1981-2010 average and was the second highest on record since at least 1900. This marks the 9th of the last 10 years when SAT anomalies were at least 1°C warmer than the 1981-2010 mean. Driving this annual extreme were anomalously warm conditions across much of the Eurasian Arctic for most of the first seven months of 2020 and during the summer over the central Arctic basin. These air temperature extremes both contributed to and in part were caused by extremes in the Arctic sea ice. Sea ice loss in spring 2020 was particularly early in the East Siberian Sea and Laptev Sea regions. During June, ice extent in the Laptev Sea dropped to record low levels for that time of year. More broadly, both winter and summer sea ice extent extremes continued declining trends. In 2020, the end of winter extent was the 11th lowest in the 42-year satellite record and the end of summer extent was the second lowest, 2012 being the record minimum year. Satellite-derived sea ice thickness (available only since 2010) showed both the winter maximum and late summer minimum to be near the lowest in the decade since data collection began.

The terrestrial Arctic environment is very sensitive to air temperature at varying time scales, especially during spring and autumn. The snow cover (or lack thereof) exerts a strong control on weather and climate, as well as on the larger ecosystem, through reflection of incoming solar energy and its insulating effect on the ground's ability to gain or lose heat. Snow accumulation during the 2019/20 winter was above normal across the entire Arctic. However, the exceptional spring warmth across the

Eurasian Arctic resulted in the lowest June snow cover extent in this region since the observational record began in 1967. The May Arctic snow cover extent during the 1981-2020 period is decreasing at a rate of 3.7% per decade, with a much higher rate of loss (15% per decade) for June over this same period.

Variably in the seasonality of snow cover is an important control on wildland fire activity in high northern latitudes. Arctic wildfires occur primarily, though not exclusively, in the boreal forest (Taiga), the world's largest terrestrial biome. In this region wildfires are highly variable in space and time, driven by sub-seasonal drying of fuel over weeks and controlled by climate. Increasing trends in air temperature and fuel availability over the 41-year record (1979-2019) suggest that conditions are becoming more favorable for fire growth, with more intense burning, more fire growth episodes, and greater consumption of fuels. The extreme wildfires in 2020 in Sakha Republic offer another example of the impact of the extreme warm spring and summer air temperatures in the Eurasian Arctic.

Tundra productivity (i.e., greenness) is sensitive to summer air temperature but in complex ways, with other factors playing a significant role, such as the characteristics and timing of the spring snow retreat. In North America, tundra productivity for the 2019 growing season rebounded strongly from the previous year, in tandem with record summer warmth following the cold summer of 2018. Since 2016, greenness trends have diverged strongly by continent; peak summer greenness has declined sharply in North America but has remained above the long-term mean in Eurasia. (Note that unlike other ARC Vital Signs, satellite-based tundra vegetation analysis lags a year behind other essays due to data processing constraints. See ARC2019 for details on surface air temperatures during 2019.)

Ocean surface temperatures (SSTs) in the Arctic during spring and summer are strongly tied to sea ice presence or absence as well as ocean currents and atmospheric parameters. August 2020 mean SSTs were ~1-3°C warmer than the 1982-2010 August mean over most of the Arctic Ocean. Exceptionally warm SSTs in the Laptev and Kara Seas distinguished August 2020 SSTs, coinciding with the early loss of sea ice in this region. The strong interannual variability in spatial patterns of SST bears a close relationship to early summer sea ice concentrations because the regions of low sea ice area allow more direct solar heating of the exposed surface waters. August mean SSTs show statistically significant warming trends for 1982-2020 in most regions of the Arctic Ocean that are ice-free in August. Also tied to sea ice and ocean temperature conditions is productivity at the bottom of the marine food web. During July and August 2020, a ~600 km long region in the Laptev Sea of the Eurasian Arctic showed much higher primary productivity (~2 times higher for July and ~6 times higher for August) than the same months of the 2003-2019 multiyear average.

Air temperatures, storminess, sea ice and ocean conditions are major factors in permafrost coastal erosion. Permafrost coasts in the Arctic make up more than 30% of Earth's coastlines. A high proportion of Arctic residents live in the coastal zone, where industrial, commercial, tourist, and military presences are also expanding. Since the early 2000s, erosion of permafrost coasts in the Arctic has increased at nearly all observational sites where data extending back to approximately 1960 or 1980 are available. Permafrost coasts along the US and Canadian Beaufort Sea experienced the largest increase in erosion rates, ranging from +80 to +160%, when comparing data from the 1980s and 2000s with the 2010s.

The Greenland ice sheet is the largest Northern Hemisphere remnant of the Pleistocene glaciation, holding enough water to raise the global sea level by 7.4 meters. High regional variability in temperatures, albedo, and ice loss characterized the 2019/20 season across the Greenland ice sheet. Overall, during September 2019-June 2020, the ice sheet experienced higher ice loss than the 1981-2010

average but lower than the record 2018/19 loss. Glaciers and ice sheets outside of Greenland also continued a trend of significant ice loss, dominated largely by ice loss from Alaska and Arctic Canada.

As an example of the impact of changing conditions on marine mammals, ARC2020 includes an essay on bowhead whales, one of the iconic megafauna of the Arctic and the only "true" arctic baleen species, with a range confined to icy sub-arctic and arctic waters. They have been a staple resource for coastal Indigenous peoples from the Russian Far East to Greenland for millennia. Nearly hunted to extinction by commercial whaling in the 19th and 20th centuries, populations in the Pacific Arctic and East Canada/West Greenland region are thought to have now recovered to early 19th century levels. The population size of bowheads in the Pacific Arctic has increased in the past 30 years likely due to increases in ocean primary production as well as the northward transport of the zooplankton on which they feed.

Observations are the backbone of scientific inquiry. While remote sensing provides vital large-scale data, many important parameters can only be gathered in situ. For nearly half a century, NOAA's Barrow Observatory, just northeast of Utqiaġvik, Alaska, has observed the atmosphere and terrestrial system from what was intended to be a temporary building. After years of planning, a new facility opened in 2020, enabling the Observatory to continue existing work and affording greater collaboration with other researchers. The 2019/20 period also brought the greatest international research effort conducted in the Arctic sea ice pack in more than 20 years, the Multidisciplinary drifting Observatory for the Study of Arctic Climate (MOSAiC). Focused on data gathering to improve understanding of the physical processes occurring at high latitudes, this legacy dataset will enable research to improve modeling and predictive capabilities for years to come.

2020 marks the 15th year of the ARC. In 2006 it was clear that the Arctic was changing. However, the complexity of change was less understood and the rapidity of change that would occur in just a few years, highlighted by the (then) record-smashing low September 2007 sea ice extent, was unanticipated. In concert, an analysis of data products used to support the ARC over the course of its 15 years, along with a newly developed custom ARC data portal, reveals that the evolution of tools and available data has advanced the quality and accessibility of observations. Another important development of the last 15 years is the strengthened commitments to collaborate with the Indigenous peoples of the Arctic so that their integrated, cumulative, holistic understanding of the Arctic environment acquired over many generations critically contributes to today's shared understanding of the changes occurring across the region.

Consistent with past ARCs, across the ARC2020 essays runs the theme of variability, both in time and place. While sometimes referred to as "the new normal," in reality, most parts of the Arctic environmental system are continuing to change very rapidly, with each ARC providing a snapshot of "where things are now." As the past 15 years of ARCs have vividly demonstrated, the Arctic of yesterday is different from today, and the Arctic of today is not predictive of tomorrow.

Acknowledgments - Past and Present Arctic Report Card Editors

While NOAA has supported the production of the Arctic Report Card since 2006, the content from year to year is formally arranged by a small group of dedicated editors that support the efforts and fruition of the Report Card, from inception in June to the press release in December. This team of Arctic scientists brings their unique backgrounds in shaping the Report Card, providing a rigorous internal review of the

essays, refining the content by identifying systems-level linkages, and providing a guiding eye and vision for the highly praised Arctic Report Card videos and website.

On behalf of the NOAA Arctic Report Card production team, thank you to past and present Editors for your dedication and service to this hallmark publication.

James E. Overland (2006 - 2017)
Jacqueline Richter-Menge (2006 - 2020)
Martin O. Jeffries (2011 - 2016, 2018, 2019)
Jeremy T. Mathis (2016)
Emily B. Osborne (2017, 2018)
Matthew L. Druckenmiller (2019, 2020)
Richard L. Thoman (2020)

Please visit the Arctic Report Card's Meet the Editors webpage to learn more about a few of these Editors.

December 7, 2020

A 15-year Retrospective

DOI: 10.25923/5h6n-j448

J. Richter-Menge[1], M. L. Druckenmiller[2], and R. L. Thoman[3,4]*

[1]Institute of Northern Engineering, University of Alaska Fairbanks, Fairbanks, AK, USA
[2]National Snow and Ice Data Center, University of Colorado Boulder, Boulder, CO, USA
[3]Alaska Center for Climate Assessment and Policy, University of Alaska Fairbanks, Fairbanks, AK, USA
[4]International Arctic Research Center, University of Alaska Fairbanks, Fairbanks, AK, USA
*with important contributions from numerous ARC authors

First issued in 2006 to address the need for timelier communication of Arctic change to a broad audience, Arctic Report Card (ARC) 2020 marks the 15th anniversary of this annual, peer-reviewed publication. In recognition of this milestone, the ARC2020 editorial team has taken a step back to consider how observing, understanding, and communicating Arctic change have evolved over the course of the 15-year ARC series. To be clear, warming temperatures in the Arctic, and around the globe, were recorded decades before ARC2006 was published. A look back at ARC2006, however, reveals a community of observers who were just beginning to grasp the scope and persistence of the Arctic change we would witness and document over the next 15 years. Lost on most was the rapid rate of the changes to come. From the ARC2006 Executive Summary:

> *'...during 2000-2005 the Arctic system showed signs of continued warming. However, there are a few indications that certain elements may be recovering and returning to recent climatological norms (for example, the central Arctic Ocean and some wind patterns). These mixed tendencies further illustrate the sensitivity and complexity of the Arctic physical system. They underline the importance of maintaining and expanding efforts to observe and better understand this important component of the climate system to provide accurate predictions of its future state.'*

It did not take long into the ARC series to realize the Arctic region was on a path toward a 'new normal'. Dominating the 15-year storyline is the persistent and robust increasing trend in surface air temperature over the Arctic region. It is a trend that extends from the mid-1990s and continues to outpace the rate of increase in global temperatures by a factor of two. In response to the upward trend in air temperatures, there is an equally persistent and robust record of significant ice loss throughout the region during the 15 years of the ARC.

As it turns out, the first publication in 2006 coincided with a cusp of transformation in the sea ice cover, which is literally and figuratively central to the Arctic system. The 2007 September minimum sea ice extent stunned scientists and grabbed world-wide media attention with a new record minimum that was 23% below the previous record low set in 2005. Just five years later, in 2012, the 2007 record was overtaken by a September minimum sea ice extent that was 18% below 2007. The 2012 record low still stands as of 2020. However, in the 14 years since ARC2006 the late summer sea ice minimum extent has never returned to pre-2007 values. The impacts of this significant reduction in the extent of the summer sea ice cover, accompanied by equally notable changes in the thickness of the sea ice cover, reach well

beyond the Arctic environmental system. Sea ice loss has significantly increased accessibility to Arctic waters for shipping and commercial enterprises. At the same time, these changes are challenging the traditional ways of life for coastal Indigenous communities. Reductions in the sea ice cover may also be linked to shifts in weather in the mid-latitudes.

There have been other consequential surprises. For example, 15 years ago, researchers were just beginning to see signals of rapid changes in the Greenland Ice Sheet, via the increasing rate of ice motion at glaciers on both coasts of Greenland. Currently, the Greenland Ice Sheet is losing ice mass at an average rate that is almost four times higher than reported at the turn of the century, just 20 years ago. At the current rate of ice melt, Greenland is the largest contributor to global sea level rise, increasing sea level 0.7mm/year. Arctic-wide glaciers and ice caps outside of the Greenland Ice Sheet also show a consistent trend of increasing ice loss, contributing approximately 0.4 mm/year. Taken together, these annual contributions add more to the global rise in sea level than Antarctica and are already acutely felt by coastal communities during storms, storm surges, and high tides. In the face of increasing air temperatures, changes to the Arctic snow cover over land during the past 15 years are in line with expectations: as air temperatures have warmed, snow cover has melted earlier in spring, and started to accumulate later in autumn. However, at -15.5% per decade over the period 1981-2020, the rate of loss of the terrestrial snow cover extent in June exceeds even the high pace of sea ice reduction in September, which is -12.8% per decade. Fifteen years ago, the notion that widespread degradation of permafrost on Alaska's North Slope would start before the end of the 21st century was still in question. Yet, as documented in ARC, permafrost loss in this region of the high Arctic is already widespread and impacting coastline stability, built infrastructure and terrestrial ecosystems. Today, it is anticipated that progressive deep thawing of permafrost in this region may begin in 30-40 years.

The ARC series has also exposed the connections and complexity within the Arctic environmental system. For instance, with each summer there has been a progressive warming of surface waters in the seas that surround the Arctic Ocean, which is associated with the decrease in sea ice extent. The loss of sea ice allows for increased solar energy absorption by the relatively dark ocean surface, leading to an increase in sea surface temperatures. The increase in sea surface temperatures, in turn, leads to more melting of the sea ice cover. Similarly, the increased melting of terrestrial snow and land ice, which reflect sunlight, increasingly exposes the darker land surfaces, which absorb the sunlight. Through these linkages, the sustained ice and snow melt and warming sea and land temperatures in the Arctic have drawn attention to the dominant role of the ice-albedo feedback, one of the most prominent global climate feedbacks. The ARC series also illustrates that changes in the characteristics of the sea ice cover, ocean, and land cascade into changes in the marine (e.g., increases in primary productivity, fish distribution, bowhead whale feeding behavior) and terrestrial ecosystems (e.g., increases in vegetation growth on the tundra, increasing wildfire activity, increasing coastal erosion).

The ARC series reveals a storyline that goes beyond long-term trends. Enveloping every strong trendline is the equally strong signal of interannual variability, evident by the year-to-year jumps that are ubiquitous throughout the climate records showcased by the ARC. It is these jumps, superimposed on the climate trends, that have often stolen the show during an ARC press release, especially when they are associated with new records (e.g., extreme air or ocean temperatures, extreme ice loss, etc.). Much research is concentrated around understanding the underlying causes behind interannual variability, realizing that this variability provides a window into the connections throughout the Arctic and global systems and the forces driving the observed trendlines. Connections throughout the Arctic system and linkages between the Arctic and global environmental systems are now much better recognized and understood than they were 15 years ago. However, much work remains to be done, motivated by the

awareness that knowledge gained in understanding these connections and linkages is a key to improved predictions of future change, on seasonal to decadal time scales. Improved predictions enable improved planning capability for local, regional, and global populations who must anticipate, cope, and adapt to the warming environment.

The intensity of the change in the Arctic environment, peppered by numerous record setting events, has broadened the awareness of change and concerns around the associated impacts well beyond the Arctic research community. With the increased awareness has come increased resources, enabling more research, encouraging interdisciplinary project teams, improving research and communication networks, increasing access to data and commercial resources, and facilitating international and national cooperation. Important technological advances have also been made; chief among them are satellite-based observational capabilities. The Arctic is a harsh environment that challenges the deployment and maintenance of long-term in situ observational networks. Satellites offer a remote platform that allows a continuous pan-Arctic perspective, with many observations that are widely available in near-real time. For instance, development of gravity measurements from space (especially the GRACE and GRACE-FO satellites) have revolutionized measurements of changes in land-based ice masses. Similarly, advances in satellite-based altimetry, employed by CryoSat-2 and ICESat-2, are providing unprecedented new data on sea ice thickness and the depth and distribution of snow on the sea ice cover. High resolution satellite imagery is also proving an essential tool for daily wildfire management in Alaska and northwest Canada and for understanding the details of changes in tundra vegetation. With that said, in situ observations continue to provide an important complement to remote sensing observations, often providing insight on causality. The recent MOSAiC project, highlighted in ARC2020, is an excellent example of how resources and research can come together, across international lines, to provide step changes in documenting and understanding the changing Arctic. When it comes to documenting climate-related changes, it important to acknowledge the need for sustained observational records that extend for decades. The challenge standing in the way of achieving multi-decadal observational records is typically funding and coordination, as opposed to technology.

One of the most important changes to take place over the course of the ARC series is the increased recognition of the roles of Indigenous Peoples of the Arctic for understanding Arctic change. There is a growing appreciation for the deep and long-term knowledge of the environment held by those who have called the Arctic home for millennia, who are an integral part of the Arctic system on which their lives depend. Though this Indigenous knowledge base seems an obvious resource, respectful and equitable partnerships with Western scientists have been long in coming and are very much a work-in-progress. ARC2019 welcomed the first contribution from members of Indigenous communities, highlighting changing conditions in the Bering Sea region. The contribution was enthusiastically received. Having taken this first step, the ARC remains committed to routinely featuring the voices of Indigenous Peoples and knowledge from Indigenous-led research, helping to facilitate an increase in the exchange and inclusion of information from diverse knowledge systems.

Over the course of its 15 years, ARC has achieved the goal of providing timely updates on the state of the Arctic environment to an increasingly broad and diverse audience. The annual ARC press release has become highly anticipated by the national and international news media and generates one of the most widely viewed events on NOAA's Climate.gov website. This achievement reflects the work of hundreds of people. Many have contributed their time and expertise to the writing and editing of the essays, which form the core of every ARC. Behind the scenes are also teams producing the webpage, developing highlight videos, guiding the content format, organizing and promoting the public release, implementing the peer review, participating in the peer review…the list goes on. To each and every one of you, a

hearty 'Thank you!' for your important contributions. The ARC team looks forward to continuing to provide annual updates on the state of the Arctic, documenting the condition of this unique and fascinating region that is an integral part of our planet.

November 10, 2020

The Observational Foundation of the Arctic Report Card – a 15-Year Retrospective Analysis on the Arctic Observing Network (AON) and Insights for the Future System

DOI: 10.25923/ahj5-z336

S. Starkweather[1,2], H. Shapiro[3], S. Vakhutinsky[4], and M. Druckenmiller[4]

[1]Cooperative Institute for Research in Environmental Sciences, University of Colorado Boulder, Boulder, CO, USA
[2]Earth System Research Laboratory, NOAA, Boulder, CO, USA
[3]Arctic Research Consortium of the United States, Fairbanks, AK, USA
[4]National Snow and Ice Data Center, Boulder, CO, USA

Highlights

- Since 2007, the overall performance of the Arctic Observing Network (AON) and its data products that support the Vital Signs of the Arctic Report Card (ARC) has increased from "Fair" to "Good", according to expert input to a Value Tree Assessment. Advancements in the AON have resulted in moderate to significant improvements in five out of seven ARC Vital Sign metrics, however persistent constraints and significant observing gaps still exist, limiting understanding and posing uncertainty.
- Important additions to the observing system and advancements in process-level understanding of the Arctic environment account for these improvements to the ARC.
- A public data portal has been developed at the Arctic Data Center to house a searchable catalog of these data products (Arctic Report Card Data Portal).

Introduction

Over the last 15 years, observations of the Arctic environment have revealed broad, system-wide, and cumulative changes, with potentially catastrophic consequences to Arctic and global society (Richter-Menge et al. 2019; IPCC 2019; CAFF 2017, 2019; AMAP 2017; AC 2009, 2016; ICC 2008, 2014). Yet relative to other regions, structural gaps in sustained observing systems have hampered scientific understanding of the drivers and implications of these changes (Lee et al. 2019; Murray et al. 2018; AOS EOC 2018). Arctic observing systems encounter many challenges. Extreme physical conditions drive up the cost and limit the capabilities of conventional technology systems. A lack of regional infrastructure, including telecommunications, also increases costs and constrains deployments and real-time transmissions. The patchwork of national approaches across eight Arctic states and other observing partners increases planning complexity.

These challenges and imperatives gave rise to the vision of an internationally coordinated Arctic Observing Network (AON; NRC 2006) of sustained and integrated observations targeting the most

critical aspects of a rapidly changing Arctic. Tracking, evaluating, and continuously improving the quality of the AON in support of these outcomes, for both research and operational systems, is a critical effort. The inception of the AON vision coincided with the first publication date of the Arctic Report Card (ARC), which is significant because the ARC is an example of a key product that benefits from the AON's improvements. The 15-year archive of the ARC, along with input from the subject matter experts who have authored it, provide a substantial foundation for a retrospective analysis exploring how the AON's support of the ARC has changed over this period.

Analysis approach

Strategic improvement to the complex of Arctic observations (for example, see essay *Barrow Arctic Observatory*) requires a comprehensive evidence base that systematically identifies gaps and opportunities for optimized investment. Such an evidence base must recognize the interconnected nature of Arctic observations and their connection to delivering public value. Value Tree Analysis (VTA) is a multi-criteria decision support methodology that supports these objectives (IDA 2017). Through expert elicitation, a process which synthesizes the opinions of authorities on a subject, VTA systematically links observational inputs (i.e., satellite or in situ measurements) to the value-added data product and application outputs they support, ultimately linking those outputs to desired outcomes. The desired outcomes in the value tree are specified by a benefit framework. The International Arctic Observing Assessment Framework (IAOAF) was developed by international partners to support analyses specifically for the AON (IDA 2017).

The methodology of VTA is used to weigh the relative impact of individual observing systems and data products, while revealing up- and downstream dependencies across the system. The completed analysis generates a systems-level view of how the value derived from Earth observations propagates forward to achieve societal benefit. The results of a VTA can also reveal where value propagation terminates due to technical hurdles, like prolonged latencies in the delivery of a parameter. By generating a cohesive view of these issues, VTA provides funders and policymakers with an evidence base for informing decisions to strategically fill observing gaps and remove impediments to value propagation.

Analysis scope

The ARC-focused analysis covers the period from 2007 to 2020, using the seven ARC parameters now termed Vital Signs. These parameters have been covered most consistently throughout the ARC series. Under each Vital Sign, this analysis centers on the data products, both observational and model-derived, that support key findings. Key findings are defined as those that establish the annual status of a key variable (e.g., terrestrial snow cover extent) in the context of its long-term trend. Authors from each Vital Sign validated the catalog of data products referenced in the 15-year history of their essay and independently provided the weights and performance scores in the VTA, based on their collective expertise.

Findings

Since 2007, over the course of the ARC series, Vital Signs have employed more than 100 different data products to support key findings of Arctic change. In ARC2020, the 27 data products employed were largely derived from gridded products based on satellite or blended analyses (14), but were also supported by reanalyses or modeled products (8) and in situ networks (5). Reanalyses and model

products themselves are fed by a complex of observational inputs, the full accounting of which exceeded the scope of this analysis. Hence, the 27 observing system inputs to the ARC-focused analysis reflects a conservative count of data inputs. The need for multinational and interagency support for the systems that underpin ARC findings is evident in the mix of products, which are developed for both operational (8) and research (19) purposes, supported by the US, Canada, Japan, and European nations. In an effort to support transparency around the key findings of the ARC2020, a specialty public data portal has been developed at the Arctic Data Center to house a searchable catalog of these data products.

The results of the VTA revealed the diverse scope of inputs required to develop the seven ARC Vital Signs (see Fig. 1 and Glossary of Acronyms for this discussion). The most widely used observing systems are the Passive Microwave (PM) satellite (currently DMSP/SSMIS), NASA's hyperspectral MODIS satellite, and in situ automated weather stations (AWS). Given the persistent issues with atmospheric reanalysis and satellite retrievals near the surface in high latitudes, AWS networks continue to provide critical insights on surface conditions. The PM provides high utility for cryospheric observations, even under cloudy conditions, making it a good fit for the Arctic. The dependence of five Vital Signs on the PM (four shown in Fig. 1; a fifth, Ocean Primary Productivity, did not meet the criticality threshold for inclusion in the graphic) reveals an important vulnerability given that the last satellite is beyond its planned life without a replacement scheduled (Lavergne et al. 2019). This contrasts with the Normalized Difference Vegetation Index (NDVI, see essay *Tundra Greenness*) that is redundantly supported by multiple systems (MODIS, AVHRR, and LandSat). Here, authors note that they choose to work with AVHRR, despite its lower spatial resolution, because the longer record (compared to MODIS) and comprehensive coverage (compared to LandSat) better supports the goals of the ARC.

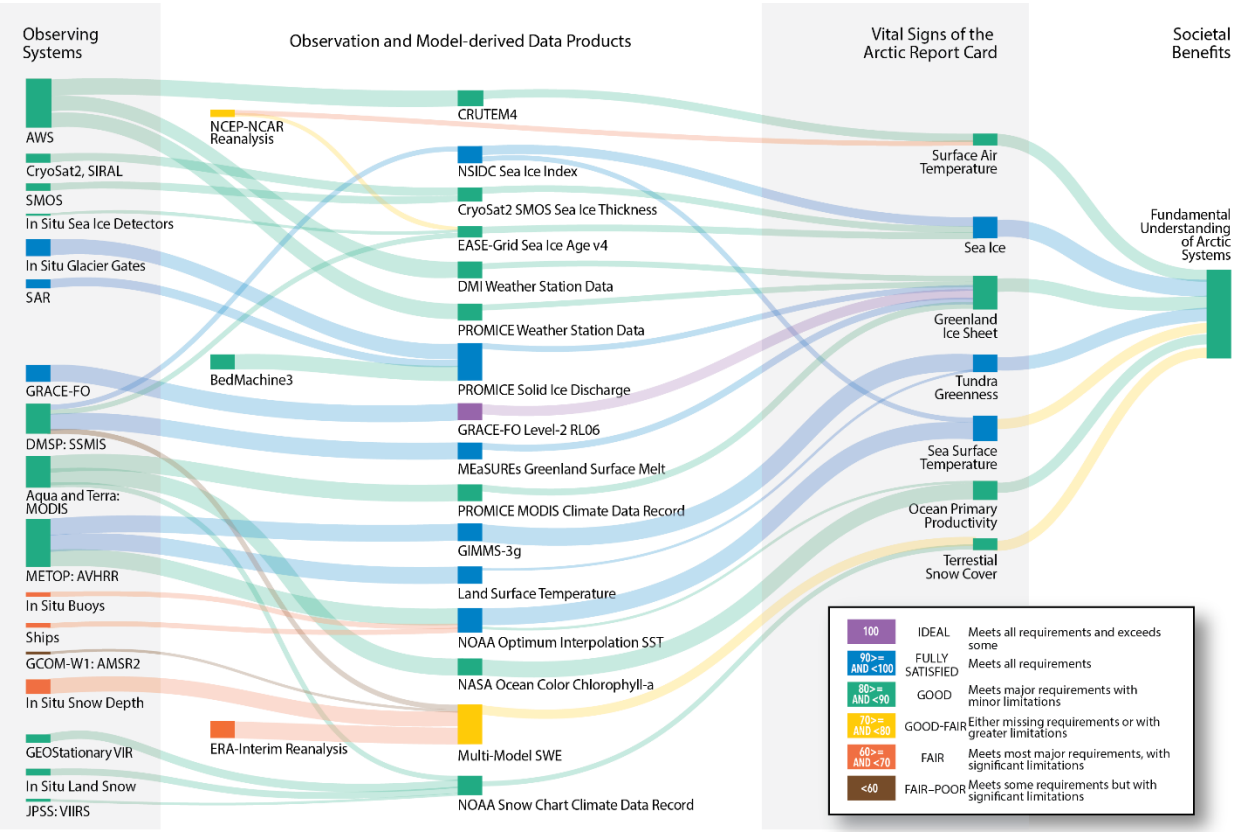

Fig. 1. Value Tree Analysis (VTA) for the ARC2020, in support of Fundamental Understanding of Arctic Systems.

Observing system value in support of the seven ARC Vital Signs propagates forward (left to right) through observation and model-derived data products, then Vital Signs to societal benefit. Color coding indicates a performance score for nodes (see insert), averaged across all uses; links are weighted (indicated by line thickness) based on their criticality to downstream value. The VTA indicates the Vital Signs were most relevant to the IAOAF Societal Benefit Area (SBA): Fundamental Understanding of Arctic Systems (composite score = 74), but also provided value to SBAs like Environmental Quality (not shown, 59) and Marine and Coastal Ecosystems and Processes (not shown, 49). See Glossary for acronyms.

Most authors reported that the objective of the ARC itself, which primarily is to support rapid reporting of key findings, became a driver for the types of products they used in combination with their own preferences or desire to maintain continuity. For example, earlier versions of the ARC essay on ocean conditions included findings related to ocean temperature and salinity profiles, both of which were derived from scores of in situ instruments and ship cruises. While the consolidation of those observations into comprehensive findings was informative, it hindered the primary ARC objective of rapid assimilation of quality-assured data collections and was abandoned. In some cases, authors specifically developed climate data records to support their work on ARC and related assessments, meaning ARC has become a driving force in improving the AON. For example, a series of improvements to MODIS-derived albedo estimates since 2007 have resulted in the establishment of a Climate Data Record (Box et al. 2017, and essay *Greenland Ice Sheet*). Overall, from an ARC2020 perspective, authors reported a composite, weight-normalized observing system performance of 81 and data product performance of 86 (see Key in Fig.1 for all performance scores in this essay). Both ratings, which fall into the category of 'Good', are specific to the ARC itself and not reflective of the performance of the AON across all applications. Authors' combined ratings for how well their essay supported the IAOAF Societal Benefit Area (SBA) Fundamental Understanding of Arctic Systems (77) reflects that even an 'Ideal' Vital Sign would not address all the requirements of this SBA due to its breadth.

For the Value Tree Analysis, authors were asked to rate the performance of their ARC Vital Sign (i.e., how well the Vital Sign does at conveying long-term trends in the subject of interest) and how it has changed since it first appeared in the ARC (Table 1). Over the last 15 years, five of seven Vital Signs have seen moderate (+10) to large (+40) performance improvements. Taken as a composite across all Vital Signs, the quality of the AON and its data products in support of ARC has risen from a performance score of 61 to 84, or from 'Fair' to 'Good'(see Key in Fig.1) The Greenland (+30) and Sea Ice (+20) Vital Signs both credit their gains to new observations. In the case of Greenland, these include the GRACE satellite's Greenland mass balance observations and a new network of AWS stations across Greenland (Fausto and Van As 2019). For Sea Ice, both CryoSat and ICESat provide new capabilities to estimate sea ice thickness from space-borne radar and laser altimeters, respectively. The Tundra Greenness and Surface Air Temperature authors credit the improvements in their performance (+40 and +10, respectively) to improved representation of Arctic processes in models and data products. Terrestrial Snow Cover (+40) authors credit improved understanding of uncertainty across seasons.

Table 1. 2007 and 2020 Performance Ratings and Context, provided by Vital Sign authors and using scale as presented in Key of Fig. 1.

Vital Sign	Performance Rating, 2007 or first year in the ARC	Performance Rating, 2020	What accounts for changes in the ratings? (In the words of the Vital Signs' authors)
Surface Air Temperature	60	70	"Over the last 15 years, there have been weather model improvements [...] which have improved the quality of Arctic air temperature forecasts and reanalyses, particularly downstream of AWS sites. Within the last decade, the addition of AWS sites in Alaska and coastal Greenland and on the Greenland Ice Sheet (e.g., PROMICE sites) has also improved the depiction of Arctic Surface Air Temperature." Thomas Ballinger
Sea Ice	60	80	"[2007] Sea ice extent was available, but there was no real ice thickness information for most of the Arctic Ocean, and ice type information was limited...[2020] CryoSat-2 and ICESat-2 are now providing comprehensive thickness info. Also long-term ice age is available." Walt Meier
Greenland Ice Sheet	50	80	"We are now able to comment on most ice sheet changes using observational records. Records are longer and our confidence in results and understanding of ice sheet processes is significantly advanced. There are multiple sources for a number of important observations, and many more observational (especially remote sensing) tools now." Twila Moon
Tundra Greenness	50	90	"[2007] Originally, there were issues with the dataset at high latitudes, specifically > 72 degrees north. [2020] Since [then], [...], we have worked extensively with the dataset developers to improve the quality of the data at high latitudes." Howard Epstein
Sea Surface Temperature	90	90	"[These ratings are] not 100 percent because of limitations of spatial resolution, which is a shortcoming in coastal regions where Sea Surface Temperature variability over small spatial scales is significant." Mary Louise Timmermans
Ocean Primary Productivity	80	80	"The same satellite data sets have been used since 2011, [...] not much changed here, however, with a longer time series, the statistical significance of the change can be more accurate." Karen Frey

Vital Sign	Performance Rating, 2007 or first year in the ARC	Performance Rating, 2020	What accounts for changes in the ratings? (In the words of the Vital Signs' authors)
Terrestrial Snow Cover	40	80	"In the early years of the Arctic Report Card, we only analyzed the trend in snow cover extent using two products. Over time, we added new datasets from remote sensing and models. This has provided more comprehensive information on how Arctic snow is changing (snow extent, duration, snow water equivalent), and increased confidence in the trends. Over the past fifteen years, a wide range of reference data has also been used to improve our understanding of seasonal changes to Arctic snow." Lawrence Mudryk

While these improvements are encouraging, there are still significant gaps in the AON of relevance to ARC Vital Signs. For this reason, authors were also asked about needed future improvements to the AON and its data products that would increase the performance score of their essays. The Terrestrial Snow Cover authors indicated that new earth observation capabilities, such as Ku-band radar, are needed to improve estimates of snow water equivalent (SWE) across the Arctic (particularly in mountain areas), which would allow better validation of other SWE analyses over these regions. Sea Ice authors would like to include snow depth and melt ponding over sea ice in the essay, as well as representations of melt-onset and freeze-up dates. They note that these observations are largely available, but there is a significant time lag in the preparation of the data products. Sea Surface Temperature and Sea Ice estimates are poorly resolved in coastal areas, indicating a need for higher resolution in their respective satellite systems. In the case of Ocean Primary Productivity, NASA's PACE mission may address needs for higher accuracy chlorophyll-*a* concentrations in the optically complex Arctic waters, but this would not address the limitations of visible band instruments under the persistently cloudy Arctic conditions.

Conclusions

Earth observations are a public good for which policy makers require a strong evidence base to maximize the benefits that observing systems yield. The catalog of data products from the ARC provides a meaningful input to such an evidence base, particularly in support of the IAOAF SBA Fundamental Understanding of the Arctic System. The data products and observing systems that have formed the basis for the ARC Vital Signs have matured since 2007, due to both sponsorship of new observations and focused improvements to data products. While the improvements observed over the seven Vital Signs are encouraging, it is important to note that the results of this analysis are biased by that which has been possible to consistently observe in the Arctic. There are many critical topics worthy of the type of assessment presented in the ARC, but the absence of related observations and data products on a timely and consistent basis eliminates them from consideration. There is a pressing need to strategically identify the most urgently needed improvements for this broader scope of concerns. The quality of the AON in support of scientific assessments is a critical indicator that should itself be monitored. The ARC and these methodologies provide a starting point for such comprehensive analyses.

Glossary of acronyms

Satellites or Sensors:

AMSR2 - Advanced Microwave Scanning Radiometer
AVHRR - Advanced Very High Resolution Radiometer
DMSP - Defense Meteorological Satellite Program
GCOM-W1 - Global Change Observation Mission
GRACE - Gravity Recovery and Climate Experiment
JPSS - Joint Polar Satellite System
MODIS - Moderate Resolution Imaging Spectroradiometer
SAR - Synthetic Aperture Radar
SIRAL - SAR/Interferometric Radar Altimeters
SMOS - Soil Moisture and Ocean Salinity mission
SSMIS - Special Sensor Microwave Imager/Sounder
VIIRS - Visible Infrared Imaging Radiometer Suite
VIR - Visible and Infrared

Data Centers/Products/Terms:

AWS - Automated Weather Station
CRUTEM - Climatic Research Unit Temperature
DMI - Danish Meteorological Institute
EASE-Grid - Equal Area Scalable Earth Grid
ECMWF - European Centre for Medium-range Weather Forecasts
ERA - ECMWF Reanalysis
MEaSUREs - Making Earth Science Data Records for Use in Research Environments
NCEP - National Center for Environmental Prediction
NCAR - National Center for Atmospheric Research
NSIDC - National Snow and Ice Data Center
PROMICE - Program for the Monitoring of the Greenland Ice Sheet

References

Arctic Council (AC), 2009: Arctic Marine Shipping Assessment 2009 Report. B. Ellis and L. Brigham, Eds., 194 pp., https://oaarchive.arctic-council.org/handle/11374/54.

Arctic Council (AC), 2016: Arctic Resilience Report. M. Carson and G. Peterson, Eds. Stockholm Environment Institute and Stockholm Resilience Centre, Stockholm, Sweden, http://www.arctic-council.org/arr.

Arctic Monitoring and Assessment Program (AMAP), 2017: Snow, water, ice and permafrost. Summary for policy-makers. Arctic Monitoring and Assessment Programme (AMAP), Oslo, Norway, 20 pp., https://www.amap.no/documents/doc/snow-water-ice-and-permafrost.-summary-for-policy-makers/1532.

Arctic Observing Summit Executive Organizing Committee (AOS EOC), 2018: Report of the 4th Arctic Observing Summit: AOS 2018, Davos, Switzerland, 24-26 June 2018. International Study of Arctic Change (ISAC) Program Office, Arctic Institute of North America, Calgary, Canada.

Box, J. E., D. van As, and K. Steffen, 2017: Greenland, Canadian and Icelandic land ice albedo grids (2000-2016). *Geol. Surv. Den. Greenl.*, **38**, 53-56.

Conservation of Arctic Flora and Fauna (CAFF), 2017: State of fresh water report. Conservation of Arctic Flora and Fauna International Secretariat, Akureyri, Iceland, https://www.caff.is/freshwater/freshwater-monitoring-publications/488-state-of-the-arctic-freshwater-biodiversity-report-full-report.

Conservation of Arctic Flora and Fauna (CAFF), 2019: State of the arctic marine biodiversity report. Conservation of Arctic Flora and Fauna International Secretariat, Akureyri, Iceland, https://www.caff.is/marine/marine-monitoring-publications/state-of-the-arctic-marine-biodiversity-report.

Fausto, R. S., and D. van As, 2019: Programme for monitoring of the Greenland ice sheet (PROMICE): Automatic weather station data. Version: v03, Dataset published via Geological Survey of Denmark and Greenland, https://doi.org/10.22008/promice/data/aws.

Institute for Defense Analyses (IDA), 2017: International Arctic Observations Assessment Framework. IDA Science and Technology Policy Institute, Washington, DC, U.S.A., and Sustaining Arctic Observing Networks, Oslo, Norway, 73 pp., https://www.arcticobserving.org/news/268-international-arctic-observations-assessment-framework-released.

Intergovernmental Panel on Climate Change (IPCC), 2019: IPCC Special Report on the Ocean and Cryosphere in a Changing Climate [H. -O. Pörtner, D. C. Roberts, V. Masson-Delmotte, P. Zhai, M. Tignor, E. Poloczanska, K. Mintenbeck, A. Alegría, M. Nicolai, A. Okem, J. Petzold, B. Rama, and N. M. Weyer (eds.)], in press.

Inuit Circumpolar Council-Canada (ICC), 2008: The Sea Ice is Our Highway: An Inuit Perspective on Transportation in the Arctic. https://www.inuitcircumpolar.com/project/the-sea-ice-is-our-highway-an-inuit-perspective-on-transportation-in-the-arctic/.

Inuit Circumpolar Council (ICC), 2014: The Sea Ice Never Stops: Circumpolar Inuit Reflections on Sea Ice Use and Shipping in Inuit Nunaat. https://www.inuitcircumpolar.com/project/the-sea-ice-never-stops-circumpolar-inuit-reflections-on-sea-ice-use-and-shipping-in-inuit-nunaat/.

Lavergne, T., and Coauthors, 2019: Version 2 of EUMETSAT OSI SAF and ESA CCi sea ice concentration climate data records. *Cryosphere*, **12**, 49-78, https://doi.org/10.5194/tc-13-49-2019.

Lee, C. M., and Coauthors, 2019: A Framework for the development, design and implementation of a sustained Arctic ocean observing system. *Front. Mar. Sci.*, **6**, 451, https://doi.org/10.3389/fmars.2019.00451.

Murray, M. S., R. D. Sankar, and G. Ibarguchi, 2018: The Arctic Observing Summit, Background and Synthesis of Outcomes 2013-2016. International Study of Arctic Change (ISAC) Program Office, Arctic Institute of North America, Calgary, Canada.

National Research Council (NRC), 2006: Toward an integrated Arctic Observing Network. The National Academies Press, Washington, DC, https://doi.org/10.17226/11607.

Richter-Menge, J., M. L. Druckenmiller, and M. Jeffries, Eds., 2019: Arctic Report Card 2019, https://www.arctic.noaa.gov/Report-Card.

November 21, 2020

Surface Air Temperature

DOI: 10.25923/gcw8-2z06

T. J. Ballinger[1], J. E. Overland[2], M. Wang[2,3], U. S. Bhatt[4], E. Hanna[5], I. Hanssen-Bauer[6], S. -J. Kim[7], R. L. Thoman[1], and J. E. Walsh[1]

[1]International Arctic Research Center, University of Alaska Fairbanks, Fairbanks, AK, USA
[2]Pacific Marine Environmental Laboratory, NOAA, Seattle, WA, USA
[3]Cooperative Institute for Climate, Ocean, and Ecosystem Studies, University of Washington, Seattle, WA, USA
[4]Geophysical Institute, University of Alaska Fairbanks, Fairbanks, AK, USA
[5]School of Geography and Lincoln Centre for Water and Planetary Health, University of Lincoln, Lincoln, UK
[6]Norwegian Meteorological Institute, Blindern, Oslo, Norway
[7]Korea Polar Research Institute, Incheon, Republic of Korea

Highlights

- October 2019-September 2020 represented the second warmest 12-month period of observed surface air temperatures (SAT) over Arctic land during the last century.
- Remarkably warm Siberian SAT occurred in the first half of 2020, with near-surface air temperatures 3-5°C above average during boreal winter (JFM) and spring (AMJ).
- A persistent, strong, and zonal jet stream over the mid-to-high latitudes led to warmer than average SAT over northern Eurasia and colder than normal SAT over Alaska and Greenland in winter and spring.

Introduction

Surface air temperatures (SAT) represent one of the strongest indicators of Arctic change over the last 50 years (Box et al. 2019). While SAT patterns across the Arctic vary on a seasonal and annual basis, there has been a strong, positive trend toward warming pan-Arctic land SAT over the last five decades (Fig. 1). This warming has distinctly impacted the Arctic cryosphere, most notably through the decline of sea-ice extent across the annual cycle (Stroeve and Notz 2018; see essay *Sea Ice*), decreased mass balance of ice sheets and glaciers (Hanna et al. 2020; see essay *Greenland Ice Sheet*), and increased permafrost temperatures (Biskaborn et al. 2019). Ecosystems in the region are also highly sensitive to SAT trends and extreme temperature events. For example, increased trends in terrestrial vegetation productivity and "greening" of the Arctic tundra are largely attributed to the strong influence of multidecadal SAT warming (Myers-Smith et al. 2020; see essay *Tundra Greenness*). These warming-induced Arctic system changes have been especially pronounced during the last 15 years, spanning the history of the Arctic Report Card. In this essay, we summarize the seasonal and annual Arctic SAT conditions over the last year (October 2019-September 2020), relative to recent decades.

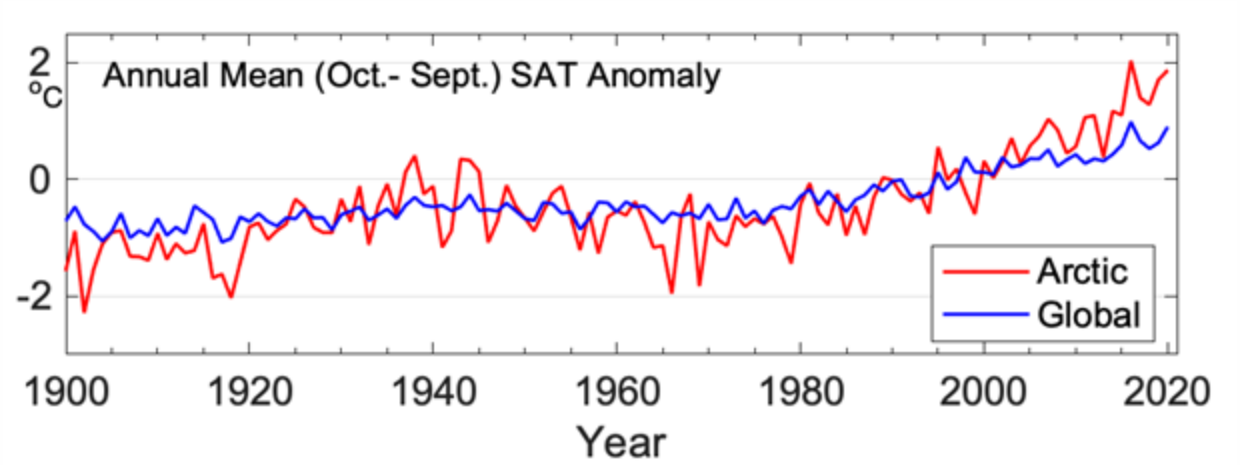

Fig. 1. Mean annual SAT anomalies (in °C) for terrestrial weather stations located in the Arctic (60-90° N; blue line) and globally (red line) for the 1900-2020 period, relative to the 1981-2010 means. Source: CRUTEM4 SAT data (Jones et al. 2012) are obtained from the Climate Research Unit (University of East Anglia) and Met Office.

Mean annual surface air temperature over Arctic lands

The Arctic annual mean SAT anomaly for October 2019 through September 2020 was 1.9°C warmer than the 1981-2010 average for land areas between 60 and 90°N (Fig. 1). This marks the second highest observed SAT anomaly behind 2016 for Arctic lands since at least 1900 and continues a current pattern of 7 consecutive years (and 9 of the last 10 years) where SAT anomalies were at least 1°C warmer than the 1981-2010 mean. Since 2000, average Arctic SAT anomalies have more than doubled global anomalies (Fig. 1) due to a phenomenon known as Arctic Amplification, which is likely driven by a combination of processes that operate on different space and time scales. Heat and moisture transport through atmospheric circulation and winds, as well as oceanic heat transport to the Arctic from low-to-middle latitudes, contribute to the enhanced warming on an annual scale. Mechanisms within the Arctic also modulate air temperatures, and these processes tend to vary by the season. For example, terrestrial snow and sea-ice cover losses resulting in a decrease in surface albedo tend to be major factors driving summertime warming, while tropospheric temperature and cloud-radiative feedbacks play a major role in air temperature increases during winter months (Pithan and Mauritsen 2014; Cohen et al. 2020).

Seasonal surface air temperature patterns

To provide seasonal perspectives, patterns of near-surface air temperature anomalies and extremes are highlighted for autumn 2019 (October-December [OND]) and winter (January-March [JFM]), spring (April-June [AMJ]), and summer (July-September [JAS]) 2020 (Fig. 2). These seasonal divisions are used to coincide with annual cycles of key Arctic components, such as the melt onset of snow and sea-ice cover during spring and the September sea-ice minimum.

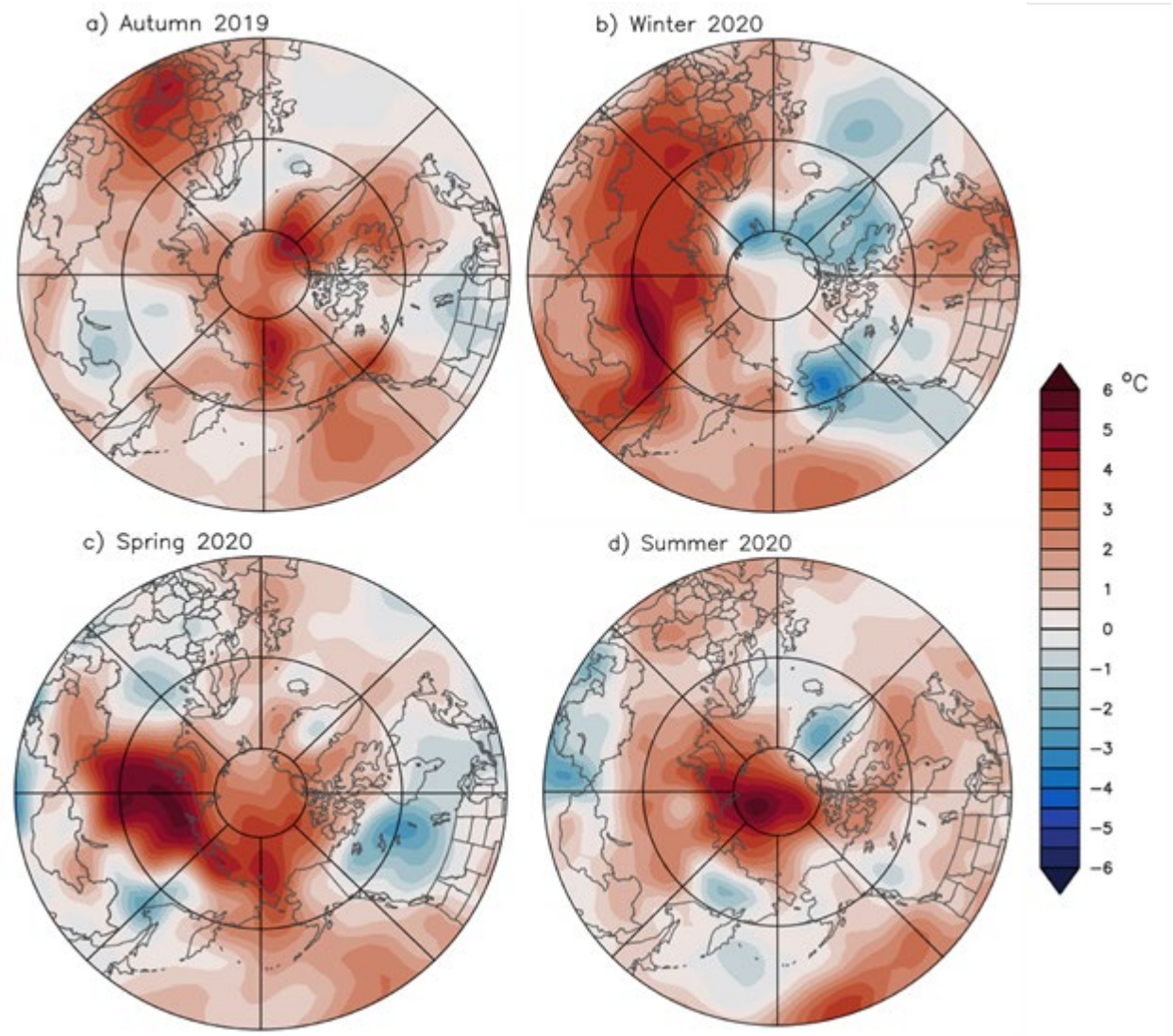

Fig. 2. Near-surface (925 hPa) seasonal air temperature anomaly patterns (in °C) for (a) autumn 2019, (b) winter 2020, (c) spring 2020, and (d) summer 2020, relative to the 1981-2010 means. The 925 hPa layer located just above the surface is used to emphasize large spatial temperature patterns rather than local surface features. Source: NCEP/NCAR reanalysis air temperature data (Kalnay et al. 1996) are obtained from the NOAA Physical Science Laboratory.

Autumn 2019. Positive (i.e., relatively warm) air temperature anomalies were found across most of the Arctic Ocean (Fig. 2a). The largest anomalies (4°C) were found in the Chukchi Sea and across northern Greenland. Similar to autumn 2018 (see essay *Sea Ice* in Arctic Report Card 2019), freeze-up in the Chukchi Sea, as well as in the Laptev and Kara Seas, in 2019 was slowed by diminished sea ice and retention of heat from the previous summer in the upper ocean (see essays *Sea Surface Temperature* and *Sea Ice*). The transfer of this upper ocean heat to the atmosphere likely played a major role in the air temperature anomalies, especially in the absence of southerly winds into the region, which are more typically responsible for the transport of warm air into the region (Fig. 3a). A trough over the Canadian Archipelago helped transport warm air from the south to support the development of large positive air temperature anomalies over northern Greenland (see essay *Greenland Ice Sheet*).

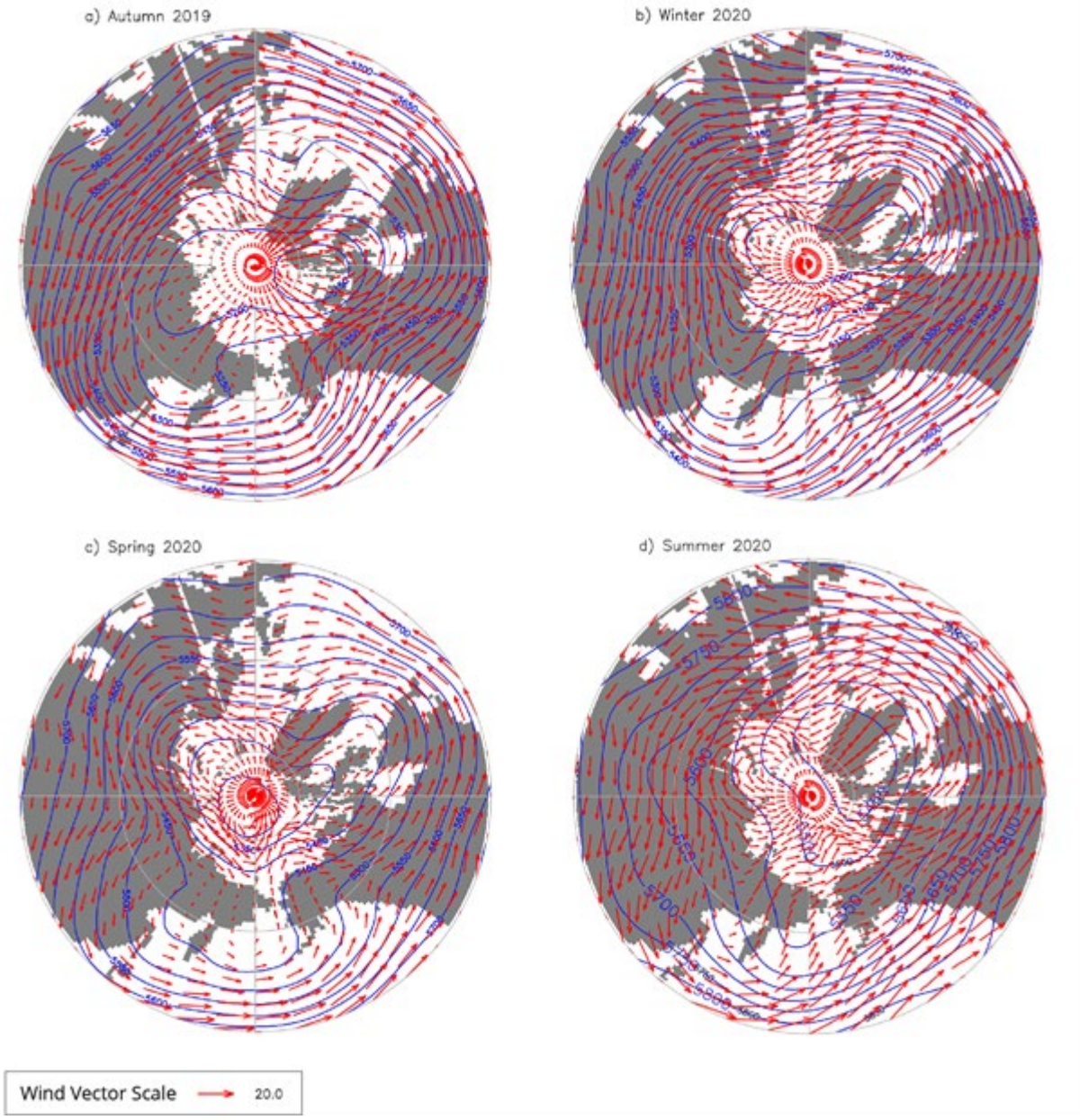

Fig. 3. Atmospheric circulation patterns described by 500 hPa geopotential heights (GPH; blue contours) and winds (red vectors) for (a) autumn 2019, (b) winter 2020, (c) spring 2020, and (d) summer 2020. GPH values are in meters (m) from the surface and the wind vector scale indicates winds of 20 meters per second. For reference, these mid-troposphere winds flow clockwise and counterclockwise around high and low pressure and hence GPH values, respectively. Source: NCEP/NCAR reanalysis GPH data (Kalnay et al. 1996) are obtained from the NOAA Physical Sciences Laboratory.

Winter 2020. The winter air temperature patterns were characterized by above-average temperature anomalies stretching from eastern Europe to central Siberia. An extensive area of air temperature anomalies of 3-5°C occurred in north-central Siberia (Fig. 2b). In contrast, areas extending eastward from Alaska to Greenland and Svalbard showed abnormally cold air temperatures. For example, Svalbard weather stations observed winter temperatures 1.4-2.6°C below normal. It was a particularly cold March at Svalbard Airport and Ny-Ålesund where monthly average air temperatures were 3°C and

4.5°C below average, respectively (https://klimaservicesenter.no/observations/). Arctic Alaska was also anomalously cold and stormy, with the North Slope experiencing the lowest average winter SAT since 2012 (1.4°C below average) marked by the coldest February (5.1°C below average) since 1990 (https://www.ncdc.noaa.gov/cag/divisional/time-series).

A persistent, strong jet stream over the mid-to-high latitudes this past winter (Fig. 3b) supported westerly winds, stormy weather conditions, and relatively mild northern Eurasian temperatures, and conversely trapped frigid Arctic air over Atlantic Arctic waters and the Alaskan and Greenland sectors of the North American Arctic. This anomalous circulation pattern impacted the MOSAiC Expedition, accelerating the icebreaker's drift across the central Arctic Ocean (see essay *MOSAiC*). These warm air temperature anomalies (Fig. 2b) and zonal jet stream orientation (air flow parallel to latitude lines; Fig. 3b) reflect common conditions that occur during the positive phase of the Arctic Oscillation (AO). The AO is an index used to describe the Northern Hemisphere mid-to-high latitude atmospheric circulation. Figure 4a shows the strong, positive correlation between winter AO and near-surface air temperature across Eurasia (i.e., AO and air temperature increases are closely related) and strong, negative correlation across much of the eastern Canadian Arctic, Greenland, and northwest Atlantic Arctic waters. These relationships are relevant to winter 2020, as the AO index was at a record high dating back to 1950 (winter AO = 2.83; Fig. 4b), supporting the observed regional patterns of Arctic air temperature extremes, including the above-average temperatures over north-central Siberia.

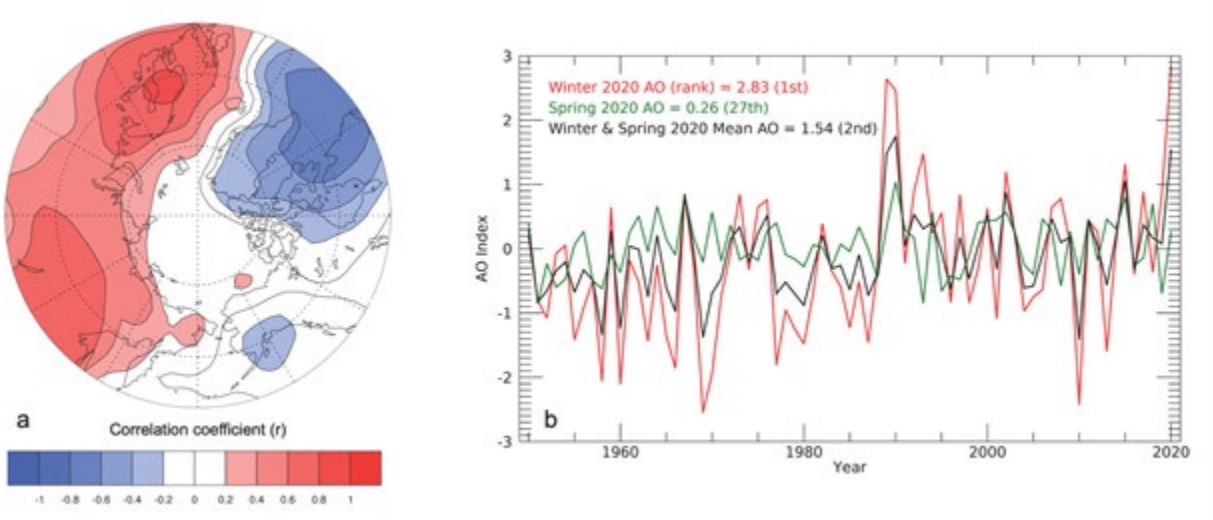

Fig. 4. (a) The spatial correlation between winter Arctic Oscillation (AO) index values and near-surface (925 hPa) air temperatures for the 1950-2020 period. (b) Time series of AO index values from 1950-2020 for winter (January-March; red), spring (April-June; green), and the average of winter and spring months (January-June; black). The AO data are normalized for the 1979-2000 period. The 2020 value and rank for each time series are listed in the legend, with the winter 2020 AO ranking 1st (i.e., the highest value) for the 1950-2020 period. Source: NCEP/NCAR reanalysis air temperature data (Kalnay et al. 1996) are obtained from the NOAA Physical Sciences Laboratory, and the AO data (Thompson and Wallace 1998) are from the NOAA Climate Prediction Center.

Spring 2020. Warm air temperature anomalies characterized much of the Arctic Ocean and coastal zones during spring (Fig. 2c). Persisting from winter, warm air temperatures continued over north-central Siberia with near-surface air temperatures 5°C above the 1981-2010 mean. Late June was especially warm in the region, with 38°C (100.4°F) observed at Verkhoyansk, Russia, on 20 June (Overland and Wang 2020). The relatively warm air temperatures and warm air advection in this region prompted record-low spring snow cover extent (see essay *Terrestrial Snow Cover*) and early onset of

sea-ice melt along the Eurasian Arctic coast. The sea-ice melt season in the Laptev and Kara Seas began nearly 30 days earlier than the 1981-2010 average (http://nsidc.org/arcticseaicenews/2020/08/steep-decline-sputters-out/). The shape of the jet stream, with a trough over eastern Europe, helped transfer warm lower-latitude air to the north-central Siberian Arctic and adjacent marine areas to support these air temperature and sea-ice extremes (Fig. 3c).

Summer 2020. Summer air temperatures were especially warm for the Central Arctic Ocean, extending toward the Siberian Arctic (5°C above average; Fig. 2d). Warm anomalies over north-central Siberia were weaker relative to the previous winter and spring, though the strength of the warm anomaly rapidly increased toward the sector's coastal areas extending into the Kara and Laptev Seas. A monthly mean air temperature record high was set in July at Svalbard Airport (9.8°C), which is 0.8°C above the previous record value from 2016 and 3.4°C above average. Ny-Ålesund also set a similar record in July (8°C), which is 0.7°C above the previous record value from 2019 and 2.7°C above normal. The trough-ridge jet stream pattern atop the Siberian coast (Fig. 3d) steered warm air off the continent into the Kara and Laptev Seas and contributed to sea-ice and sea surface temperature anomalies through the ice-albedo feedback (see essay *Sea Surface Temperature*).

References

Biskaborn, B. K., and Coauthors, 2019: Permafrost is warming at a global scale. *Nat. Commun.*, **10**, 264, https://doi.org/10.1038/s41467-018-08240-4.

Box, J. E., and Coauthors, 2019: Key indicators of Arctic climate change: 1971-2017. *Environ. Res. Lett.*, **14**, 045010, https://doi.org/10.1088/1748-9326/aafc1b.

Cohen, J., and Coauthors, 2020: Divergent consensuses on Arctic amplification influence on midlatitude severe winter weather. *Nat. Climate Change*, **10**, 20-29, https://doi.org/10.1038/s41558-019-0662-y.

Hanna, E., and Coauthors, 2020: Mass balance of the ice sheets and glaciers – Progress since AR5 and challenges. *Earth-Sci. Rev.*, **201**, 102976, https://doi.org/10.1016/j.earscirev.2019.102976.

Jones, P. D., D. H. Lister, T. J. Osborn, C. Harpham, M. Salmon, and C. P. Morice, 2012: Hemispheric and large-scale land-surface air temperature variations: An extensive revision and an update to 2010. *J. Geophys. Res.*, **117**, D05127, https://doi.org/10.1029/2011JD017139.

Kalnay, E., and Coauthors, 1996: The NCEP/NCAR 40-year reanalysis project. *Bull. Amer. Meteor. Soc.*, **77**, 437-472, https://doi.org/10.1175/1520-0477(1996)077<0437:TNYRP>2.0.CO;2.

Myers-Smith, and Coauthors, 2020: Complexity revealed in the greening of the Arctic. *Nat. Climate Change*, **10**, 106-117, https://doi.org/10.1038/s41558-019-0688-1.

Overland, J. E., and M. Wang, 2020: The 2020 Siberian heat wave. *Int. J. Climatol.*, https://doi.org/10.1002/joc.6850.

Pithan, F., and T. Mauritsen, 2014: Arctic amplification dominated by temperature feedbacks in contemporary climate models. *Nat. Geosci.*, **7**, 181-184, https://doi.org/10.1038/NGEO2071.

Stroeve, J., and D. Notz, 2018: Changing state of Arctic sea ice across all seasons. *Environ. Res. Lett.*, **13**, 103001, https://doi.org/10.1088/1748-9326/aade56.

Thompson, D. W. J., and J. M. Wallace, 1998: The Arctic oscillation signature in the wintertime geopotential height and temperature fields. *Geophys. Res. Lett.*, **25**, 1297-1300, https://doi.org/10.1029/98GL00950.

November 12, 2020

Terrestrial Snow Cover

DOI: 10.25923/p6ca-v923

L. Mudryk[1], A. Elias Chereque[2], R. Brown[1], C. Derksen[1], K. Luojus[3], and B. Decharme[4]

[1]Climate Research Division, Environment and Climate Change Canada, Ottawa, ON, Canada
[2]Department of Physics, University of Toronto, Toronto, ON, Canada
[3]Arctic Research Centre, Finnish Meteorological Institute, Helsinki, Finland
[4]Centre National de Recherches Météorologiques, Toulouse, France

Highlights

- Extremely high spring 2020 temperatures across Siberia resulted in the lowest June snow extent across the Eurasian Arctic observed in the 54-year satellite record.
- The record Eurasian minimum spring snow extent occurred despite larger than normal winter snowpack accumulation through April.
- Long-term changes in Arctic spring snow extent show similar reductions across both North America and Eurasia. The trend in Arctic peak snow water equivalent differs over North America (negative trend) and Eurasia (little change), but the combined Arctic peak snow water equivalent total is decreasing.

Introduction

Snow covers the Arctic land surface (land areas north of 60° N) for up to 9 months each year, and influences the surface energy budget, ground thermal regime, and freshwater budget of the Arctic (Brown et al. 2017). Snow also interacts with vegetation, affects biogeochemical activity, and influences migration and access to forage for wildlife, which impacts terrestrial and aquatic ecosystems (Callaghan et al. 2011). The assessment provided here is based on an ensemble of datasets derived from satellite observations and reconstructions of snow cover from snowpack models driven by atmospheric reanalyses. Collectively, this basis provides a reliable picture of Arctic snow cover variability over the last five decades.

Snow across the Arctic land surface can be characterized by multiple variables: how much area is covered by snow (snow cover extent - SCE), how long snow remains on the land surface (snow cover duration - SCD), and how much water is stored in solid form by the snowpack (a function of the snow depth and density, commonly expressed as snow water equivalent - SWE). We examine each of these variables in turn for the 2019/20 Arctic snow season.

Snow cover extent

Snow cover extent (SCE) anomalies (relative to the 1981-2010 climatology) for the Arctic in spring 2020 were computed separately for the North American and Eurasian terrestrial sectors of the Arctic. Anomalies were derived from the NOAA snow chart climate data record, which extends from 1967 to

present (Fig. 1). SCE anomalies over the Eurasian Arctic were strongly negative in May (4th lowest). Additional melt through June associated with a Siberian heat wave (see essay *Surface Air Temperature*) resulted in the lowest Eurasian June SCE in the entire 54-year record. North American Arctic spring SCE anomalies in 2020 were below average in both May and June (8th and 10th lowest, respectively).

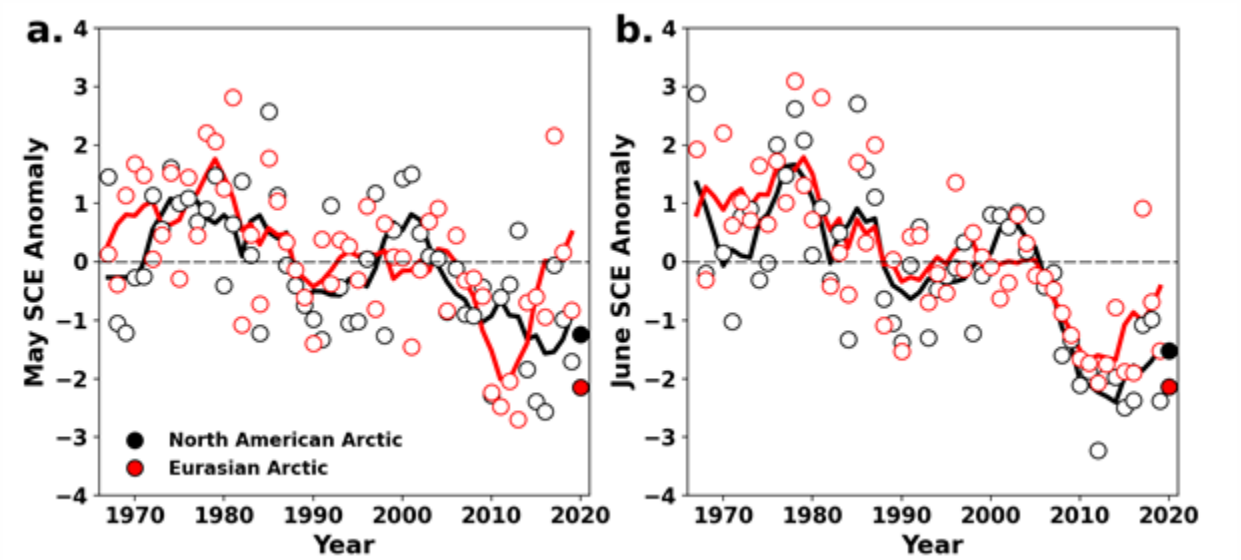

Fig. 1. Monthly snow cover extent (SCE) for Arctic land areas (>60° N) for (a) May and (b) June from 1967 to 2020, a 54-year record. Anomalies are relative to the average for 1981-2010 and standardized (each observation differenced from the mean and divided by the standard deviation, and thus unitless). Solid black and red lines depict 5-year running means for North America and Eurasia, respectively. Filled circles are used to highlight 2020 anomalies. Source: Estilow et al. (2015), Robinson et al. (2012).

Snow cover duration

Snow cover duration (SCD) anomalies across the Arctic region for the 2019/20 snow season (Fig. 2) were derived from the NOAA daily Interactive Multisensor Snow and Ice Mapping System (IMS) snow cover product, produced at 24 km resolution since 1998. Anomalies in the total number of days with snow cover were computed separately for both halves of the snow season: August 2019 to January 2020, referred to as "onset period," and February 2020 to July 2020, referred to as "melt period." SCD during the onset period (Fig. 2a) was close to normal over much of the Arctic, with values reflecting a slightly later start over the eastern Canadian Arctic (Baffin Island and Northern Quebec) and slightly earlier than normal onset over coastal eastern Siberia and the Scandinavian peninsula. The marked difference between Arctic and sub-Arctic Europe is linked to a strong positive mode of the East Atlantic (EA) pattern in atmospheric variability associated with above-average surface temperatures in Europe (see Fig 2a in essay *Surface Air Temperature*). SCD during the melt period (Fig. 2b) over the North American Arctic indicate a combination of late and early melt with more persistent snow occurring in southern Nunavut and early melt occurring in parts of the northeast (e.g., Baffin Island) and across parts of Alaska and Yukon Territory. Over Eurasia, later than normal melt occurred over the Scandinavian peninsula, likely due to larger than normal accumulation (Fig. 3) from an earlier start to the snow season and above-normal winter precipitation. In marked contrast, and despite the larger than normal accumulation of snow through April (Fig. 3a), springtime temperatures averaging more than 5 degrees above normal (see essay *Surface Air Temperature*) resulted in snow melting up to a month early across extensive areas of central Siberia.

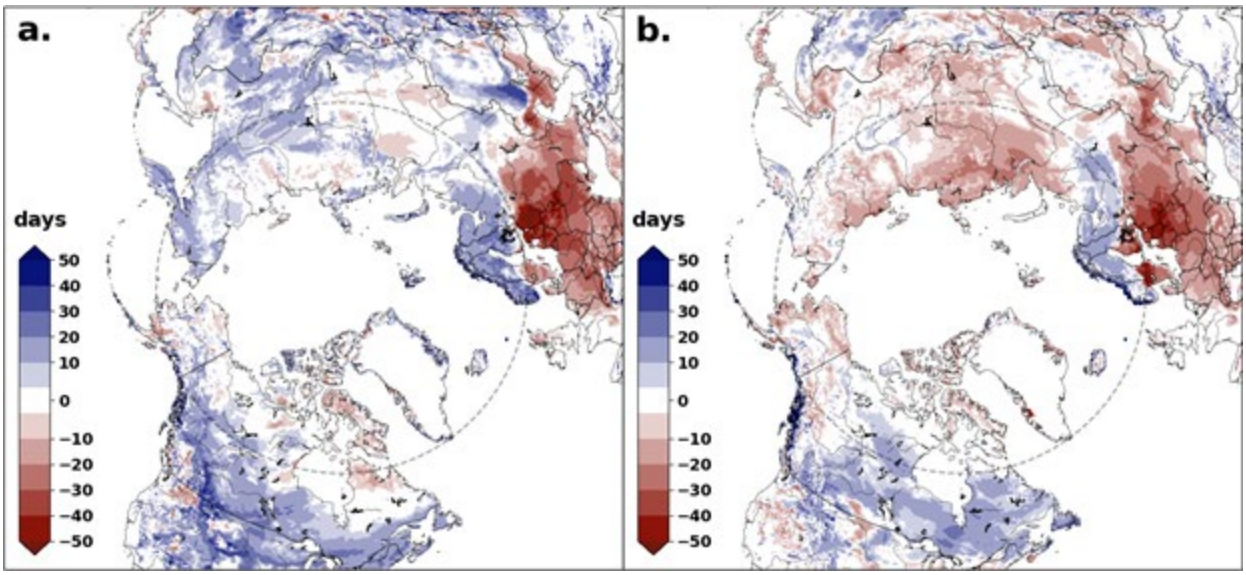

Fig. 2. Snow cover duration (SCD in days) anomalies (difference from 1998-2018 mean; red = shorter SCD than average; blue = longer SCD than average) across the (a) snow onset period (Aug 2019-Jan 2020); and (b) snow melt period (Feb 2020-Jul 2020). The grey circle marks the latitude 60° N; land north of this defines Arctic land areas considered in this study. Source: Helfrich et al. (2007), U.S. National Ice Center (2008).

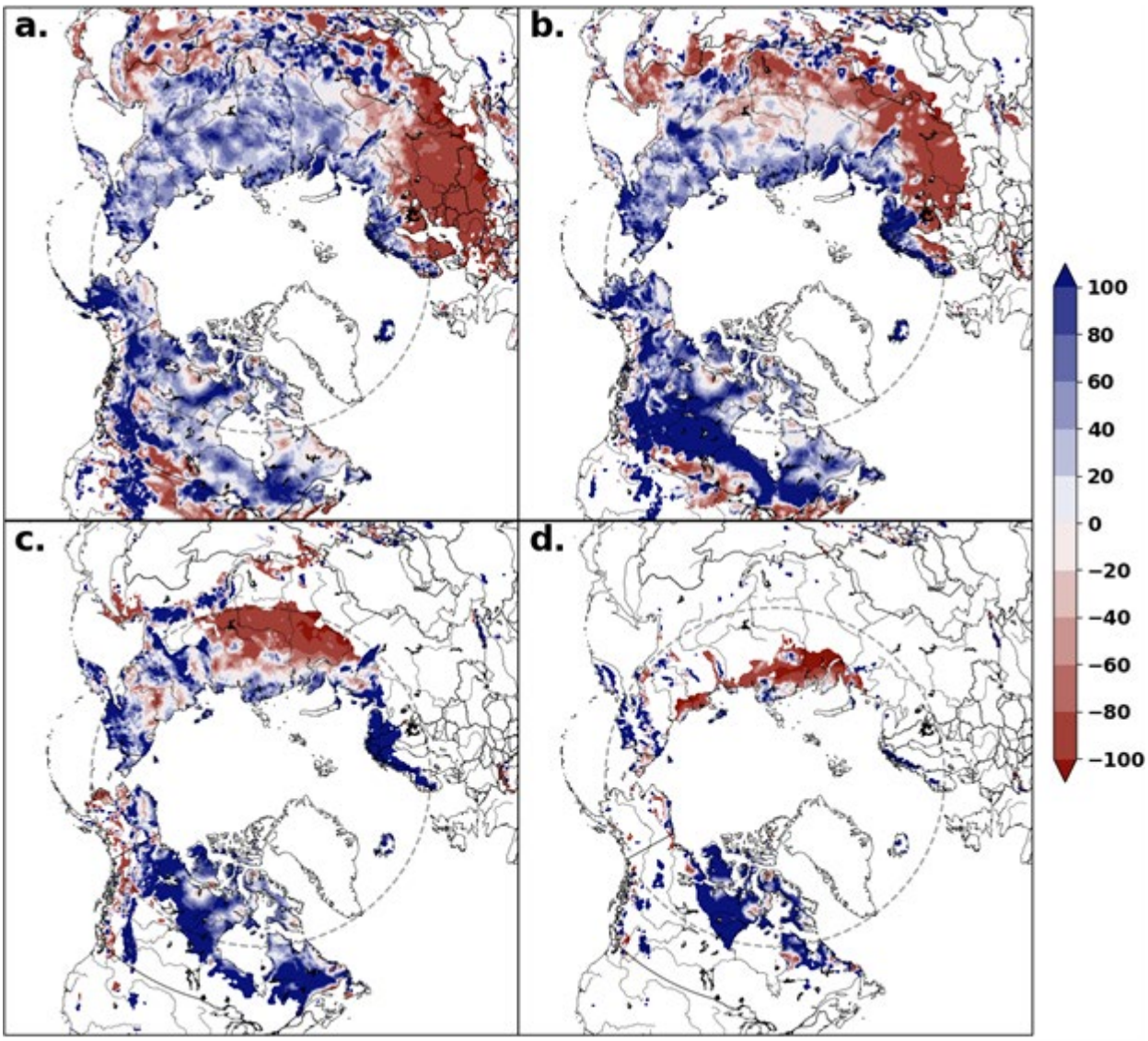

Fig. 3. Snow depth anomalies (% of the 1999-2018 average) in 2020 for (a) March, (b) April, (c) May, and (d) June. The grey circle marks the latitude 60° N. Source: Brasnett (1999), Brown and Brasnett (2010).

Snow depth

Snow depth anomalies (Fig. 3) were derived from the Canadian Meteorological Centre (CMC) daily gridded global snow depth analysis, which combines air temperature and precipitation analyses with the assimilation of surface snow depth observations. This approach is required to obtain hemispheric estimates of snow depth because in situ observations alone are too spatially sparse to be representative. Snow accumulation over the 2019/20 season resulted in above-average March snow depth across the Arctic. In parts of the North American Arctic, deep snow persisted throughout the spring (Apr-Jun). Across central Siberia, changes in monthly snow depth from April to June signified strong melt, which led to the lowest Eurasian Arctic June snow extent in the full observational record, despite the anomalously deep March snowpack.

Snow water equivalent

Four products were utilized to generate a multi-dataset SWE anomaly time series (1981-2020) for April (Fig. 4): (1) The Modern-Era Retrospective Analysis for Research and Applications version 2 (MERRA-2); (2) a simple temperature index model driven by ERA-interim meteorology described in Brown et al. (2003); (3) the physical snowpack model, Crocus, also driven by ERA-Interim meteorology (Note: Crocus data were not included for 2019 or 2020 due to data availability); and (4) the European Space Agency GlobSnow product derived through a combination of satellite passive microwave data and climate station observations. The use of multiple SWE products allows for the determination of inter-product spread through the time series. SWE estimates for April 2020 indicate above-normal snow accumulation over both the Eurasian and North American Arctic, consistent with deeper-than-normal April snow depths shown in Fig. 3b.

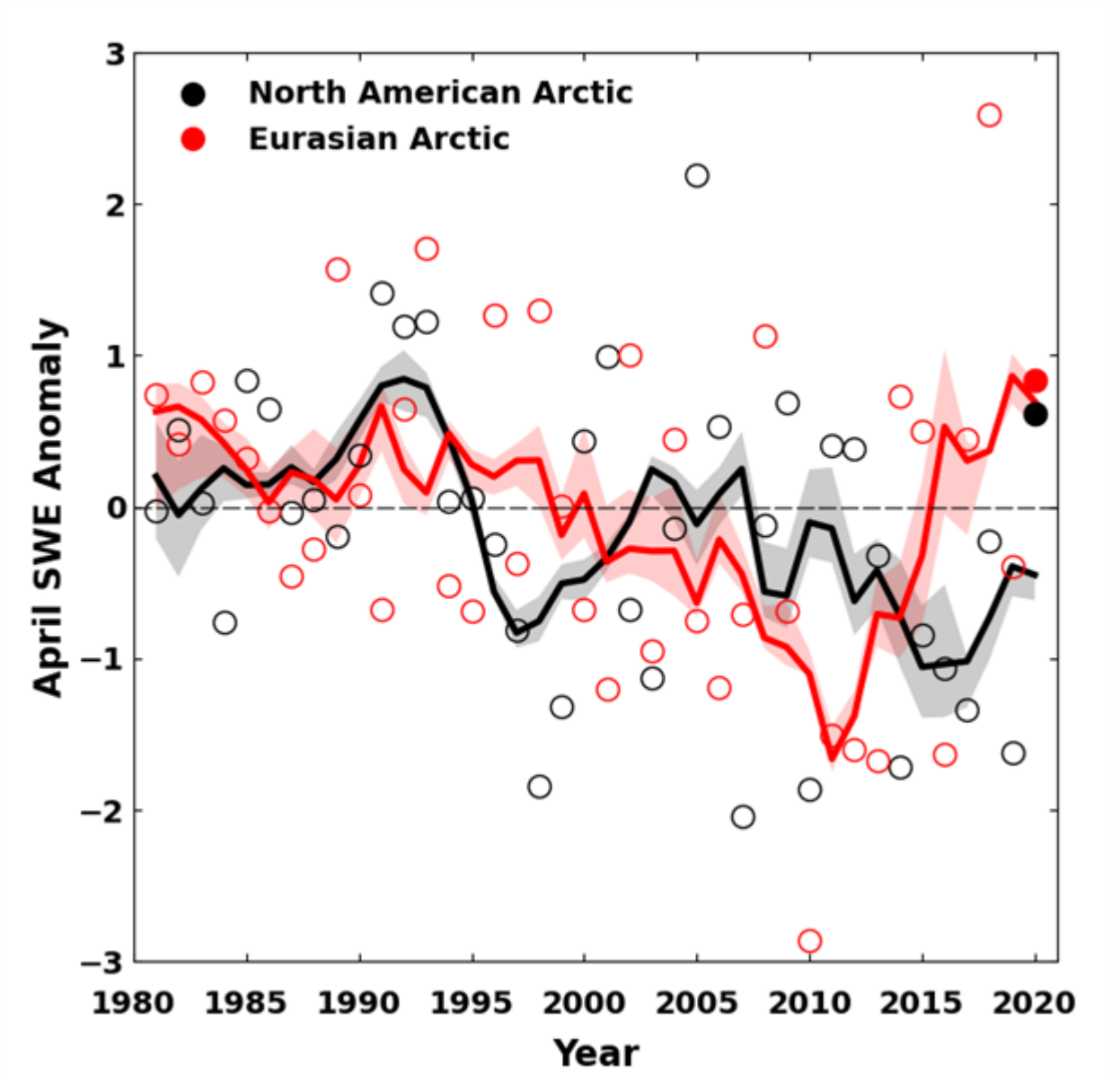

Fig. 4. Mean April SWE anomalies for Arctic land areas calculated for North American (black) and Eurasian (red) sectors of the Arctic. Anomalies are relative to the average for 1981-2010 and standardized (each observation

differenced from the mean and divided by the standard deviation, and thus unitless). Filled circles are used to highlight 2020 anomalies. Solid black and red lines depict 5-year running means for North America and Eurasia, respectively, and the spread among the running means for individual datasets is shown in shading. Sources: MERRA2: Gelaro et al. (2017) and GMAO (2015); temperature index model: Brown et al. (2003); Crocus: Brun et al. (2013); GlobSnow: Takala et al. (2011), www.globsnow.info/.

Summary and long-term trends

In summary, snow accumulation during the 2019/20 winter was above normal across the entire Arctic. Nonetheless, extreme springtime temperatures over central Siberia were high enough to result in the lowest Eurasian June SCE documented across the 54-year satellite record. Anomalies of SCE over North America were more moderate, though still negative, due to a combination of regions with deeper, more persistent snow and regions that experienced early melt.

Long-term trends for total Arctic SCE, derived from the data presented in Fig. 1, are negative: -3.7 ± 2.0% decade^{-1}, and -15.5 ± 6.1% decade^{-1} for May and June, respectively (1981-2020). These trends are on the higher end of estimates from a range of sources, as discussed in Mudryk et al. (2017, 2020). The April trend in Arctic SWE over the 1981-2020 period, calculated from the data presented separately for each continent in Fig. 4, is -2.6 ± 1.8% decade^{-1}, representing a decrease of more than 10% over the entire Arctic since 1981.

References

Brasnett, B., 1999: A global analysis of snow depth for numerical weather prediction. *J. Appl. Meteor.*, **38**, 726-740.

Brown, R., B. Brasnett, and D. Robinson, 2003: Gridded North American monthly snow depth and snow water equivalent for GCM evaluation. *Atmos.-Ocean.*, **41**, 1-14.

Brown, R. D., and B. Brasnett, 2010: Canadian Meteorological Centre (CMC) Daily Snow Depth Analysis Data, Version 1. Boulder, Colorado USA. NASA National Snow and Ice Data Center Distributed Active Archive Center. https://doi.org/10.5067/W9FOYWH0EQZ3, (last access: 27 July 2020).

Brown, R., D. Vikhamar Schuler, O. Bulygina, C. Derksen, K. Luojus, L. Mudryk, L. Wang, and D. Yang, 2017: Arctic terrestrial snow cover. *Snow, Water, Ice and Permafrost in the Arctic (SWIPA) 2017*, Arctic Monitoring and Assessment Programme (AMAP), Oslo, Norway, 25-64.

Brun, E., V. Vionnet, A. Boone, B. Decharme, Y. Peings, R. Valette, F. Karbou, and S. Morin, 2013: Simulation of Northern Eurasian local snow depth, mass, and density using a detailed snowpack model and meteorological reanalyses. *J. Hydrometeor.*, **14**, 203-219, https://doi.org/10.1175/JHM-D-12-012.1.

Callaghan, T., and Coauthors, 2011: The changing face of Arctic snow cover: A synthesis of observed and projected changes. *Ambio*, **40**, 17-31, https://doi.org/10.1007/s13280-011-0212-y.

Estilow, T. W., A. H. Young, and D. A. Robinson, 2015: A long-term Northern Hemisphere snow cover extent data record for climate studies and monitoring. *Earth Sys. Sci. Data*, **7**(1), 137-142, https://doi.org/10.5194/essd-7-137-2015.

Gelaro, R., and Coauthors, 2017: The Modern-Era Retrospective Analysis for Research and Applications, Version 2 (MERRA-2). *J. Climate*, **30**, 5419-5454, https://doi.org/10.1175/JCLI-D-16-0758.1.

GMAO (Global Modeling and Assimilation Office), 2015: MERRA-2tavg1_2d_lnd_Nx:2d, 1-Hourly, Time-Averaged, Single-Level, Assimilation, Land Surface Diagnostics V5.12.4, Greenbelt, MD, USA, Goddard Earth Sciences Data and Information Services Center (GESDISC), https://doi.org/10.5067/RKPHT8KC1Y1T, (last access: 26 August 2020).

Helfrich, S., D. McNamara, B. Ramsay, T. Baldwin, and T. Kasheta, 2007: Enhancements to, and forthcoming developments in the Interactive Multisensor Snow and Ice Mapping System (IMS). *Hydrol. Process.*, **21**, 1576-1586.

Mudryk, L. R., P. J. Kushner, C. Derksen, and C. Thackeray, 2017: Snow cover response to temperature in observational and climate model ensembles. *Geophys. Res. Lett.*, **44**, 919-926, https://doi.org/10.1002/2016GL071789.

Mudryk, L., M. Santolaria-Otín, G. Krinner, M. Ménégoz, C. Derksen, C. Brutel-Vuilmet, M. Brady, and R. Essery, 2020: Historical Northern Hemisphere snow cover trends and projected changes in the CMIP6 multi-model ensemble. *Cryosphere*, **14**, 2495-2514, https://doi.org/10.5194/tc-14-2495-2020.

Robinson, D. A., T. W. Estilow, and NOAA CDR Program, 2012: NOAA Climate Data Record (CDR) of Northern Hemisphere (NH) Snow Cover Extent (SCE), Version 1 [r01]. NOAA National Centers for Environmental Information, https://doi.org/10.7289/V5N014G9, (last access: 27 July 2020).

Takala, M., K. Luojus, J. Pulliainen, C. Derksen, J. Lemmetyinen, J. –P. Kärnä, and J. Koskinen, 2011: Estimating Northern Hemisphere snow water equivalent for climate research through assimilation of space-borne radiometer data and ground-based measurements. *Remote Sens. Environ.*, **115**, 3517-3529, https://doi.org/10.1016/j.rse.2011.08.014.

U.S. National Ice Center, 2008: IMS Daily Northern Hemisphere Snow and Ice Analysis at 1 km, 4 km, and 24 km Resolutions, Version 1. Boulder, Colorado USA. NSIDC: National Snow and Ice Data Center, https://doi.org/10.7265/N52R3PMC, (last access: 27 July 2020).

November 9, 2020

Greenland Ice Sheet

DOI: 10.25923/ms78-g612

T. A. Moon[1,2], M. Tedesco[3,4], J. E. Box[5], J. Cappelen[6], R. S. Fausto[5], X. Fettweis[7], N. J. Korsgaard[5], B. Loomis[8], K. D. Mankoff[5], T. Mote[9], C. H. Reijmer[10], C. J. P. P. Smeets[11], D. van As[5], and R. S. W. van de Wal[10,11]

[1]Cooperative Institute for Research in Environmental Sciences, University of Colorado Boulder, Boulder, CO, USA
[2]National Snow and Ice Data Center, Boulder, CO, USA
[3]Lamont Doherty Earth Observatory of Columbia University, Palisades, NY, USA
[4]Goddard Institute of Space Studies, NASA, New York, NY, USA
[5]Geological Survey of Denmark and Greenland, Copenhagen, Denmark
[6]Danish Meteorological Institute, Copenhagen, Denmark
[7]University of Liege, Liege, Belgium
[8]Goddard Space Flight Center, NASA, Greenbelt, MD, USA
[9]Department of Geography, University of Georgia, Athens, GA, USA
[10]Institute for Marine and Atmospheric Research Utrecht, Utrecht University, Utrecht, The Netherlands
[11]Department of Physical Geography, Utrecht University, Utrecht, The Netherlands

Highlights

- During September 2019-August 2020 the Greenland ice sheet experienced ice loss that was higher than the 1981-2010 average but substantially lower than the record 2018/19 losses.
- Abnormal cyclonic atmospheric circulation centered over Greenland promoted normal or colder-than-average conditions for the interior and east, with higher air temperatures in the north, southwest, and many coastal regions.
- Albedo during summer 2020 was above average at the ice-sheet-wide scale, with below average albedo in the north and south but above average in the central and interior regions, mostly aligning with temperature anomalies.

Introduction

The Greenland ice sheet sits atop the world's largest island and holds the equivalent of 7.4 m of potential sea level rise (Morlighem et al. 2017). Following a period of relative stability from the 1970s to early 1990s, the ice sheet began losing ice at an accelerating rate and has now experienced annual net ice loss every year since 1998 (Mouginot et al. 2019). The largest annual mass losses since regular monitoring began in the 1950s occurred in 2012 and 2019, with losses of -464 ± 62 Gt and -532 ± 58 Gt, respectively (Sasgen et al. 2020; estimates including all Greenland glaciers and peripheral ice caps and excluding Ellesmere Island). The record ice loss in 2019 is equivalent to ~1.5 mm global sea level rise. Total ice loss in 2020 (-293 ± 66 Gt) is substantially less than these record years, in part due to cooler summer surface air temperatures and relatively bright surface conditions in the central regions. Overall, the number of melt days was slightly above average but with large regional variation.

To capture the annual cycle of accumulation (ice gain) and ablation (ice loss), Greenland measurements are commonly synthesized from September through August. Hence, the seasons in this essay are delineated as autumn (September through November, SON), winter (December through February, DJF), spring (March through May, MAM), and summer (June through August, JJA).

Atmospheric conditions and surface air temperature

Atmospheric circulation anomalies over Greenland during summer 2020 created strong regional differences in surface air temperatures. Abnormal cyclonic circulation promoted near-to-below-average air temperatures in the interior and east. Warmer-than-average conditions, however, impacted the southern, northern, and most coastal regions (see Fig. 2 in essay *Surface Air Temperature*). The summer 2020 circulation anomaly pattern was the opposite to that of 2019, helping to facilitate more moderate Greenland ice loss.

The high regional variability was evident at in situ measurement sites. Measurements at 20 Danish Meteorological Institute (DMI) weather stations reported near-to-above-average temperatures compared to the 1981-2010 mean, with the exception of winter 2019-2020, when temperatures were near to below average at almost all DMI stations. Measurements at 8 weather station transects of the Programme for Monitoring of the Greenland Ice Sheet (PROMICE) indicate average summer (JJA) temperatures at the ice sheet margin relative to the 1981-2010 period, except at stations KPC_L (+0.6 ± 0.3°C anomaly), SCO_L (+0.6 ± 0.4°C), KAN_L (+0.5 ± 0.4°C), and THU_L (+1.2 ± 0.4°C) (Fausto and van As 2019; transect locations in Fig. 3). In the ice sheet interior, Summit Station observations show near to slightly above normal temperatures for autumn 2019, spring 2020, and summer 2020, while winter 2019/20 was significantly colder than average.

Albedo

Ice sheet albedo is also important for influencing surface melt. Albedo, which is the fraction of surface sunlight reflected, is dependent on ice sheet surface conditions. A high albedo means more sunlight is reflected (bright), while a low albedo leads to greater sunlight absorption (dark). During the summer season, absorbed sunlight is the dominant energy source for snow and ice melt in the Greenland ablation area (the peripheral region across which all winter snow is melted away during the following summer) (van den Broeke et al. 2011). Estimated via the MODIS satellite (Moderate Resolution Imaging Spectroradiometer; after Box et al. 2017), the 2020 summer ice-sheet-wide albedo (80.8%) was near the 2000-2020 average (79.1%) (Fig. 1b), with dark anomalies in the south and north and bright anomalies across the mid-section (Fig. 1a).

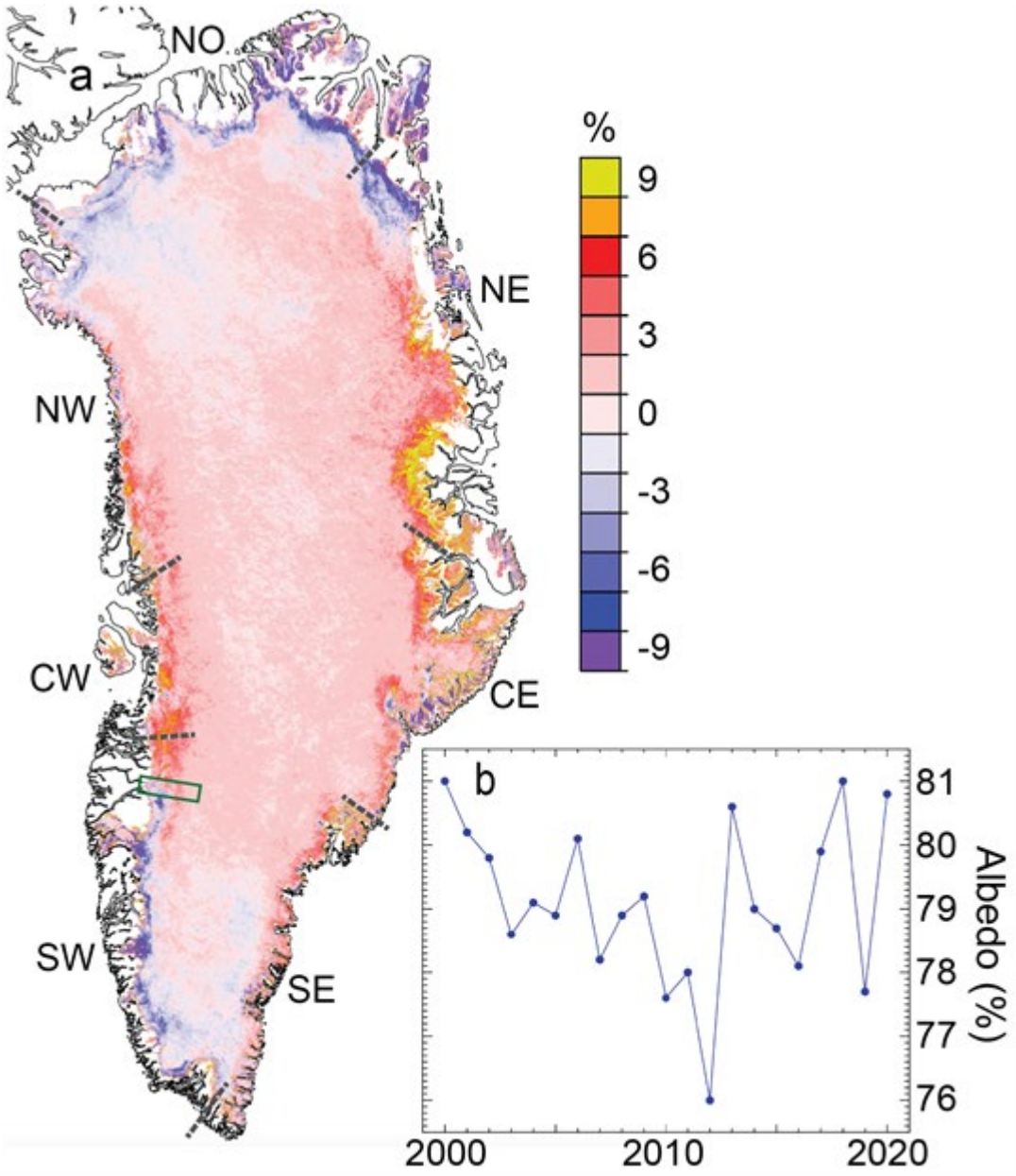

Fig. 1. (a) Albedo anomaly map for summer (JJA) 2020, relative to a 2000-2009 reference period. Region boundaries are marked for the north (NO), northeast (NE), central east (CE), southeast (SE), southwest (SW), central west (CW), and northwest (NW), with a green box indicating the K-transect zone. (b) Time series for summer albedo of Greenland snow and ice.

Surface melting

Daily satellite observations from the Special Sensor Microwave Imager/Sounder (SSMIS) passive microwave radiometer allow estimates of surface melt spatial extent and duration (e.g., Mote 2007; Tedesco et al. 2013). Estimates of the daily melt extent across the Greenland ice sheet exceeded the 1981-2010 median (i.e., conditions were warmer) on more than half of the days during summer 2020 (Fig. 2a). The maximum daily extent reached 33.8% of the ice sheet surface on 10 July, lower than the

average maximum extent (1981-2010) of 39.8% (Fig. 2a), though the cumulative melt-day extent for 2020 was 29.2% higher (18.6 million km^2) than the 1981-2010 average (14.4 million km^2).

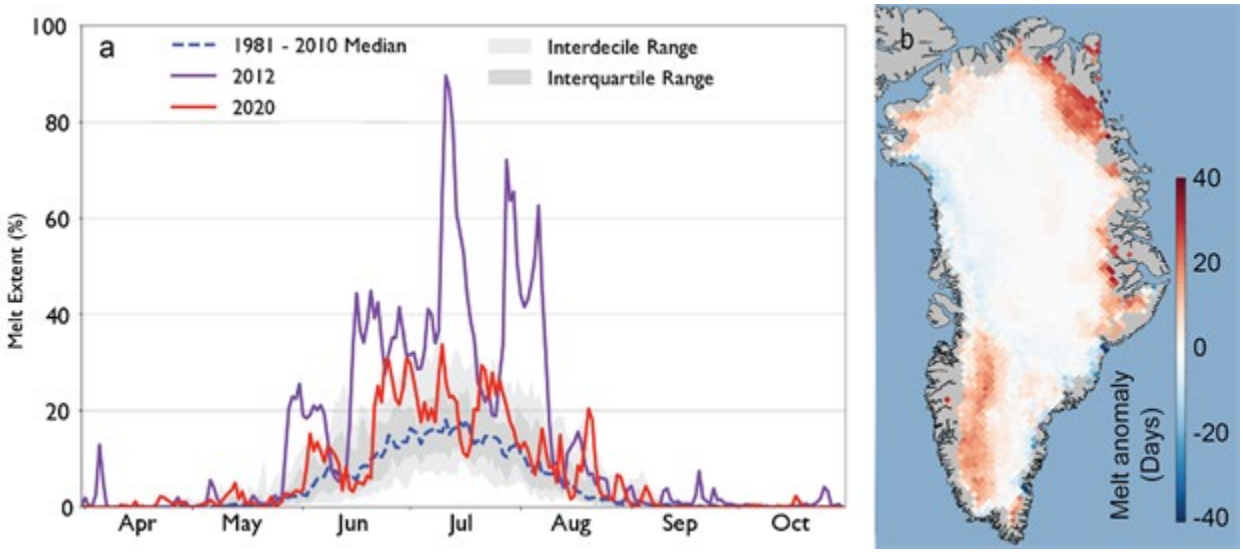

Fig. 2. (a) SSMIS-derived surface melt area as a percentage of the ice sheet area during 2020 (solid red) and 2012 (solid purple). (b) Summer 2020 melt anomaly (in number of melting days) with respect to the 1981-2010 period and estimated from spaceborne passive microwave observations.

Compared to previous summers, melt duration exceeded the mean for most of the southwest and northeast ablation zone. The northeastern periphery of the ice sheet had more than 30 additional days with melt compared to the mean (Fig. 2b). However, in much of the accumulation zone and the west central periphery of the ice sheet, melt duration was below the 1981-2010 mean (Fig. 2b). This region broadly corresponds to a region of positive albedo anomalies (Fig. 1b) and the patterns are also consistent with surface air temperature anomalies (see essay *Surface Air Temperature*). Discrepancies between the melt duration and ablation anomalies, which can result from summer snowfall, occurred in the east central periphery of the ice sheet.

Surface mass balance

Along with meteorology, the PROMICE weather stations record surface mass balance including ice ablation along the ice sheet perimeter. Referencing values to the 1981-2010 mean following van As et al. (2016), 2020 ablation anomalies at 5 out of 8 sites along the ice sheet margin were near average, within uncertainty. At stations KPC_L (northeast), KAN_L (southwest), and THU_L (northwest) ablation was above average with positive anomaly values of 33 ± 29%, 22 ± 20%, and 66 ± 49%, respectively (Fig. 3). For the 30-year measurement record (1990-2020) available from the K-transect (67° N) in the southwestern ablation zone (region indicated in Fig. 1a), summer 2020 ablation was close to the measurement period mean.

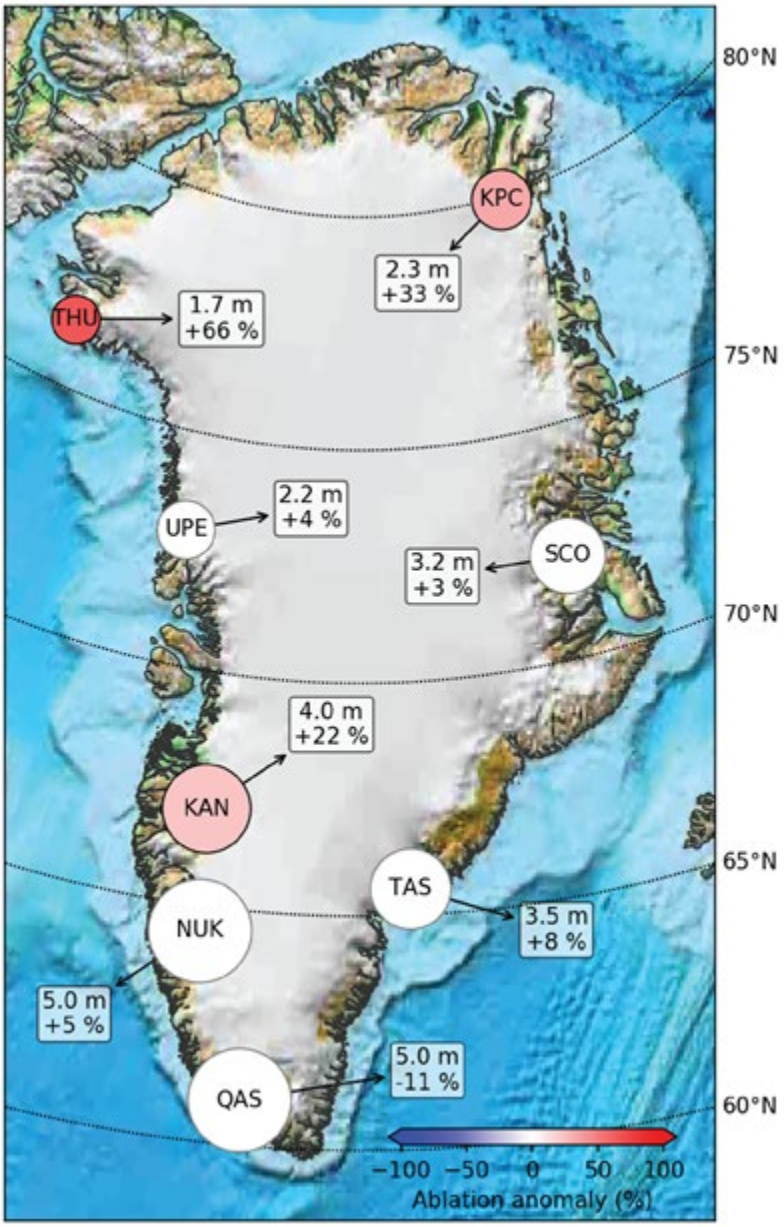

Fig. 3. Net ablation in 2020 measured by PROMICE weather stations along the Greenland ice sheet margin, referenced to the 1981-2010 standard period following van As et al. (2016). Circle size is scaled to the ablation in m of ice equivalent, and color its anomaly value. White circles with gray outlines indicate anomaly values not exceeding methodological and measurement uncertainty.

Ice discharge and glaciers

Along with surface ice melt, the Greenland ice sheet loses mass via calving of icebergs from glaciers in contact with the ocean (solid ice discharge). PROMICE combines ice thickness estimates with ice velocity measurements based on Sentinel-1 satellite data to create a high temporal resolution solid ice discharge product integrated over Greenland (following Mankoff et al. 2020). For 1981-2010, the average total discharge was ~460 ± 46 Gt yr^{-1}, while average discharge during 2010-2019 was ~487 ± 49 Gt yr^{-1}. As of 21 October 2020, solid ice discharge for 2020 reached an average of 506 ± 50 Gt yr^{-1}, with the largest

contributions from the southeast, following by the northwest (see Fig. 1a for regions). Discharge from the central east is slightly greater than from the central west, with the smallest contributions from the northeast, north, and southwest.

If solid ice discharge is more rapid than replacement of glacier ice from ice flow, the glacier front or ice edge will retreat and glacier area is lost. The 2019/20 end-of-melt-season area changes for 47 Greenland tidewater glacier fronts (selected to provide regional coverage and include major glaciers) show a net area loss of 55.4 km^2, compared to an average yearly loss of 99.5 km^2 for these glaciers since 1999 (Fig. 4a). Of the 47 glaciers measured during 2019/20 (Fig. 4b), 20 retreated, 12 advanced, and 15 were stable (within ±0.2 km^2), contrasting somewhat with the higher area loss during 2018/19 in which only six glaciers advanced, 29 retreated, and 12 were stable. (Note: Ice loss values are derived following Andersen et al. (2019) using Landsat, Aster, and, since 2015, exclusively Sentinel-2 optical satellite imagery.)

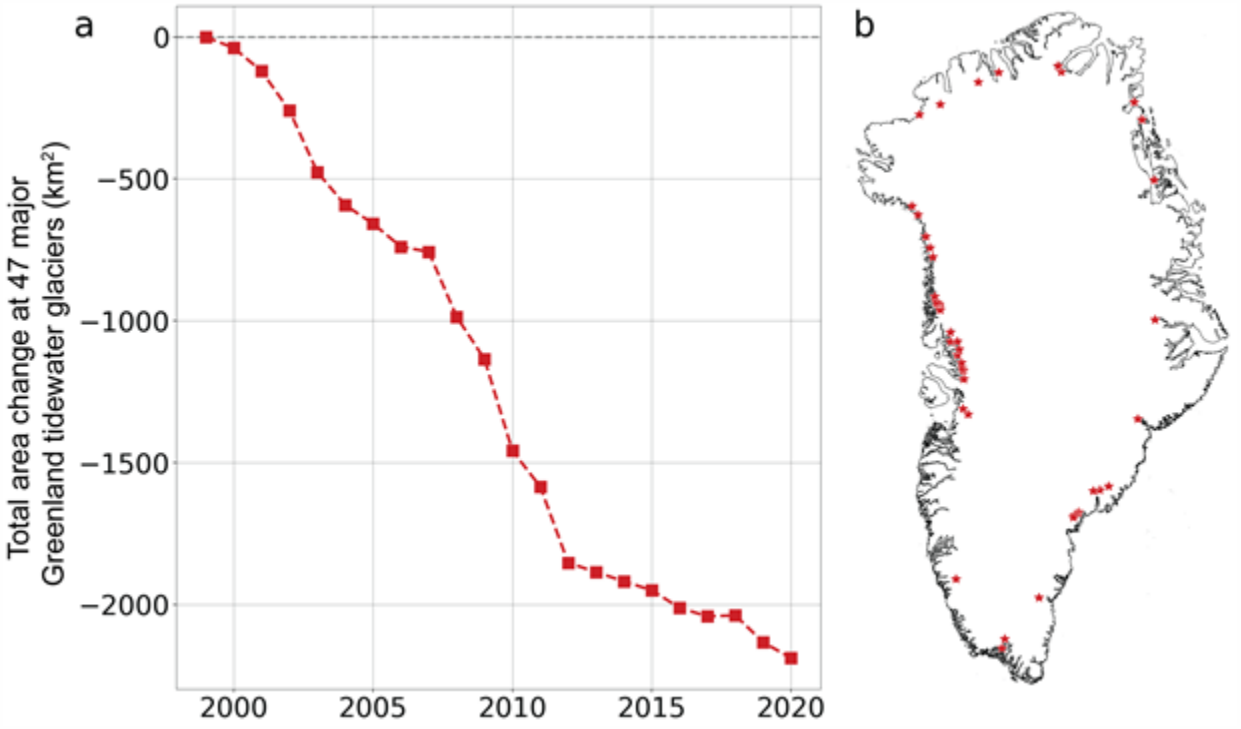

Fig. 4. (a) Total area change at 47 major Greenland tidewater glaciers. Glaciers are sampled from across the ice sheet periphery at the locations shown in (b).

Total mass balance

The total mass change of the ice sheet must be measured to evaluate annual contributions to sea level rise. The GRACE (Gravity Recovery and Climate Experiment, 2002-2017) and GRACE-FO (Follow On, 2018-present) satellite missions have revolutionized the ability to monitor mass changes on the Earth's surface. Over the full span of both missions, the average rate of mass loss for the Greenland ice sheet is 268 ± 14 Gt yr^{-1} (2-σ model fit uncertainties reported) (Fig. 5). Over the 2018/19 season, a new record annual mass loss of 532 ± 58 Gt was observed (Sasgen et al. 2020), marking a dramatic change from the decreased annual mass losses of about 100 Gt yr^{-1} over 2017/18. GRACE-FO data extending through August 2020 show that the September 2019-August 2020 annual mass loss is -293 ± 66 Gt, above the multi-mission average but substantially lower than was observed in 2019 (Fig. 5).

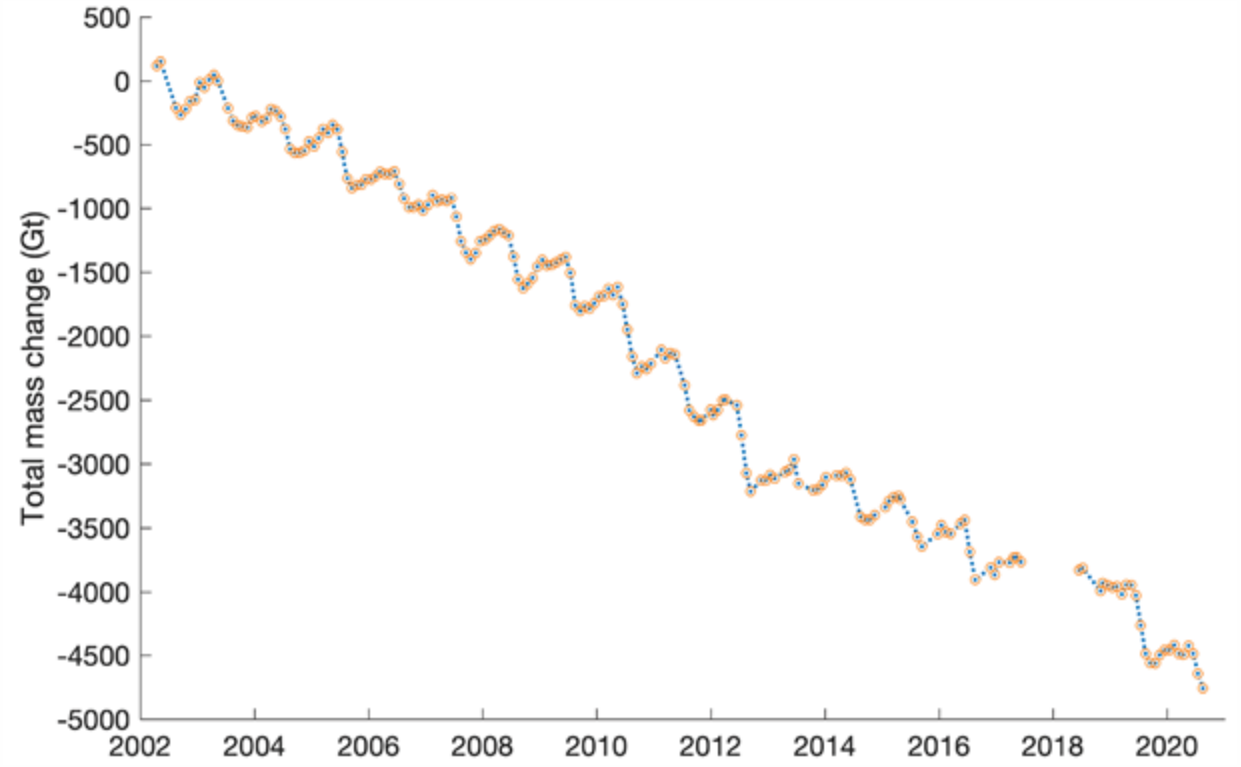

Fig. 5. Total mass change (Gt) of the Greenland ice sheet from April 2002 to August 2020 determined from GRACE (2002-2017) and GRACE–FO (2018-Present). An averaging kernel (Wahr et al. 1998) is applied to the JPL RL06 Level 2 monthly spherical harmonic solutions after the applied corrections: Geocenter (Sun et al. 2016; https://podaac-tools.jpl.nasa.gov/drive/files/allData/grace/docs/TN-13_GEOC_JPL_RL06.txt); C_{20} and C_{30} (Loomis et al. 2019b, 2020; https://podaac-tools.jpl.nasa.gov/drive/files/allData/gracefo/docs/TN-14_C30_C20_GSFC_SLR.txt); and glacial isostatic adjustment (Peltier et al. 2018; ICE-6G_D). The applied averaging kernel has been tuned to match the trends observed by the NASA GSFC mascons (Loomis et al. 2019a), which was designed to mitigate leakage of other nearby mass change signals into the Greenland ice sheet estimates.

Acknowledgments

Financial support for measurements along the K-transect was received from the Dutch Polar Program of NWO. Data from the Programme for Monitoring of the Greenland Ice Sheet (PROMICE) and the Greenland Analogue Project (GAP) were provided by the Geological Survey of Denmark and Greenland (GEUS) at http://www.promice.dk. T. M. was supported by the University of Colorado Boulder Cooperative Institute for Research in Environmental Sciences. M. T. was supported by National Science Foundation ANS #1713072, National Science Foundation PLR-1603331, NASA MAP #80NSSC17K0351, NASA #NNX17AH04G, and the Heising-Simons foundation.

References

Andersen, J. K., and Coauthors, 2019: Update of annual calving front lines for 47 marine terminating outlet glaciers in Greenland (1999-2018). *Geol. Surv. Den. Greenl.*, **43**, e2019430202, https://doi.org/10.34194/GEUSB-201943-02-02.

Box, J. E., D. van As, and K. Steffen, 2017: Greenland, Canadian and Icelandic land ice albedo grids (2000-2016). *Geol. Surv. Den. Greenl.*, **38**, 53-56.

Fausto, R. S., and D. van As, 2019: Programme for monitoring of the Greenland ice sheet (PROMICE): Automatic weather station data, version: v03, Geological Survey of Denmark and Greenland, https://doi.org/10.22008/promice/data/aws (last access: 14 September 2020).

Loomis, B. D., S. B. Luthcke, and T. J. Sabaka, 2019a: Regularization and error characterization of GRACE mascons. *J. Geodesy*, **93**, 1381–1398, https://doi.org/10.1007/s00190-019-01252-y.

Loomis, B. D., K. E. Rachlin, and S. B. Luthcke, 2019b: Improved Earth oblateness rate reveals increased ice sheet losses and mass-driven sea level rise. *Geophys. Res. Lett.*, **46**, 6910-6917, https://doi.org/10.1029/2019GL082929.

Loomis, B. D., K. E. Rachlin, D. N. Wiese, F. W. Landerer, and S. B. Luthcke, 2020: Replacing GRACE/GRACE-FO C30 with satellite laser ranging: Impacts on Antarctic Ice Sheet mass change. *Geophys. Res. Lett.*, **47**(3), e2019GL085488, https://doi.org/10.1029/2019gl085488.

Mankoff, K. D., A. Solgaard, W. Colgan, A. P. Ahlstrøm, S. A. Khan, and R. S. Fausto, 2020: Greenland Ice Sheet solid ice discharge from 1986 through March 2020. *Earth Syst. Sci. Data*, 12, 1367–1383, https://doi.org/10.5194/essd-12-1367-2020.

Morlighem, M., and Coauthors, 2017: BedMachine v3: Complete bed topography and ocean bathymetry mapping of Greenland from multibeam echo sounding combined with mass conservation. *Geophys. Res. Lett.*, **44**(21), 11051-11061, https://doi.org/10.1002/2017GL074954.

Mote, T., 2007: Greenland surface melt trends 1973-2007: Evidence of a large increase in 2007. *Geophys. Res. Lett.*, **34**, L22507, https://doi.org/10.1029/2007GL031976.

Mouginot, J., and Coauthors, 2019: Forty-six years of Greenland Ice Sheet mass balance from 1972 to 2018. *Proc. Natl. Acad. Sci. USA*, **116**(19), 9239–9244, https://doi.org/10.1073/pnas.1904242116.

Peltier, W. R., D. F. Argus, and R. Drummond, 2018: Comment on "An Assessment of the ICE-6G_C (VM5a) Glacial Isostatic Adjustment Model" by Purcell et al. *J. Geophys. Res.-Solid Earth*, **123**, 2019-2018, https://doi.org/10.1002/2016JB013844.

Sasgen, I., and Coauthors, 2020: Return to rapid ice loss in Greenland and record loss in 2019 detected by the GRACE-FO satellites. *Commun. Earth. Environ.*, **1**, 8, https://doi.org/10.1038/s43247-020-0010-1.

Sun, Y., R. Riva, and P. Ditmar, 2016: Optimizing estimates of annual variations and trends in geocenter motion and J_2 from a combination of GRACE data and geophysical models. *J. Geophys. Res.-Solid Earth*, **121**, 8352–8370, https://doi.org/10.1002/2016JB013073.

Tedesco, M., X. Fettweis, T. Mote, J. Wahr, P. Alexander, J. Box, and B. Wouters, 2013: Evidence and analysis of 2012 Greenland records from spaceborne observations, a regional climate model and reanalysis data. *Cryosphere*, **7**, 615-630, https://doi.org/10.5194/tc-7-615-2013.

van As, D., R. S. Fausto, J. Cappelen, R. S. van de Wa, R. J. Braithwaite, H. Machguth, and PROMICE project team, 2016: Placing Greenland ice sheet ablation measurements in a multi-decadal context. *GEUS Bull.*, **35**, 71-74, https://doi.org/10.34194/geusb.v35.4942.

van den Broeke, M. R., C. J. P. P. Smeets, and R. S. W. van de Wal, 2011: The seasonal cycle and interannual variability of surface energy balance and melt in the ablation zone of the west Greenland ice sheet. *Cryosphere*, **5**, 377-390, https://doi.org/10.5194/tc-5-377-2011.

Wahr, J., M. Molenaar, and F. Bryan, 1998: Time variability of the Earth's gravity field: Hydrological and oceanic effects and their possible detection using GRACE. *J. Geophys. Res.-Solid Earth*, **103**(B12), 30205-30229, https://doi.org/10.1029/98JB02844.

November 9, 2020

Sea Ice

DOI: 10.25923/n170-9h57

D. Perovich[1], W. Meier[2,3], M. Tschudi[4], S. Hendricks[5], A. A. Petty[6], D. Divine[7], S. Farrell[8], S. Gerland[7], C. Haas[5], L. Kaleschke[5], O. Pavlova[7], R. Ricker[5], X. Tian-Kunze[5], M. Webster[9], and K. Wood[10,11]

[1]Thayer School of Engineering, Dartmouth College, Hanover, NH, USA
[2]Cooperative Institute for Research in Environmental Sciences, University of Colorado Boulder, Boulder, CO, USA
[3]National Snow and Ice Data Center, Boulder, CO, USA
[4]Aerospace Engineering Sciences, University of Colorado, Boulder, CO, USA
[5]Alfred Wegener Institute, Helmholtz Centre for Polar and Marine Research, Bremerhaven, Germany
[6]Goddard Space Flight Center, NASA, Greenbelt, MD, USA
[7]Norwegian Polar Institute, Fram Centre, Tromsø, Norway
[8]NOAA Earth System Science Interdisciplinary Center, University of Maryland, College Park, MD, USA
[9]Geophysical Institute, University of Alaska Fairbanks, Fairbanks, AK, USA
[10]Cooperative Institute for Climate, Ocean, and Ecosystem Studies, University of Washington, Seattle, WA, USA
[11]Pacific Marine Environmental Laboratory, NOAA, Seattle, WA, USA

Highlights

- The Arctic sea ice cover continues declining trends in the summer minimum and winter maximum extents. In 2020, end of winter extent was the 11th lowest and the end of summer extent was the 2nd lowest in the satellite record (1979-2020).
- Maximum Northern Hemisphere sea ice volume in April 2020 was 18,785 km^3, approximately 1,000 km^3 below the 2010-2019 average. October 2020 sea ice volume showed the lowest value (4.627 km^3) in the past 10 years because of the second largest summer loss of 15.215 km^3.
- Sea ice melt onset and opening was very early in the Siberian coastal region, related to very warm spring and early summer air temperatures and offshore winds.

Introduction

Arctic sea ice is an important part of the climate system. Its higher albedo reflects much of the incoming solar radiation during the summer, keeping the region cooler than an ice-free environment. The sea ice cover acts as a physical barrier between the ocean and the atmosphere, limiting energy and moisture exchange. Ice formation and melt substantially modify the biogeochemical balance of the upper ocean. Sea ice also acts as a platform for charismatic megafauna and other components of the ecosystem. Finally, it is both a facilitator and hazard to human activities in the Arctic. In 2020, the Arctic sea ice cover continued the declining trends in extent, thickness, and volume.

For sea ice, 2020 was marked by very warm spring conditions (see essay *Surface Air Temperature*), leading to early ice loss, particularly in the East Siberian and Laptev Sea regions. During June, Laptev Sea

ice extent dropped to record-low levels for that time of year, which led to particularly warm sea surface temperatures later in the summer (see essay *Sea Surface Temperature)*. Ocean warmth also led to a slow freeze-up in autumn 2019, which led to warm autumn air temperatures (see essay *Surface Air Temperature*) and may have helped pre-condition sea ice in the region for the early melt in spring 2020. In contrast to recent years, early season ice loss in the Beaufort and Chukchi Seas was near the 1981 to 2010 climatological average; however, those seas experienced rapid late loss and ended the summer far below average. This late-summer loss in the Pacific sector drove a faster-than-normal late-August and early September ice loss and had implications for primary productivity (see essay *Ocean Primary Productivity*). The large-scale conditions described here complement and provide context for the in situ observations from the MOSAiC expedition during October 2019 to October 2020 (see essay *MOSAiC*).

Sea ice extent

Sea ice extent is a common metric of Arctic sea ice conditions because of its long and consistent record from satellite-borne passive microwave sensors, now covering 42 years. The substantial decline in extent since 1979 is one of the most iconic indicators of climate change. In September 2020, the average monthly extent was 3.92 million km^2 (Fig. 1), the second lowest monthly extent in the 42-year satellite record. The linear trend of the monthly average extent for 1979 to 2020 is -82,700 km^2 per year or -13.1% per decade relative to the 1981-2010 average (Fig. 2). On 15 September 2020, the annual minimum Arctic sea ice extent of 3.74 million km^2 was reached (Fig. 2). This was the second lowest extent in the satellite record and only the second minimum extent below 4 million km^2.

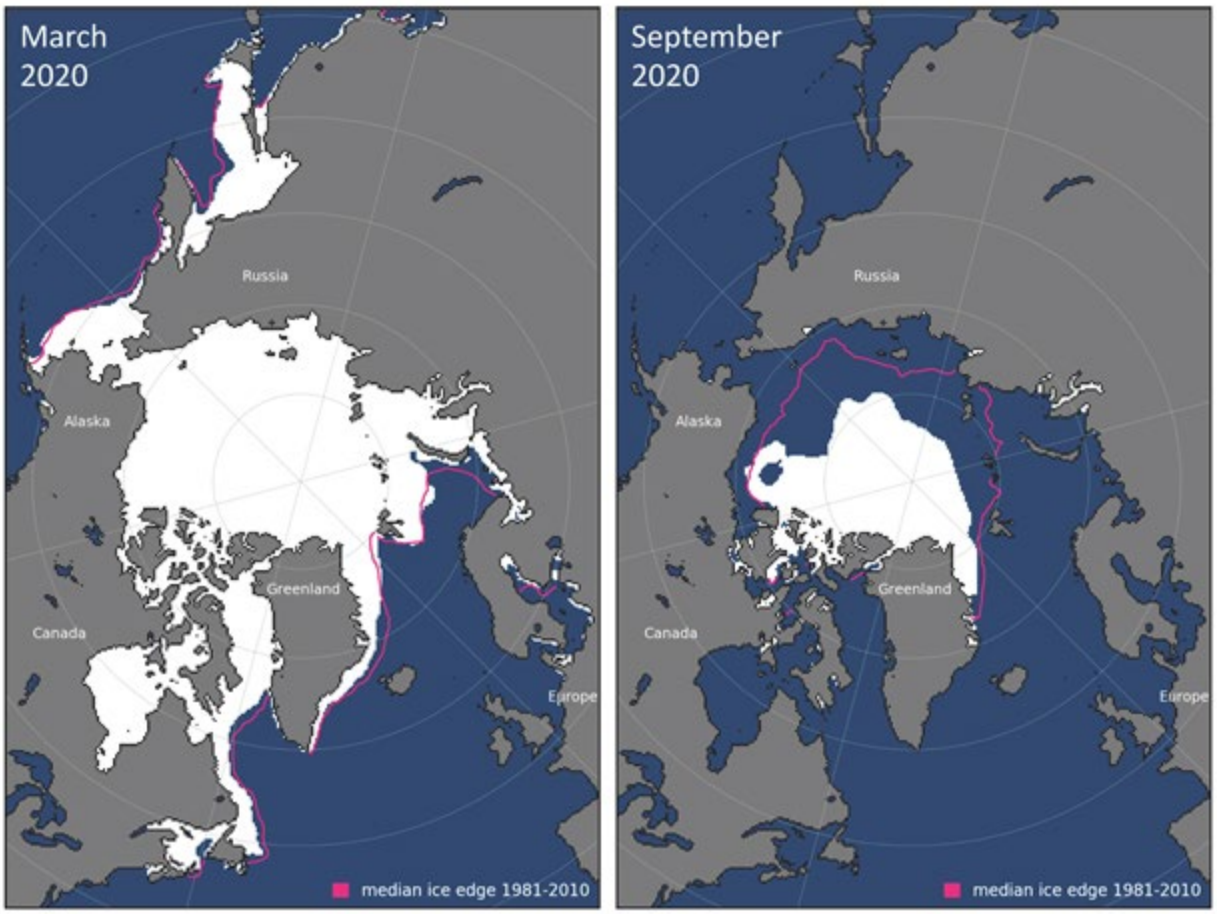

Fig. 1. Monthly average sea ice extent map for (left) March 2020 and (right) September 2020.

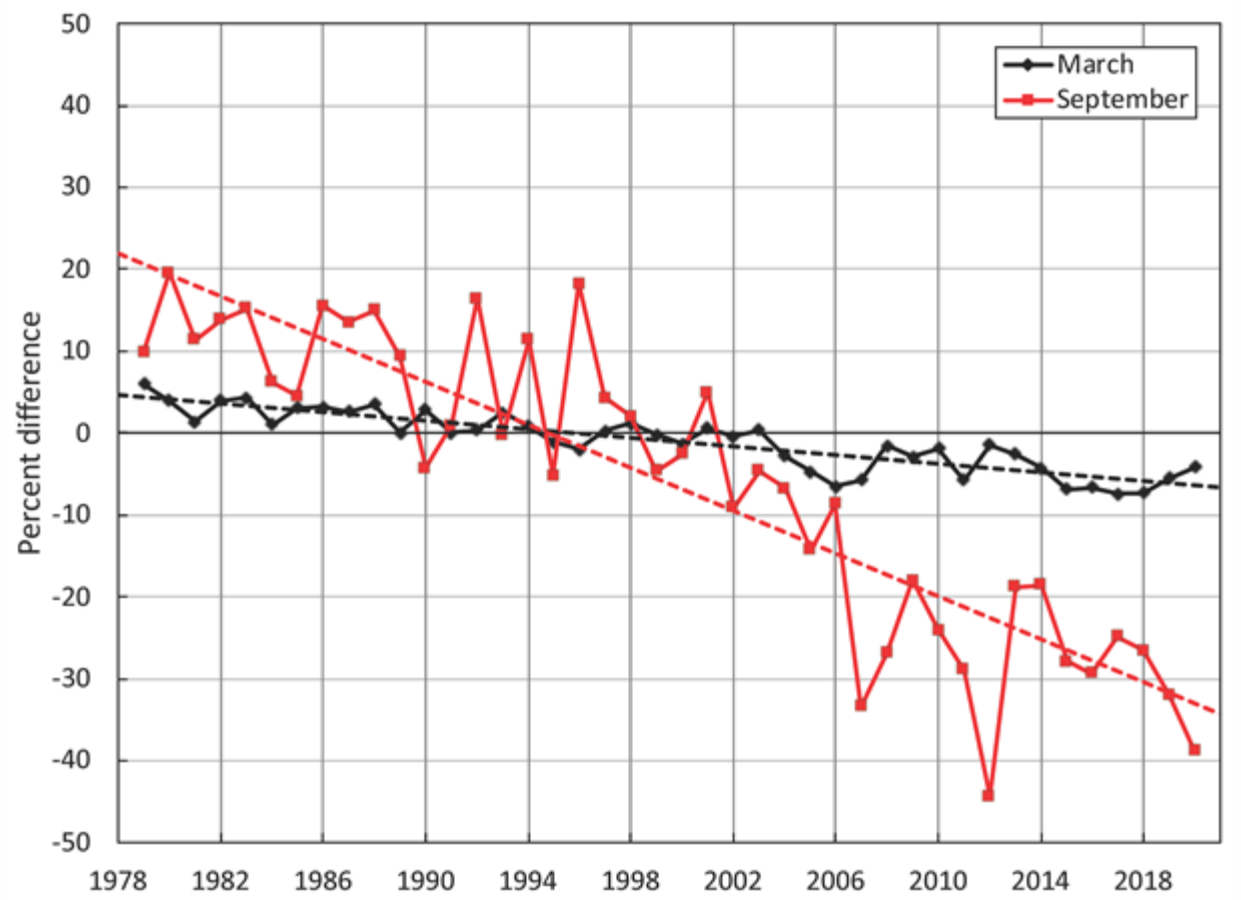

Fig. 2. Monthly sea ice extent (solid lines) and linear trend lines (dashed lines) for March (black) and September (red) 1979 to 2020.

March is the typical month of the maximum annual extent; March 2020 extent was 14.79 million km^2 (Fig. 1) and the month has experienced a significant decline of -40,400 km^2 (-2.6% per decade) (Fig. 2). On 5 March 2020, the annual maximum sea ice extent was reached, 15.05 million km^2, the 11th lowest in the satellite record and the highest since 2013.

The values presented here are from the NSIDC Sea Ice Index (Fetterer et al. 2017), based on passive microwave-derived sea ice concentrations from the NASA Team algorithm (Cavalieri et al. 1996; Maslanik and Stroeve 1999). There are several other passive microwave-derived products (e.g., Ivanova et al. 2014), including the EUMETSAT OSI-SAF CCI climate data record (Lavergne et al. 2019). All products have some limitations and uncertainties (e.g., Kern et al. 2019), but overall the trends agree well (Comiso et al. 2017).

The last 14 years (2007-2020) of the satellite record are the lowest 14 extents in the 42-year satellite record. Fourteen years represents one third of the record, with three such periods in the record. Each of the three 14-year periods show distinct characteristics. The first period, 1979-1992, was marked by a fairly slow decline of -6.9% per decade (relative to the 1981-2010 average climatology). The rate of extent loss accelerated during the second 14-year period, 1993-2006, nearly doubling to -13.3% per decade. The most recent 14-year period has seen the extent loss slow to -4.0% per decade. This number, however, reflects a changed Arctic with consistently low extent throughout the period. The average

minimum extents dropped for each period: 6.85 million km^2 for 1979-1992, 6.13 million km^2 for 1993-2006, and 4.44 million km^2 for 2007-2020.

Age of the sea ice

The age of sea ice is also a key descriptor of the state of the sea ice cover. It serves as an indicator for ice physical properties, including snow cover, surface roughness, optical properties, melt pond coverage, salinity, and thickness. Older ice tends to be thicker and thus more resilient to changes in short-term atmospheric and oceanic variations compared to younger ice. The age of the ice is determined using satellite observations and drifting buoy records to track ice parcels over several years (Tschudi et al. 2020). This method has been used to provide a record of the age of the ice since the early 1980s (Tschudi et al. 2019).

The oldest ice (> 4 years old) was once a major component of the Arctic sea ice cover, but now makes up just a small fraction of the March Arctic Ocean ice pack (Fig. 3). In 1985, 33% of the ice pack was very old ice (> 4 years), but by March 2020 old ice only constituted 4.4% of the ice pack within the Arctic Ocean. The total extent of the oldest ice declined from 2.70 million km^2 in March 1985 to 0.34 million km^2 in March 2020. The March 2020 extent of > 4 year old ice increased from the record-low year in 2019 when it was only 1.2% (0.09 million km^2) of the ice cover. This increase was due to 3-4 year old ice surviving a year and aging into > 4 year old ice. The 3-4 year old cover dropped from 6.4% in 2019 to 3.7% in 2020. Overall the percentage of ice 3 years and older was effectively unchanged. Note that these percentages are relative to ice in the Arctic Ocean region (Fig. 3, bottom inset); areas in the peripheral seas outside of this region have little or no older ice and thus do not show any change over time.

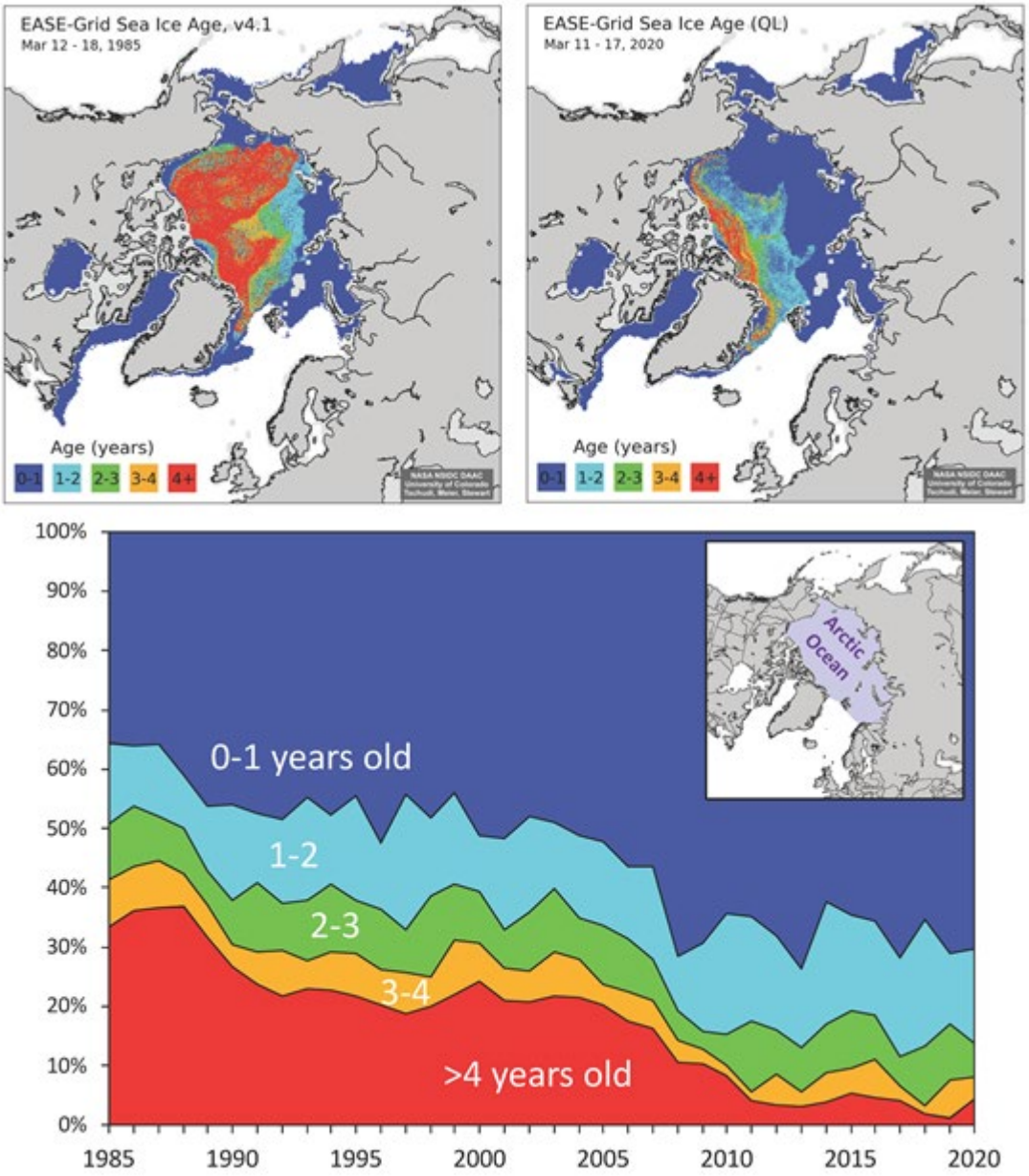

Fig. 3. Late winter sea ice age coverage map for the week of 12-18 March 1985 (upper left) and 11-17 March 2020 (upper right). Bottom: Sea ice age percentage within the Arctic Ocean for the week of 11-18 March 1985-2020. Data are from NSIDC (Tschudi et al. 2019, 2020).

Sea ice thickness and volume

Satellite altimetry has enabled the continuous retrieval of sea ice thickness and volume estimates over the entire Arctic basin, starting with the ESA CryoSat-2 radar altimeter, launched in 2010. This was followed in 2018 by the launch of the NASA Ice, Cloud, and land Elevation 2 laser altimeter. Thus, there are now two independent altimetry-based estimates of thickness and volume.

Altimeter measurements have higher relative errors for thin ice because of the achievable precision of the elevation. Using an optimal interpolation scheme, the CryoSat-2 estimates have been combined with

thin ice (< 1 m) estimates from the ESA Soil Moisture Ocean Salinity (SMOS) instrument, launched in 2009, to obtain an optimal estimate across thin and thick ice regimes (Ricker et al. 2017). When combined with sea ice concentration, the CryoSat-2/SMOS record of ice thickness is used to indicate variability in sea ice volume.

The time series of sea ice volume from CryoSat-2/SMOS, spanning October 2019 to April 2020, is shown in Fig. 4a relative to the daily range in sea ice volume over the previous nine winters. Northern Hemisphere sea ice volume grew by 14,185 km^3 during the winter 2019/20 season, increasing from 5,657 km^3 in October 2019 to 19,842 km^3 in April 2020. Sea ice volume in winter 2019/20 was consistently below the average of all 10 years. By the end of winter, ice volume in April 2020 was approximately 1,000 km^3 (~5%) below the 2010-2019 average and near the lowest volume of the 10 years for April. This record suggests that while September sea ice extent decline has been somewhat slower over the 2010-2019 period, the ice has continued to thin and the low volume during 2019/20 likely helped pre-condition the ice for larger summer extent loss, leading to the second lowest minimum in September 2020.

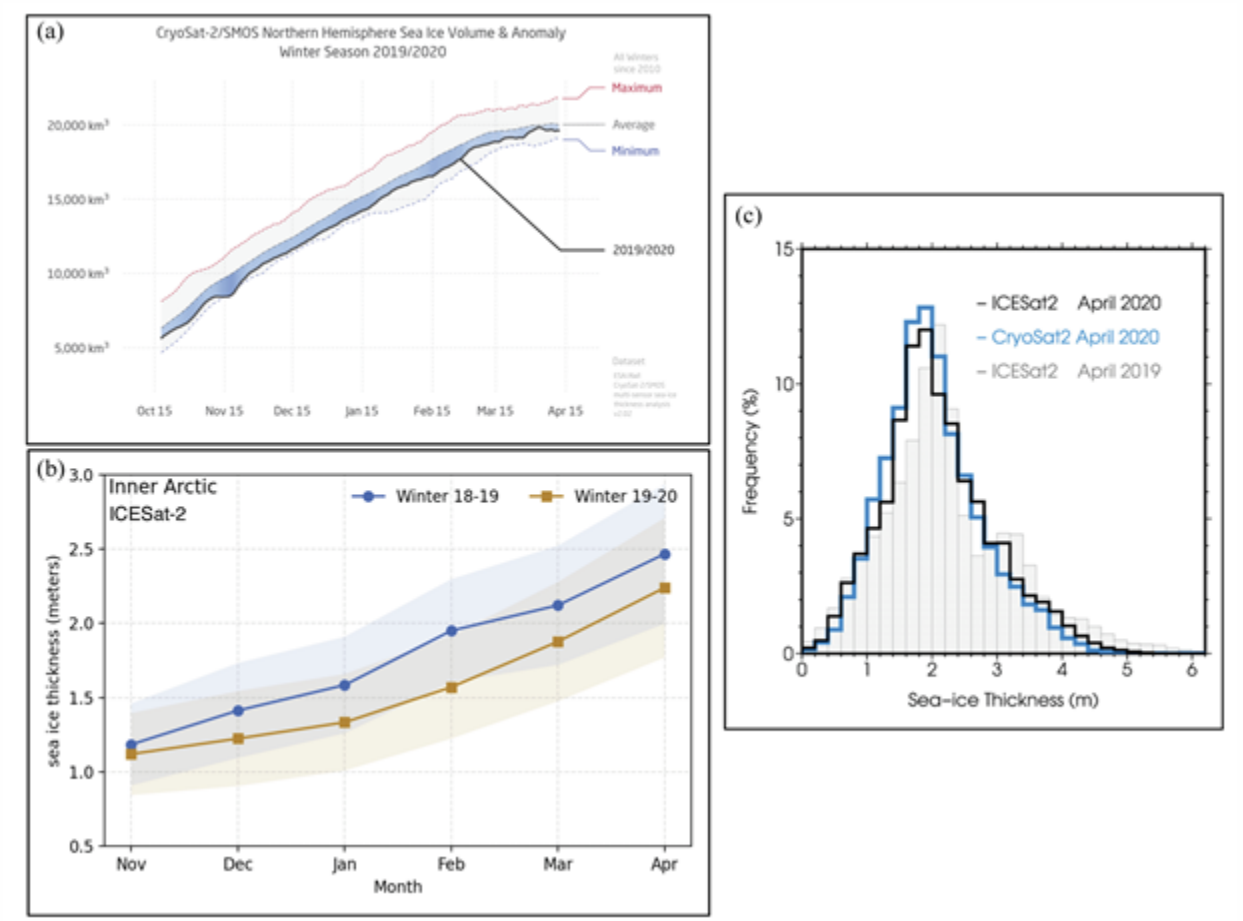

Fig. 4. (a) Time series of Northern Hemisphere sea ice volume from CryoSat-2/SMOS in winter 2019/20, spanning 15 October 2019 to 15 April 2020 (black line). The 10-year climatology range (gray shading) for winter 2010/11 through winter 2019/20 bounded by the daily lowest (Minimum, blue dashed line), highest (Maximum, red dashed line), and average (gray dot-dashed line) sea ice volume in the climatology. Blue shading represents the amount below average of the 2019/20 volume. (b) Monthly thickness from the gridded ICESat-2 product (snow depth/density from modified Warren et al. (1999) climatology) for November to April of 2018/19 (blue) and 2019/20 (brown). Shading represents the mean thickness uncertainty as described in Petty et al. (2020). (c)

Thickness distribution from ICESat-2 and CryoSat-2 thickness estimates for April 2020 and comparison with ICESat-2 April 2019.

Sea ice thickness from ICESat-2 (Fig. 4b) also indicates a thinner winter ice cover with an April 2020 mean (modal) thickness of 2.2 +/- 0.5 m, slightly lower than April 2019. The longer CryoSat-2 record can provide a longer-term context to complement the two years of ICESat-2 data. Both sensors have similar modal thickness and thickness distributions (Fig. 4c) suggesting that two independent instruments can provide consistent but complementary information on thickness.

The below-average sea ice volume at the end of winter in April 2020 was driven by wide areas of below-average sea ice thickness in the central Arctic Basin and on the Russian continental shelves (Fig. 5). However, ice thickness in April 2020 was above average in the Beaufort Sea, as well as in the Barents Sea and north of Svalbard (Fig. 5, right side), where the latter was likely caused by an increase in southward advection of thick multiyear sea ice. This advection was observed by the MOSAiC expedition as their drift was more rapid than expected (see essay *MOSAiC*).

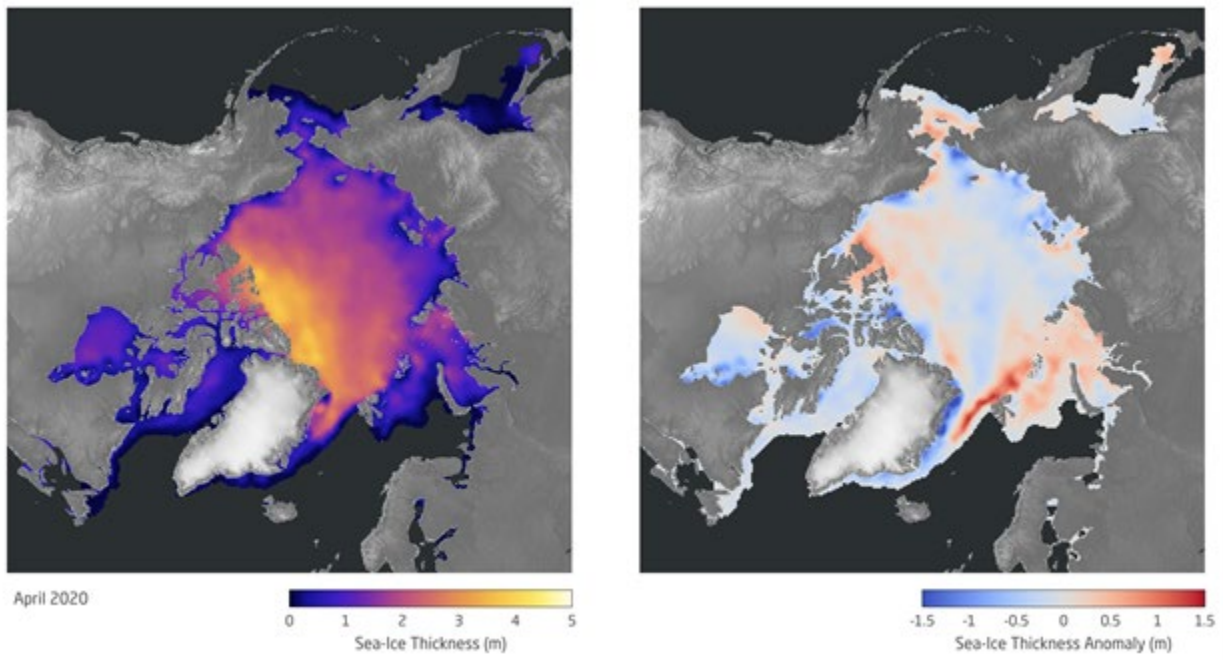

Fig. 5. (left) Sea ice thickness for April 2020 from the multi-sensor CryoSat-2/SMOS sea ice thickness analysis product. (right) Sea ice thickness anomaly for April 2020 relative to the 2011 to 2019 winter average. (Data source: AWI/ESA CryoSat-2 & SMOS multi-sensor sea-ice thickness v2.02. Data available at: ftp://ftp.awi.de/sea_ice/product/cryosat2_smos/v202/nh/.

These changes in ice thickness from 2019 are seen particularly in the Fram Strait region, the area between northeast Greenland and Svalbard. Fram Strait is the main exit route for sea ice drifting out of the central Arctic Ocean. Sea ice in Fram Strait has been monitored by the Norwegian Polar Institute since the early 1990s, and trends over the period 1990-2014 show a decrease in both ice thickness and ice volume (Spreen et al. 2020). In August/September 2020, ice drifting through Fram Strait consisted mainly of first-year sea ice, with some sporadic occurrences of older ice. In shallow areas of the shelf east of northeast Greenland, grounded icebergs previously provided conditions well-suited for forming or maintaining multiyear fast ice (e.g., Wang et al. 2020), but in September 2020 few fast ice floes were observed. Sea ice thicknesses in western Fram Strait in August/September 2020 ranged from 1.06 to

3.43 m, with a modal thickness of 1.6 m. Ice thickness in the Fram Strait in August/September 2020 is inferred from 34 direct measurements made on four ice stations, mainly on thicker second year and multiyear ice floes.

Sea ice melt over the spring and summer of 2020 led to volume loss of 15,215 km^3, as indicated by the CryoSat-2/SMOS measurements in October 2020, leading to an annual minimum volume of 4,627 km^3, the lowest volume in the 10 years of the CryoSat-2/SMOS data record. The spring/summer volume loss was only the second largest loss of sea ice over a melt season (after 2011) due to the low volume at the beginning of the 2020 melt season. Thus, the summer volume loss, record low end-of-summer volume, and the second lowest annual minimum extent marks 2020 as one of the more extreme years in the modern satellite record.

References

Cavalieri, D. J., C. L. Parkinson, P. Gloersen, and H. J. Zwally, 1996 (updated yearly): Sea Ice Concentrations from Nimbus-7 SMMR and DMSP SSM/I-SSMIS Passive Microwave Data, Version 1. NASA National Snow and Ice Data Center Distributed Active Archive Center, Boulder, CO, USA, https://doi.org/10.5067/8GQ8LZQVL0VL.

Comiso, J.C., W.N. Meier, and R. Gersten, 2017. Variability and trends in the Arctic sea ice cover: Results from different techniques. *J. Geophys. Res.*, **122**, 6883-6900, https://doi.org/10.1002/2017JC012768.

Fetterer, F., K. Knowles, W. N. Meier, M. Savoie, and A. K. Windnagel, 2017 (updated daily): Sea Ice Index, Version 3. NSIDC: National Snow and Ice Data Center, Boulder, CO, USA, https://doi.org/10.7265/N5K072F8. [Accessed 27 August 2020].

Ivanova, N., O. M. Johannessen, L. T. Pedersen, and R. T. Tonboe, 2014: Retrieval of Arctic sea ice parameters by satellite passive microwave sensors: A comparison of eleven sea ice concentration algorithms. *IEEE Trans. Geosci. Rem. Sens.*, **52**(11), 7233-7246, https://doi.org/10.1109/TGRS.2014.2310136.

Kern, S., T. Lavergne, D. Notz, L. T. Pedersen, R. T. Tonboe, R. Saldo, and A. M. Sørensen, 2019: Satellite passive microwave sea-ice concentration data set intercomparison: closed ice and ship-based observations. *Cryosphere*, **13**, 3261-3307, https://doi.org/10.5194/tc-13-3261-2019.

Lavergne, T., and Coauthors, 2019: Version 2 of the EUMETSAT OSI SAF and ESA CCI sea-ice concentration climate data records. *Cryosphere*, **13**, 49-78, https://doi.org/10.5194/tc-13-49-2019.

Maslanik, J., and J. Stroeve, 1999: Near-Real-Time DMSP SSMIS Daily Polar Gridded Sea Ice Concentrations, Version 1. NASA National Snow and Ice Data Center Distributed Active Archive Center, Boulder, CO, USA, https://doi.org/10.5067/U8C09DWVX9LM.

Petty, A. A., N. T. Kurtz, R. Kwok, T. Markus, and T. A. Neumann, 2020: Winter Arctic sea ice thickness from ICESat-2 freeboards. *J. Geophys. Res.-Oceans*, **125**, e2019JC015764, https://doi.org/10.1029/2019JC015764.

Ricker, R., S. Hendricks, L. Kaleschke, X. Tian-Kunze, J. King, and C. Haas, 2017: A weekly Arctic sea-ice thickness data record from merged CryoSat-2 and SMOS satellite data. *Cryosphere*, **11**, 1607-1623, https://doi.org/10.5194/tc-11-1607-2017.

Spreen, G., L. de Steur, D. Divine, S. Gerland, E. Hansen, and R. Kwok, 2020: Arctic sea ice volume export through Fram Strait from 1992 to 2014. *J. Geophys. Res.-Oceans,* **125**, e2019JC016039, https://doi.org/10.1029/2019JC016039.

Tschudi, M. A., W. N. Meier, and J. S. Stewart, 2020: An enhancement to sea ice motion and age products at the National Snow and Ice Data Center (NSIDC). *Cryosphere*, **14**, 1519-1536, https://doi.org/10.5194/tc-14-1519-2020.

Tschudi, M., W. N. Meier, J. S. Stewart, C. Fowler, and J. Maslanik, 2019: EASE-Grid Sea Ice Age, Version 4. NASA National Snow and Ice Data Center Distributed Active Archive Center, Boulder, CO, USA, https://doi.org/10.5067/UTAV7490FEPB.

Wang, C., J. Negrel, S. Gerland, D. V. Divine, P. Dodd, and M. A. Granskog, 2020: Thermodynamics of fast ice off the northeast coast of Greenland (79° N) over a full year (2012-2013). *J. Geophys. Res.-Oceans*, **125**, e2019JC015823, https://doi.org/10.1029/2019JC015823.

Warren, S. G., I. G. Rigor, N. Untersteiner, V. F. Radionov, N. N. Bryazgin, Y. I. Aleksandrov, and R. Colony, 1999: Snow depth on Arctic sea ice. *J. Climate*, **12**, 1814-1829, https://doi.org/10.1175/1520-0442(1999)012<1814:SDOASI>2.0.CO;2.

December 8, 2020

Sea Surface Temperature

DOI: 10.25923/v0fs-m920

M. -L. Timmermans[1] and Z. Labe[2]

[1]Yale University, New Haven, CT, USA
[2]Colorado State University, Fort Collins, CO, USA

Highlights

- August mean sea surface temperatures (SSTs) in 2020 were ~1-3°C warmer than the 1982-2010 August mean over most of the Arctic Ocean.
- August mean SSTs show statistically significant warming trends for 1982-2020 in most regions of the Arctic Ocean that are ice-free in August.
- August mean SSTs in 2020 were exceptionally warm in parts of the Kara and Laptev Seas, up to ~5°C warmer than 1982-2010 August mean values, associated with early seasonal ice loss in these regions and anomalously warm surface air temperatures over northern Eurasia.

Introduction

Summer sea surface temperatures (SST) in the Arctic Ocean are driven mainly by the amount of incoming solar radiation absorbed by the sea surface. Solar warming of the Arctic surface ocean is influenced by the distribution of sea ice (with greater warming occurring in ice-free regions), cloud cover, ocean optical properties, and upper-ocean stratification. Discharge of warm Arctic river waters can provide an additional source of heat to the surface marginal seas. In the Barents and Chukchi Seas, there is also a contribution to ocean heat by the advection of warm water from the North Atlantic and North Pacific Oceans, respectively. Arctic SSTs are an essential indicator of the role of the ice-albedo feedback mechanism in any given summer melt season. As the area of sea ice cover decreases (see essay *Sea Ice*), more incoming solar radiation is absorbed by the ocean and, in turn, the warmer ocean melts more sea ice. In addition, warmer SSTs are associated with delayed autumn freeze-up and increased ocean heat storage throughout the year. Marine ecosystems are influenced by SST, which affects the timing and development of primary and secondary production cycles, as well as available habitat for upper trophic and temperature-sensitive species. Finally, with respect to carbon cycling, warmer SSTs increase the surface-ocean partial pressure of CO_2 (pCO_2), which reduces the air-ocean pCO_2 gradient and therefore the ocean uptake of CO_2 from the atmosphere. A study published this year indicates that increased SSTs in recent years may have reduced air-ocean exchange of CO_2 by as much as 50% (DeGrandpre et al. 2020).

SST data presented in this section are a blend of in situ and satellite measurements from December 1981 to present, taken from the monthly mean NOAA Optimum Interpolation (OI) SST Version 2 product (OISSTv2) (Reynolds et al. 2002, 2007). Compared to purely in situ temperature measurements, the OISSTv2 product explains about 80% of the variance, with an overall cold bias via its tendency to underestimate SST by 0.02°C (Stroh et al. 2015). The OISSTv2 product uses a linear relationship with sea ice concentration to infer SST, with SST constrained to -1.8°C (the freezing point of seawater with a salinity of 33 g kg^{-1} at the sea surface) where ice concentration is 100% (Reynolds et al. 2007). Variations

in freezing temperature as a result of variations in sea surface salinity (not accounted for in the algorithm) imply that OISSTv2 SSTs under sea ice can be too cool by up to 0.2°C, with the highest errors in the fresher surface waters of the Canada Basin. August mean SSTs provide the most appropriate representation of Arctic Ocean summer SSTs because they are not affected by the cooling and subsequent sea ice growth that typically takes place in the latter half of September. The period 1982-2010 is used as a climatological reference.

August 2020 mean SSTs ranged from 7 to 10°C in the southern Chukchi and Barents Seas to approximately 1 to 3°C in the interior Arctic Ocean marginal seas that are ice-free in August (Fig. 1a). SSTs in August 2020 were consistent with sustained mean August SST warming trends from 1982 to 2020 over much of the Arctic Ocean, with statistically significant (at the 95% confidence interval) linear warming trends of up to +1°C per decade (Fig. 1b); mean August SSTs for the entire Arctic (the Arctic Ocean and marginal seas north of 67° N) exhibit a linear warming trend of 0.03 ± 0.01°C yr^{-1}. The cooling trend in mean August SSTs in the northern Barents Sea region remains a notable exception (see Timmermans et al. 2020).

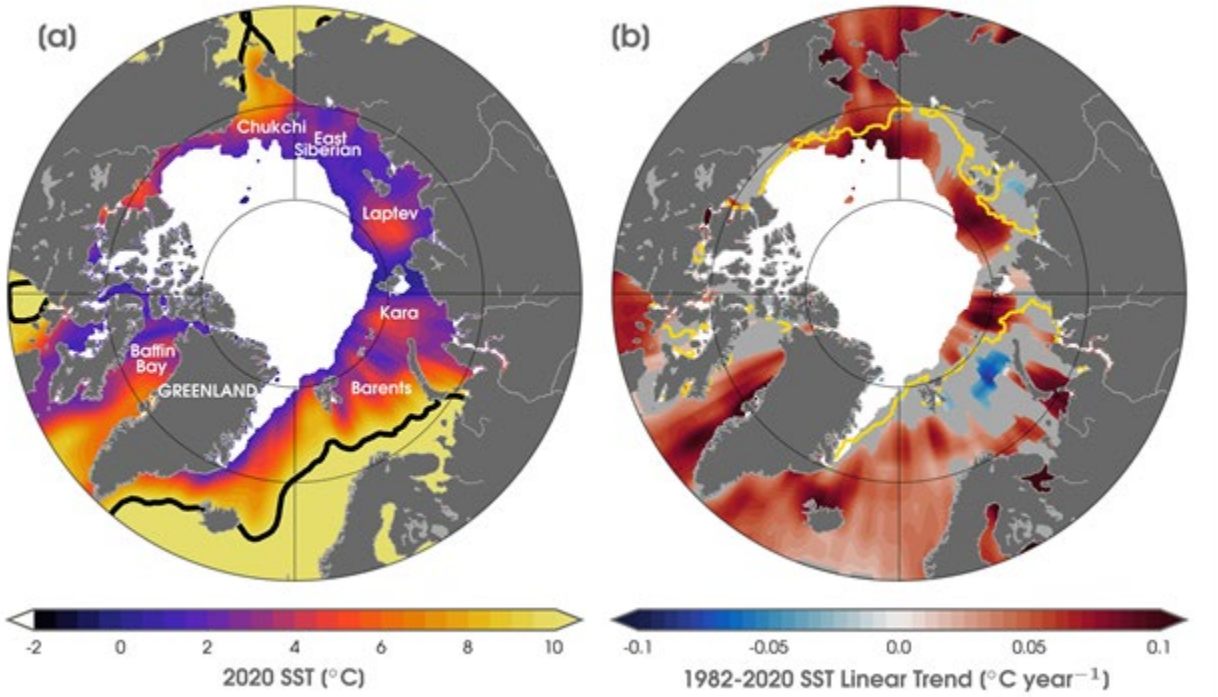

Fig. 1. (a) Mean SST (°C) in August 2020. White shading is the August 2020 mean sea ice extent, and black contours indicate the 10°C SST isotherm. (b) Linear SST trend (°C yr^{-1}) for August of each year from 1982 to 2020. The trend is only shown for values that are statistically significant at the 95% confidence interval; the region is grey otherwise. The yellow line indicates the median ice edge for August 1982-2010. White shading is the August 2020 mean sea ice extent. (Sources: SST data are from the NOAA OISSTv2; sea ice extent and ice-edge data are from NOAA/NSIDC Climate Data Record of Passive Microwave Sea Ice Concentration, Version 3; Peng et al. 2013; Meier et al. 2017.)

Long-term trends

August 2020 mean SSTs were around 1-3°C warmer than the 1982-2010 August mean over most of the Arctic Ocean's marginal seas (Fig. 2a). The warmest SSTs were observed in the Laptev and Kara Seas, with values up to 5.5°C warmer than the 1982-2010 August mean (Fig. 2a). Conversely, similar to August 2019 conditions, the northern Barents Sea region was marked by anomalously cool SSTs in August 2020, up to 1.5°C cooler than the 1982-2010 mean (Fig. 2), contributing further to the region's long-term cooling trend. Relative to August 2019, August 2020 SSTs were up to 4°C cooler in the Chukchi and Beaufort Sea region and a few degrees warmer overall in the Kara and Laptev Seas (Fig. 2b). The strong interannual variability in spatial patterns of SST bear a close relationship to early summer sea ice concentrations, with direct solar heating of the exposed surface waters in regions of low sea ice area, and likely an active ice-albedo feedback.

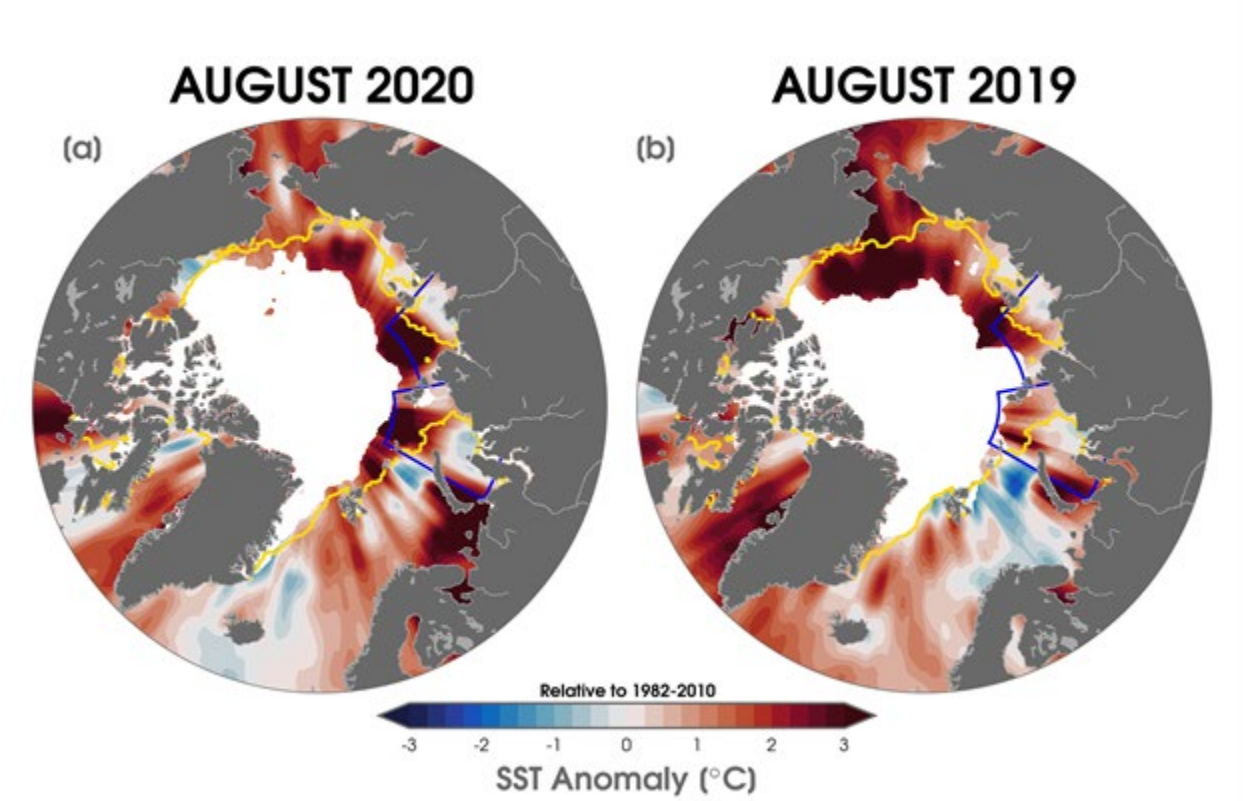

Fig. 2. SST anomalies (°C) in (a) August 2020 and (b) August 2019 relative to the August 1982–2010 mean. The yellow line indicates the median ice edge for August 1982–2010 and white shading indicates the mean sea-ice extent in (a) August 2020 (b) and August 2019. The two regions marked by blue boxes indicate the Kara and Laptev seas and relate to data presented in Fig. 3. (Sources: SST data are from the NOAA OISSTv2; sea-ice extent and ice-edge data are from NOAA/NSIDC Climate Data Record of Passive Microwave Sea Ice Concentration, Version 3; Peng et al., 2013; Meier et al., 2017.)

Anomalously warm SSTs in the Laptev and Kara Seas distinguished the August 2020 SST field. Kara Sea SSTs are becoming warmer in August with a linear warming trend over 1982-2020 of 0.03 ± 0.01°C yr^{-1} (Fig. 3a). Although not statistically significant, Laptev Sea August mean SSTs also appear to be warming, with a linear trend of 0.02 ± 0.02°C yr^{-1} (Fig. 3b). The interplay between regional sea ice cover and solar absorption is evident in the low sea ice extents in August 2020 in these seas (Fig. 2c,d, and see essay *Sea*

Ice). Both regions also saw exceptionally low sea ice extents in July 2020, with Laptev Sea sea ice extent showing a record minimum for July. In addition, observations indicate increased heat fluxes from the deeper ocean (i.e., warmer waters sourced from the Atlantic Ocean) into the mixed layer in the eastern Eurasian Basin, from around 3-4 W/m2 in 2007-08 to more than 10 W/m2 in 2016-18 (Polyakov et al. 2020). This may also contribute to generally warmer SSTs in the region, although the relative influences of direct solar warming and heat fluxed into the mixed layer from below have not been quantified.

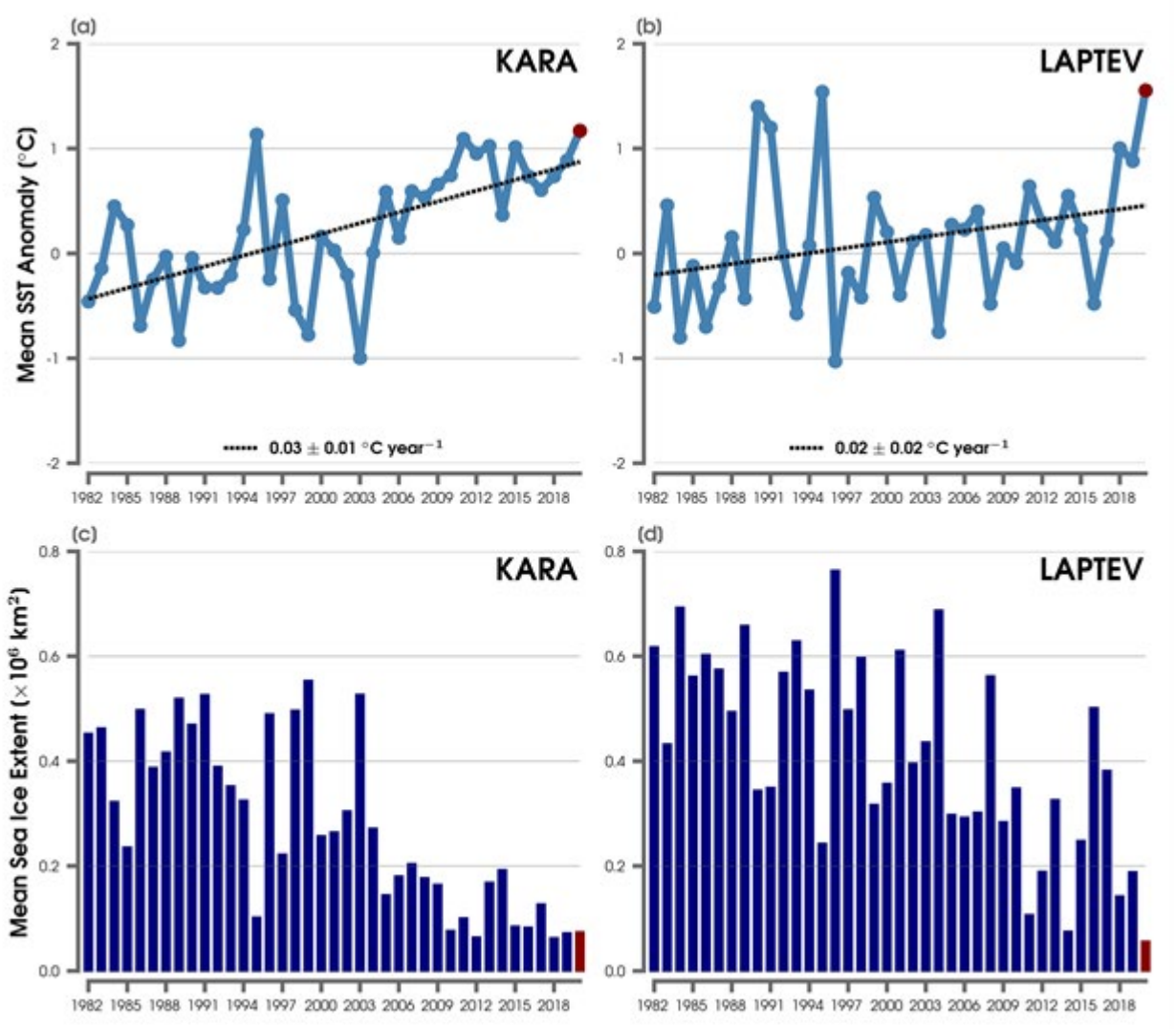

Fig. 3. Area-averaged SST anomalies (°C) for August of each year (1982-2020) relative to the 1982–2010 August mean for (a) the Kara Sea and (b) the Laptev Sea regions shown by blue boxes in Fig. 2. The dotted lines show the linear SST anomaly trends over the period shown, and numbers in the legends indicate the trends in °C year^{-1} (with 95% confidence intervals). August sea ice extents calculated over the (c) Kara and (d) Laptev Sea domains. Sea ice extent data are from NSIDC Sea Ice Index, Version 3 (Fetterer et al. 2017) using a regional mask introduced by Meier et al. (2007), available at nsidc.org.

References

DeGrandpre, M., W. Evans, M. -L. Timmermans, R. Krishfield, B. Williams, and M. Steele, 2020: Changes in the arctic ocean carbon cycle with diminishing ice cover. *Geophys. Res. Lett.*, **47**, e2020GL088051, https://doi.org/10.1029/2020GL088051.

Fetterer, F., K. Knowles, W. N. Meier, M. Savoie, and A. K. Windnagel, 2017 (updated daily): Sea Ice Index, Version 3: Regional Daily Data. National Snow and Ice Data Center (NSIDC), Boulder, CO, USA, https://doi.org/10.7265/N5K072F8.

Meier, W., J. Stroeve, and F. Fetterer, 2007: Whither Arctic sea ice? A clear signal of decline regionally, seasonally and extending beyond the satellite record. *Ann. Glaciol.*, **46**, 428-434, https://doi.org/10.3189/172756407782871170.

Meier, W. N., F. Fetterer, M. Savoie, S. Mallory, R. Duerr, and J. Stroeve. 2017: NOAA/NSIDC Climate Data Record of Passive Microwave Sea Ice Concentration, Version 3. [Indicate subset used]. National Snow and Ice Data Center (NSIDC), Boulder, CO, USA, https://doi.org/10.7265/N59P2ZTG.

Peng, G., W. N. Meier, D. J. Scott, and M. H. Savoie, 2013: A long-term and reproducible passive microwave sea ice concentration data record for climate studies and monitoring. *Earth Syst. Sci. Data*, **5**, 311-318, https://doi.org/10.5194/essd-5-311-2013.

Polyakov, I. V., and Coauthors, 2020: Weakening of the cold halocline layer exposes sea ice to oceanic heat in the eastern Arctic Ocean. *J. Climate*, **33**(18), 8107-8123, https://doi.org/10.1175/JCLI-D-19-0976.1.

Reynolds, R. W., N. A. Rayner, T. M. Smith, D. C. Stokes, and W. Wang, 2002: An improved in situ and satellite SST analysis for climate. *J. Climate*, **15**, 1609-1625, https://doi.org/10.1175/1520-0442(2002)015<1609:AIISAS>2.0.CO;2.

Reynolds, R. W., T. M. Smith, C. Liu, D. B. Chelton, K. S. Casey, and M. G. Schlax, 2007: Daily high-resolution-blended analyses for sea surface temperature. *J. Climate*, **20**, 5473-5496, https://doi.org/10.1175/2007JCLI1824.1, and see http://www.esrl.noaa.gov/psd/data/gridded/data.noaa.oisst.v2.html.

Stroh, J. N., G. Panteleev, S. Kirillov, M. Makhotin, and N. Shakhova, 2015: Sea-surface temperature and salinity product comparison against external in situ data in the Arctic Ocean. *J. Geophys. Res. Oceans*, **120**, 7223-7236, https://doi.org/10.1002/2015JC011005.

Timmermans, M. -L., Z. Labe, and C. Ladd, 2020: Sea surface temperature [in "State of the Climate in 2019"]. *Bull. Amer. Meteor. Soc.*, **101**(8), S249-S251, https://doi.org/10.1175/BAMS-D-20-0086.1.

November 9, 2020

Arctic Ocean Primary Productivity: The Response of Marine Algae to Climate Warming and Sea Ice Decline

DOI: 10.25923/vtdn-2198

K. E. Frey[1], J. C. Comiso[2], L. W. Cooper[3], J. M. Grebmeier[3], and L. V. Stock[2]

[1]Graduate School of Geography, Clark University, Worcester, MA, USA
[2]Cryospheric Sciences Laboratory, Goddard Space Flight Center, NASA, Greenbelt, MD, USA
[3]Chesapeake Biological Laboratory, University of Maryland Center for Environmental Science, Solomons, MD, USA

Highlights

- Satellite estimates of ocean primary productivity (i.e., the rate at which marine algae transform dissolved inorganic carbon into organic material) showed higher values for 2020 (relative to the 2003-2019 mean) for seven of the nine investigated regions (with the Sea of Okhotsk and Bering Sea showing lower than average values).
- All regions continue to exhibit positive trends over the 2003-2020 period, with the strongest trends in the Eurasian Arctic, Barents Sea, and Greenland Sea.
- During July and August 2020, a ~600 km long region in the Laptev Sea of the Eurasian Arctic showed much higher chlorophyll-*a* concentrations (~2 times higher for July and ~6 times higher for August) than the same months of the multiyear average (2003-2019), associated with very early loss of sea ice in spring and summer (see essay *Sea Ice*).

Introduction

Autotrophic single-celled algae living in sea ice (ice algae) and water column (phytoplankton) are the main primary producers in the Arctic Ocean. Through photosynthesis, they transform dissolved inorganic carbon into organic material. Consequently, primary production provides a key ecosystem service by providing energy to the entire food web in the oceans. Primary productivity is strongly dependent upon light availability and the presence of nutrients, and thus is highly seasonal in the Arctic. The melting and retreat of sea ice during spring are strong drivers of primary production in the Arctic Ocean and its adjacent shelf seas, owing to enhanced light availability and stratification (Barber et al. 2015; Leu et al. 2015; Ardyna et al. 2017). Recent studies have emphasized that primary production occurs under lower light conditions and earlier in the seasonal cycle than previously recognized (Randelhoff et al. 2020). Other studies suggest that increased nutrient supply have also influenced overall production (Henley et al. 2020; Lewis et al. 2020). Furthermore, while declines in Arctic sea ice extent over the past several decades (see essay *Sea Ice*) have contributed substantially to shifts in primary productivity throughout the Arctic Ocean, the response of primary production to sea ice loss has been both seasonally and spatially variable (e.g., Tremblay et al. 2015; Hill et al. 2018).

Here we present satellite-based estimates of algal chlorophyll-*a* (occurring in all species of phytoplankton), based on ocean color, and subsequently provide calculated primary production estimates. These results are shown for ocean areas with less than 10% sea ice concentration and, therefore, do not include production by sea ice algae or under-ice phytoplankton blooms, which can be significant (e.g., Lalande et al. 2019).

Chlorophyll-*a*

Measurements of the algal pigment chlorophyll (e.g., chlorophyll-*a*) serve as a proxy for the amount of algal biomass present (e.g., Behrenfeld and Boss 2006) as well as overall plant health. The complete, updated Moderate Resolution Imaging Spectroradiometer (MODIS)-Aqua satellite chlorophyll-*a* record for the northern polar region for the years 2003-2020 serves as a time series against which individual years can be compared. For this reporting, we show mean monthly chlorophyll-*a* concentrations calculated as a percentage of the 2003-2019 average, which was chosen as the reference period in order to maximize the length of the satellite-based time series.

The data presented in Fig. 1 show the ratio of chlorophyll-*a* concentrations for 2020 to chlorophyll-*a* concentrations for the multiyear average from 2003 to 2019 expressed as percentages, where patterns are spatially and temporally heterogeneous across the Arctic Ocean. These patterns are often associated with the timing of the seasonal break-up and retreat of the sea ice cover (Fig. 2) (see essay *Sea Ice*): high percentages tend to occur in regions where the break-up is relatively early, while low percentages tend to occur in regions where the break-up is delayed. The most notable enhanced values in 2020 occurred during July and August, with high concentrations of chlorophyll-*a* occurring in the Laptev Sea of the Eurasian Arctic (Figs. 1c, d), linked with very early sea ice loss and exceptionally warm conditions in the Laptev Sea in August 2020 (see essays *Sea Surface Temperature* and *Sea Ice*). In particular, this regional increase in chlorophyll-*a* concentrations extended ~600 km in length and exhibited on average ~2 times higher (July) and ~6 times higher (August) concentrations compared to the 2003-2019 average. Additional widespread increases in chlorophyll-*a* concentrations occurred along the ice edge in the Greenland Sea during May and June (Figs. 1a, b) associated with increases in sea ice to the west (Figs. 2a, b), as well as in the Barents Sea during May (Fig. 1a). Some of the lowest percentages of chlorophyll-*a* concentrations (i.e., low primary productivity) occurred in the northern Bering Sea during May, June, and August (Figs. 1a, b, and d) and in the Barents Sea in June, July, and August (Fig. 1b, c, and d).

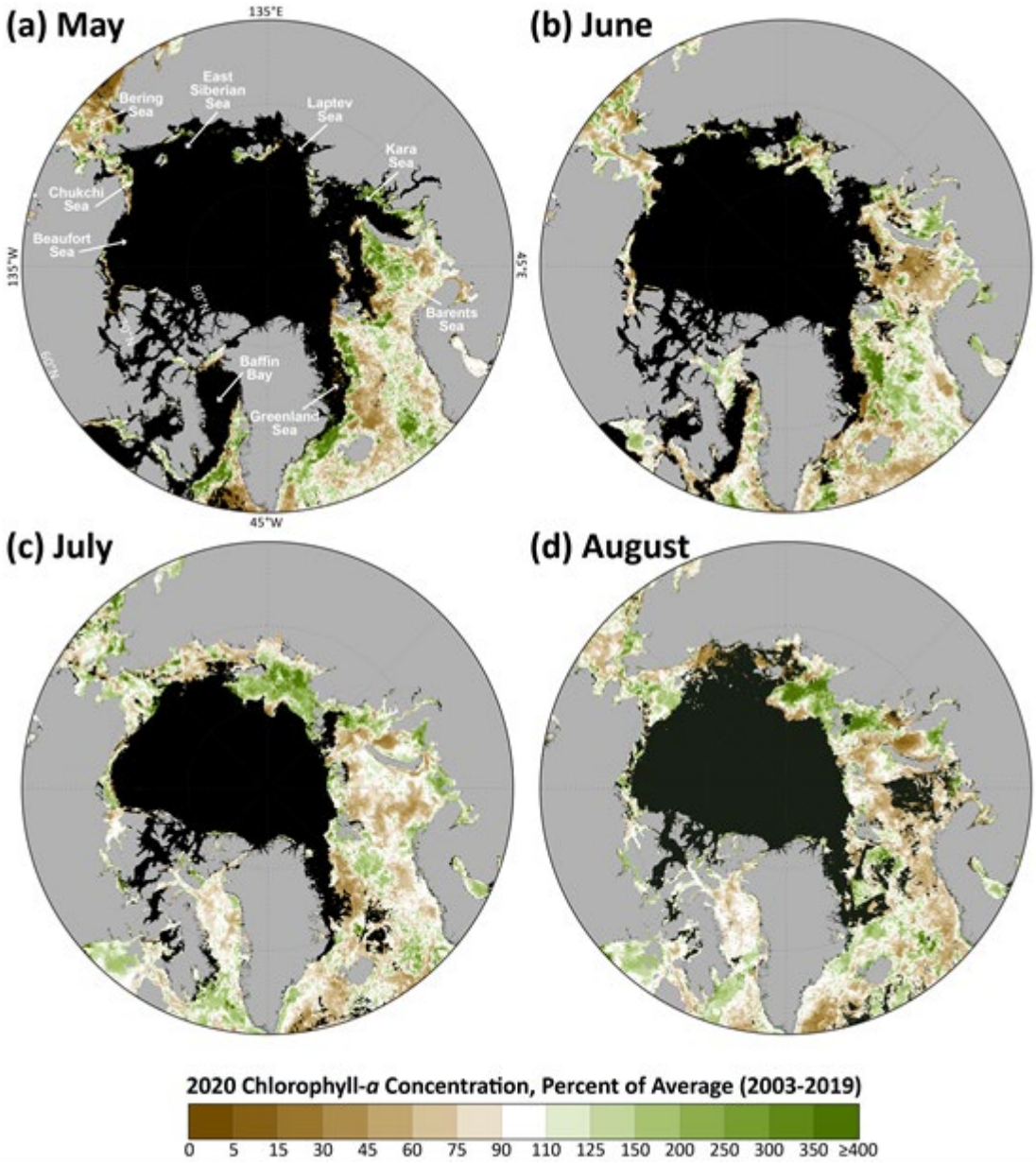

Fig. 1. Mean monthly chlorophyll-*a* concentrations during 2020, shown as a percent of the 2003-2019 average for (a) May, (b) June, (c) July, and (d) August. The black regions represent areas where no data are available (owing to either >10% sea ice concentrations or cloud cover). Satellite-based chlorophyll-*a* data across the pan-Arctic region were derived using the MODIS-Aqua Reprocessing 2018.0, chlor_a algorithm: http://oceancolor.gsfc.nasa.gov/.

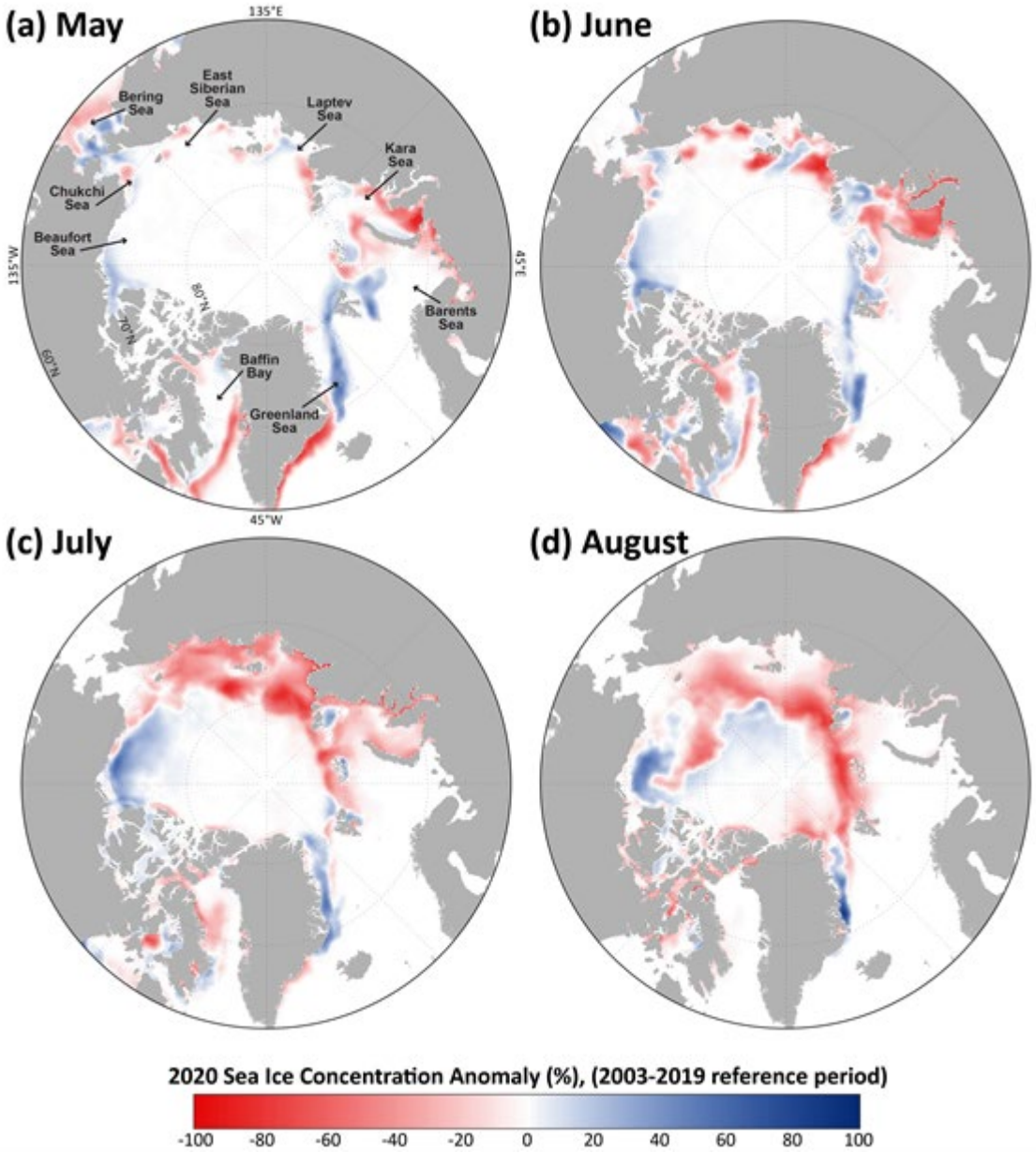

Fig. 2. Sea ice concentration anomalies (%) in 2020 (compared to a 2003-2019 mean reference period) for (a) May, (b) June, (c) July, and (d) August. Satellite-based sea ice concentrations were derived from the Special Sensor Microwave/Imager (SSM/I) and Special Sensor Microwave Imager/Sounder (SSMIS) passive microwave instruments, calculated using the Goddard Bootstrap (SB2) algorithm (Comiso et al. 2017a,b).

As noted above, some of the lowest percentages of chlorophyll-*a* concentrations observed in 2020 occurred over the shelf region of the Bering Sea during May, June, and August (Figs. 1a, b, and d). During June, these low percentages extended northward through the Bering Strait and onto the Chukchi Shelf (Fig. 1b). It is unclear from the satellite time series what role sea ice may be playing in these reductions of chlorophyll-*a* concentrations. For instance, 2020 experienced a resurgence of seasonal sea ice cover across the northern Bering Sea and Bering Strait region (e.g., Fig. 2a) compared to drastic reductions observed in 2018 (Frey et al. 2018; Stabeno and Bell 2019) and 2019 (Frey et al. 2019) (see essay *Sea Ice*), yet chlorophyll-*a* concentrations in the region do not appear to respond in a consistent way to

these potential sea ice forcings. In general, knowing how regions experience changes in chlorophyll-*a* concentrations alongside dramatic losses of sea ice cover provides insight into what to expect with future sea ice declines. However, while many of these observed patterns are directly linked to sea ice variability (and therefore light availability), it is noteworthy that there are other important factors at play that add to the complexity of observed chlorophyll-*a* concentrations such as the distribution and availability of nutrients (e.g., Giesbrecht et al. 2019; Lewis et al. 2020). The impacts of sea ice decline on specific water column phytoplankton properties, such as community composition and carbon biomass (Neeley et al. 2018), as well as broader ecosystem responses (Duffy-Anderson et al. 2019) will also be critical to continue to monitor. Furthermore, it is important to reiterate that the satellite ocean color data do not account for early-season under-ice blooms that may contribute substantially to primary productivity in these regions (e.g., Arrigo et al. 2012). Deployment of a new sediment trap array in the northern Bering Sea, together with a mooring array in autumn 2020 should improve understanding of seasonal carbon production and export in this region, just as new year-round results reported from the Chukchi Ecosystem Observatory in the northern Chukchi Sea (Lalande et al. 2020) have improved understanding of annual production.

Primary Production

Chlorophyll-*a* concentrations give an estimate of the total standing stock of algal biomass. However, rates of primary production (i.e., the production of organic carbon via photosynthesis) provide a different perspective since not all algae present in the water column are necessarily actively producing. Primary productivity can be estimated by combining remotely sensed chlorophyll-*a* concentrations with sea surface temperatures, incident solar irradiance, and mixed layer depths (see caption in Fig. 3 for references to details of the method for estimation). Estimates of ocean primary productivity for nine regions (and the average of these nine regions) across the Arctic (relative to the 2003-2019 reference period) were assessed (Fig. 3, Table 1). In particular, the Eurasian Arctic designation includes the Kara Sea, Laptev Sea, and East Siberian Sea, whereas the Amerasian Arctic designation includes the Chukchi Sea, Beaufort Sea, and Canadian Archipelago region. The defined North Atlantic region is south of 60° N and east of 45° W, and as such is not inclusive of the Labrador or Greenland seas. Our results show above average primary productivity for 2020 in all regions except for the Sea of Okhotsk and Bering Sea (Fig. 3, Table 1). In the longer term, positive trends in primary productivity occurred in all regions during the period 2003-2020 (Fig. 3, Table 1). Statistically significant positive trends occurred in the Eurasian Arctic, Barents Sea, Greenland Sea, Hudson Bay, Baffin Bay/Labrador Sea, North Atlantic, and for the average of the nine regions. The steepest trends over the 2003-2020 period were found for the Eurasian Arctic (12.83 g C/m^2/yr/decade, or a ~37.7% increase), the Barents Sea (9.32 g C/m^2/yr/decade, or a ~21.0% increase), and the Greenland Sea (6.34 g C/m^2/yr/decade, or a ~18.7% increase). In summary, while observations of primary productivity have shown complex interannual and spatial patterns over the 2003-2020 study period, overall we observe increasing trends across all sectors of the Arctic Ocean.

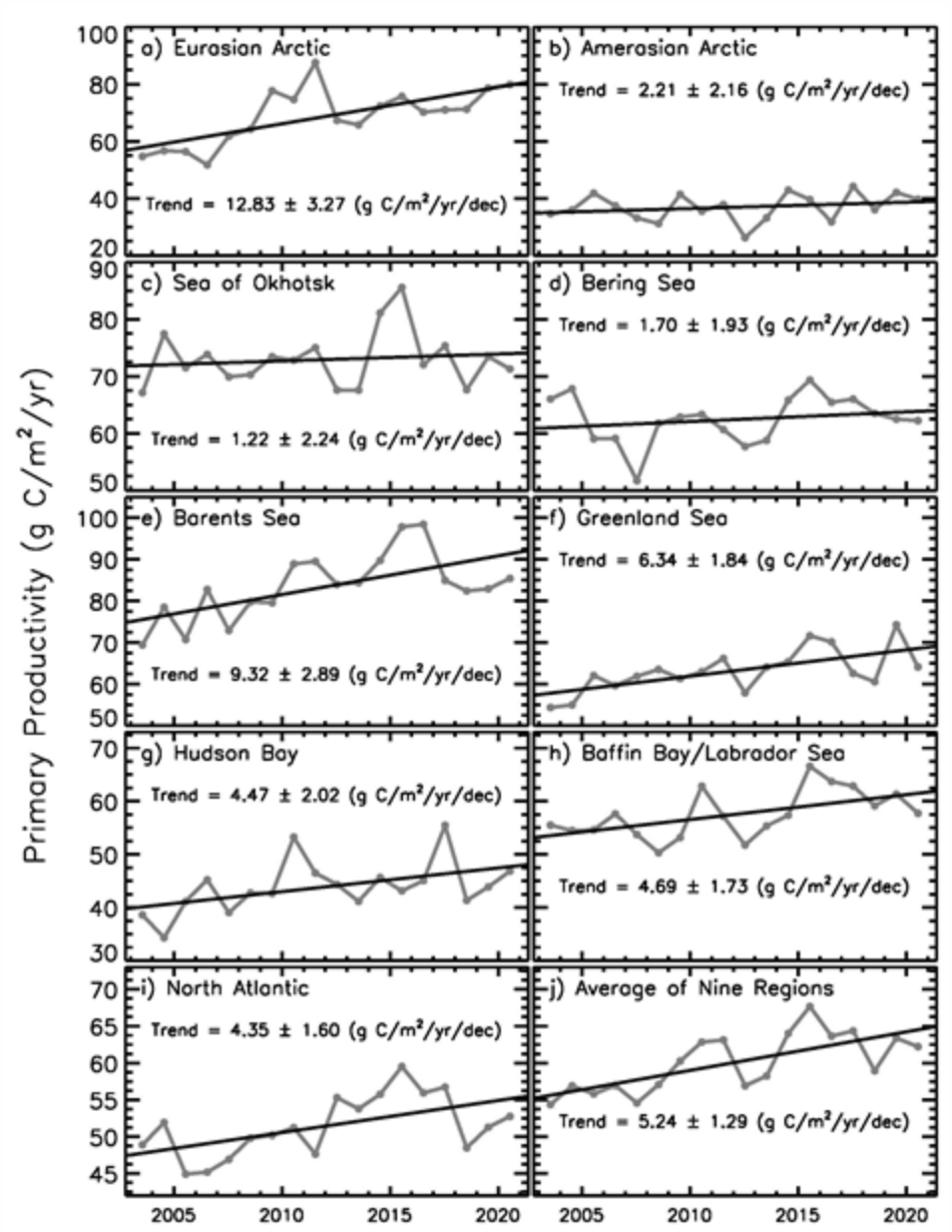

Fig. 3. Primary productivity (2003-2020, March-September only) in nine different regions of the Northern Hemisphere (for a definition of the regions see Comiso 2015), as well as the average of these nine regions, derived using chlorophyll-*a* concentrations from MODIS-Aqua data, the NOAA 1/4° daily Optimum Interpolation Sea Surface Temperature dataset (or daily OISST) that uses satellite sea surface temperatures from AVHRR, and additional parameters. Values are calculated based on the techniques described by Behrenfeld and Falkowski (1997) and represent net primary productivity. Additional information regarding these data can be found in Table 1.

Table 1. Linear trends, statistical significance, percent change, and primary productivity anomalies in 2020 (March-September) in the nine regions (and overall average) as shown in Fig. 3. Utilizing the Mann-Kendall test for trend, values in bold are significant at the 95% confidence level. The percent change was estimated from the linear regression of the 18-year time series.

Region	Trend, 2003-20 (g C/m^2/yr/decade)	Mann-Kendall *p* -value	% Change	2020 Anomaly (g C/m^2/yr) from a 2003-19 reference period	2020 Primary Productivity (% of the 2003-19 average)
Eurasian Arctic	**12.83**	0.001	37.7	11.74	117.2
Amerasian Arctic	2.21	0.260	10.7	2.90	107.9
Sea of Okhotsk	1.22	0.601	2.9	-1.75	97.6
Bering Sea	1.70	0.002	4.7	-0.20	99.7
Barents Sea	**9.32**	0.004	21.0	2.09	102.5
Greenland Sea	**6.34**	0.021	18.7	0.98	101.6
Hudson Bay	**4.47**	0.039	18.9	3.12	107.1
Baffin Bay/Labrador Sea	**4.69**	0.007	14.9	0.24	100.4
North Atlantic	**4.35**	0.001	15.5	1.37	103.8
Average of nine regions	**5.24**	0.001	16.0	2.28	103.8

Acknowledgments

K. Frey would like to acknowledge financial support by the National Science Foundation Arctic Observing Network (AON) Program (Grants 1702137 and 1917434).

References

Ardyna, M., M. Babin, E. Devred, A. Forest, M. Gosselin, P. Raimbault, and J. -É. Tremblay, 2017: Shelf-basin gradients shape ecological phytoplankton niches and community composition in the coastal Arctic Ocean (Beaufort Sea). *Limnol. Oceanogr.*, **62**, 2113-2132, https://doi.org/10.1002/lno.10554.

Arrigo, K. R., and Coauthors, 2012: Massive phytoplankton blooms under Arctic sea ice. *Science*, **336**, 1408, https://doi.org/10.1126/science.1215065.

Barber, D. G., and Coauthors, 2015: Selected physical, biological and biogeochemical implications of a rapidly changing Arctic Marginal Ice Zone. *Prog. Oceanogr.*, **139**, 122-150, https://doi.org/10.1016/j.pocean.2015.09.003.

Behrenfeld, M. J., and E. Boss, 2006: Beam attenuation and chlorophyll concentration as alternative optical indices of phytoplankton biomass. *J. Mar. Res.*, **64**, 431-451.

Behrenfeld, M. J., and P. G. Falkowski, 1997: Photosynthetic rates derived from satellite-based chlorophyll concentration. *Limnol. Oceanogr.*, **42**(1), 1-20.

Comiso, J. C., 2015: Variability and trends of the global sea ice covers and sea levels: effects on physicochemical parameters. Climate and fresh water toxins, L. M. Botana, M. C. Lauzao, and N. Vilarino, Eds., De Gruyter, Berlin, Germany.

Comiso, J. C., R. A. Gersten, L. V. Stock, J. Turner, G. J. Perez, and K. Cho, 2017a: Positive trend in the Antarctic sea ice cover and associated changes in surface temperature. *J. Climate*, **30**, 2251-2267, https://doi.org/10.1175/JCLI-D-16-0408.1 .

Comiso, J. C., W. N. Meier, and R. Gersten, 2017b: Variability and trends in the Arctic Sea ice cover: Results from different techniques. *J. Geophys. Res.-Oceans*, **122**, 6883-6900, https://doi.org/10.1002/2017JC012768.

Duffy-Anderson, J. T., and Coauthors, 2019: Responses of the northern Bering Sea and southeastern Bering Sea pelagic ecosystems following record-breaking low winter sea ice. *Geophys. Res. Lett.*, **46**, 9833-9842, https://doi.org/10.1029/2019GL083396.

Frey, K. E., J. C. Comiso, L. W. Cooper, J. M. Grebmeier and L. V. Stock, 2018: Arctic Ocean Primary Productivity: The response of marine algae to climate warming and sea ice decline. *Arctic Report Card 2018*, E. Osborne, J. Richter-Menge, and M. Jeffries, Eds., https://www.arctic.noaa.gov/Report-Card.

Frey, K. E., J. C. Comiso, L. W. Cooper, J. M. Grebmeier and L. V. Stock, 2019: Arctic Ocean Primary Productivity: The response of marine algae to climate warming and sea ice decline. *Arctic Report Card 2019*, J. Richter-Menge, M. L. Druckenmiller, and M. Jeffries, Eds., https://www.arctic.noaa.gov/Report-Card.

Giesbrecht, K. E., D. E. Varela, J. Wiktor, J. M. Grebmeier, B. Kelly, and J. E. Long, 2019: A decade of summertime measurements of phytoplankton biomass, productivity and assemblage composition in the Pacific Arctic Region from 2006 to 2016. *Deep-Sea Res. Part II Top. Stud. Oceanogr.*, **162**, 93-113, https://doi.org/10.1016/j.dsr2.2018.06.010.

Henley, S. F., M. Porter, L. Hobbs, J. Braun, R. Guillaume-Castel, E. J. Venables, E. Dumont, and F. Cottier, 2020: Nitrate supply and uptake in the Atlantic Arctic sea ice zone: seasonal cycle, mechanisms and drivers. *Philos. Trans. Royal Soc. A*, **378**, 20190361, https://doi.org/10.1098/rsta.2019.0361.

Hill, V., M. Ardyna, S. H. Lee, and D. E. Varela, 2018: Decadal trends in phytoplankton production in the Pacific Arctic Region from 1950 to 2012. *Deep-Sea Res. Part II Top. Stud. Oceanogr.*, **152**, 82-94, https://doi.org/10.1016/j.dsr2.2016.12.015.

Lalande, C., J. M. Grebmeier, R. R. Hopcroft and S. Danielson, 2020: Annual cycle of export fluxes of biogenic matter near Hanna Shoal in the northeast Chukchi Sea. *Deep-Sea Res. Part II Top. Stud. Oceanogr.*, **177**, 104730, https://doi.org/10.1016/j.dsr2.2020.104730.

Lalande, C., E. -M. Nöthig, and L. Fortier, 2019: Algal export in the Arctic Ocean in times of global warming. *Geophys. Res. Lett.*, **46**, 5959-5967, https://doi.org/10.1029/2019GL083167.

Leu, E., C. J. Mundy, P. Assmy, K. Campbell, T. M. Gabrielsen, M. Gosselin, T. Juul-Pedersen, and R. Gradinger, 2015: Arctic spring awakening – Steering principles behind the phenology of vernal ice algal blooms. *Prog. Oceanogr.*, **139**, 151-170, https://doi.org/10.1016/j.pocean.2015.07.012.

Lewis, K. M., G. L. van Dijken, and K. R. Arrigo, 2020: Changes in phytoplankton concentration now drive increased Arctic Ocean primary production. *Science*, **369**, 198-202, https://doi.org/10.1126/science.aay8380.

Neeley, A. R., L. A. Harris, and K. E. Frey, 2018: Unraveling phytoplankton community dynamics in the northern Chukchi Sea under sea-ice-covered and sea-ice-free conditions. *Geophys. Res. Lett.*, **45**, 7663-7671, https://doi.org/10.1029/2018GL077684.

Randelhoff, A., and Coauthors, 2020: Arctic mid-winter phytoplankton growth revealed by autonomous profilers. *Sci. Adv.*, **6**, eabc2678, https://doi.org/10.1126/sciadv.abc2678.

Stabeno, P., and S. W. Bell, 2019: Extreme conditions in the Bering Sea (2017-2018): record-breaking low sea-ice extent. *Geophys. Res. Lett.*, **46**, 8952-8959, https://doi.org/10.1029/2019GL083816.

Tremblay J. -É., L. G. Anderson, P. Matrai, P. Coupel, S. Bélanger, C. Michel, and M. Reigstad, 2015: Global and regional drivers of nutrient supply, primary production and CO_2 drawdown in the changing Arctic Ocean. *Prog. Oceanogr.*, **139**, 171-196, https://doi.org/10.1016/j.pocean.2015.08.009.

November 16, 2020

Tundra Greenness

DOI: 10.25923/46rm-0w23

G. V. Frost[1], U. S. Bhatt[2], H. E. Epstein[3], I. Myers-Smith[4], G. K. Phoenix[5], L. T. Berner[6], J. W. Bjerke[7], B. C. Forbes[8], M. J. Macander[1], S. J. Goetz[6], J. T. Kerby[9], T. Park[10,11], M. K. Raynolds[12], H. Tømmervik[7], and D. A. Walker[12]

[1]Alaska Biological Research, Inc., Fairbanks, AK, USA
[2]Geophysical Institute, University of Alaska Fairbanks, Fairbanks, AK, USA
[3]Department of Environmental Sciences, University of Virginia, Charlottesville, VA, USA
[4]School of GeoSciences, University of Edinburgh, Edinburgh, UK
[5]Department of Animal and Plant Sciences, University of Sheffield, Sheffield, UK
[6]School of Informatics, Computing and Cyber Systems, Northern Arizona University, Flagstaff, AZ, USA
[7]Norwegian Institute for Nature Research, FRAM - High North Research Centre for Climate and the Environment, Tromsø, Norway
[8]Arctic Centre, University of Lapland, Rovaniemi, Finland
[9]Aarhus Institute of Advanced Studies, Aarhus University, Aarhus, Denmark
[10]Ames Research Center, NASA, Mountain View, CA, USA
[11]Bay Area Environmental Research Institute, Moffett Field, Mountain View, CA, USA
[12]Institute of Arctic Biology, University of Alaska Fairbanks, Fairbanks, AK, USA

Highlights

- In North America, tundra productivity for the 2019 growing season (the most recent data available) rebounded strongly from the previous year, in tandem with record summer warmth following the cold summer of 2018.
- Since 2016, greenness trends have diverged strongly by continent; peak summer greenness has declined sharply in North America but has remained above the long-term mean in Eurasia.
- The long-term satellite record (1982-2019) indicates "greening" across most of the Arctic but some regions exhibit "browning," underscoring the dynamic linkages that exist between tundra ecosystems and other elements of a changing Arctic system.

The Arctic tundra biome occupies Earth's northernmost landmasses and forms a "wreath" of treeless vegetation that encircles the Arctic Ocean. Arctic tundra ecosystems are strongly influenced by warming air temperatures (Bjorkman et al. 2020), and thus have become a focal point of global environmental change. One of the most conspicuous impacts of a warming Arctic climate and declining sea ice has been an increase in the productivity, or "greenness" of tundra vegetation (Lawrence et al. 2008; Bhatt et al. 2010; see essays *Surface Air Temperature* and *Sea Ice*). Tundra greenness has been monitored by Earth-observing satellites since the early 1980s and was identified as a key vital sign of the Arctic in the first Arctic Report Card published in 2006 (Richter-Menge et al. 2006). Satellites continue to monitor tundra greenness to the present day, although at the time of writing the record is only available through the 2019 growing season due to data processing requirements. Arctic greening has continued but interannual variability in greenness has increased over the past decade and trends have not been uniform from place to place or from year to year (Bhatt et al. 2013; National Academies of Sciences,

Engineering and Medicine 2019; Myers-Smith et al. 2020). This interannual variability results from the dynamic linkages that connect the vegetation, atmosphere, sea ice, permafrost, seasonal snow, soils, disturbance processes, and wildlife of the Arctic (Duncan et al. 2020).

The combination of gradual and abrupt changes occurring in Arctic landscapes have consequences that extent beyond other elements of the Arctic environment, to the global atmosphere and climate system (Post et al. 2019). Changes in the species composition, height, and biomass of tundra vegetation impact the biogeochemical cycling of carbon and nutrients in Arctic soils (Hewitt et al. 2019; Natali et al. 2019; Turetsky et al. 2019; Hugelius et al. 2020), as well as the distribution of snow on the landscape, the timing of spring snowmelt, and the exchange of energy between Earth's atmosphere and permafrost (Wilcox et al. 2019; Grünberg et al. 2020). Permafrost thaw can dramatically affect vegetation, as well as surface topography, geomorphology, and surface wetness (Farquharson et al. 2019; Turetsky et al. 2020), which can further amplify changes to wildlife habitats (Kwon et al. 2019; Andruko et al. 2020; Skarin et al. 2020) and the availability of subsistence resources that are vital to the economy and food security of Arctic peoples (Bronen et al. 2020; Herman-Mercer et al. 2020).

In late 1981, NOAA Earth-observing satellites began acquiring daily "snapshots" of global vegetation productivity using the Advanced Very High Resolution Radiometer (AVHRR). This dataset has continued through the 2019 Arctic growing season. Satellite observations of tundra productivity use a spectral index termed the Normalized Difference Vegetation Index (NDVI), which is sensitive to the unique way in which green vegetation reflects light in the Red and Near-Infrared wavelengths. NDVI values are strongly correlated with the quantity of aboveground vegetation, or "greenness," of Arctic tundra (Raynolds et al. 2012). The dataset reported here is the Global Inventory Modeling and Mapping Studies 3g V1.2 dataset (GIMMS-3g+), which is based upon corrected and calibrated AVHRR data. GIMMS-3g+ consists of a global composite of the maximum NDVI value observed every 15-16 days within 1/12° grid cells, or "pixels" (Pinzon and Tucker 2014). We use two metrics based on GIMMS-3g+. MaxNDVI is the peak NDVI value for the calendar year and corresponds to maximum aboveground live biomass during the Arctic summer, typically recorded in late July or early August. TI-NDVI is the time-integrated NDVI, calculated as the sum of all biweekly NDVI values >0.05 (i.e., collected during the growing season) and is correlated with the total aboveground vegetation productivity over the summer. Average NDVI values for North American tundra are lower than in Eurasia because a large proportion of the North American Arctic lies in the very cold, dry High Arctic and a comparatively shorter period of time has been available for soils development after Pleistocene glaciation in this region (Walker et al. 2005).

The GIMMS-3g+ record indicates both MaxNDVI and TI-NDVI have increased across most of the Arctic over the last 38 years (1982-2019) (Figs. 1a,b). There is strong regional variability in trends, however, with areas of strong greening on Alaska's North Slope, the Low Arctic of mainland Canada, and the Chukotka Peninsula in far eastern Russia. Tundra greenness appears to be declining ("browning"), however, in southwestern Alaska, the Canadian Arctic Archipelago, and northwestern Siberia. Regional "hotspots" of trend are generally consistent between the two NDVI metrics, but the declines in TI-NDVI tend to be more pronounced than for MaxNDVI.

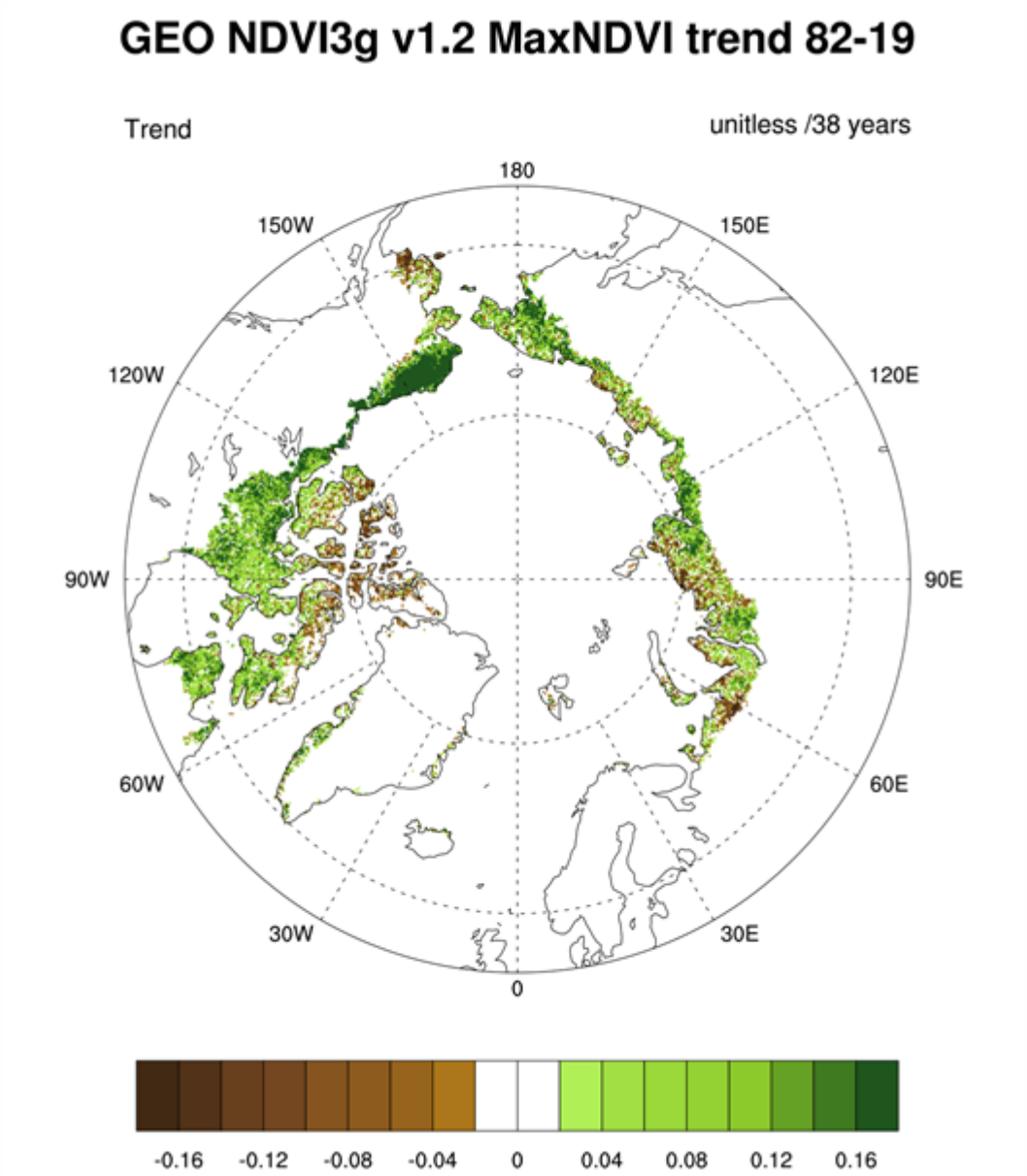

Fig. 1a. Magnitude of the overall trend in MaxNDVI (Maximum Normalized Difference Vegetation Index) for the 38-year period, 1982–2019.

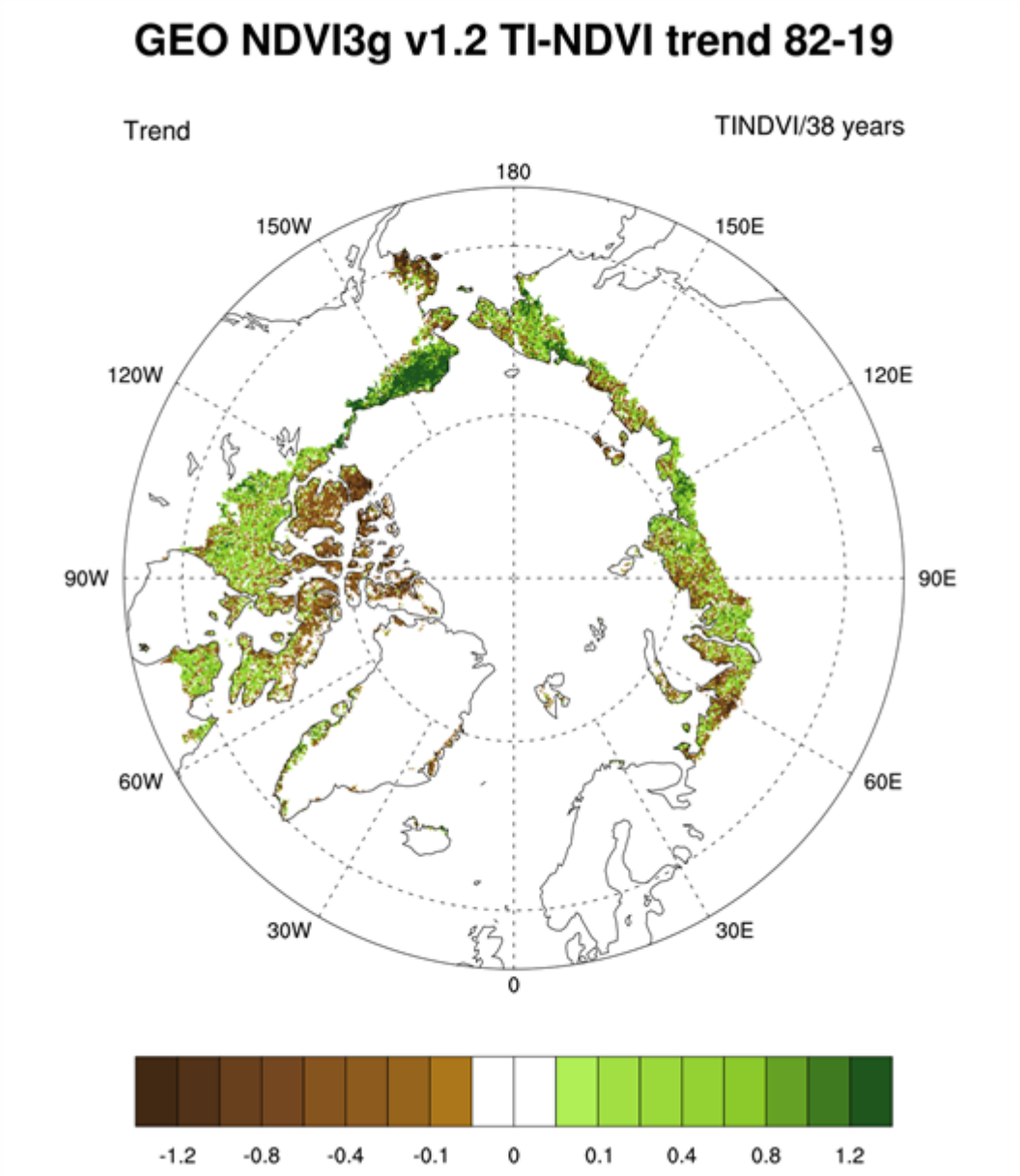

Fig. 1b. Magnitude of the overall trend in TI-NDVI (Time-integrated Normalized Difference Vegetation Index) for the 38-year period, 1982–2019.

In 2019, the mean MaxNDVI value for the circumpolar Arctic declined 2% from the previous year (Fig. 2a), marking the third straight year of MaxNDVI decline after the record high value set in 2016. Over the last 3 years, there have been striking contrasts in MaxNDVI variability by continent. In the Eurasian Arctic, the 2019 value was similar to the preceding four years, being 3% higher than the 1982-2019 mean. In the North American Arctic, however, the 2019 MaxNDVI value was the lowest in the record since 1996 and was 2% below the long-term mean. In contrast to MaxNDVI, there was a 5% increase in circumpolar mean TI-NDVI from the previous year (Fig. 2b). This increase was particularly strong in the North American Arctic, where TI-NDVI rebounded after the unusually slow growing season of 2018 associated with relatively cold summer temperatures (Overland et al. 2018). The 2019 TI-NDVI marked the third largest single-year increase (9%) in the entire record for North America. Nonetheless, the 2019

TI-NDVI for the circumpolar region was 4% lower than the 1982-2019 mean, marking the second lowest value since 1993.

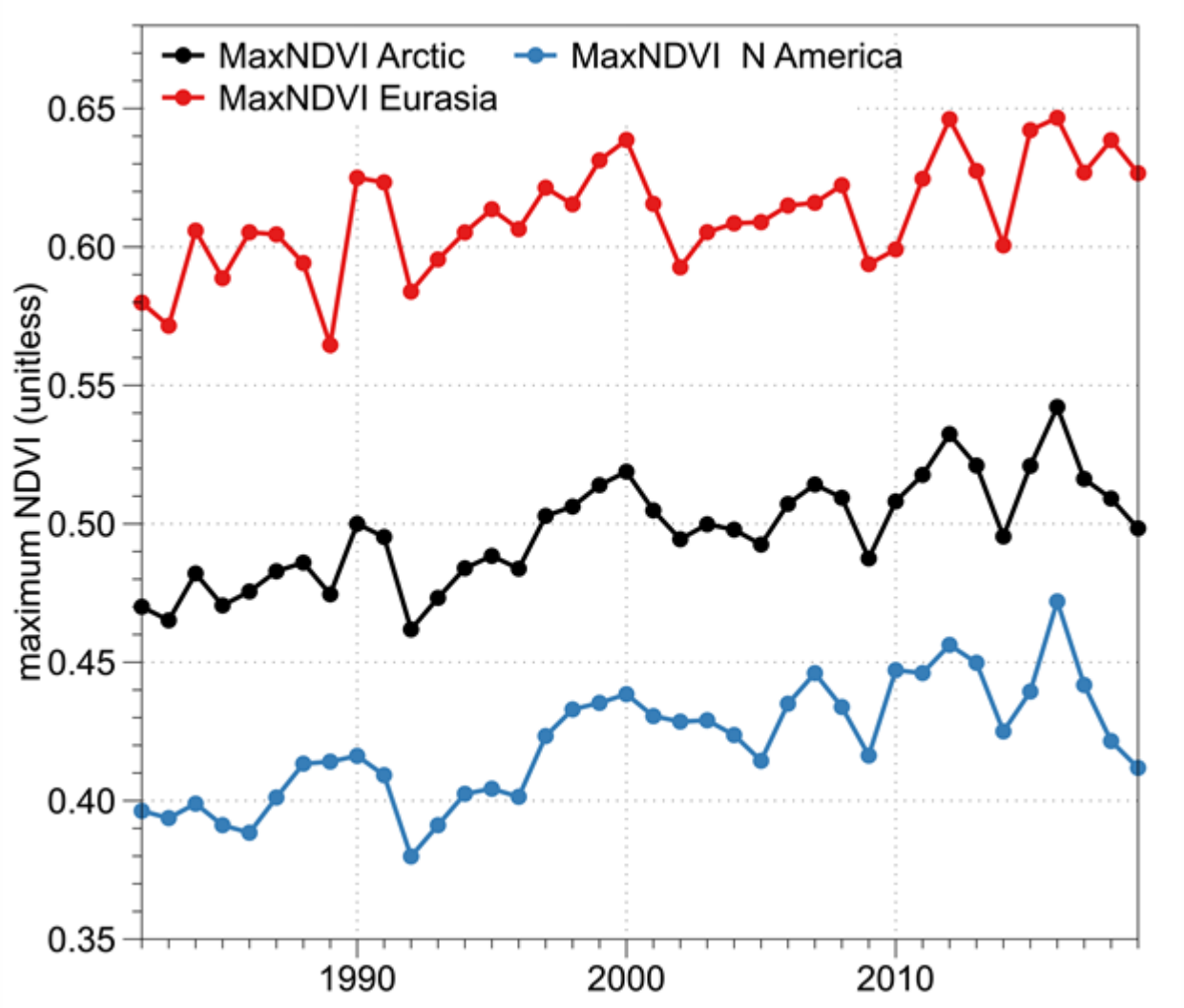

Fig. 2a. MaxNDVI (Maximum Normalized Difference Vegetation Index) during 1982-2019 for the North American Arctic (bottom, in blue), Eurasian Arctic (top, in red), and the circumpolar Arctic (middle, in black).

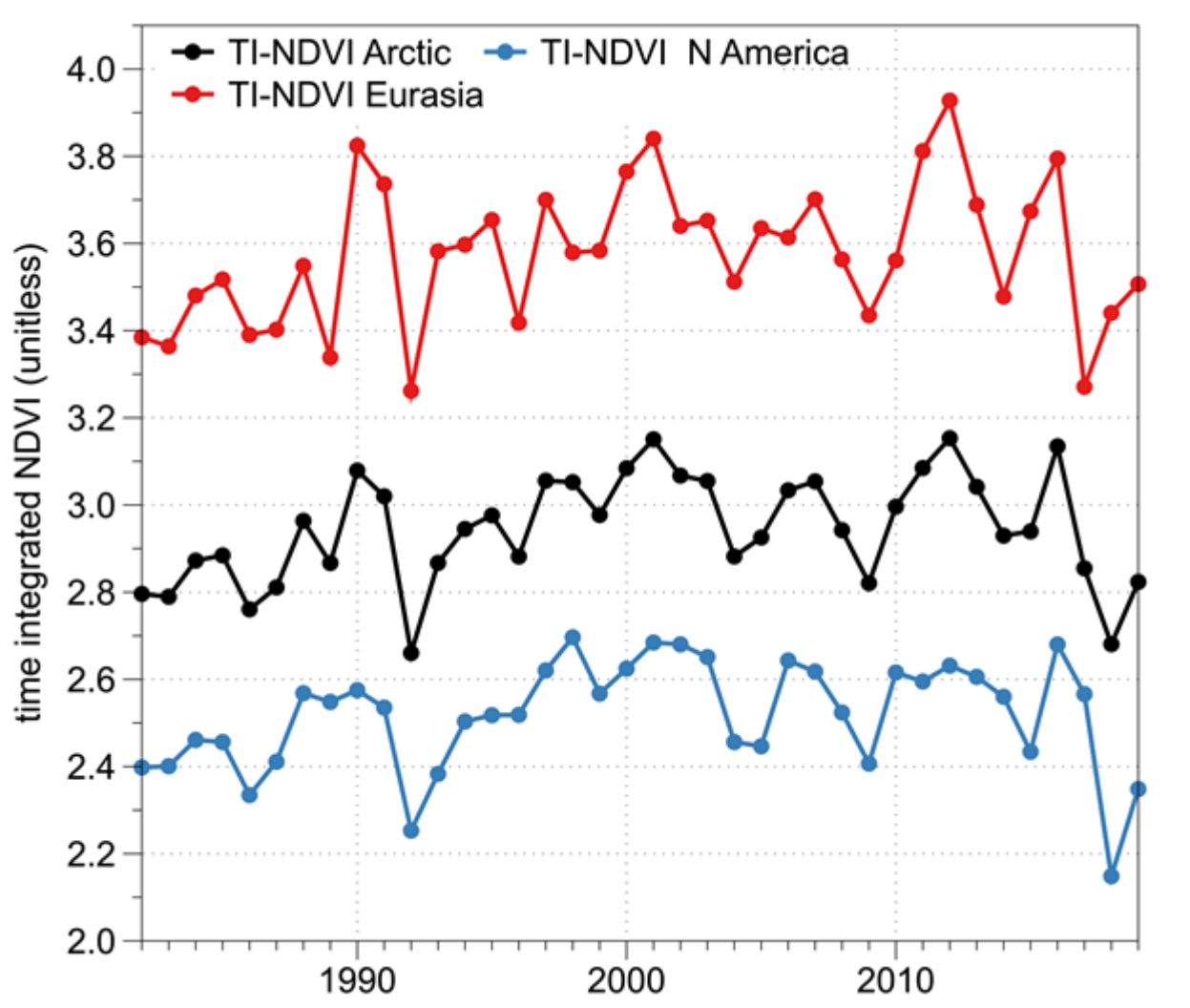

Fig. 2b. TI-NDVI (Time-integrated Normalized Difference Vegetation Index) during 1982-2019 for the North American Arctic (bottom, in blue), Eurasian Arctic (top, in red), and the circumpolar Arctic (middle, in black).

The AVHRR sensors that record NDVI also record Land Surface Temperature (LST), a key control of tundra productivity that provides context for understanding spatio-temporal patterns of tundra greenness and phenology (Arndt et al. 2019; Park et al. 2019; Xu et al. 2019, 2020). A useful metric of growing conditions is the Summer Warmth Index (SWI), the sum of mean monthly LST values for months with mean temperatures above freezing, expressed as °C-months. The 2019 growing season was the warmest in the entire record for both continents; the mean SWI for the full circumpolar region (39.0°C-months) broke the previous record (34.9°C-months in 2016; Overland et al. 2019). In the North American Arctic, record warmth was especially noteworthy because summer temperatures averaged well below normal in the previous year. Interestingly, the record warmth in the North American Arctic was not accompanied by strong increases in MaxNDVI in 2019, possibly due to lag effects arising from cold conditions a year earlier.

Greening dominates trends in Arctic NDVI since 1982. Many site-specific studies have detected an associated increase in the abundance of taller plants, particularly tundra shrubs (Bjorkman et al. 2018; Andreu-Hayles et al. 2020, Shevtsova et al. 2020; Thomas et al. 2020). However, greening is not

happening everywhere. Over the past 15 years, browning—a reduction in plant biomass that can occur as a trend over decadal timescales, or as an abrupt, extreme event within a year—has emerged as an increasingly important phenomenon (Phoenix and Bjerke 2016) that is now contributing to greater complexity of Arctic vegetation trends (Myers-Smith et al. 2020). Browning trends can arise from reduced summer warmth or prolonged winter snow cover that reduce productivity (Bieniek et al. 2015; Cao et al. 2020). Episodic events can also cause die-back or removal of vegetation, including wildfire (Rocha and Shaver 2011; Frost et al. 2020; see essay *Wildland Fire*), permafrost thaw (Turetsky et al. 2020; Verdonen et al. 2020), abrupt temperature changes or extreme weather events (Bokhorst et al. 2009), and herbivore and pest outbreaks (Lund et al. 2017; Prendin et al. 2020). Severe event-driven browning led to major reductions in ecosystem CO_2 fluxes in the European Arctic (Treharne et al. 2020). While Arctic warming is likely to continue to drive greening, drivers of browning are also increasing in frequency (Hu et al. 2015; Vikhamar-Schuler et al. 2016; Wu et al. 2020), highlighting the emergence of increased variability as a component of Arctic climate change.

GIMMS-3g+ is a legacy dataset that provides by far the longest continuous record for the entire Arctic of any spaceborne record. However, MaxNDVI datasets compiled from more recent satellites with higher spatial resolution can be used to corroborate the GIMMS-3g+ record and provide context for understanding what the NDVI changes represent on the ground. Estimates of the proportion of statistically significant NDVI trends vary with 42% greening and 3% browning during 1982-2014 in GIMMS-3g+ (Park et al. 2016), to 20% greening and 4% browning during 2000-2016 in 30 m resolution Landsat data (Berner et al. 2020), and 13% greening and 1% browning during 2000-2018 for 250 m resolution Moderate Resolution Imaging Spectroradiometer (MODIS) data (Myers-Smith et al. 2020). The different spatial resolutions and durations of satellite time-series make direct comparisons difficult, but the picture that emerges from spaceborne datasets is that of an overall greener Arctic (Beamish et al. 2020; Myers-Smith et al. 2020). A rapidly growing area of Arctic greening research is the incorporation of new types of high-resolution data collection to bridge scale gaps between satellite observations and ground-based ecological monitoring (Cunliffe et al. 2020; Siewert and Olofsson 2020; Yang et al. 2020; Assmann et al. 2020). Airborne and drone data collection campaigns in recent years are also shedding new light on Arctic greening (Miller et al. 2019). Continued monitoring of Arctic landscapes from space and field studies improves our understanding of Arctic environmental change and its implications in Earth's northernmost lands and beyond.

References

Andreu-Hayles, L., B. V. Gaglioti, L. T. Berner, M. Levesque, K. J. Anchukaitis, S. J. Goetz, and R. D'Arrigo, 2020: A narrow window of summer temperatures associated with shrub growth in Arctic Alaska. *Environ. Res. Lett.*, **15**, 105012, https://doi.org/10.1088/1748-9326/ab897f.

Andruko, R., R. Danby, and P. Grogan, 2020: Recent growth and expansion of birch shrubs across a Low Arctic landscape in continental Canada: Are these responses more a consequence of the severely declining caribou herd than of climate warming? *Ecosystems*, **23**, 1362-1379, https://doi.org/10.1007/s10021-019-00474-7.

Arndt, K. A., and Coauthors, 2019: Arctic greening associated with lengthening growing seasons in Northern Alaska. *Environ. Res. Lett.*, **14**, 125018, https://doi.org/10.1088/1748-9326/ab5e26.

Assmann, J. J., I. Myers-Smith, J. Kerby, A. M. Cunliffe, and G. N. Daskalova, 2020: Drone data reveal heterogeneity in tundra greenness and phenology not captured by satellites. *Environ. Res. Lett.*, **15**, 125002, https://doi.org/10.1088/1748-9326/abbf7d.

Beamish, A., and Coauthors, 2020: Recent trends and remaining challenges for optical remote sensing of Arctic tundra vegetation: A review and outlook. *Remote Sens. Environ.*, **246**, 111872, https://doi.org/10.1016/j.rse.2020.111872.

Berner, L. T., and Coauthors, 2020: Summer warming explains widespread but not uniform greening in the Arctic tundra biome. *Nat. Commun.*, **11**, 4621, https://doi.org/10.1038/s41467-020-18479-5.

Bhatt, U., and Coauthors, 2010: Circumpolar Arctic tundra vegetation change linked to sea ice decline. *Earth Interact.*, **14**, 1-20, https://doi.org/10.1175/2010EI315.1.

Bhatt, U., and Coauthors, 2013: Recent declines in warming and vegetation greening trends over Pan-Arctic tundra. *Remote Sens.*, **5**, 4229-4254, https://doi.org/10.3390/rs5094229.

Bieniek, P. A., and Coauthors, 2015: Climate drivers linked to changing seasonality of Alaska coastal tundra vegetation productivity. *Earth Interact.*, **19**, 1-29, https://doi.org/10.1175/EI-D-15-0013.1.

Bjorkman, A. D., and Coauthors, 2018: Plant functional trait change across a warming tundra biome. *Nature*, **562**, 57-62, https://doi.org/10.1038/s41586-018-0563-7.

Bjorkman, A. D., and Coauthors, 2020: Status and trends in Arctic vegetation: Evidence from experimental warming and long-term monitoring. *Ambio*, **49**, 678-692, https://doi.org/10.1007/s13280-019-01161-6.

Bokhorst, S. F., J. W. Bjerke, H. Tømmervik, T. V. Callaghan, and G. K. Phoenix, 2009: Winter warming events damage sub-Arctic vegetation: consistent evidence from an experimental manipulation and a natural event. *J. Ecol.*, **97**, 1408-1415, https://doi.org/10.1111/j.1365-2745.2009.01554.x.

Bronen, R., D. Pollock, J. Overbeck, D. Stevens, S. Natali, and C. Maio, 2020: Usteq: integrating indigenous knowledge and social and physical sciences to coproduce knowledge and support community-based adaptation. *Polar Geogr.*, **43**, 188-205, https://doi.org/10.1080/1088937X.2019.1679271.

Cao, R., Y. Feng, X. Liu, M. Shen, and J. Zhou, 2020: Uncertainty of vegetation green-up date estimated from vegetation indices due to snowmelt at northern middle and high latitudes. *Remote Sens.*, **12**, 190, https://doi.org/10.3390/rs12010190.

Cunliffe, A. M., J. J. Assmann, G. Daskalova, J. T. Kerby, and I. H. Myers-Smith: Aboveground biomass corresponds strongly with drone-derived canopy height but weakly with greenness (NDVI) in a shrub tundra landscape. *Environ. Res. Lett.*, **15**(12), 125004, https://doi.org/10.1088/1748-9326/aba470.

Duncan, B. N., and Coauthors, 2020: Space-based observations for understanding changes in the Arctic-boreal zone. *Rev. Geophys.*, **58**, e2019RG000652, https://doi.org/10.1029/2019RG000652.

Farquharson, L. M., V. E. Romanovsky, W. L. Cable, D. A. Walker, S. V. Kokelj, and D. Nicolsky, 2019: Climate change drives widespread and rapid thermokarst development in very cold permafrost in the Canadian High Arctic. *Geophys. Res. Lett.*, **46**, 6681-6689, https://doi.org/10.1029/2019GL082187.

Frost, G. V., R. A. Loehman, L. B. Saperstein, M. J. Macander, P. R. Nelson, D. P. Paradis, and S. M. Natali, 2020: Multi-decadal patterns of vegetation succession after tundra fire on the Yukon-Kuskokwim Delta, Alaska. *Environ. Res. Lett.*, **15**, 025003, https://doi.org/10.1088/1748-9326/ab5f49.

Grünberg, I., E. J. Wilcox, S. Zwieback, P. Marsh, and J. Boike, 2020: Linking tundra vegetation, snow, soil temperature, and permafrost. *Biogeosciences*, **17**, 4261-4279, https://doi.org/10.5194/bg-17-4261-2020.

Herman-Mercer, N. M., R. A. Loehman, R. C. Toohey, and C. Paniyak, 2020: Climate- and disturbance-driven changes in subsistence berries in coastal Alaska: Indigenous knowledge to inform ecological inference. *Hum. Ecol.*, **48**, 85-99, https://doi.org/10.1007/s10745-020-00138-4.

Hewitt, R. E., D. L. Taylor, H. Genet, A. D. McGuire, and M. C. Mack, 2019: Below-ground plant traits influence tundra plant acquisition of newly thawed permafrost nitrogen. *J. Ecol.*, **107**, 950-962, https://doi.org/10.1111/1365-2745.13062.

Hu, F. S., P. E. Higuera, P. Duffy, M. L. Chipman, A. V. Rocha, A. M. Young, R. Kelly, and M. C. Dietze, 2015: Arctic tundra fires: natural variability and responses to climate change. *Front. Ecol. Environ.*, **13**, 369-377, https://doi.org/10.1890/150063.

Hugelius, G., and Coauthors, 2020: Large stocks of peatland carbon and nitrogen are vulnerable to permafrost thaw. *P. Natl. A. Sci.*, **117**, 20438-20446, https://doi.org/10.1073/pnas.1916387117.

Kwon, E., and Coauthors, 2019: Geographic variation in the intensity of warming and phenological mismatch between Arctic shorebirds and invertebrates. *Ecol. Monogr.*, **89**, e01383, https://doi.org/10.1002/ecm.1383.

Lawrence, D. M., A. G. Slater, R. A. Tomas, M. M. Holland, and C. Deser, 2008: Accelerated Arctic land warming and permafrost degradation during rapid sea ice loss. *Geophys. Res. Lett.*, **35**, L11506, https://doi.org/10.1029/2008GL033985.

Lund, M., K. Raundrup, A. Westergaard-Nielsen, E. López-Blanco, J. Nymand, and P. Aastrup, 2017: Larval outbreaks in West Greenland: Instant and subsequent effects on tundra ecosystem productivity and CO_2 exchange. *Ambio*, **46**, 26-38, https://doi.org/10.1007/s13280-016-0863-9.

Miller, C. E., and Coauthors, 2019: An overview of ABoVE airborne campaign data acquisitions and science opportunities. *Environ. Res. Lett.*, **14**, 080201, https://doi.org/10.1088/1748-9326/ab0d44.

Myers-Smith, I. H., and Coauthors, 2020: Complexity revealed in the greening of the Arctic. *Nat. Climate Change*, **10**, 106-117, https://doi.org/10.1038/s41558-019-0688-1.

Natali, S. M., and Coauthors, 2019: Large loss of CO_2 in winter observed across the northern permafrost region. *Nat. Climate Change*, **9**, 852-857, https://doi.org/10.1038/s41558-019-0592-8.

National Academies of Sciences, Engineering and Medicine, 2019: Understanding northern latitude vegetation greening and browning: proceedings of a workshop, A. Melvin, Ed. The National Academies Press.

Overland, J. E., E. Hanna, I. Hanssen-Bauer, S. -J. Kim, J. E. Walsh, M. Wang, U. S. Bhatt, and R. L. Thoman, 2018: Surface Air Temperature. Arctic Report Card 2018, E. Osborne, J. Richter-Menge, and M. Jeffries, Eds., https://www.arctic.noaa.gov/Report-Card.

Overland, J. E., E. Hanna, I. Hanssen-Bauer, S. -J. Kim, J. E. Walsh, M. Wang, U. S. Bhatt, R. L. Thoman, and T. J. Ballinger, 2019: Surface Air Temperature. Arctic Report Card 2019, J. Richter-Menge, M. L. Druckenmiller, and M. Jeffries, Eds., http://www.arctic.noaa.gov/Report-Card.

Park, T., and Coauthors, 2016: Changes in growing season duration and productivity of northern vegetation inferred from long-term remote sensing data. *Environ. Res. Lett.*, **11**, 084001, https://doi.org/10.1088/1748-9326/11/8/084001.

Park, T., and Coauthors, 2019: Changes in timing of seasonal peak photosynthetic activity in northern ecosystems. *Glob. Change Biol.*, **25**, 2382-2395, https://doi.org/10.1111/gcb.14638.

Phoenix, G. K., and J. W. Bjerke, 2016: Arctic browning: extreme events and trends reversing arctic greening. *Glob. Change Biol.*, **22**, 2960-2962, https://doi.org/10.1111/gcb.13261.

Pinzon, J. E., and C. J. Tucker, 2014: A non-stationary 1981-2012 AVHRR NDVI3g time series. *Remote Sens.*, **6**, 6929-6960, https://doi.org/10.3390/rs6086929.

Post, E., and Coauthors, 2019: The polar regions in a 2°C warmer world. *Sci. Advances*, **5**, eaaw9883, https://doi.org/10.1126/sciadv.aaw9883.

Prendin, A. L., and Coauthors, 2020: Immediate and carry-over effects of insect outbreaks on vegetation growth in West Greenland assessed from cells to satellite. *J. Biogeogr.*, **47**, 87-100, https://doi.org/10.1111/jbi.13644.

Raynolds, M. K., D. A. Walker, H. E. Epstein, J. E. Pinzon, and C. J. Tucker, 2012: A new estimate of tundra-biome phytomass from trans-Arctic field data and AVHRR NDVI. *Remote Sens. Lett.*, **3**, 403-411, https://doi.org/10.1080/01431161.2011.609188.

Richter-Menge, J., and Coauthors, 2006: State of the Arctic Report. NOAA/OAR/PMEL, https://www.arctic.noaa.gov/Report-Card/Report-Card-Archive.

Rocha, A. V., and G. R. Shaver, 2011: Postfire energy exchange in arctic tundra: the importance and climatic implications of burn severity. *Glob. Change Biol.*, **17**, 2831-2841, https://doi.org/10.1111/j.1365-2486.2011.02441.x.

Shevtsova, I., B. Heim, S. Kruse, J. Schröder, E. I. Troeva, L. A. Pestryakova, E. S. Zakharov, and U. Herzschuh, 2020: Strong shrub expansion in tundra-taiga, tree infilling in taiga and stable tundra in central Chukotka (north-eastern Siberia) between 2000 and 2017. *Environ. Res. Lett.*, **15**, 085006, https://doi.org/10.1088/1748-9326/ab9059.

Siewert, M. B., and J. Olofsson, 2020: Scale-dependency of Arctic ecosystem properties revealed by UAV. *Environ. Res. Lett.*, **15**, 094030, https://doi.org/10.1088/1748-9326/aba20b.

Skarin, A., M. Verdonen, T. Kumpula, M. Macias-Fauria, M. Alam, J. T. Kerby, and B. C. Forbes, 2020: Reindeer use of low Arctic tundra correlates with landscape structure. *Environ. Res. Lett.*, **15**, 115012, https://doi.org/10.1088/1748-9326/abbf15.

Thomas, H. J. D., and Coauthors, 2020: Global plant trait relationships extend to the climatic extremes of the tundra biome. *Nat. Commun.*, **11**, 1351, https://doi.org/10.1038/s41467-020-15014-4.

Treharne, R., J. W. Bjerke, H. Tømmervik, and G. K. Phoenix, 2020: Extreme event impacts on CO_2 fluxes across a range of high latitude, shrub-dominated ecosystems. *Environ. Res. Lett.*, **15**, 104084, https://doi.org/10.1088/1748-9326/abb0b1.

Turetsky, M. R., and Coauthors, 2019: Permafrost collapse is accelerating carbon release. *Nature*, **569**, 32-34, https://doi.org/10.1038/d41586-019-01313-4.

Turetsky, M. R., and Coauthors, 2020: Carbon release through abrupt permafrost thaw. *Nat. Geosci.*, **13**, 138-143, https://doi.org/10.1038/s41561-019-0526-0.

Verdonen, M., L. T. Berner, B. C. Forbes, and T. Kumpula, 2020: Periglacial vegetation dynamics in Arctic Russia: decadal analysis of tundra regeneration on landslides with time series satellite imagery. *Environ. Res. Lett.*, **15**, 105020, https://doi.org/10.1088/1748-9326/abb500.

Vikhamar-Schuler, D., K. Isaksen, J. E. Haugen, H. Tømmervik, B. Luks, T. V. Schuler, and J. W. Bjerke, 2016: Changes in winter warming events in the Nordic arctic region. *J. Climate*, **29**, 6223-6244, https://doi.org/10.1175/JCLI-D-15-0763.1.

Walker, D. A., and Coauthors, 2005: The circumpolar Arctic vegetation map. *J. Veg. Sci.*, **16**, 267-282.

Wilcox, E. J., D. Keim, T. de Jong, B. Walker, O. Sonnentag, A. E. Sniderhan, P. Mann, and P. Marsh, 2019: Tundra shrub expansion may amplify permafrost thaw by advancing snowmelt timing. *Arctic Sci.*, **5**, 202-217, https://doi.org/10.1139/as-2018-0028.

Wu, W., X. Sun, H. Epstein, X. Xu, and X. Li, 2020: Spatial heterogeneity of climate variation and vegetation response for Arctic and high-elevation regions from 2001-2018. *Environ. Res. Commun.*, **2**, 011007, https://doi.org/10.1088/2515-7620/ab6369.

Xu, X., W. J. Riley, C. D. Koven, and G. Jia, 2019: Heterogeneous spring phenology shifts affected by climate: supportive evidence from two remotely sensed vegetation indices. *Environ. Res. Commun.*, **1**, 091004, https://doi.org/10.1088/2515-7620/ab3d79.

Xu, X., W. J. Riley, C. D. Koven, G. Jia, and X. Zhang, 2020: Earlier leaf-out warms air in the north. *Nat. Climate Chang*e, **10**, 370-375, https://doi.org/10.1038/s41558-020-0713-4.

Yang, D., and Coauthors, 2020: A multi-sensor Unoccupied Aerial System improves characterization of vegetation composition and canopy properties in the Arctic tundra. *Remote Sens.*, **12**, 2638, https://doi.org/10.3390/rs12162638.

November 9, 2020

Glaciers and Ice Caps Outside Greenland

DOI: 10.25923/nwqq-8736

G. J. Wolken[1,2], B. Wouters[3,4], M. Sharp[5], L. M. Andreassen[6], D. Burgess[7], J. Kohler[8], and B. Luks[9]

[1]International Arctic Research Center, University of Alaska Fairbanks, Fairbanks, AK, USA
[2]Alaska Division of Geological & Geophysical Surveys, Fairbanks, AK, USA
[3]Institute for Marine and Atmospheric Research, Utrecht University, Utrecht, The Netherlands
[4]Department of Geoscience & Remote Sensing, Delft University of Technology, Delft, The Netherlands
[5]Department of Earth and Atmospheric Sciences, University of Alberta, Edmonton, AB, Canada
[6]Section for Glaciers, Ice and Snow, Norwegian Water Resources and Energy Directorate, Oslo, Norway
[7]Geological Survey of Canada, Ottawa, ON, Canada
[8]Norwegian Polar Institute, Tromsø, Norway
[9]Institute of Geophysics, Polish Academy of Sciences, Warsaw, Poland

Highlights

- Observations of glaciers and ice caps outside Greenland from 2018 and 2019 (the most recent data available) show regional variations in mass change, and a continuing trend of significant ice loss throughout the Arctic.
- Ice loss in 2018 and 2019 was dominated largely by melting in Alaska, Arctic Canada, and Svalbard, in association with anomalously warm air temperatures, with 2019 producing the most negative mass balance year on record for the combined Alaska glaciers.
- The estimated total mass loss for Arctic glaciers and ice caps as a whole during the combined GRACE and GRACE-FO period (2002-19) is -164 ± 23.8 Gt yr^{-1}, which is equal to a global sea level rise contribution of approximately 0.4 mm yr^{-1}.

Introduction

Numerous glaciers and ice caps, in multiple climatic zones, occupy land areas in the Arctic outside Greenland. They exist where the rate of snow accumulation exceeds the rate of melt by atmospheric heat. Although their potential longer-term contribution to sea level rise is small compared to the ice sheets of Antarctica and Greenland, on the short term these smaller land ice masses have contributed disproportionately to recent sea level rise in response to continued atmospheric warming (Gardner et al. 2011, 2013; Jacob et al. 2012; Millan et al. 2017; Wouters et al. 2019). Observations of glaciers and ice caps from 2018 and 2019 (the most recent data available) show regional variations in mass change and a continuing trend of significant ice loss throughout the Arctic and especially in Alaska and Arctic Canada.

Measurements of glacier mass change allow us to assess the state, or health, of a glacier and how it influences changes in global mean sea level. Glaciers gain mass by snow accumulation and lose mass through surface melt and runoff and, where they terminate in the ocean or a lake, by iceberg calving. The annual mass balance is traditionally measured over a 'balance year' that, in the Arctic, is often defined operationally to extend from September to August of the following year. Positive annual mass

balance values indicate a gain in mass over the balance year, whereas negative mass balance values indicate a loss in mass. This summary considers the annual mass balance in two ways: the climatic mass balance, which is the difference between the annual mass gain by snow accumulation and the annual mass loss by surface melting and runoff, and the total mass balance is given by the mass gain by snow accumulation minus runoff and iceberg calving. Of the 27 glaciers currently monitored for mass balance across the Arctic (Fig. 1), only three (Kongsvegen (Svalbard), Hansbreen (Svalbard), and Devon Ice Cap (Canada)) are tidewater glaciers, which lose mass by iceberg calving into the ocean.

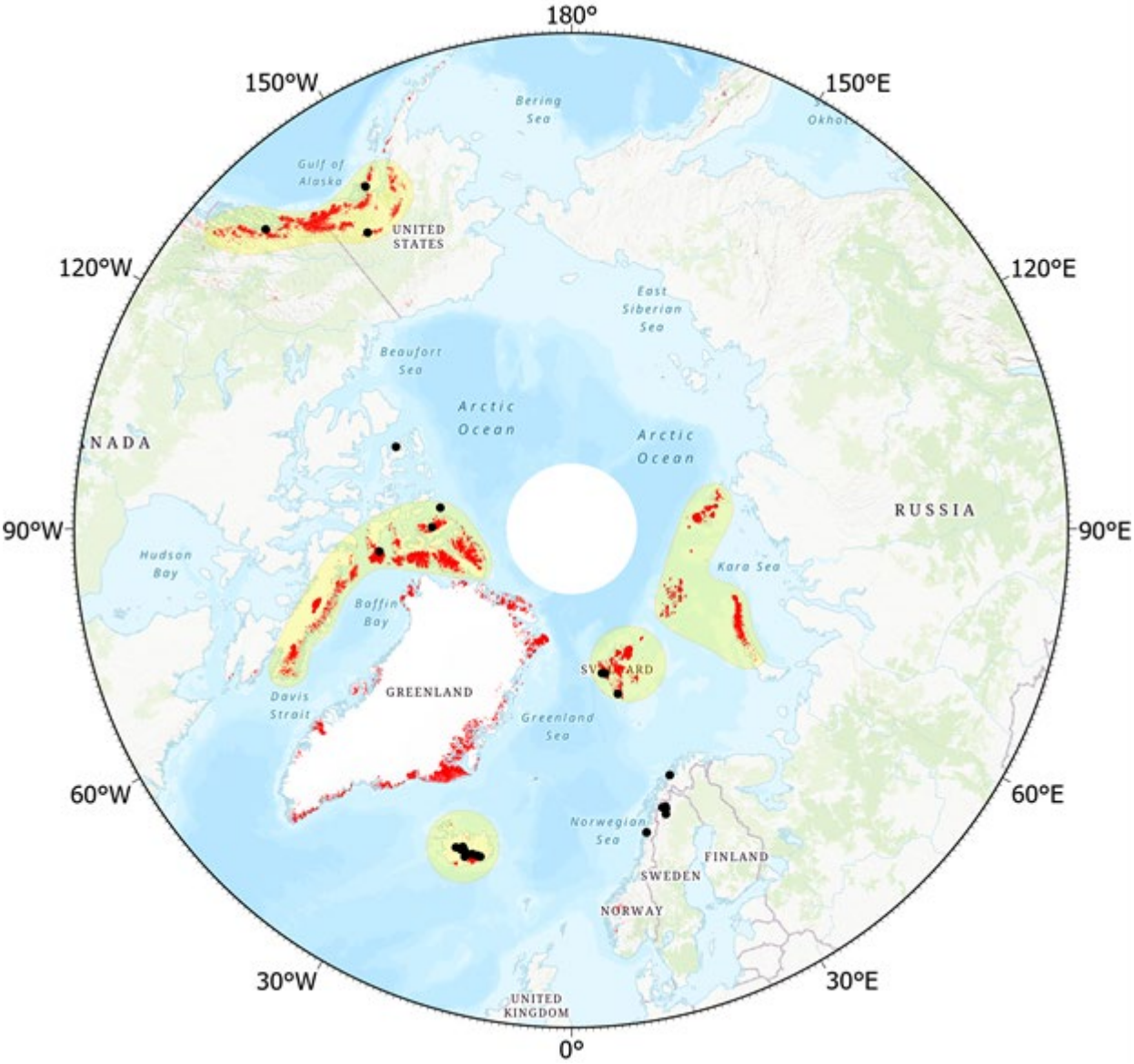

Fig. 1. Arctic glaciers and ice caps (red), including ice caps in Greenland separate from the ice sheet (Pfeffer et al. 2014). Black dots indicate the locations of regularly monitored glaciers in the Arctic. Yellow shading shows the GRACE- and GRACE-FO-derived mass anomaly domains, used to estimate changes in regional annual glacier mass balance total mass balance for the heavily glacierized regions of the Arctic.

Climatic mass balance

At the time of reporting, climatic mass balance measurements for mass balance year 2018/19 are available from 10 of the 27 monitored Arctic glaciers (three in Alaska, four in Svalbard, two in Norway, and one in Arctic Canada). This limited data availability is due to latency in seasonal measurements at some glaciers and because some of these data are still provisional. Therefore, to provide a more complete assessment of the state of Arctic glaciers and ice caps, we also report on 25 glaciers for mass balance year 2017/18 (World Glacier Monitoring Service [WGMS] 2017; Kjøllmoen et al. 2019). For the Arctic as a whole, the mean climatic mass balance values for 2017/18 and 2018/19 were negative, indicating overall mass loss.

Negative balances were recorded for 16 of the 25 glaciers (64%) in 2017/18 (in Alaska, Svalbard, and northern Scandinavia) and 9 (36%) registered positive balances (in Arctic Canada and Iceland). Relative to the 1985-2015 mean values of climatic mass balance, 12 of the 25 were more negative and 13 were more positive than the mean. The positive anomalies observed for the nine individual glaciers during 2017/18 contrast with the mainly negative annual mass balance anomalies that have driven the current trend of continued mass loss observed throughout the Arctic since the mid-1950s (Fig. 2). With the exception of the Svalbard region (where there has been no obvious recent acceleration of mass loss rates), rapid mass loss across the five regions generally began during the 1990s (van Pelt et al. 2019; Zemp et al. 2019). In 2018/19, climatic mass balance values reported for glaciers in Alaska, Svalbard, Norway, and Arctic Canada were as a whole more negative than the long-term mean. For the combined Alaska glaciers, 2018/19 was the most negative mass balance year on record and marked the seventh consecutive year of strongly negative anomalies in the Alaska region.

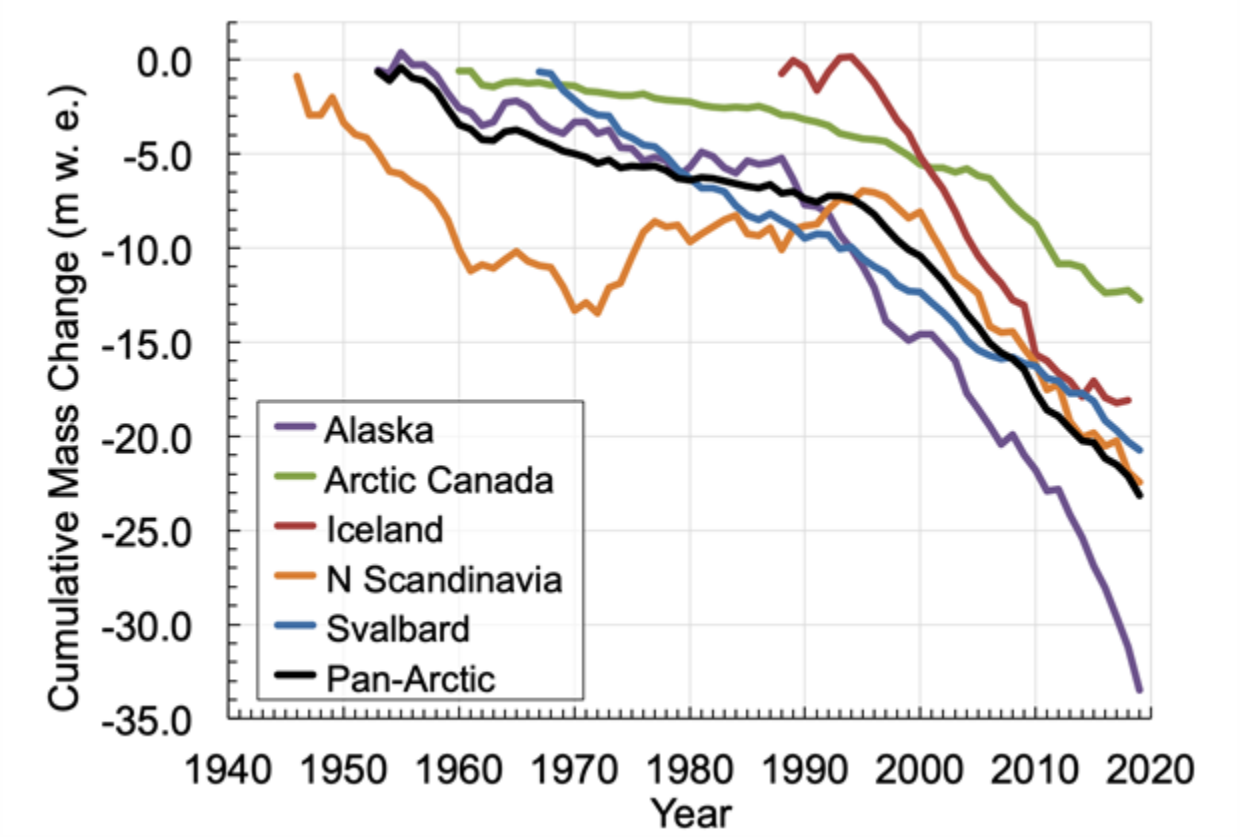

Fig. 2. Cumulative climatic mass balance in meters of water equivalent (m w.e.) for monitored glaciers in five

regions of the Arctic and for the Arctic as a whole (Pan-Arctic), through the 2018/19 balance year. Mean balances are calculated for glaciers monitored in each region in each year and these means are summed over the period of record. Note that monitoring periods vary between regions and that the number and identity of glaciers monitored in a given region may vary between years. (Source: WGMS 2017.)

Surface melting

The climatic mass balance of glaciers in the Arctic is strongly controlled by changes in air temperature. Positive balance anomalies in Arctic Canada and Iceland during 2017/18 were likely influenced by frequent low-pressure systems in the central Arctic generating persistent cloud cover that reduced solar heating during summer (Overland et al. 2019). The negative balances of glaciers in Alaska, northern Scandinavia, and Svalbard in 2017/18 were most likely linked to melt increases caused by positive air temperature anomalies during autumn from the surface to 850 hPa, relative to the 1981-2010 climatology (data from NCEP-NCAR Reanalysis; Overland et al. 2019). In 2018/19, negative balance values reported for glaciers in Alaska, Arctic Canada, and Svalbard were also associated with anomalously warm air temperatures at 850 hPa and persistent ridges of high pressure over Arctic Russia, Arctic Canada, and Alaska. Strong positive air temperature anomalies (2.5°-3.5°C at 1000-850 hPa) in 2018/19, associated with southerly winds and warm air (Overland et al. 2020), produced the most negative mass balance year on record for the combined Alaska glaciers. For example, the 2019 average summer air temperature at Wolverine Glacier in south-central Alaska was 11.1°C, marking the hottest summer in the 52-year record and 3.2°C higher than the 1981-2010 climatological mean (Fig. 3). Over the period of record at Wolverine Glacier (1967-2019), mean summer temperatures have increased 1°C, at a rate of 0.02°C yr^{-1} ($p < 0.02$; O'Neel et al. 2019).

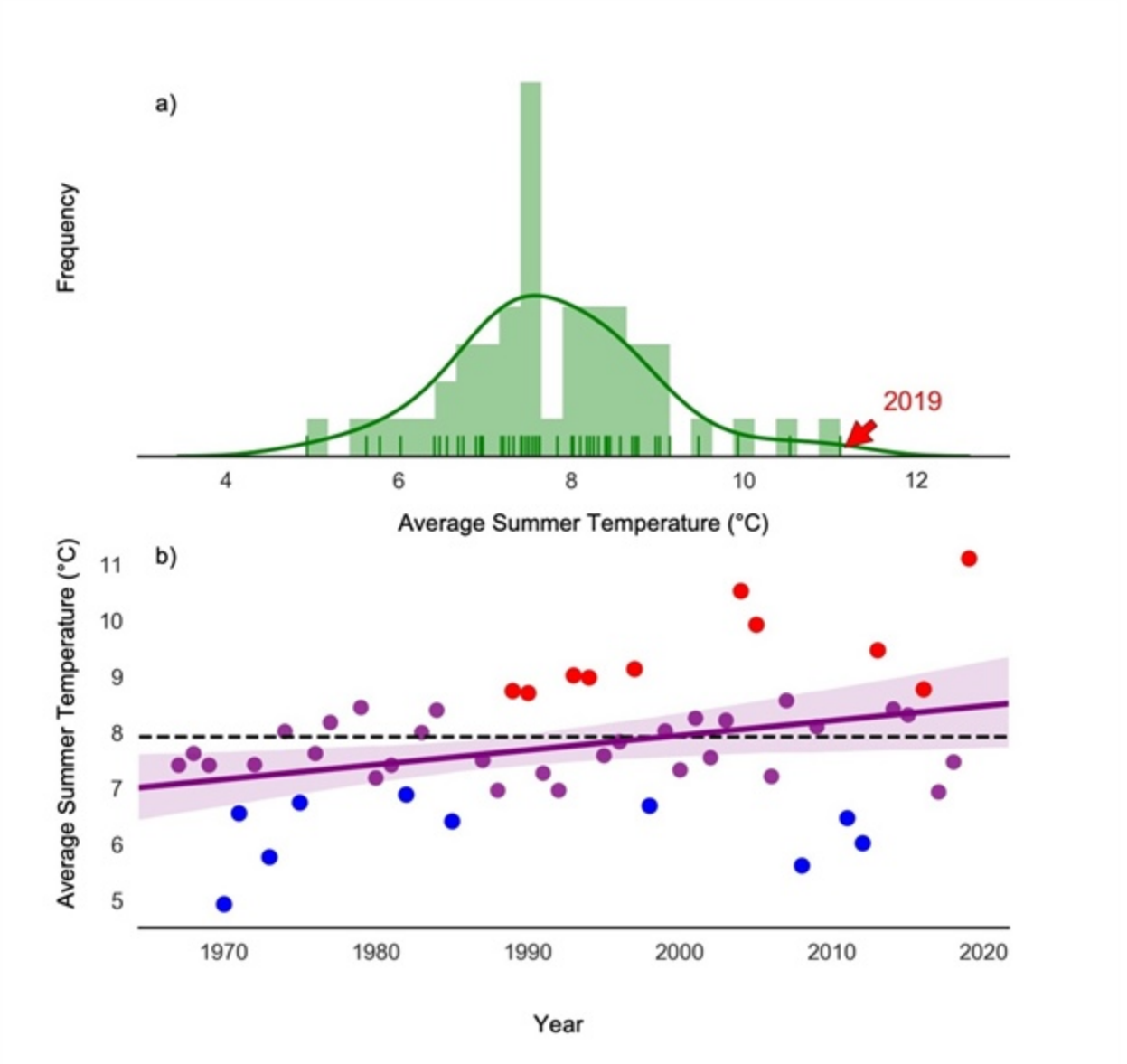

Fig. 3. Summer air temperatures at Wolverine Glacier, Alaska from 1967 to 2019, at 990-m elevation. The summer season is defined as June, July, and August following Bieniek and Walsh (2017). (a) Distribution of mean summer temperatures, shown with a histogram (bar plot) and probability density function estimate (smoothed curve). Small vertical lines show each individual year's summer temperature, with Summer 2019 labeled for emphasis. (b) Time series of mean summer temperature, with the 10 warmest years shown as red dots, and the 10 coldest years shown as blue dots. An ordinary least squares trend line is fit through all data and is shown in purple ($p < 0.02$), and an envelope of uncertainty about this line is shaded in light purple. The horizontal dashed line represents the mean summer temperature for the 1981-2010 climatology.

Total mass balance

The regional total glacier mass balance in the heavily glacierized regions of the Arctic can be estimated from time series of cumulative regional mass anomalies, here derived using GRACE (2002-17) and GRACE FO (2018-present) satellite gravimetry (Fig. 1; Wouters et al. 2019). For the Arctic glaciers and ice caps as a whole, the overall mass balance was strongly negative during the combined GRACE and

GRACE-FO period (2002-19), with the record dominated largely by ice mass loss from Arctic Canada and Alaska (Fig. 4). The estimated mass loss trends during this period for five regions in the Arctic are: -66 ± 10 Gt yr^{-1} (Alaska); -63 ± 8.2 Gt yr^{-1} (Arctic Canada); -9 ± 1.8 Gt yr^{-1} (Iceland); -14 ± 3.2 Gt yr^{-1} (Arctic Russia); and -12 ± 0.6 Gt yr^{-1} (Svalbard), with estimated uncertainties (at 2 std. dev.) including corrections for glacial isostatic adjustment and terrestrial hydrology. The Arctic-wide estimate for mass loss from glaciers and ice caps outside of Greenland is equal to a global sea level rise contribution of approximately 0.4 mm yr^{-1}. By comparison, Greenland currently contributes about 0.7 mm yr^{-1} (see essay *Greenland Ice Sheet*). When normalized by area, glaciers and ice caps outside Greenland are currently producing more melt per unit area than all land ice on Greenland. For the Arctic as a whole (glaciers and ice caps plus the Greenland Ice Sheet) the current rate of contribution to global sea level rise is 1.1 mm yr^{-1}.

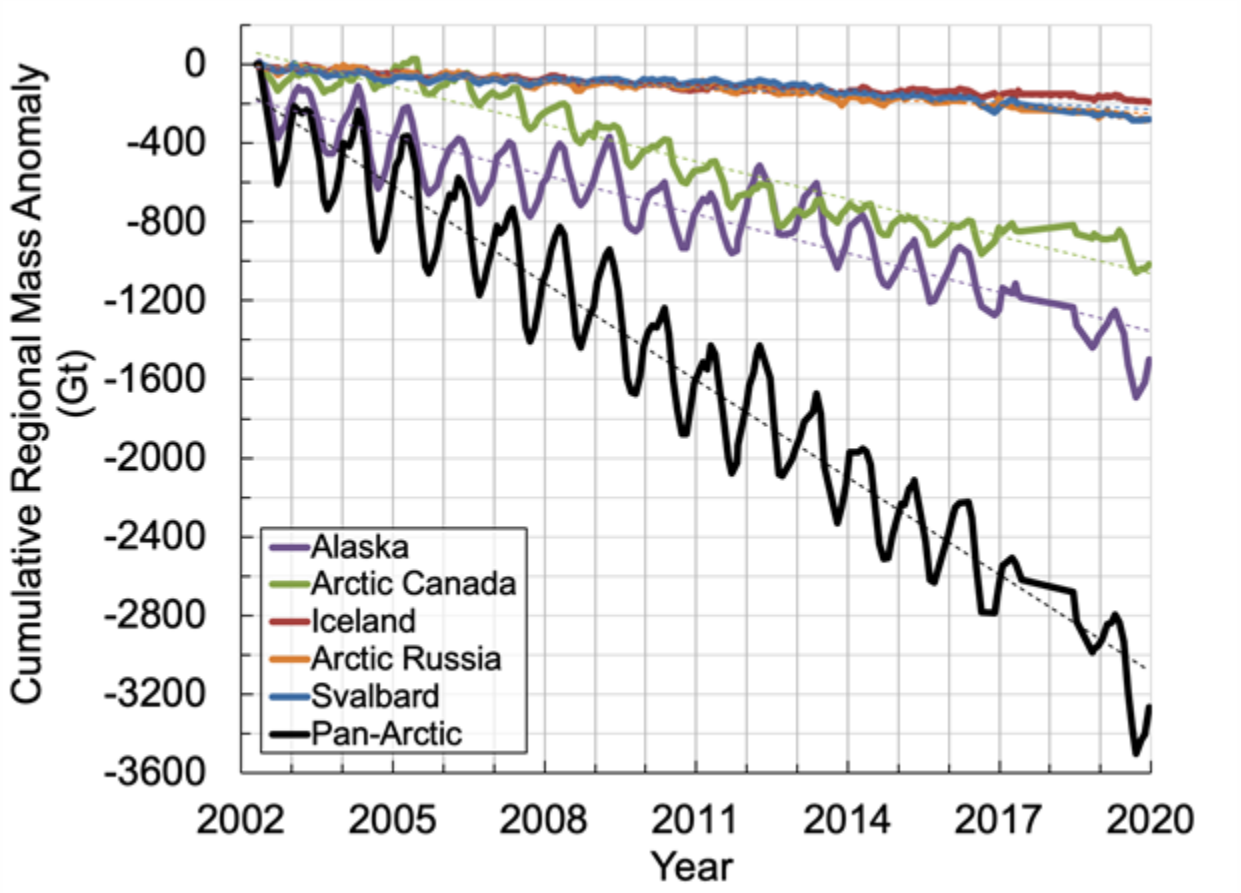

Fig. 4. Cumulative changes in regional total stored water for 2002-19 (Gt), derived using GRACE and GRACE-FO satellite gravimetry. A measurement gap exists between the GRACE and GRACE-FO missions from July 2017 to May 2018 through which linear interpolation is applied.

Acknowledgments

The authors would like to thank E. H. Baker and S. O'Neel, U.S. Geological Survey, Alaska Science Center, Anchorage, Alaska, for data contributions to this report.

References

Bieniek, P. A., and J. E. Walsh, 2017: Atmospheric circulation patterns associated with monthly and daily temperature and precipitation extremes in Alaska. *Int. J. Climatol.*, **37**, 208-217, https://doi.org/10.1002/joc.4994.

Gardner, A. S., and Coauthors, 2011: Sharply increased mass loss from glaciers and ice caps in the Canadian Arctic Archipelago. *Nature*, **473**, 357-360, https://doi.org/10.1038/nature10089.

Gardner, A. S., and Coauthors, 2013: A reconciled estimate of glacier contributions to sea level rise: 2003-2009. *Science*, **340**, 852-857, https://doi.org/10.1126/science.1234532.

Jacob, T., J. Wahr, W. T. Pfeffer, and S. Swenson, 2012: Recent contributions of glaciers and ice caps to sea level rise. *Nature*, **482**, 514-518, https://doi.org/10.1038/nature10847.

Kjøllmoen, B., L. M. Andreassen, H. Elvehøy, and M. Jackson, 2019: Glaciological investigations in Norway 2018, NVE Rapport 46-2019, 84 pp +app.

Millan, R., J. Mouginot, and E. Rignot, 2017: Mass budget of the glaciers and ice caps of the Queen Elizabeth Islands, Canada from 1991-2015. *Environ. Res. Lett.*, **12**, 024016, https://doi.org/10.1088/1748-9326/aa5b04.

O'Neel, S., and Coauthors, 2019: Reanalysis of the US Geological Survey Benchmark Glaciers: long-term insight into climate forcing of glacier mass balance. *J. Glaciol.*, **65**(253), 850-866, https://doi.org/10.1017/jog.2019.66.

Overland, J. E., E. Hanna, I. Hanssen-Bauer, S. -J. Kim, J. E. Walsh, M. Wang, and U. S. Bhatt, 2019: Surface air temperature [in "State of the Climate in 2018"]. *Bull. Amer. Meteor. Soc.*, **100**(9), S142-S143, https://doi.org/10.1175/2019BAMSStateoftheClimate.1.

Overland, J. E., T. J. Ballinger, E. Hanna, I. Hanssen-Bauer, S. -J. Kim, J. E. Walsh, M. Wang, U. S. Bhatt, and R. L. Thoman, 2020: Surface air temperature [in "State of the Climate in 2018"]. *Bull. Amer. Meteor. Soc.*, **101**(7), S8-S10, https://doi.org/10.1175/2020BAMSStateoftheClimate.1.

Pfeffer, W. T., and Coauthors, 2014: The Randolph Glacier Inventory: a globally complete inventory of glaciers. *J. Glaciol.*, **60**(221), 537-552, https://doi.org/10.3189/2014JoG13J176.

van Pelt, W., and Coauthors, 2019: A long-term dataset of climatic mass balance, snow conditions, and runoff in Svalbard (1957-2018). *Cryosphere*, **13**, 2259-2280, https://doi.org/10.5194/tc-13-2259-2019.

WGMS, 2017: Global Glacier Change Bulletin No. 2 (2014-2015). M. Zemp, S. U. Nussbaumer, I. Gärtner-Roer, J. Huber, H. Machguth, F. Paul, and M. Hoelzle (Eds.), ICSU(WDS)/IUGG(IACS)/UNEP/UNESCO/WMO, World Glacier Monitoring Service, Zurich, Switzerland, 244 pp. Based on database version: https://doi.org/10.5904/wgms-fog-2017-10.

Wouters, B., A. S. Gardner, and G. Moholdt, 2019: Global glacier mass loss during the GRACE satellite mission (2002-2016). *Front. Earth Sci.*, **7**, 96, https://doi.org/10.3389/feart.2019.00096.

Zemp, M., and Coauthors, 2019: Global glacier mass changes and their contributions to sea-level rise from 1961 to 2016. *Nature*, **568**, 382-386, https://doi.org/10.1038/s41586-019-1071-0.

November 14, 2020

Bowhead Whales: Recent Insights into Their Biology, Status, and Resilience

DOI: 10.25923/cppm-n265

J. C. George[1], S. E. Moore[2], and J. G. M. Thewissen[3]

[1]Department of Wildlife Management, North Slope Borough, Utqiaġvik, AK, USA
[2]Center for Ecosystem Sentinels, University of Washington, Seattle, WA, USA
[3]Department of Anatomy and Neurobiology, Northeast Ohio Medical University, Rootstown, OH, USA

Highlights

- Bowhead whales can live over 200 years and have unique anatomical and physiological attributes. Their sequenced genome holds promise for the advance of medical knowledge related to cell senescence, bone biology, and fat metabolism in mammals including humans.
- Commercial fishing and associated gear entanglement, industrial shipping, oil and gas activities including seismic exploration, and orca predation are affecting all four bowhead populations to varying degrees. Resilience of the species to these human-induced and natural ecological shifts vary by region.
- Bowhead whales are a useful indicator species that reflect variability in arctic marine ecosystems. Population size of bowheads in the Pacific Arctic has increased in the past 30 years in part due to increases in primary production as well as transport of the zooplankton north from the Bering Strait. The East Canada-West Greenland population has also increased. Conversely, the smaller bowhead populations in the Atlantic and Okhotsk Sea have remained at low numbers and are considered vulnerable or at risk.

Introduction

Bowhead whales, the only "true" arctic baleen species, are large rotund whales with a range confined to icy arctic and sub-arctic seas. The four bowhead populations, or "stocks" in management terms, are named for the seas they inhabit: Okhotsk Sea (OKH; ~218 individuals); the East Greenland, Svalbard, Barents Sea (EGSB; ~318 individuals); the East Canada-West Greenland Sea (ECWG; ~6,400 individuals); and the Bering-Chukchi-Beaufort Seas (BCB; ~16,800 individuals) (Fig. 1; Givens and Heide-Jørgensen 2021; Baird and Bickham 2021). All populations were hunted to near-extinction by commercial whaling, which ceased by the early 1900s, but the two last mentioned have nearly fully recovered. Their conservation success story was made possible by the productive collaboration of international organizations, Indigenous hunters, non-governmental organizations, and national governments (Suydam and George 2021). The two smaller populations have not recovered and are considered at high risk by the International Union for Conservation of Nature (IUCN; Givens and Heide-Jørgensen 2021).

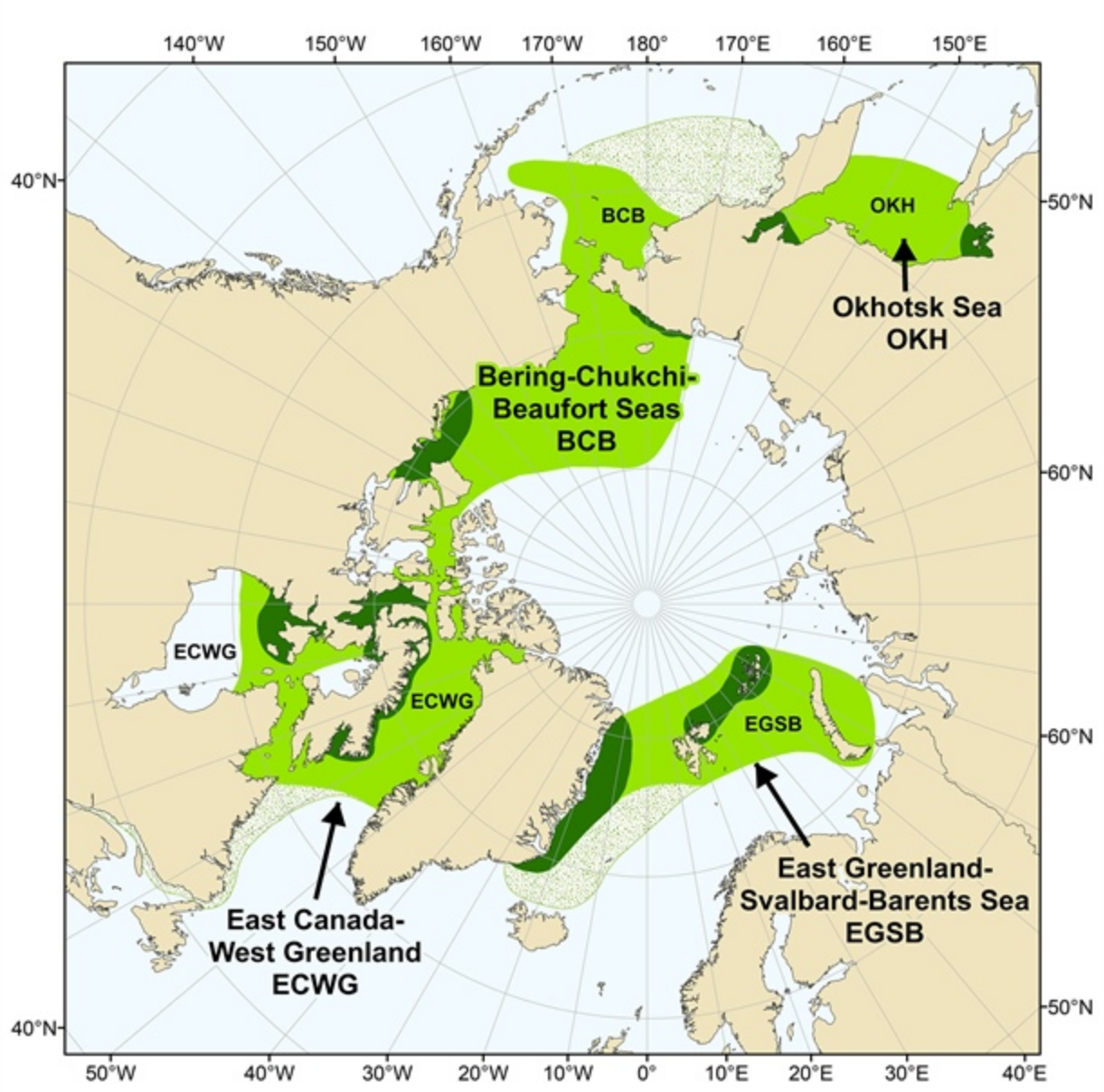

Fig. 1. Range of the four recognized bowhead whale regional populations: Bering-Chukchi-Beaufort (BCB) seas; Sea of Okhotsk (OKH); East Greenland, Svalbard, Barents Sea (EGSB); and East Canada-West Greenland Sea (ECWG). The range of the BCB and ECWG populations overlap slightly in the western Canadian Arctic archipelago. Green - current range; Dark green - areas of high summer density; Dotted - historical distribution. Source: Map by John Citta (modified from: Baird and Bickham 2021).

Compared to other whales, bowheads have greater blubber reserves, longer baleen, proportionally larger heads, and are highly adapted to live in ice-covered waters. They can break through ice up to 2 m in thickness, and feed on the small but seasonally rich zooplankton in arctic waters. They reach sexual maturity in their mid-20s, have a body temperature lower than that of most mammals, and can reach ages over 200 years (George et al. 2021a). Sea ice provides a refuge from orcas, their only natural predator, and may have allowed the evolution of many of their unusual traits.

Anatomy, physiology, and genetics

Collaborations with Indigenous whale hunters have allowed researchers to study samples from freshly harvested whales from the BCB population, providing the foundation for detailed anatomical and health assessments (Fig. 2), as well as quantification of population biology statistics, such as age composition and calf production rates (George et al. 2021a; Stimmelmayr et al. 2021). In turn, these findings have also informed oceanographic studies whereby stomach contents can be used to identify whether prey was derived from local production or transported from the Bering Sea by currents (Ashjian et al. 2021).

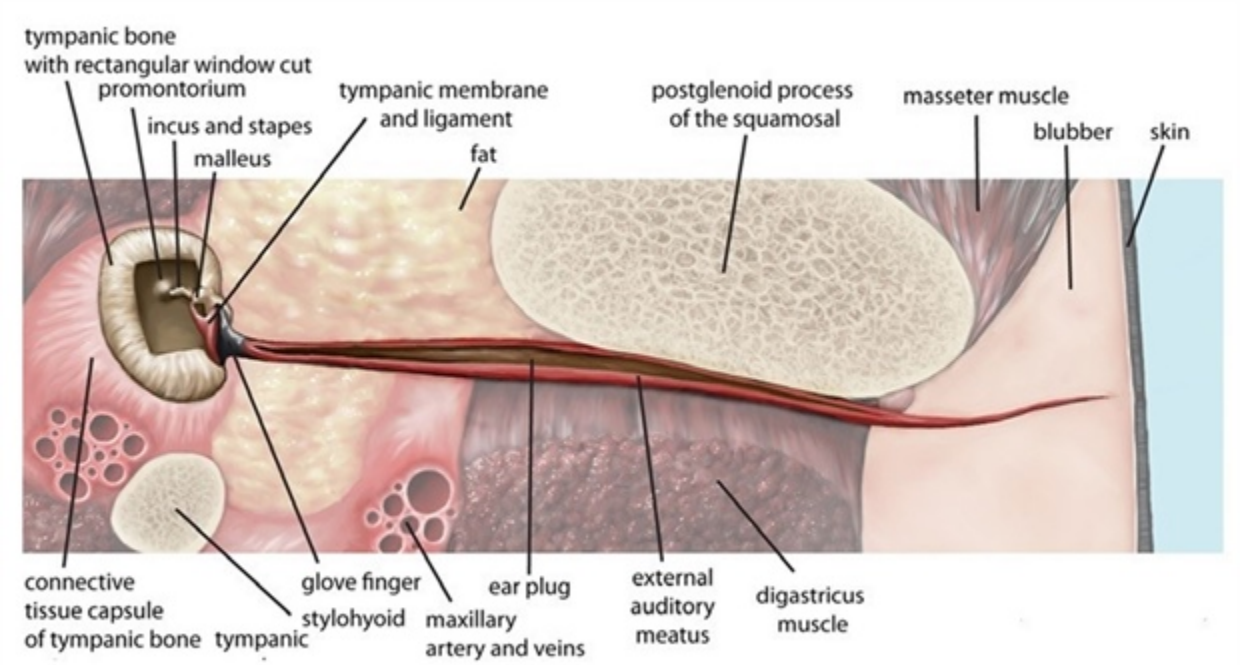

Fig. 2. Diagram of the ear of a bowhead whale (from Rehorek et al. 2020). Detailed anatomy work such as this would not be possible without collaborations with Indigenous hunters. Studies like these allow researchers to describe normal anatomy and identify disease and possible anthropogenically induced abnormalities and injuries from full-scale seismic surveys, industrial shipping, and oil and gas. Illustration by Jacqueline Dillard.

Bowhead blubber is the thickest of any cetacean (Fig. 3) and is important as an energy storage organ for times when food availability is limited (Burns 1993; George et al. 2021b). This allows bowheads to survive years of low oceanic productivity. It may also be a liability; observed avoidance of warmer waters in the Canadian Arctic (Chambault et al. 2018) and energetic models suggest bowheads are "over-insulated" and might overheat in a warming arctic. Other interpretations suggest bowheads may not be thermally stressed in part due to their relatively low metabolic rate and that the whales may simply be seeking higher prey densities in colder waters, and not directly avoiding warmer waters (George et al. 2021b; Citta et al. 2018).

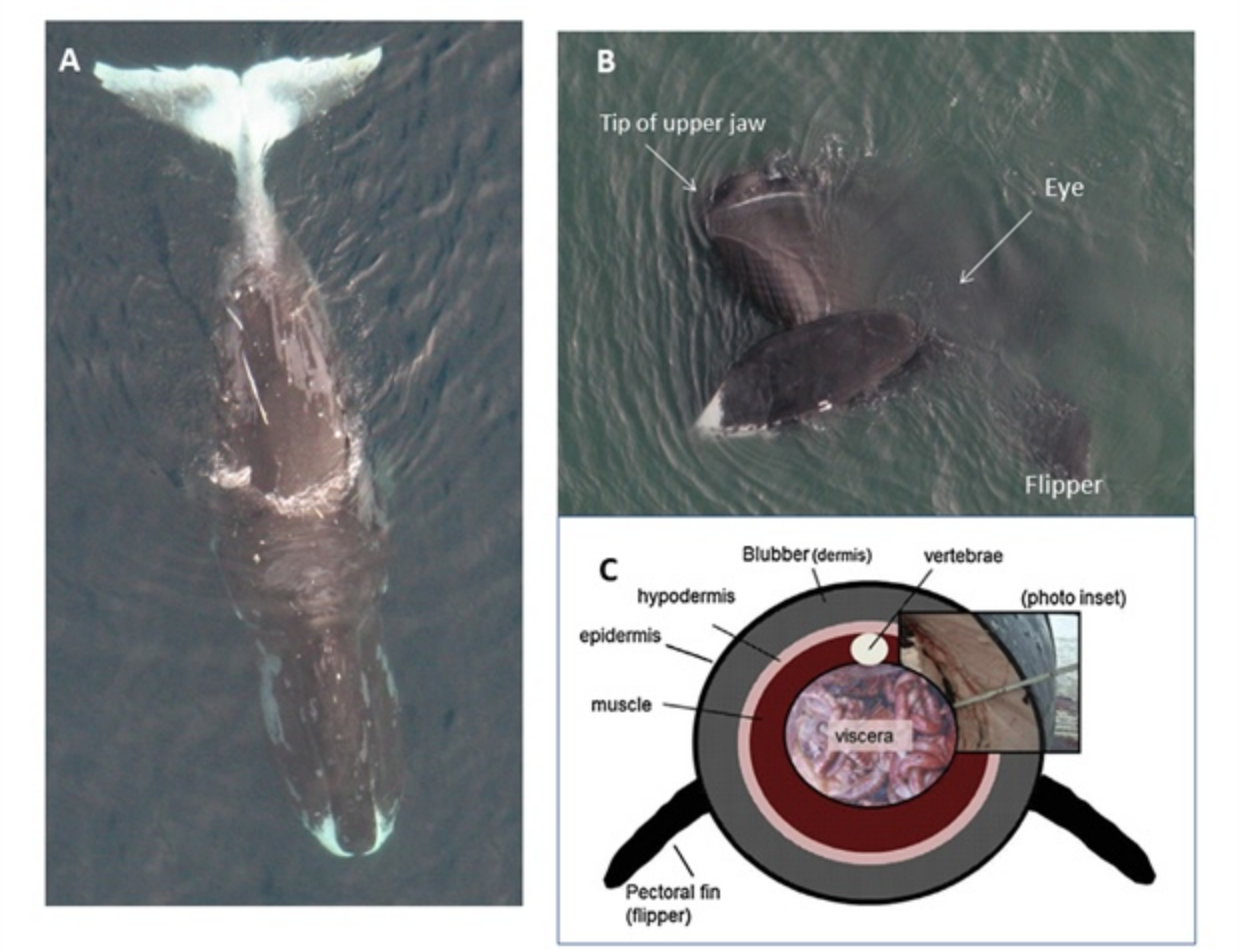

Fig. 3. (a) Large, heavily scared, and likely very old bowhead whale. The only baleen whale species endemic to the Arctic, bowheads grow to ~18 m (60 ft), weigh ~100 tons, and can live ~200 years. (b) A bowhead surfacing on its side with the mouth wide agape. These whales have the longest baleen rack of any mysticete allowing them to feed on remarkably small (1 mm) prey at relatively low densities (photo: C. George). (c) Diagram showing a cross-section of a harvested bowhead used in a body condition analysis. Increases in girth were associated with years with strong upwelling and reduced ice cover in their Beaufort Sea feeding grounds. The inset is an actual photograph of a yearling ''*ingutuq*'' bowhead showing the skin, blubber, a thick layer of fat underlying the blubber, and muscle (from: George et al. 2015).

The bowhead genome has been sequenced (Keane et al. 2015) and explored to understand the many remarkable aspects of their biology, such as their great longevity, ability to control fat deposits (Ball et al. 2013), low incidence of cancer, and bone metabolism (Cooper and Gorbunova 2021).

Regional ecology and anthropogenic threats

Loss of arctic sea ice has become an iconic signal of climate change and all bowhead populations now regularly inhabit open-water regions from at least late summer through autumn (Moore et al. 2021). Recent occurrences of wintertime sea ice loss (e.g., in the Bering sea per Stabeno et al. 2019), elevated ocean temperatures, an overall 57% increase in primary production (Lewis et al. 2020), and now-routine extensive summer sea ice retreats (see essay *Sea Ice*) indicate that bowhead habitat is undergoing rapid biophysical alteration (e.g., Huntington et al. 2020; Moore et al. 2019).

Biophysical and anthropogenic drivers in regional marine ecosystems will influence how each bowhead population fares in the current era of rapid change. For example, in the Pacific Arctic, bowheads routinely feed both on local copepods and on euphausiids (krill), which are advected through the Bering Strait (Fig. 4; Ashjian et al. 2021). Increased primary productivity and advection through Bering Strait since ~2000 seemingly have resulted in more local (copepod) and advected (krill) prey (Fig. 4), respectively, leading to improved bowhead body condition and high calf production (George et al. 2015). There is interannual variability in these biophysical drivers, however. For example, during the nearly ice-free autumn of 2019 bowhead whales were not observed feeding over the continental shelf areas of the western Beaufort Sea where they are commonly seen (Moore et al. 2021). The reason for this shift remains unclear but could have been the result of a mismatch in timing of prey delivery and whale arrival in the western Beaufort Sea. In autumn 2020, bowheads were again in abundance in the western Beaufort Sea, coincident with unprecedented wash-ups of krill on local beaches (Fig. 4).

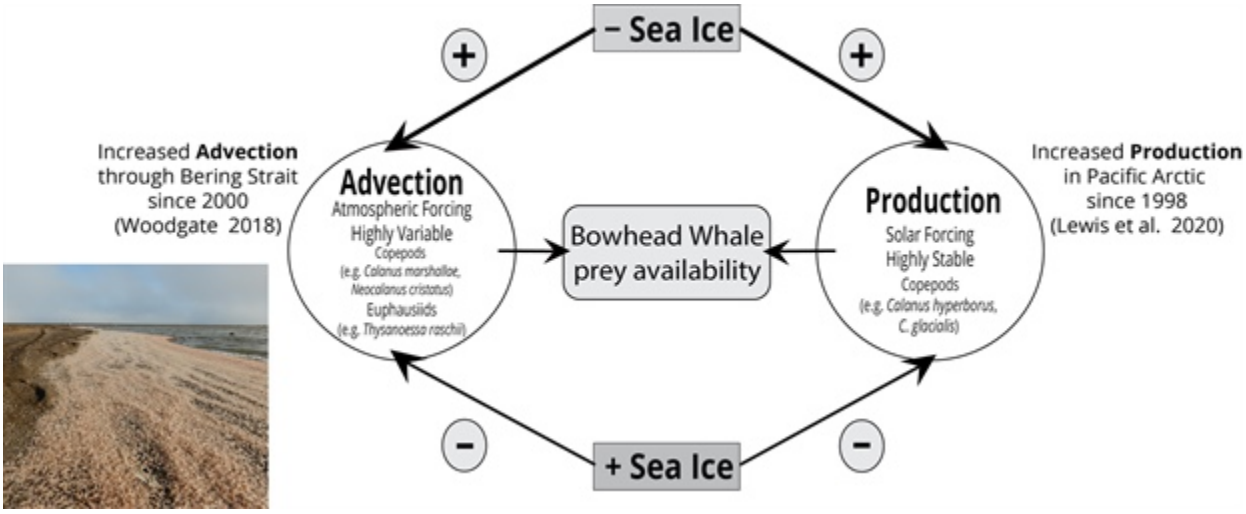

Fig. 4. Schematic summarizing biophysical drivers of bowhead prey reliant on local production (boreal copepods) and advection (e.g., euphausiids) and their relationship to sea ice (modified from Moore and Laidre 2006). In the past 20 years, with a decrease in sea ice, integrated primary production (see essay *Arctic Ocean Primary Productivity*) has increased by 96.1% in the Chukchi Sea and by 38.6% the Beaufort Sea (Lewis et al. 2020). Advection (transport) of nutrients and zooplankton has also increased (Woodgate 2018). Both of these biophysical changes have resulted in more prey and improved the body condition and health of bowheads. The inset photo is an unusual and tremendously large volume of beachcast euphausiids (or krill) near Point Barrow, Alaska in September 2020, where advection and local physical forcing trap krill to make it an important bowhead feeding area for the BCB population (Photo credit: Peter Detwiler 2020).

Increased orca predation impacts all four populations of bowheads (Breed 2021). Orcas (killer whales) in arctic regions tend to avoid sea ice unlike those in the Antarctic. With the now-common extreme Arctic summer ice retreats, orca are regularly observed in Canadian high arctic waters, leading to a sharing of habitat with bowheads. Sightings of both live and dead bowheads with orca-inflicted scars are becoming more common. Bowhead behavior is also affected (Breed 2021). Where bowheads once fed undisturbed in places such as Peel Sound, Foxe Basin, Lancaster Sound, and the Canadian Beaufort, orcas now pose a predation threat, which has led to some displacement away from these traditional summer feeding areas. Evidence of increased predation on bowheads is now a conservation concern for bowheads in the Sea of Okhotsk and the Pacific Arctic regions (Breed 2021; Willoughby et al. 2020).

Entanglement in commercial fishing gear is now considered the greatest threat to baleen whales worldwide (George et al. 2021c). Commercial fishing and crabbing are shifting north, following targeted

species and taking advantage of ice-free waters, suggesting arctic bowhead populations will encounter fishing gear more often. Evidence from aerial surveys and Indigenous-harvested individuals indicate that about 12% of bowheads in the North Pacific have entanglement scars (George et al. 2017). In addition, the harvesting of bowheads that are still entangled in commercial fishing gear has occurred several times in recent decades (George et al. 2021c). Increased underwater noise (Blackwell and Thode 2021), ship strikes, oil and gas and mineral extraction, and tourism associated with the more ice-free Arctic also pose threats, as well as induce stress in bowheads (e.g., Reeves et al. 2014).

Bowhead resilience, Indigenous Peoples, and future research

Rapid changes in bowhead whale regional habitats call into question the future of the only arctic endemic baleen whale. Moore and Reeves (2018) provide a simplified framework to assess status and resilience of each of the four bowhead populations based on population size, geographic range, flexibility in behavior and diet, and health parameters. Overall, this framework suggests that the smaller populations are at higher risk (Moore et al. 2021).

Bowhead whales are a good indicator species of arctic change because they react to annual environmental perturbations, especially those influencing prey availability, and subsequently integrate these changes into long-term measurable trends in reproduction and health. So far, two of the populations (ECWG and BCB) appear stable or increasing with strong reproduction. The remarkable and steady recovery of the BCB population since the 1980s (Givens et al. 2016) confirms that the arctic ecosystem has fewer direct anthropogenic impacts (commercial fishing, shipping, etc.) relative to other marine regions and is actually more productive in the face of sea ice loss – at least to date. The recovery of the BCB population should be ranked among the great conservation successes of the last century, particularly considering the continued sustainable harvest by Inuit peoples.

Several arctic Indigenous societies, from Chukotka to Greenland, depend on bowhead whales for food and cultural identity. The changing Arctic has the potential to deeply affect these relationships. The scientific collaborations between Indigenous peoples and researchers are critically important to both high-quality science, conservation, and arguably the survival of these human societies in a changing Arctic. (*Please note that the ARC2020 was altered by the COVID-19 pandemic; a planned essay on impacts of the changing Arctic to subsistence hunting from the viewpoints of Indigenous experts from two northwest Alaska communities had to be postponed to a future report.*)

We strongly urge continued monitoring of subsistence bowhead harvests, regular population size estimates, oceanographic sampling across their range, periodic aerial surveys, as well as health assessments based on the two harvested populations and beachcast whales whenever possible (Stimmelmayr et al. 2021). There is reason for concern due to rapid changes within the bowhead's range, but given their persistence through 4 million years of dramatic ecosystem change and intensive commercial harvests, there is also room for optimism about the future of bowhead whales, given reasonable conservation measures.

References

Ashjian, C. J., R. G. Campbell, and S. R. Okkonen, 2021: Biological environment. In: George, J. C. and J. G. M. Thewissen, Eds. The Bowhead Whale, *Balaena mysticetus*, Biology and Human Interactions. Academic Press.

Baird, A. B., and J.W. Bickham, 2021: The stocks of bowheads. In: George, J. C. and J. G. M. Thewissen, Eds. The Bowhead Whale, *Balaena mysticetus*, Biology and Human Interactions. Academic Press.

Ball, H. C., R. K. Holmes, R. L. Londraville, J. G. Thewissen, and R. J. Duff, 2013: Leptin in whales: validation and measurement of mRNA expression by absolute quantitative real-time PCR. *Plos One*, **8**(1), p.e54277.

Blackwell, S. B., and A. M. Thode, 2021: Effects of noise. In: George, J. C. and J. G. M. Thewissen, Eds. The Bowhead Whale, *Balaena mysticetus*, Biology and Human Interactions. Academic Press.

Breed, G. A., 2021: Predators and impacts of predation. In: George, J. C. and J. G. M. Thewissen, Eds. The Bowhead Whale, *Balaena mysticetus*, Biology and Human Interactions. Academic Press.

Burns, J. J., 1993: Epilog. In: Burns, J. J., Montague, J. and C. J. Cowles (eds.). The Bowhead Whale. Society for Marine Mammalogy, 787 pp.

Chambault, P., C. M. Albertsen, T. A. Patterson, R. G. Hansen, O. Tervo, K. L. Laidre, and M. P. Heide-Jørgensen, 2018: Sea surface temperature predicts the movements of an Arctic cetacean: the bowhead whale. *Sci. Rep.*, **8**(1), 9658, https://doi.org/10.1038/s41598-018-27966-1.

Citta, J. J., and Coauthors, 2018: Oceanographic characteristics associated with bowhead whale movements in the Chukchi Sea in autumn. *Deep-Sea Res. II*, **152**, 121-131. https://doi.org/10.1016/j.dsr2.2017.03.009.

Cooper, L. N., and V. Gorbunova, 2021: Molecular insights into anatomy and physiology. In: George, J. C. and J. G. M. Thewissen, Eds. The Bowhead Whale, *Balaena mysticetus*, Biology and Human Interactions. Academic Press.

George, J. C., M. L. Druckenmiller, K. L. Laidre, R. Suydam, and B. Person, 2015: Bowhead whale body condition and links to summer sea ice and upwelling in the Beaufort Sea. *Prog. Oceanogr.*, **136**, 250-262, https://doi.org/10.1016/j.pocean.2015.05.001.

George, J. C., J. G. M. Thewissen, A. Von Duyke, G. A. Breed, R. Suydam, T. L. Sformo, B. T. Person, and H.K. Brower, Jr., 2021a: Life history, growth, and form. In: George, J. C. and J. G. M. Thewissen, Eds. The Bowhead Whale, *Balaena mysticetus*, Biology and Human Interactions. Academic Press.

George, J. C., L. Horstmann, S. Fortune, Todd L. Sformo, R. Elsner, and E. Follmann. 2021b. Thermoregulation and energetics. In: George, J.C. and J. G. M. Thewissen, Eds. The Bowhead Whale, *Balaena mysticetus*, Biology and Human Interactions. Academic Press.

George, J. C., G. Sheffield, D. J. Reed, B. Tudor, R. Stimmelmayr, B. T. Person, T. Sformo, and R. Suydam, 2017: Frequency of injuries from line entanglements, killer whales, and ship strikes on Bering-Chukchi-Beaufort Seas bowhead whales. *Arctic*, **70**(1), 37-46, https://doi.org/10.14430/arctic4631.

George, J. C., G. Sheffield, B. J. Tudor, R. Stimmelmayr, and M. Moore, 2021c: Fishing gear entanglement and vessel collisions. In: George, J. C. and J. G. M. Thewissen, Eds. The Bowhead Whale, *Balaena mysticetus*, Biology and Human Interactions. Academic Press.

Givens, G. H., and Coauthors, 2016: Horvitz-Thompson whale abundance estimation adjusting for uncertain recapture, temporal availability variation, and intermittent effort. *Environmetrics*, **27**(3), 134-146, https://doi.org/10.1002/env.2379.

Givens, G. H., and M. P. Heide-Jørgensen, 2021: Abundance. In: George, J. C. and J. G. M. Thewissen, Eds. The Bowhead Whale, *Balaena mysticetus*, Biology and Human Interactions. Academic Press.

Huntington, H. P., and Coauthors, 2020: Evidence suggests potential transformation of the Pacific Arctic Ecosystem is underway. *Nat. Climate Change*, **10**, 342–348, https://doi.org/10.1038/s41558-020-0695-2.

Keane, M., and Coauthors, 2015: Insights into the evolution of longevity from the bowhead whale genome. *Cell Rep.*, **10**(1), 112-122, https://doi.org/10.1016/j.celrep.2014.12.008.

Lewis, K. M., G. L. van Kijken, and K. R. Arrigo, 2020: Changes in phytoplankton concentration now drive increased Arctic Ocean primary production. *Science*, **369**, 198-202, https://doi.org/10.1126/science.aay8380.

Moore, S. E., and K. L. Laidre, 2006: Trends in sea ice cover within habitats used by bowhead whales in the western arctic. *Ecol. Appl.*, **16**(3), 932-944.

Moore, S. E., and R. R. Reeves, 2018: Tracking arctic marine mammal resilience in an era of rapid ecosystem alteration. *PLOS Biol.*, **16**, e2006708, https://doi.org/10.1371/journal.pbio.2006708.

Moore, S. E., T. Haug, G. A. Víkingsson, and G. B. Stenson, 2019: Baleen whale ecology in arctic and subarctic seas in an era of rapid habitat alteration. *Prog. Oceanogr.*, **176**, 102118, https://doi.org/10.1016/j.pocean.2019.05.010.

Moore, S. E., J. C. George, and R. R. Reeves, 2021: Bowhead whale ecology in changing high-latitude ecosystems. In: George, J.C. and J. G. M. Thewissen, Eds. The Bowhead Whale, *Balaena mysticetus*, Biology and Human Interactions. Academic Press.

Reeves, R. R., and Coauthors, 2014: Distribution of endemic cetaceans in relation to hydrocarbon development and commercial shipping in a warming Arctic. *Mar. Policy*, **44**, 375-389.

Rehorek, S. J., R. Stimmelmayr, J. C. George, R. Suydam, D. M. McBurney, and J. G. M. Thewissen, 2020: The role of desmosomes in the ear plug formation in the bowhead whale (*Balaena mysticetus*). *Anat. Rec.*, **303**, 3035-3043, https://doi.org/10.1002/ar.24338.

Stabeno, P. J., R. L. Thoman, and K. Wood, 2019: Recent warming in the Bering Sea and its impact on the ecosystem. *Arctic Report Card 2019*, J. Richter-Menge, M. L. Druckenmiller, and M. Jeffries, Eds., https://www.arctic.noaa.gov/Report-Card.

Stimmelmayr, R., D. Rotstein, G. Sheffield, H. K. Brower, Jr., and J. C. George, 2021: Diseases and parasites. In: George, J.C. and J. G. M. Thewissen, Eds. The Bowhead Whale, *Balaena mysticetus*, Biology and Human Interactions. Academic Press.

Suydam, R., and J. C. George, 2021: Current indigenous whaling. In: George, J.C. and J. G. M. Thewissen, Eds. The Bowhead Whale, *Balaena mysticetus*, Biology and Human Interactions. Academic Press.

Willoughby, A. L., M. C. Ferguson, R. Stimmelmayr, J. T. Clarke, and A. A. Brower, 2020: Bowhead whale (*Balaena mysticetus*) and killer whale (*Orcinus orca*) co-occurrence in the US Pacific Arctic, 2009-2018: evidence from bowhead whale carcasses. *Polar Biol.*, **43**, 1669-1679, https://doi.org/10.1007/s00300-020-02734-y.

Woodgate, R. A., 2018: Increases in the Pacific inflow to the Arctic from 1990 to 2015, and insights into seasonal trends and driving mechanisms from year-round Bering Strait mooring data. *Prog. Oceanogr.*, **160**, 124-154, https://doi.org/10.1016/j.pocean.2017.12.007.

November 17, 2020

Coastal Permafrost Erosion

DOI: 10.25923/e47w-dw52

B. M. Jones[1], A. M. Irrgang[2], L. M. Farquharson[3], H. Lantuit[2], D. Whalen[4], S. Ogorodov[5], M. Grigoriev[6], C. Tweedie[7], A. E. Gibbs[8], M. C. Strzelecki[9], A. Baranskaya[5], N. Belova[5], A. Sinitsyn[10], A. Kroon[11], A. Maslakov[5], G. Vieira[12], G. Grosse[2,13], P. Overduin[2], I. Nitze[2], C. Maio[14], J. Overbeck[15], M. Bendixen[16], P. Zagórski[17], and V. E. Romanovsky[3]

[1]Institute of Northern Engineering, University of Alaska Fairbanks, Fairbanks, AK, USA
[2]Alfred Wegener Institute, Helmholtz Centre for Polar and Marine Research, Potsdam, Germany
[3]Geophysical Institute, University of Alaska Fairbanks, Fairbanks, AK, USA
[4]Natural Resources Canada, Geological Survey of Canada-Atlantic, Dartmouth, Nova Scotia, Canada
[5]Faculty of Geography, Lomonosov Moscow State University, Moscow, Russia
[6]Mel'nikov Permafrost Institute, Siberian Branch, Russian Academy of Sciences, Yakutsk, Russia
[7]Department of Biology, University of Texas El Paso, El Paso, TX, USA
[8]U.S. Geological Survey, Pacific Coastal and Marine Science Center, Santa Cruz, CA, USA
[9]Institute of Geography and Regional Development, University of Wroclaw, Wroclaw, Poland
[10]SINTEF AS, SINTEF Community, Trondheim, Norway
[11]Department of Geosciences and Natural Resource Management, University of Copenhagen, Copenhagen, Denmark
[12]Centre of Geographical Studies, Institute of Geography and Spatial Planning, University of Lisbon, Portugal
[13]Institute of Geosciences, University of Potsdam, Potsdam, Germany
[14]Geography, University of Alaska Fairbanks, Fairbanks, AK, USA
[15]Alaska Division of Geological & Geophysical Surveys, Anchorage, AK, USA
[16]Institute of Arctic and Alpine Research, University of Colorado, Boulder, CO, USA
[17]Institute of Earth and Environmental Sciences, Marie Curie Skłodowska University, Lublin, Poland

Highlights

- Since the early 2000s, erosion of permafrost coasts in the Arctic has increased at 13 of 14 sites with observational data that extend back to ca. 1960 and ca. 1980, coinciding with warming temperatures, sea ice reduction, and permafrost thaw.
- Permafrost coasts along the US and Canadian Beaufort Sea experienced the largest increase in erosion rates in the Arctic, ranging from +80 to +160%, when comparing average rates from the last two decades of the 20th century with the first two decades of the 21st century.
- The initiation of several national and international research networks in recent years has enabled closer coordination and collaboration of measurements and a better understanding of pan-Arctic permafrost coastal dynamics.

Introduction

Permafrost coasts in the Arctic make up more than 30% of Earth's coastlines (Fig. 1; Lantuit et al. 2012) and they are sensitive to Arctic Ocean/permafrost-influenced land linkages (Nielsen et al. 2020). The changes currently taking place along these coasts are both indicators and integrators of changes occurring in the global climate system. Reductions in sea ice extent and increases in the duration of the open water period (see essay *Sea Ice*), rising air (see essay *Surface Air Temperature*) and sea surface temperatures (see essay *Sea Surface Temperature*), absolute and relative sea-level rise (see essay *Greenland Ice Sheet*), warming permafrost (Biskaborn et al. 2019), subsiding permafrost landscapes (Lim et al. 2020), and increased storminess and wave heights (Casas-Prat and Wang, 2020) all interact to amplify coastal permafrost erosion (Forbes, 2011). Recent changes in these conditions have increased the vulnerability of permafrost coasts to erosion and altered coastal morphologies (Farquharson et al. 2018), ecosystems (Fritz et al. 2017), carbon export to oceans (Tanski et al. 2019), infrastructure (Fritz et al. 2017), and human subsistence lifestyles (Irrgang et al. 2018).

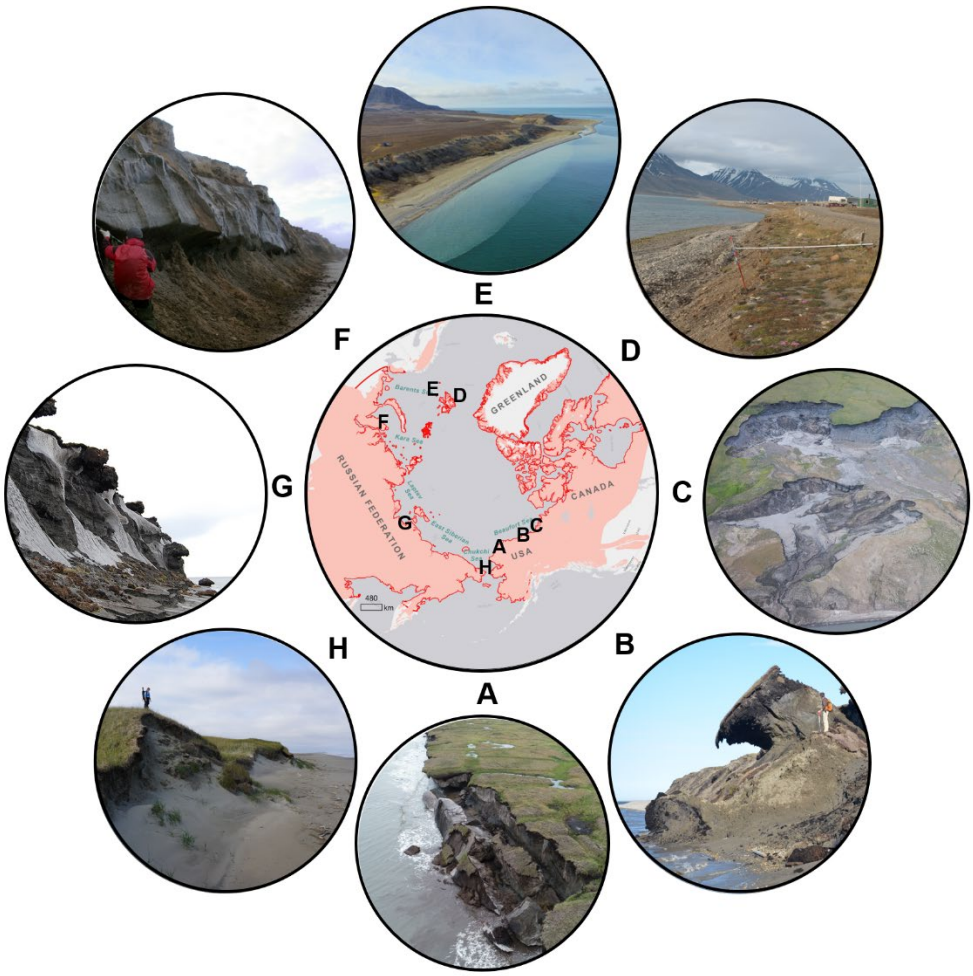

Fig. 1. Arctic permafrost region (red region in central figure) and the distribution of and variability in permafrost coasts (bold red line in central figure). (A) Ice-rich exposed permafrost bluffs at Drew Point, Alaska (photo: B. M. Jones); (B) Ice-rich and ice-poor exposed permafrost coastal bluffs at Barter Island, Alaska (photo: B. M. Jones); (C)

Permafrost-preserved buried glacial ice and retrogressive thaw slumps exposed at Herschel Island, Canada (photo: G. Vieira); (D) Mixed-type permafrost coast exposed at Adventfjorden, Svalbard (photo: E. Guégan); (E) Ice-poor permafrost coast at Calypsostranda, southern Svalbard (photo: P. Zagórski); (F) Ice-rich permafrost overlying fluvial sands with a thermo-erosional niche in the Kara Sea, Siberia (photo: A. Baranskaya); (G) Ice-rich, ice-complex deposits exposed at Muostakh Island, Siberia (photo: T. Opel); and (H) Ice-poor dune and barrier permafrost system at Cape Espenberg, Seward Peninsula, Alaska (photo: L. Farquharson).

Changes in permafrost coasts are primarily due to erosion (Lantuit et al. 2012). However, coastal change rates have high temporal and spatial variability, which is driven largely by diversity in internal and external factors. For example, sediment composition, permafrost properties, and coastline exposure contribute to the spatial variability in coastline change, while changing hydrometeorological and ocean forcing conditions determine the temporal evolution of coastline change (Shabanova et al. 2018). The highest erosion rates occur in unconsolidated sediment deposits that represent 65% of permafrost coasts in the Arctic (Lantuit et al. 2012). The remaining 35% of permafrost coasts are classified as rocky or consolidated material that exhibit more stability. In unconsolidated permafrost coasts, the presence of ice-rich permafrost is a weak but statistically significant contributor to higher coastal erosion rates (Lantuit et al. 2012). The primary drivers of erosion of ice-rich permafrost coasts are summer warmth and solar radiation (thermo-denudation) and wave action (thermo-abrasion) (Aré 1988).

Historic and contemporary decadal-scale changes

Baseline measurements of both historic and contemporary permafrost coastal change were established through the collaborative international efforts of the Arctic Coastal Dynamics program in the late 1990s and early to mid-2000s (Brown and Solomon 2000; Rachold et al. 2005). Historical benchmarks of permafrost coastal change typically integrate observations collected between the 1950s and the 1980s, with those acquired in the early to mid-2000s (Fig. 2; Lantuit et al. 2012). Data were synthesized from field observations and remote sensing-based coastline datasets. Information was compiled on measures of erosion and accumulation occurring in a specific area, and the aggregate mean was reported.

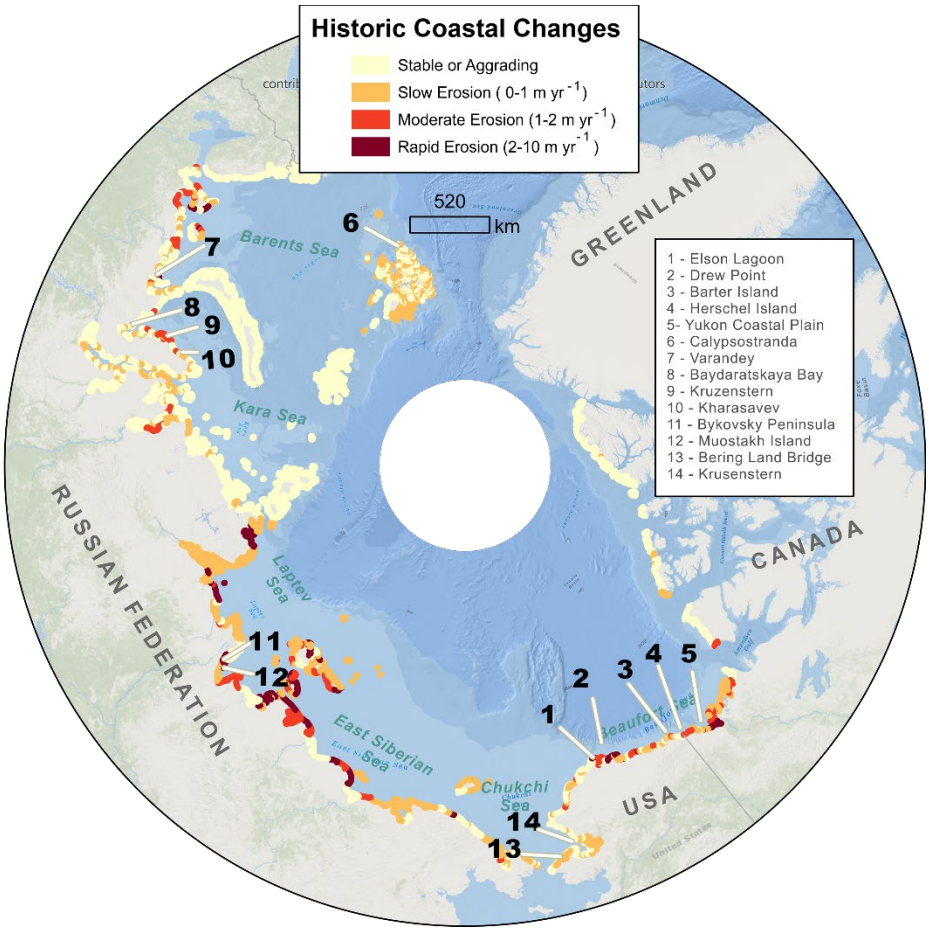

Fig. 2. Historic decadal-scale coastal change observations for permafrost coasts in the Arctic (Lantuit et al. 2012). Data are from the Arctic Coastal Dynamics database (https://doi.pangaea.de/10.1594/PANGAEA.919573) and are based on field observations and coastline change data collected between the 1950s and the 1980s, with updated positions acquired in the early to mid-2000s. The 14 sites mentioned in the essay where contemporary, decadal-scale coastal change rates exist are indicated with numbers in the map and referenced in the upper right text box. More detailed information on relative changes in erosion rates in the 21st century relative to measurements from the latter half of the 20th century are provided in Table 1.

Over the period ~1950 to ~2000, the mean Arctic-wide coastal permafrost change rate was -0.5 m yr^{-1} (where negative values indicate erosion), with substantial variability within and among different regions (Lantuit et al. 2012). According to the primary subdivisions of the Arctic Ocean, change rates have historically been highest along permafrost coasts along the US and Canadian Beaufort Sea (-1.1 m yr^{-1}), East Siberian Sea (-0.9 m yr^{-1}), Laptev Sea (-0.7 m yr^{-1}), and Kara Sea (-0.7 m yr^{-1}). Sites that were historically at or below the mean Arctic-wide coastal permafrost change rate were the Russian (-0.3 m yr^{-1}) and US (-0.5 m yr^{-1}) Chukchi Seas, Barents Sea (-0.4 m yr^{-1}), Canadian Archipelago (0.0 m yr^{-1}), and Svalbard (-0.02 m yr^{-1}) (Lantuit et al. 2012).

Since the early 2000s, observations from 14 coastal permafrost sites have been updated, providing a synopsis of how changes in the Arctic system are intensifying the dynamics of permafrost coasts in the 21st century (Table 1; Fig. 2). Observations from all but 1 of the 14 coastal permafrost sites around the Arctic indicate that decadal-scale erosion rates are increasing. The US and Canadian Beaufort Sea coasts have experienced the largest increases in erosion rates since the early 2000s. The mean annual erosion

rate in these regions has increased by 80 to 160% at the five sites with available data, with sites in the Canadian Beaufort Sea experiencing the largest relative increase. The sole available site in the Greenland Sea, on southern Svalbard, indicates an increase in mean annual erosion rates by 66% since 2000, due primarily to a reduction in nearshore sediment supply from glacial recession. At the six sites along the Barents, Kara, and Laptev Seas in Siberia, mean annual erosion rates increased between 33 and 97% since the early to mid-2000s. The only site to experience a decrease in mean annual erosion (-40%) was located in the Chukchi Sea in Alaska. Interestingly, the other site in the Chukchi Sea experienced one of the highest increases in mean annual erosion (+160%) over the same period. In general, a considerable increase in the variability of erosion and deposition intensity was also observed along most of the sites.

Table 1. Synthesis of historic and contemporary decadal-scale coastal change rates from 14 coastal permafrost sites in the Arctic. The map site number and site location are linked to information provided in Fig. 2.

Map Site Number	Site Location	Historic Decadal-Scale Change		Contemporary Decadal-Scale Change		Change in Rate	References
		Rate (m yr^{-1})	Time Period	Rate (m yr^{-1})	Time Period	Percent (%)	
Beaufort Sea							
1	Elson Lagoon	-0.90	1979 to 2000	-2.10	2000 to 2018	+133	Brown et al. 2003; Tweedie personal communication
2	Drew Point	-8.70	1979 to 2002	-17.20	2002 to 2019	+98	Jones et al. 2018; Jones personal communication
3	Barter Island	-1.50	1979 to 2000	-2.70	2000 to 2020	+80	Gibbs et al. 2020
4	Herschel Island	-0.50	1979 to 2000	-1.30	2000 to 2017	+160	Radosavljevic et al., 2016; Cunliffe et al. 2019
5	Yukon Coastal Plain	-0.60	1970 to 1990	-1.30	1990 to 2011	+117	Irrgang et al. 2018
Greenland Sea							
6	Calypsostranda	-0.06	1960 to 2005	-0.10	2005 to 2017	+66	Zagórski et al. 2020
Barents Sea							
7	Varandey	-1.60	1961 to 1998	-2.40	1998 to 2012	+50	Sinitsyn et al. 2020

Map Site Number	Site Location	Historic Decadal-Scale Change		Contemporary Decadal-Scale Change		Change in Rate	References
		Rate (m yr^{-1})	Time Period	Rate (m yr^{-1})	Time Period	Percent (%)	
Kara Sea							
8	Baydaratskaya Bay	-0.61	1964 to 2005	-1.20	2005 to 2016	+97	Novikova et al. 2018
9	Kruzenstern	-0.50	1964 to 2010	-0.90	2010 to 2019	+80	Baranskaya personal communication
10	Kharasavey	-0.90	1988 to 2006	-1.20	2006 to 2016	+33	Belova et al. 2020
Laptev Sea							
11	Bykovsky Peninsula	-3.70	1982 to 2000	-5.30	2000 to 2018	+43	Grigoriev, 2019
12	Muostakh Island	-5.40	1982 to 2000	-9.50	2000 to 2018	+76	Grigoriev, 2019
Chukchi Sea							
13	Bering Land Bridge	-0.26	1980 to 2003	-0.68	2003 to 2014	+160	Farquharson et al. 2018
14	Cape Kruzenstern	-0.22	1980 to 2003	-0.13	2003 to 2014	-40	Farquharson et al. 2018

There is overwhelming evidence that erosion at ice-rich and ice-poor unconsolidated permafrost coasts is increasing in the Arctic since the early to mid-2000s when compared to decadal-scale measurements taken between ca. 1960 and ca. 1980. Higher and more fluctuating erosion rates reflect increasing coastal dynamics associated with intensified environmental changes. These larger-scale environmental changes include increases in summer air temperature, permafrost thaw and land subsidence, rising sea levels, reductions in sea ice cover and the resulting increase in open water period, and increasingly impactful storms. Combined, these changes have led to an increase in the effect of thermo-denudation and thermo-abrasion on permafrost coasts and document the cumulative effects of climate change on the Arctic System.

The future of permafrost-affected coastal research

Ongoing coastal issues in the Arctic transcend borders. A high proportion of Arctic residents live in the coastal zone, and many derive their livelihood from terrestrial and nearshore marine resources (Forbes 2011). Industrial, commercial, tourist, and military presence in the Arctic is expanding. Each will need to grapple with coastal permafrost erosion and the related impacts on the dynamics of the nearshore zone. The socio-economic consequences of an increasingly dynamic system will become a recurring theme and have a profound impact across the Arctic, influencing human decision making and adaptation planning. For example, take the remote Yupik Village of Newtok, Alaska, located in a zone of discontinuous permafrost along the Bering Sea. Annual erosion rates as high as 22 m yr^{-1} along the low-lying bluffs of Newtok have reinforced its recent relocation efforts. In the Canadian Beaufort Sea, the natural deep-water harbor in the Hamlet of Tuktoyaktuk is protected by Tuktoyaktuk Island. This island is at risk of being breached in the next 20-25 years, exposing the harbor to larger waves and intensified erosion. With the increasingly rapid pace of environmental and social change, there is ever greater need for international collaboration between researchers and impacted local societies to focus on permafrost coasts in transition.

Fortunately, more accurate, frequent, and extensive mapping of permafrost coasts has been made possible by an increase in spatial and temporal earth observations from spaceborne and airborne platforms. Access to commercial high-resolution satellite imagery, available through national and international federally-funded research projects in the US, Europe, and Russia, has increased the number of observations by several orders of magnitude at specific key sites, relative to the previous 50 years. More readily available ancillary datasets on climate, sea ice, storms, and permafrost dynamics have increased our capacity to better model and predict future coastline positions and their impacts on infrastructure. The initiation of several national and international research networks, in recent years and in past decades, has enabled closer coordination and collaboration of measurements and a better understanding of permafrost coastal dynamics. Future efforts will focus on expanding the permafrost-affected coastal change knowledge base beyond the continuous permafrost region, to include vulnerable coasts located in the discontinuous permafrost zone as well as rocky permafrost coasts. Connections between researchers and Indigenous communities have increased beyond hub communities, which allows for a more informed dialogue and representation of key issues and the factors driving rapid changes along permafrost coasts. The formation of interdisciplinary research teams and increasing collaboration across knowledge systems, such as Western science and Indigenous knowledge, has increased the scope and breadth of studies being conducted along permafrost coasts as well as their societal relevance. Combined, these developments show great promise for understanding future changes in coastal permafrost dynamics and the potential impact on both the natural and built environments.

Acknowledgments

Benjamin Jones, Louise Farquharson, Craig Tweedie, Chris Maio, and Vladimir Romanovsky were supported by grants (OISE 1927553 and 1927137) from the US National Science Foundation Office of International Science and Engineering (OISE) and Office of Polar Programs (OPP). Anna Irrgang, Hugues Lantuit, Paul Overduin, and Gonçalo Vieira were funded by the EU project Nunataryuk (grant number 773421). Stanislav Ogorodov and Alexey Maslakov were funded by the Russian Science Foundation Project 16-17-00034 and the State Budget Theme AAAA-A16-116032810055-0. Alisa Baranskaya was funded by the Russian Foundation for Basic Research (RFBR) grant 20-35-70002. Ann Gibbs, U.S.

Geological Survey, Coastal/Marine Hazards and Resources Program. Piotr Zagórski was supported from the project of the National Science Centre (Poland) No. 2013/09/B/ST10/04141, Matt Strzelecki was supported by NAWA Bekker Programme (PPN/BEK/2018/1/00306). Ingmar Nitze and Guido Grosse were funded by the ESA GlobPermafrost and ESA CCI+ Permafrost projects. Mette Bendixen is funded by The Danish Independent Research Council with grant number 8028-00008B.

References

Aré, F., 1988: Thermal abrasion of sea coasts. Polar Geography and Geology, **12**, 1-157.

Belova, N. G., A. V. Novikova, F. Günther, and N. N. Shabanova, 2020: Spatiotemporal variability of coastal retreat rates at western Yamal Peninsula, Russia, based on remotely sensed data. *J. Coastal Res.*, **95**, 367-371, https://doi.org/10.2112/SI95-071.1.

Biskaborn, B. K., and Coauthors, 2019: Permafrost is warming at a global scale. *Nature Comm.*, **10**, 264, https://doi.org/10.1038/s41467-018-08240-4.

Brown, J., M. T. Jorgenson, O. P. Smith, and W. Lee, 2003: Long-term rates of coastal erosion and carbon input, Elson Lagoon, Barrow, Alaska. In Eighth International Conference on Permafrost, Vol 21, 101-107.

Brown, J., and S. Solomon, 2000: Arctic Coastal Dynamics-Report of an International Workshop, Woods Hole, MA, November 2-4, 1999. Geological Survey of Canada Open File 3929.

Casas-Prat, M., and X. L. Wang, 2020: Projections of extreme ocean waves in the Arctic and potential implications for coastal inundation and erosion. *J. Geophys. Res.-Oceans*, **125**, e2019JC015745, https://doi.org/10.1029/2019JC015745.

Cunliffe, A. M., G. Tanski, B. Radosavljevic, W. F. Palmer, T. Sachs, H. Lantuit, J. T. Kerby, and I. H. Myers-Smith, 2019: Rapid retreat of permafrost coastline observed with aerial drone photogrammetry. *Cryosphere*, **13**, 1513-1528, https://doi.org/10.5194/tc-13-1513-2019.

Farquharson, L. M., D. H. Mann, D. K. Swanson, B. M. Jones, R. M. Buzard, and J. W. Jordan, 2018: Temporal and spatial variability in coastline response to declining sea-ice in northwest Alaska. *Mar. Geol.*, **404**, 71-83, https://doi.org/10.1016/j.margeo.2018.07.007.

Forbes, D. L., 2011: State of the Arctic coast 2010: scientific review and outlook. Land-Ocean Interactions in the Coastal Zone, Institute of Coastal Research, 178 pp.

Fritz, M., J. E. Vonk, and H. Lantuit, 2017: Collapsing Arctic coastlines. *Nat. Climate Change*, **7**, 6-7, https://doi.org/10.1038/nclimate3188.

Gibbs, A. E., B. M. Jones, and B. M. Richmond, 2020: A GIS compilation of vector shorelines and coastal bluff edge positions, and associated rate of change data for Barter Island, Alaska: U.S. Geological Survey data release, https://doi.org/10.5066/P9CRBC5I.

Grigoriev, M. N., 2019: Coastal retreat rates at the Laptev Sea key monitoring sites. *PANGAEA*, https://doi.org/10.1594/PANGAEA.905519.

Irrgang, A. M., H. Lantuit, G. K. Manson, F. Günther, G. Grosse, and P. P. Overduin, 2018: Variability in rates of coastal change along the Yukon coast, 1951 to 2015. *J. Geophys. Res.-Earth*, **123**, 779-800, https://doi.org/10.1002/2017JF004326.

Jones, B. M., and Coauthors, 2018: A decade of remotely sensed observations highlight complex processes linked to coastal permafrost bluff erosion in the Arctic. *Environ. Res. Lett.*, **13**, 115001, https://doi.org/10.1088/1748-9326/aae471.

Lantuit, H., and Coauthors, 2012: The Arctic coastal dynamics database: a new classification scheme and statistics on Arctic permafrost coastlines. *Estuar. Coasts*, **35**, 383-400, https://doi.org/10.1007/s12237-010-9362-6.

Lim, M., D. Whalen, J. Martin, P. Mann, S. Hayes, P. Fraser, H. Berry, and D. Ouellette, 2020: Massive ice control on permafrost coast erosion and sensitivity. *Geophys. Res. Lett.*, 47, e2020GL087917, https://doi.org/10.1029/2020GL087917.

Nielsen, D. M., M. Dobrynin, J. Baehr, S. Razumov, and M. Grigoriev, 2020: Coastal erosion variability at the southern Laptev Sea linked to winter sea ice and the Arctic Oscillation. *Geophys. Res. Lett.*, **47**, e2019GL086876, https://doi.org/10.1029/2019GL086876.

Novikova, A., N. Belova, A. Baranskaya, D. Aleksyutina, A. Maslakov, E. Zelenin, N. Shabanova, and S. Ogorodov, 2018: Dynamics of permafrost coasts of Baydaratskaya Bay (Kara Sea) based on multi-temporal remote sensing data. *Remote Sens.*, **10**, 1481, https://doi.org/10.3390/rs10091481.

Rachold, V., F. E. Aré, D. E. Atkinson, G. Cherkashov, and S. M. Solomon, 2005: Arctic coastal dynamics (ACD): An introduction. *Geo-Mar. Lett.*, **25**, 63-68.

Radosavljevic, B., H. Lantuit, W. Pollard, P. Overduin, N. Couture, T. Sachs, V. Helm, and M. Fritz, 2016: Erosion and flooding—Threats to coastal infrastructure in the Arctic: a case study from Herschel Island, Yukon Territory, Canada. *Estuar. Coasts*, **39**, 900-915, https://doi.org/10.1007/s12237-015-0046-0.

Shabanova, N., S. Ogorodov, P. Shabanov, and A. Baranskaya, 2018: Hydrometeorological forcing of western Russian Arctic coastal dynamics: XX-century history and current state. *Geogr. Environ. Sustain.*, **11**, 113-129.

Sinitsyn, A. O., E. Guegan, N. Shabanova, O. Kokin, and S. Ogorodov, 2020: Fifty four years of coastal erosion and hydrometeorological parameters in the Varandey region, Barents Sea. *Coastal Eng.*,**157**, 103610, https://doi.org/10.1016/j.coastaleng.2019.103610.

Tanski, G., D. Wagner, C. Knoblauch, M. Fritz, T. Sachs, and H. Lantuit, 2019: Rapid CO_2 release from eroding permafrost in seawater. *Geophys. Res. Lett.*, **46**, 11244-11252, https://doi.org/10.1029/2019GL084303.

Zagórski, P., K. Jarosz, and J. Superson, 2020: Integrated assessment of shoreline change along the Calypsostranda (Svalbard) from remote sensing, field survey and GIS. *Mar. Geod.*, **43**, 433-471, https://doi.org/10.1080/01490419.2020.1715516.

November 9, 2020

Wildland Fire in High Northern Latitudes

DOI: 10.25923/2gef-3964

A. York[1], U. S. Bhatt[2,3], E. Gargulinski[4], Z. Grabinski[1], P. Jain[5], A. Soja[4], R. L. Thoman[6,7], and R. Ziel[1]

[1]Alaska Fire Science Consortium, International Arctic Research Center, University of Alaska Fairbanks, Fairbanks, AK, USA
[2]Department of Atmospheric Sciences, University of Alaska Fairbanks, Fairbanks, AK, USA
[3]Geophysical Institute, University of Alaska Fairbanks, Fairbanks, AK, USA
[4]National Institute of Aerospace, Langley Research Center, NASA, Hampton, VA, USA
[5]Natural Resources Canada, Canadian Forest Service, Northern Forestry Centre, Edmonton, Alberta, Canada
[6]Alaska Center for Climate Assessment and Policy, University of Alaska Fairbanks, Fairbanks, AK, USA
[7]International Arctic Research Center, University of Alaska Fairbanks, Fairbanks, AK, USA

Highlights

- Wildland fire activity in high northern latitudes is highly variable, driven by subseasonal drying over weeks, and controlled by climate.
- Under prolonged warm, dry weather conditions, the accumulated layers of partially decomposed organic matter that characterize northern ecosystems become a ready fuel source and are key to regional fire phenomena (e.g., holdover fires), to interactions with the global carbon cycle, and to impacts on other aspects of these high latitude environments.
- Increasing trends in air temperature and fuel availability over the 41-year record (1979-2019) suggest that conditions are becoming more favorable for fire growth, with more intense burning, more fire growth episodes, and greater consumption of fuels.

Introduction

Despite the low annual temperatures and short growing seasons that are characteristic of high northern latitudes (HNL), wildland fire is the dominant ecological disturbance within the region's boreal forest, the world's largest terrestrial biome. The boreal forest, also known as Taiga, is the band of mostly coniferous trees that stretches across the area north of the July 13°C isotherm in North America and Eurasia. Wildland fires also impact the tundra regions bordering the Taiga. This brief report updates our previous contribution to Arctic Report Card 2017. It summarizes evidence on variability and trends in fire disturbance in HNL, describes the fuels that characterize boreal and tundra ecosystems, and outlines how climate and subseasonal fire weather conditions in HNL influence the extent of area burned in a given year.

Regional variability

Long-term burned area data have been compiled for Alaska and Canada. These data are relatively more limited in Eurasia and arctic tundra regions, presenting challenges to developing a robust circumpolar

perspective (Kukavskaya et al. 2013; Duncan et al. 2020). Figure 1 shows the geographic extent (Fig. 1a) and time series (Fig. 1b) of annual cumulative end-of-season burned area in circumpolar HNL from 55° N to 70° N for 2001-June 2020, generated using the MODIS Global Burned Area Collection 6 Product (MCD64A1; Giglio et al. 2018). Figure 2 shows annual burned area per year in Alaska and the Northwest Territories since 1980 and in the Republic of Sakha in Siberia since 2001, including both boreal and tundra regions. These records show considerable interannual variability and that large fire years in these three regions are not coincident. Alaska and the Northwest Territories have sufficiently long time series to allow an estimate of the trend via logistic regression of large (>500,000 ha) fire seasons as shown in Fig. 2a, b. The results illustrate that high-latitude wildfire varies both geographically and across decadal timeframes, with large fire seasons becoming more likely in Alaska over the past 40 years but slightly declining in the Northwest Territories.

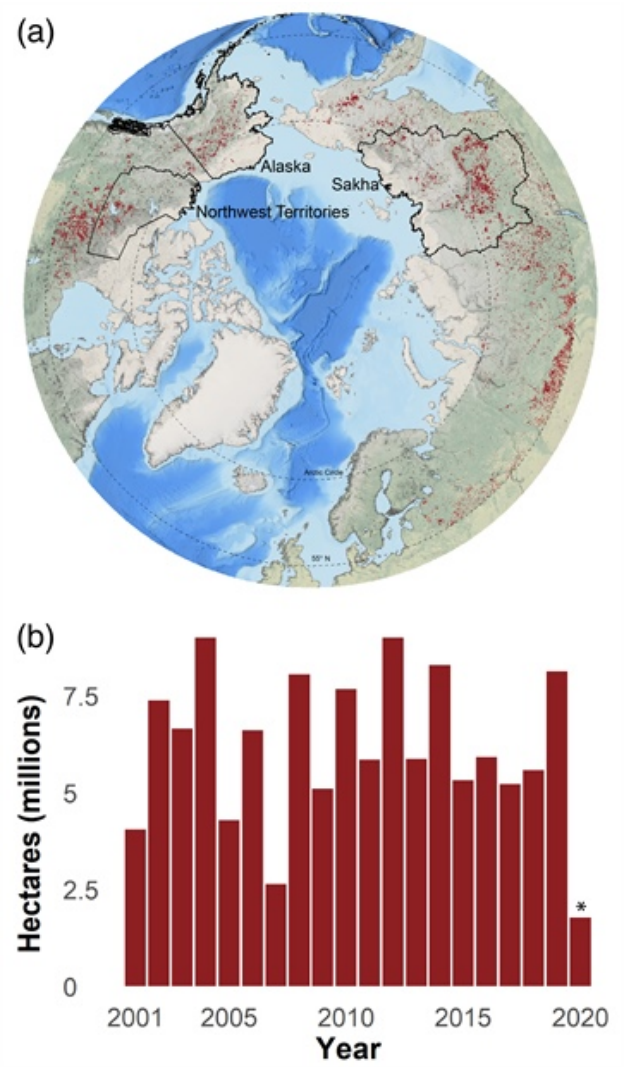

Fig. 1. Geographic extent (a) and time series (b) of annual cumulative end-of-season burned area in circumpolar high northern latitudes from 55° N to 70° N for 2001-June 2020, generated by E. Gargulinski and A. J. Soja using the MODIS Global Burned Area Collection 6 Product (MCD64A1; Giglio et al. 2018). In (a), red indicates the burned area extent, light shading indicates extent of tundra, and black outlines delineate the three regions in Fig. 2: Alaska, USA; Northwest Territories, Canada; and Republic of Sakha, Siberia, Russian Federation. Projection is lambert azimuthal equal-area North Pole. Figure by Zav Grabinski. *MODIS data are only through June 2020, due to a delay in processing following a sensor outage.

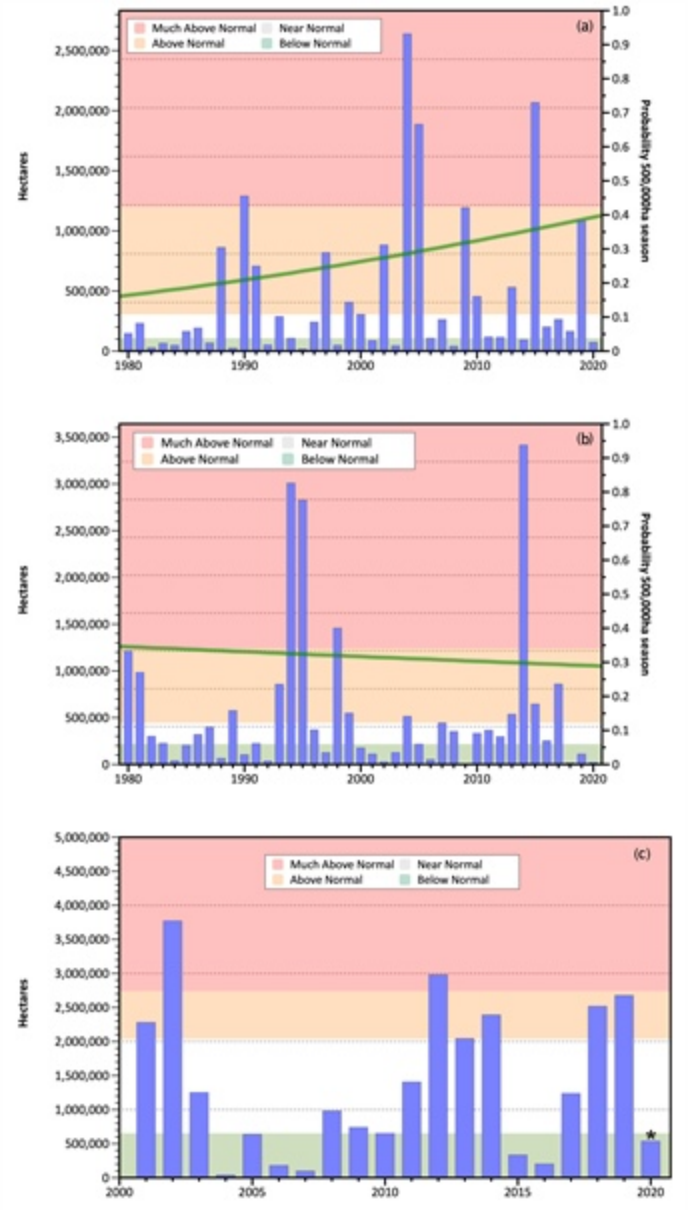

Fig. 2. Time series of burned area (in ha) in (a) Alaska 1980-2020, (b) Northwest Territories 1980-2020, and (c) Republic of Sakha 2001-June 2020, using regional definitions given in Figure 1a. "Normal" is the middle tercile (33rd-66th percentiles) of the observed distribution. In (a) and (b), the green line indicates logistic regression showing the probability of burned area of at least 500K ha. Data sources: Alaska Interagency Coordination Center (2020); Canadian National Forestry Database (2020); Sakha data are provided by A. J. Soja and E. Gargulinski. 2020 data for Alaska and NWT are preliminary. *MODIS data for Sakha are only through June 2020, missing the July burning, which typically dominates the fire season in Sakha. Figure by Rick Thoman.

Most area burned in HNL occurs during sporadic episodes of large fire growth, preceded by extended periods of drying and accompanied by anomalously hot and dry conditions (Flannigan et al. 2009). For example, 50% of the area burned in Alaska from 2002 to 2010 was consumed in just 36 days (Barrett et al. 2016). Significant weather events, such as prolonged warm dry weather, associated with blocking high pressure systems, and convective lightning storms are responsible for much of the variability in fire history (Hayasaka et al. 2016). In both Alaska and Canada, lightning-caused fires are responsible for the

majority of area burned (AICC 2020; Hanes et al. 2019), in part because lightning-ignited fires are more likely to be remote and subject to lower levels of suppression, compared to human-caused fires.

Recent large fire seasons in HNL driven by unusually warm and dry conditions include:

- 2018 in Sweden, where record May and July temperatures led to burned area of 24 thousand ha, more than 8 times the 2008-17 average (San-Miguel-Ayanz et al. 2019)
- 2019 in Alaska (Fig 2a), where 719 fires burned more than 1 million ha. Drought- and wind-driven fires in late August destroyed homes, businesses, and electric power infrastructure, and disrupted tourism and other economic activity (AICC 2020)
- The 2019 and 2020 fire seasons in Sakha (Fig 2c), which are unprecedented in the 20-year MODIS record in terms of an earlier start to the fire season and their northern extent, with some fires burning only about 11 km from the Chukchi Sea. From March through June in both 2019 and 2020, burned area was greater than 2.9 times the 20-year mean. Typically, most burning in such HNL occurs in July. Fires burned primarily in montane sub-arctic ecosystems across landscapes underlain by permafrost. (See essay *Surface Air Temperature* for information on the extreme temperature departures associated with these fires.)

Beyond immediate threats to lives and property, wildland fire has multiple impacts on HNL environments and residents. Smoke can be widespread and compromise human health, particularly in vulnerable populations. Wildfire smoke also limits visibility and constrains aviation operations, including those supporting fire suppression and detection. Black carbon derived from wildfires travels considerable distances, up to 4000 km or more, and accelerates surface melting and thawing of snow and ice by lowering the surface albedo (Thomas et al. 2017). Combustion removes the insulation provided by soil organic matter and accelerates permafrost degradation and associated disturbance of the land surface in both boreal and tundra soils, which can have multiple impacts (Jones et al. 2015). For example, the thawing of ice-rich permafrost (thermokarst) may lead to surface subsidence and hydrological changes (Romanovsky et al. 2017).

Climatological and ecosystem influences

Climate is a dominant control of fire activity on interannual and decadal scales. The relationship between climate and fire is strongly nonlinear in both boreal and tundra ecosystems, with the likelihood of fire occurrence within a 30-year period much higher where mean July temperatures exceed 13.4°C (56°F) (Young et al. 2017). HNL fire regimes appear to be responding to recent environmental changes associated with the warming climate (Soja et al. 2007; Hanes et al. 2019). Although highly variable, burned area has increased over the past several decades in much, but not all, of boreal North America (Hanes et al. 2019 and references therein). Lightning ignitions have increased in the region since 1975 and largely drove the extreme 2014 Northwest Territories and 2015 Alaska fire seasons (Veraverbeke et al. 2017). In Alaska, lightning activity increased during 1986-2015, as did summer temperatures (Bieniek et al. 2020). Partain et al. (2016) found that recent anthropogenically driven climate change increased the likelihood of the extremely dry fuel conditions seen in Alaska in 2015 by 34-60%.

Dominant vegetation varies considerably across the HNL, and species-specific traits in the conifers that carry fire in boreal forests affect regional fire regimes (Rogers et al. 2015). HNL ecosystems are also characterized by extremely limited decomposition due to low average annual air temperatures. Accumulated partially decomposed organic matter is widespread in boreal and arctic systems, often forming thick layers of potentially flammable carbon-rich moss (i.e., duff) and peat, generally termed soil

organic matter (Fig.3a). This large pool of biomass is estimated to contain 30-40% of global soil carbon (Lorenz and Lal 2010). Under long daylengths in June and July, these fuelbeds can dry rapidly over weeks (versus seasonal curing in arid climates at lower latitudes), increasing flammability even before drought reaches significant levels (Ziel et al. 2020). Once established in these fuels, fires can smolder for long periods and may form deep hot ash pits (Fig. 3b) that can overwinter to re-emerge in spring (Wheeling, 2020). At least 10 fires overwintered in the Northwest Territories from 2014-2015 (Wohlberg 2015) and at least 40 in Alaska from 2005-2020 (AICC 2020). Satellite imagery suggests that a large number of overwintering fires in Siberia from 2019 jumpstarted the 2020 season (Wheeling, 2020).

Fig. 3. (a) Profile of duff plug from black spruce woodland in Fairbanks, AK. Photo by Zav Grabinski. (b) Firefighter indicating the depth (approximately 30 cm) of an ash pit on the McKinley fire, August 2019. Firefighters and homeowners have been injured in hot ash pits following fires during drought conditions that allowed deep burning into duff layers. Photo by R. Saba, Alaska Incident Management Team.

The combustion of soil organic matter in boreal and arctic fires has large impacts on the global carbon cycle, including potential positive feedbacks to climate warming through direct emissions from combustion and accelerated decomposition and thermokarsting (Walker et al. 2019). Additional feedbacks from fire to HNL ecosystems include interactions with vegetation succession (Mekonnen et al. 2019 and references therein), biogeochemical cycles (Bond-Lamberty et al. 2007), energy balance (Potter et al. 2019), and hydrology (Liu et al. 2005).

Reflecting the importance of cumulative drying on fuelbed flammability, the Canadian Forest Fire Danger Rating System (CFFDRS) uses its Buildup Index (BUI) (Wotton 2009) as a numerical rating of fuel availability for consumption. BUI is derived from daily accounting of surface temperature, relative humidity, and 24-hour rainfall totals. In boreal and arctic systems BUI reflects the flammability of duff fuels below the surface. As BUI crosses significant thresholds, fires can burn more intensely, spread more aggressively, and pose more problems for suppression. Surface air temperatures effectively represent the influence of solar radiation and moisture deficits as well as fuel heating on ignition and fire spread.

Figure 4 shows 2 m air temperature and BUI trends and time series for boreal and tundra regions of Eurasia and North America in June for the 41-year period of record (1979-2019), calculated using the European Center Reanalysis version 5 (ERA5) (McElhinny et al. 2020). Widespread increases in temperature and BUI in both June and July (data not shown) and on both continents suggest that conditions are becoming more favorable for fire growth, with increases in cumulative drying and flammability likely to result in more intense burning, more fire growth episodes, and greater consumption of fuels.

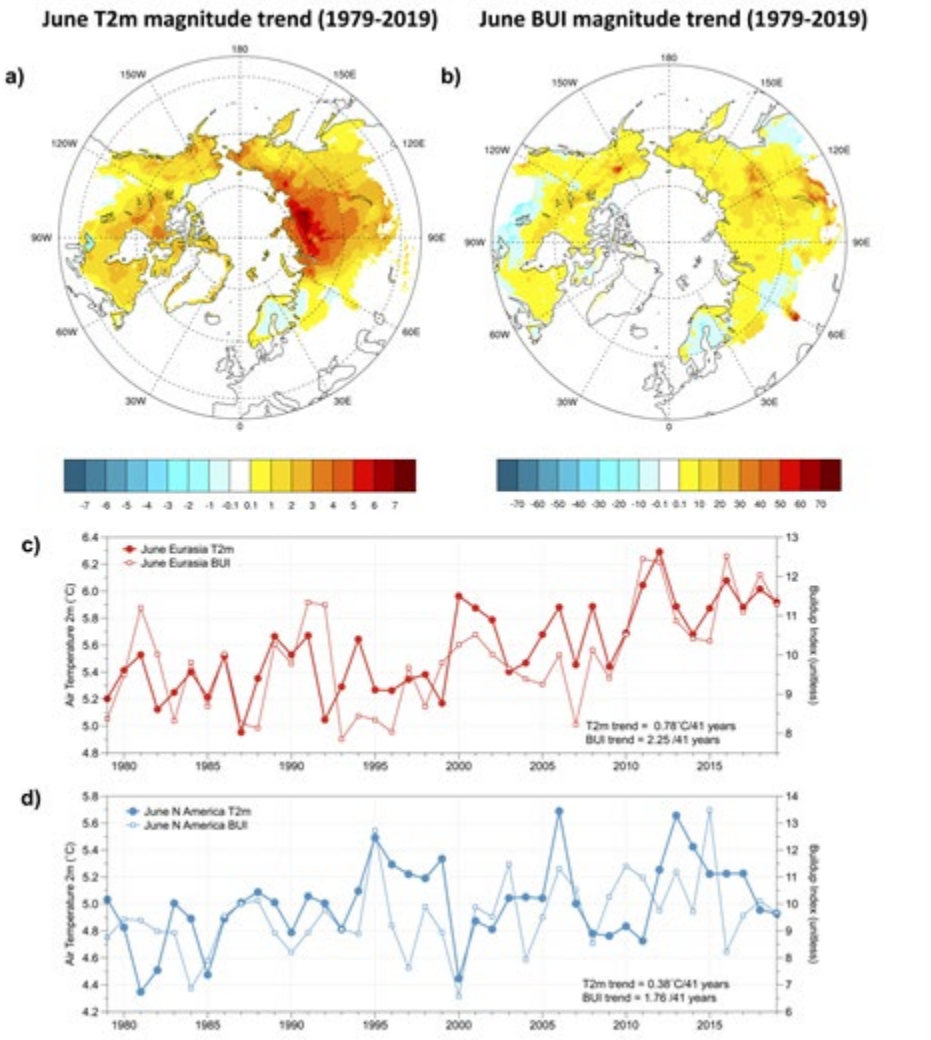

Fig. 4. Boreal and tundra air temperature at 2 m (T2m, in °C) trend (a) and Buildup Index (BUI, unitless) trend (b) in June for the full 1979-2019 period, from the European Center Reanalysis version 5 (ERA5). June T2m and BUI time series for boreal and tundra areas of Eurasia (c) and North America (d). Figure by Uma Bhatt.

These observations of area burned, BUI, and temperature are consistent with analyses projecting significant increases (up to four-fold) in burned area in HNL ecosystems by the end of the 21st century under a range of climate change scenarios (French et al. 2015; Young et al. 2017; Yue et al. 2015, and references therein). Because specific fire events depend on multiple interacting factors, the resulting changes in HNL fire regimes will vary greatly over space and time. However, all evidence indicates that northern ecosystems will become increasingly vulnerable to wildland fire and its impacts.

References

Alaska Interagency Coordination Center (AICC), 2020: Alaska fire history data. https://fire.ak.blm.gov/predsvcs/intel.php, accessed 10 September 2020.

Barrett, K., T. Loboda, A. D. McGuire, H. Genet, E. Hoy, and E. Kasischke, 2016: Static and dynamic controls on fire activity at moderate spatial and temporal scales in the Alaskan boreal forest. *Ecosphere*, **7**(11), e01572, https://doi.org/10.1002/ecs2.1572.

Bieniek, P. A., U. S. Bhatt, A. York, J. E. Walsh, R. Lader, H. Strader, R. H. Ziel, R. R. Jandt, and R. L. Thoman, 2020: Lightning variability in dynamically downscaled simulations of Alaska's present and future summer climate. *J. Appl. Meteor. Climatol.*, **59**, 1139-1152, https://doi.org/10.1175/JAMC-D-19-0209.1.

Bond-Lamberty, B., S. D. Peckham, D. E. Ahl, and S. T. Gower, 2007: Fire as the dominant driver of central Canadian boreal forest carbon balance. *Nature*, **450**(7166), 89-92. https://doi.org/10.1038/nature06272.

Canadian National Forestry Database, 2020: Area burned by jurisdiction. http://nfdp.ccfm.org/en/data/fires.php, accessed September 10, 2020.

Duncan, B. N., and Coauthors, 2020: Space-based observations for understanding changes in the arctic-boreal zone. *Rev. Geophys.*, **58**, e2019RG000652, https://doi.org/10.1029/2019RG000652.

Flannigan, M., B. Stocks, M. Turetsky, and M. Wotton, 2009: Impacts of climate change on fire activity and fire management in the circumboreal forest. *Glob. Change Biol.*, **15**, 549-560, https://doi.org/10.1111/j.1365-2486.2008.01660.x.

French, N. H. F., L. K. Jenkins, T. V. Loboda, M. Flannigan, R. Jandt, L. L. Bourgeau-Chavez, and M. Whitley, 2015: Fire in arctic tundra of Alaska: past fire activity, future fire potential, and significance for land management and ecology. *Int. J. Wildland Fire*, **24**(8), 1045-1061, https://doi.org/10.1071/WF14167.

Giglio, L., L. Boschetti, D. P. Roy, M. L. Humber, and C. O. Justice, 2018: The Collection 6 MODIS burned area mapping algorithm and product. *Remote Sens. Environ.*, **217**, 72-85. https://doi.org/10.1016/j.rse.2018.08.005.

Hanes, C. C., X. Wang, P. Jain, M. A. Parisien, J. M. Little, and M. D. Flannigan, 2019: Fire-regime changes in Canada over the last half century. *Can. J. For. Res.*, **49**(3), 256-269, https://doi.org/10.1139/cjfr-2018-0293.

Hayasaka, H., H. L. Tanaka, and P. A, Bieniek, 2016: Synoptic-scale fire weather conditions in Alaska. *Polar Sci.*, **10**(3), 217-226, https://doi.org/10.1016/j.polar.2016.05.001.

Jones, B., G. Grosse, C. D. Arp, E. A. Miller, L. Liu, D. J. Hayes, and C. F. Larsen, 2015: Recent Arctic tundra fire initiates widespread thermokarst development. *Sci. Rep.*, **5**, 15865, https://doi.org/10.1038/srep15865.

Kukavskaya, E. A., A. J. Soja, A. P. Petkov, E. I. Ponomarev, G. A. Ivanova, and S. G Conard, 2013: Fire emissions estimates in Siberia: evaluation of uncertainties in area burned, land cover, and fuel consumption. *Can. J. For. Res.*, **43**, 493-506, https://doi.org/10.1139/cjfr-2012-0367.

Liu, H., J. T. Randerson, J. Lindfors, and F. S. Chapin, 2005: Changes in the surface energy budget after fire in boreal ecosystems of interior Alaska: An annual perspective. *J. Geophys. Res.*, **110**(D13), D13101, https://doi.org/10.1029/2004JD005158.

Lorenz, K., and R. Lal, 2010: Carbon Sequestration in Forest Ecosystems, pp. 159-205, Springer Netherlands, https://doi.org/10.1007/978-90-481-3266-9.

McElhinny, M., J. F. Beckers, C. Hanes, M. Flannigan, and P. Jain, 2020: A high-resolution reanalysis of global fire weather from 1979 to 2018 - overwintering the Drought Code. *Earth Syst. Sci. Data*, **12**, 1823-1833, https://doi.org/10.5194/essd-12-1823-2020.

Mekonnen, Z. A., W. J. Riley, J. T. Randerson, R. F. Grant, and B. M. Rogers, 2019: Expansion of high-latitude deciduous forests driven by interactions between climate warming and fire. *Nat. Plants*, **5**, 952-958, https://doi.org/10.1038/s41477-019-0495-8.

Partain, J. L., and Coauthors, 2016: An assessment of the role of anthropogenic climate change in the Alaska fire season of 2015 [in "Explaining Extremes of 2015 from a Climate Perspective"]. *Bull. Amer. Met. Soc.*, **97**(12), S14-S18, https://doi.org/10.1175/BAMS-D-16-0149.1.

Potter, S., and Coauthors, 2019: Climate change decreases the cooling effect from postfire albedo in boreal North America. *Glob. Change Biol.*, **26,** 1592-1607, https://doi.org/10.1111/gcb.14888.

Romanovsky, V., and Coauthors, 2017: Changing permafrost and its impacts. In: Snow, Water, Ice and Permafrost in the Arctic (SWIPA) 2017. pp. 65-102. Arctic Monitoring and Assessment Programme (AMAP), Oslo, Norway.

Rogers, B. M., A. J. Soja, M. L. Goulden, and J. T. Randerson, 2015: Influence of tree species on continental differences in boreal fires and climate feedbacks. *Nat. Geosci.*, **8**(3), 228-234, https://doi.org/10.1038/ngeo2352.

San-Miguel-Ayanz, J., and Coauthors, 2019: Forest Fires in Europe, Middle East and North Africa 2018. EUR 29856 EN, Publications Office of the European Union, Luxembourg. https://doi.org/10.2760/1128.

Soja, A. J., and Coauthors, 2007: Climate-induced boreal forest change: predictions versus current observations. *Glob. Planet. Change*, **56**, 274-296, https://doi.org/10.1016/j.gloplacha.2006.07.028.

Thomas, J. L., and Coauthors, 2017: Quantifying black carbon deposition over the Greenland ice sheet from forest fires in Canada. *Geophys. Res. Lett.*, **44**, 7965-7974, https://doi.org/10.1002/2017GL073701.

Veraverbeke, S., B. M. Rogers, M. L. Goulden, R. R. Jandt, C. E. Miller, E. B. Wiggins, and J. T. Randerson, 2017: Lightning as a major driver of recent large fire years in North American boreal forests. *Nat. Climate Change*, **7**, 529-534, https://doi.org/10.1038/nclimate3329.

Walker, X. J., and Coauthors, 2019: Increasing wildfires threaten historic carbon sink of boreal forest soils. *Nature*, **572**, 520-523, https://doi.org/10.1038/s41586-019-1474-y.

Wheeling, K., 2020: The rise of zombie fires. *Eos*, **101**, https://doi.org/10.1029/2020EO146119.

Wohlberg, M., 2015: 'Well on our way to another record drought code year': NWT fire manager. Northern Journal, June 23, 2015, https://norj.ca/2015/06/well-on-our-way-to-another-record-drought-code-year-nwt-fire-manager/.

Wotton, B. M., 2009: Interpreting and using outputs from the Canadian Forest Fire Danger Rating System in research applications. *Environ. Ecol. Stat.*, **16**, 107-131, https://doi.org/10.1007/s10651-007-0084-2.

Young, A. M., P. E. Higuera, P. A. Duffy, and F. S. Hu, 2017: Climatic thresholds shape northern high-latitude fire regimes and imply vulnerability to future climate change. *Ecography*, **40**, 606-617, http://dx.doi.org/10.1111/ecog.02205.

Yue, X., L. J. Mickley, J. A. Logan, R. C. Hudman, M. V. Martin, and R. M. Yantosca, 2015: Impact of 2050 climate change on North American wildfire: consequences for ozone air quality. *Atmos. Chem. Phys.*, **15**, 10033-10055, https://doi.org/10.5194/acp-15-10033-2015.

Ziel, R. H., P. A. Bieniek, U. S. Bhatt, H. Strader, T. S. Rupp, and A. York, 2020: A comparison of fire weather indices with MODIS fire days for the natural regions of Alaska. *Forests*, **11**, 516, https://doi.org/10.3390/f11050516.

November 12, 2020

The MOSAiC Expedition: A Year Drifting with the Arctic Sea Ice

DOI: 10.25923/9g3v-xh92

M. D. Shupe[1,2], M. Rex[3], K. Dethloff[3], E. Damm[4], A. A. Fong[4], R. Gradinger[5], C. Heuzé[6], B. Loose[7], A. Makarov[8], W. Maslowski[9], M. Nicolaus[4], D. Perovich[10], B. Rabe[4], A. Rinke[3], V. Sokolov[8], and A. Sommerfeld[3]

[1]Cooperative Institute for Research in Environmental Sciences, University of Colorado Boulder, Boulder, CO, USA
[2]Physical Sciences Laboratory, NOAA, Boulder, CO, USA
[3]Alfred Wegener Institute, Helmholtz Center for Polar and Marine Research, Potsdam, Germany
[4]Alfred Wegener Institute, Helmholtz Center for Polar and Marine Research, Bremerhaven, Germany
[5]Department of Arctic and Marine Biology, University of Tromsø, Tromsø, Norway
[6]Department of Earth Sciences, University of Gothenburg, Göteborg, Sweden
[7]Graduate School of Oceanography, University of Rhode Island, South Kingston, RI, USA
[8]Arctic and Antarctic Research Institute, St. Petersburg, Russia
[9]Department of Oceanography, Naval Postgraduate School, Monterey, CA, USA
[10]Thayer School of Engineering, Dartmouth College, Hanover, NH, USA

Highlights

- An international and interdisciplinary team made comprehensive observations of the atmosphere, sea ice, ocean, ecosystem, and biogeochemistry over an annual cycle in the Central Arctic.
- The MOSAiC year was characterized, above all, by a thin and dynamic sea ice pack, reflecting the impact of the multi-decadal warming trend in global air temperatures on the Arctic region.
- The unprecedented data set will foster cross-cutting, process-based research that will advance understanding, bolster observational techniques from the surface and satellites, and enable improved modeling and predictive capabilities.

The Arctic sea ice has a story to tell. It is a story of change and transformation on daily, seasonal, and decadal scales. It is a story of complex interactions and feedbacks, of processes that link the ice in myriad ways with the Arctic and global systems. It is a story that has been difficult to represent with numerical models. To better understand this story has been one of the primary objectives of the Multidisciplinary drifting Observatory for the Study of Arctic Climate (MOSAiC). MOSAiC is a scientific odyssey centered on a yearlong expedition into the heart of the Arctic, to explore the story of the changing sea ice, to unravel the interdependent processes involved, and to reveal the implications of this change.

Motivation

The changing Arctic has many societally-relevant implications. As the sea ice declines the Arctic is opening for expanded commerce, resource development, tourism, and shipping (Alvarez et al. 2020). Local communities and ecosystems are affected (e.g., Cooley et al. 2020). Arctic change may also be linked with large-scale circulation patterns that influence mid-latitude weather (Cohen et al. 2020) and global ocean structure (Sévellec et al. 2017). For all these implications, it is essential to understand the changing Arctic system at a level that can be represented in our predictive models. For example, to successfully operate in the Arctic requires reliable forecasts of sea ice on sub-seasonal to seasonal time scales. Moreover, higher-quality regional and global weather predictions rely on improved representation of hemispheric-scale interactions with a changing Arctic. To assess current and future ecosystem health necessitates models that realistically link physical and biological systems. Long-term societal planning requires coupled climate models that produce robust predictions of future changes. Importantly, all of these modeling priorities rely on accurate representation of processes and feedbacks that depict how the Earth system behaves and responds to perturbations. Essential processes cut across the Arctic system, linking the atmosphere, sea ice, ocean, and land through physical, chemical, and biological pathways.

The expedition

To address this need for cross-disciplinary, process-level understanding and thereby advance models, an international consortium of world-leading Arctic researchers, institutions, and funding agencies envisioned, planned, and executed the most comprehensive exploration of the central Arctic system to date. The MOSAiC expedition started in September 2019 as the German icebreaker *Polarstern* left Norway, traveled through the northern Laptev Sea, and moored itself inside the freezing sea ice pack (Fig. 1). Over the following weeks, racing the setting sun, the research team established an ice camp around the ship called the Central Observatory (CO), complete with paths, powerlines, sampling areas, and clusters of instruments. Simultaneously, a distributed network of quasi-autonomous systems was installed by the Russian icebreaker *Akademik Federov* at scales of 5-40 km in all directions surrounding the CO to assess spatial variability and scale. For the following 10 months this intensive constellation of research assets passively drifted with the sea ice across the central Arctic, following the Transpolar Drift, until reaching the ice edge in Fram Strait on 31 July 2020, nearly 1800 km from its starting position (Fig. 2). Thereafter, *Polarstern* was relocated further north, to continue this full-year endeavor through September 2020. Along the way, partner icebreakers supported periodic resupply and personnel rotations, scientific aircraft probed the atmosphere and surface in more detail, and an unprecedented collection of satellite observations for the region was assembled.

Fig. 1. *Polarstern* during polar night, with crack in the ice. (Photo: Matthew Shupe)

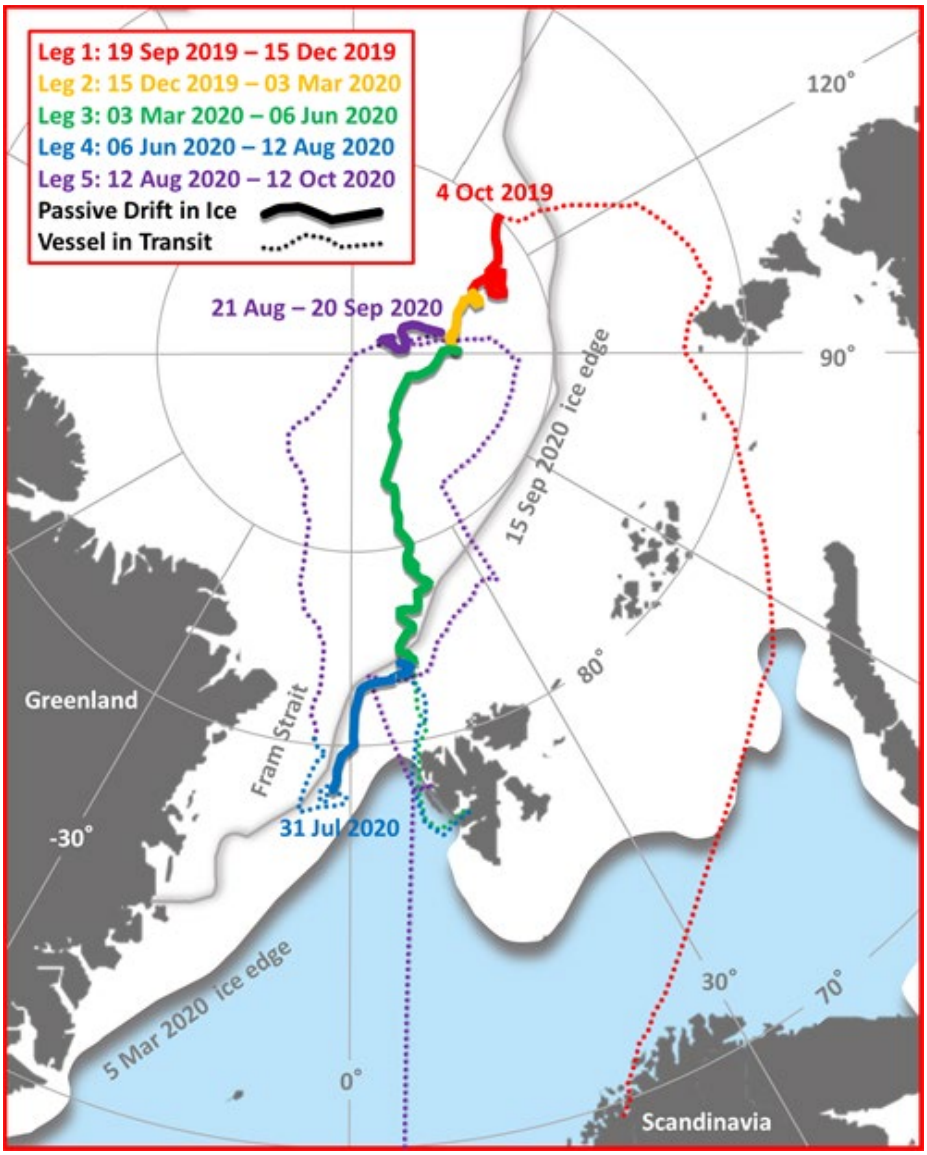

Fig. 2. The MOSAiC Expedition route, including the passive drift of the MOSAiC ice camp (solid) with dates of drift annotated, and in transit movements of *Polarstern* (dashed) delineated by legs (colors).

Modeled after Nansen's historic Fram expedition (Nansen 1897), the Surface Heat Budget of the Arctic Ocean (SHEBA) experiment (Uttal et al. 2002), and the long-standing Russian North Pole drifting stations (Frolov et al. 2005), MOSAiC took the concept to a new level of sophistication, interdisciplinarity, and comprehensiveness. It captured a full year in the Arctic ice, linking continuous seasons and their transitions, including the rarely observed central Arctic winter. It represented a tremendously diverse and modern set of observations probing the atmosphere, sea ice, ocean, ecosystem, and biogeochemistry, all designed to enable cross-disciplinary process research. Lastly, it was designed to serve a broad user community, including important international modeling activities such as the World Meteorological Organization's Polar Prediction Project (Jung et al. 2016).

Navigating challenges to reveal opportunities

The quest to understand the story of the Arctic sea ice is not an easy one, and the MOSAiC expedition, like many in the past, was beset by challenges that at times threatened parts of the program. Yet, with these challenges came unprecedented opportunities for a deeper scientific understanding.

Challenges started with simply finding an ice floe to moor the ship and conduct observations, as the ice in the target region was thinner than expected and transected with foreboding ridges. In the end a floe was selected with a heavily ridged inner core, which originally formed on the Siberian Shelf (Krumpen et al. 2020), to provide stability over a years' drift. This floe was wrapped with thinner ice, some newly forming, to offer insight into the new, thinner Arctic ice pack. Yet even before on-ice installations were complete, ice dynamics started to pose a huge challenge that would persist for most of the year: frequent and dramatic cracks in the ice. Leads opened and ridges formed, limiting access and power to instrument sites, and forcing relocation of installations. On many occasions the heightened dynamics hindered the ability to measure the processes responsible for these very dynamics! Early on it became clear that MOSAiC was to have a front row seat to observe an evolving, highly dynamic ice pack.

As the calendar turned to early 2020, a stagnant circulation pattern over the central Arctic led to record-high positive values of the Arctic Oscillation Index with warm air moving over the sea ice pack from north-central Siberia (see essay *Surface Air Temperature*) and record ozone loss in the lower stratosphere (Wohltmann et al. 2020). While representing a unique opportunity to witness this unprecedented, and unexpected, circulation pattern, the pattern also pushed *Polarstern* across the central Arctic faster than anticipated, about three times as fast as Nansen's historic expedition along a similar route. During the progressing spring, further ice dynamics eventually destroyed much of the original CO domain.

After a brief exit from the ice from late May to early June due to another major challenge—the global coronavirus pandemic—*Polarstern* rejoined its network of autonomous measurements and moored to a new position on the MOSAiC floe to observe summer melt (Fig. 3). An earlier-than-expected entry into Fram Strait and a retreating ice edge foretold a rapid melt and impending end. However, a fortunate lull in ice dynamics enabled a consistent and comprehensive assessment of the melt, the associated formation of freshwater lenses, and their impacts on vertical exchange and structure of the atmosphere-ice-ocean system. The remarkable stability of the floe's ridged core enabled the unique opportunity to follow this floe to the very end of its lifecycle a few kilometers from the open ocean. Measurements continued to the last possible moment, ending with a spectacular disintegration of the floe as equipment was lifted onboard.

Fig. 3. *Polarstern* and the second Central Observatory. (Photo: Markus Rex)

To bring MOSAiC full circle, and achieve the full year in ice, *Polarstern* ventured back northward through areas of thinner-than-average sea ice (see essay *Sea Ice*). After establishing a new camp on 21 August 2020 (Fig. 4), the expedition was again confronted with ice dynamics fracturing the very ice being studied. But now the sea ice started a transition toward freeze-up. In these waning days, the expedition quantified the loss of energy from the upper ocean, and the subtle changes in surface reflectance as melt ponds froze over and were dusted with the season's first snows. All of these processes worked together to send the ice back into the autumn freeze, reminiscent of conditions when the expedition began a year earlier.

Fig. 4. Part of the MOSAiC ice camp in September 2020, with tethered balloon, meteorological tower, and other installations on the ice. (Photo: Marcel Nicolaus)

Groundwork for the future

Through MOSAiC we have learned much about studying the new Arctic. The thinning ice pushes us to adjust how we observe this Arctic system and to consider new approaches for interdisciplinary and autonomous measurements. The expedition built tremendous capacity, exposing scores of early career scientists to the challenges of field research. MOSAiC also demonstrated the strength of international collaboration by bringing together funding from 20 nations and participants from at least 37 nations. During all stages of the planning, field expedition, scientific analysis, and outreach, the MOSAiC consortium, through intense cooperation and mutual support has accomplished much more collectively than would have been possible through individual disciplinary or national efforts.

At this early stage, it is not known what all will be learned from the MOSAiC year; the pieces have not yet been assembled and synthesized. But it is obvious that the sea ice has revealed a great deal of its story over the course of this scientific adventure. It is a story of thinner and more dynamic ice, with likely impacts on upper ocean mixing, the exchange of gases, aerosols, and moisture with the atmosphere and clouds, the seasonal cycle of productivity, and the evolution of surface reflectance, to name a few key processes. MOSAiC was in an opportune place and time to experience this story, and to collect the data with which to explore it. These data, the legacy of MOSAiC, are now starting to become publicly available and will be entirely so by 1 January 2023. In the years to come, the scientific community will embark on a further journey to harness this wealth of new information toward advancing knowledge, enhancing observational techniques, improving model predictions, and broadening global awareness of the changing Arctic.

Acknowledgments

MOSAiC was led by the Alfred Wegener Institute, Helmholtz Center for Polar and Marine Research with significant funding from the German Federal Ministry of Education and Research. US contributions were provided by the National Science Foundation, Department of Energy, NOAA and NASA. Many other international agencies and institutions made significant contributions.

References

Alvarez, J., D. Yumashev, and G. Whiteman, 2020: A framework for assessing the economic impacts of Arctic change. *Ambio*, **49**, 407-418, https://doi.org/10.1007/s13280-019-01211-z.

Cohen, J., and Coauthors, 2020: Divergent consensuses on Arctic amplification influence on midlatitude severe winter weather. *Nat. Climate Change*, **10**, 20-29, https://doi.org/10.1038/s41558-019-0662-y.

Cooley, S. W., J. C. Ryan, L. C. Smith, C. Horvat, B. Pearson, B. Dale, and A. H. Lynch, 2020: Coldest Canadian Arctic communities face greatest reductions in shorefast sea ice. *Nat. Climate Change*, **10**, 533-538, https://doi.org/10.1038/s41558-020-0757-5.

Frolov, I. E., Z. M. Gudkovich, V. F. Radionov, A. V. Shirochkov, and L. A. Timokhov, 2005: The Arctic Basin: results from the Russian drifting stations. Praxis Publishing. Chischester, 270 pp.

Jung, T., and Coauthors, 2016: Advancing Polar prediction capabilities on daily to seasonal time scales. *Bull. Amer. Meteor. Soc.*, **97**, 1631-1647, https://doi.org/10.1175/BAMS-D-14-00246.1.

Krumpen, T., and Coauthors, 2020: The MOSAiC ice floe: sediment-laden survivor from the Siberian shelf. *Cryosphere*, **14**, 2173-2187, https://doi.org/10.5194/tc-14-2173-2020.

Nansen, F., 1897: Farthest north: Being the record of a voyage of exploration of the ship "Fram" 1893-96 and of a fifteen months' sleigh journey by Dr. Nansen and Lieut. Johansen. Harper and Brothers, https://doi.org/10.1037/12900-000.

Sévellec, F., A. V. Fedorov, and W. Liu, 2017: Arctic sea-ice decline weakens the Atlantic meridional overturning circulation. *Nat. Climate Change*, **7**, 604-610, https://doi.org/10.1038/nclimate3353.

Uttal, T., and Coauthors, 2002: Surface heat budget of the Arctic Ocean. *Bull. Amer. Meteor. Soc.*, **83**, 255-276, https://doi.org/10.1175/1520-0477(2002)083<0255:SHBOTA>2.3.CO;2.

Wohltmann, I., and Coauthors, 2020: Near-complete local reduction of Arctic stratospheric ozone by severe chemical loss in spring 2020. *Geophys. Res. Lett.*, **47**, e2020GL089547, https://doi.org/10.1029/2020GL089547.

November 9, 2020

Integrating Models and Observations to Better Predict a Changing Arctic Sea Ice Cover

DOI: 10.25923/bx13-ja71

M. M. Holland[1], M. Bushuk[2], A. Jahn[3], and A. Roberts[4]

[1]Climate and Global Dynamics Laboratory, National Center for Atmospheric Research, Boulder, CO, USA
[2]Geophysical Fluid Dynamics Laboratory, NOAA, Princeton, NJ, USA
[3]Department of Atmospheric and Oceanic Sciences and Institute of Arctic and Alpine Research, University of Colorado, Boulder, CO, USA
[4]Theoretical Division, Los Alamos National Laboratory, Los Alamos, NM, USA

Highlights

- Recent advances, including the use of large model ensembles, satellite simulators for remotely-sensed data comparisons, and data assimilation techniques, have enabled more informative use of Arctic observations for climate simulation assessment, improvements in models, and better forecast initialization.
- These advances in integrating models and observations have increased the skill and utility of Arctic sea ice predictions across timescales from seasons to centuries.

Introduction

The Arctic is rapidly changing in response to rising greenhouse gas concentrations. To better prepare for Arctic change, reliable predictions are needed across a range of timescales. This includes sub-seasonal forecasts that aid near-term planning to multi-decadal projections that allow for informed decisions on climate change mitigation and adaptation. The sources of predictability differ across timescales. Accurate initial conditions are critical for near-term forecasts while longer-term climate projections are subject to assumptions on future climate drivers, such as changing greenhouse gas emissions. These predictions use physics-based models to represent the atmosphere, ocean, sea ice, and land. These models simulate the evolution of environmental conditions on timescales of hours to centuries, and have skillfully predicted Arctic change. Innovative methods for simulation assessment, model development, and forecast initialization are allowing better integration of models and observations to advance predictions.

Using observations to assess climate simulations

Comparison of simulated climate with observations can identify model deficiencies, which may influence the reliability of climate predictions. However, making appropriate comparisons is fraught with challenges. Arctic in situ measurements are sparse and represent single locations instead of the aggregate spatial quantities represented in a model. Remotely sensed data have spatial sampling more comparable to models, albeit often at higher resolution. They rely on algorithms to translate measured signals into environmental properties, which can result in incompatible definitions between remotely

sensed and simulated variables. Most observational records are short, typically a few decades or less, and subsurface measurements (e.g., under sea ice) are particularly limited.

A number of new approaches are enabling better use of observations for assessing simulation of Arctic climate. Climate models simulate climate variations over time, including variability that occurs both naturally and in response to external drivers like rising greenhouse gas concentrations. However, the naturally occurring variations are chaotic, meaning that while models simulate these variations, their temporal evolution will not match that of the observations. The advent of large ensembles in which many climate simulations are performed with the same external drivers, but with different simulated natural variations (e.g., Deser et al. 2020), allows us to compare the single observed realization within the envelope of simulated climates. This enables a fairer assessment of simulation quality in light of naturally occurring variability (e.g., for sea ice examples, see Swart et al. 2015; Jahn et al. 2016).

The compilation of remotely-sensed sea ice data beyond ice concentration, such as ice thickness and seasonal indicators (e.g., onset of melt or freeze-up), is enabling more in-depth process-based assessment, which can help identify the cause of model biases. For example, seasonal sea ice change indicators were used in a recent model assessment to reveal that melt onset is simulated too early in many CMIP6 models (Fig. 1; Smith et al. 2020). It also revealed that a bias in melt onset can compensate for a thin ice cover, leading to simulated September extents consistent with observations, but for the wrong physical reasons (Smith et al. 2020). Such process-based model assessments can provide insights on model development needs that can ultimately improve predictions and projections.

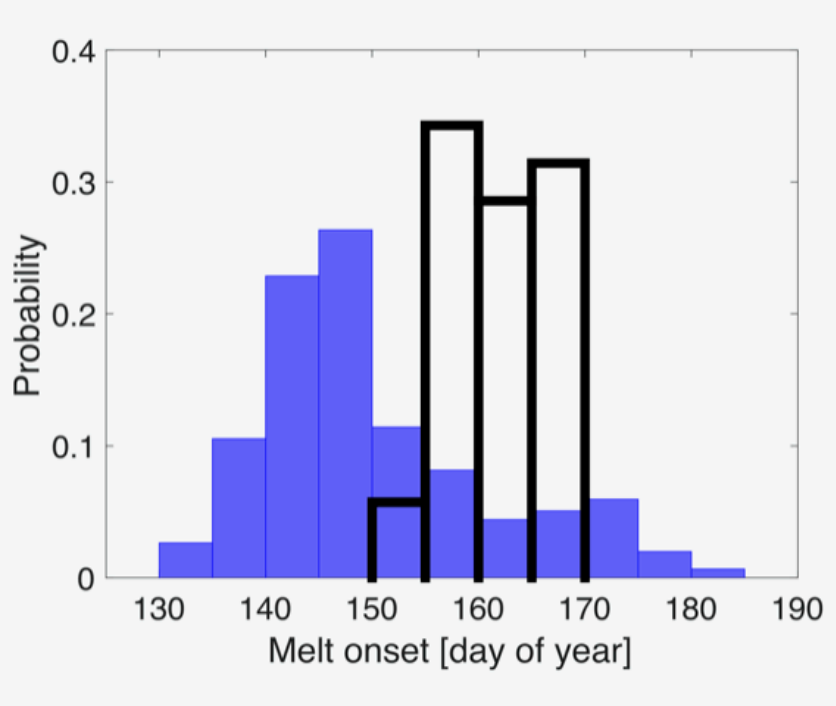

Fig. 1. Using 1979-2013 melt onset data for process-based model assessment; histogram of melt onset date from observations (black; Steele et al. 2019) and CMIP6 models (blue). Based on CMIP6 data from Smith et al. (2020).

Assessment efforts using remotely sensed data have also made advances through the development of satellite simulators within climate models (e.g., Yu et al. 1996). These simulators convert model variables into the remotely sensed measurement quantities, allowing for a direct comparison of the two. Cloud-property simulators (e.g., Bodas-Salcedo et al. 2011) have become widely used and several sea-ice

simulators currently under development show promise for better interpreting remotely sensed information for climate modeling (e.g., Burgard et al. 2020a,b).

Using observations to improve models

Measurements are critical for improving the representation of processes within models and are most useful for model development when collated to describe multiple aspects of Arctic phenomena. For this, observations are commonly combined in two distinct ways: First, long records of variables with broad spatial coverage are used to ascertain the likelihood of a simulated state, and its compatibility with observations. Examples of this type of application include quantification of skill and bias of simulated Arctic variability and mean state, for example, for sea ice extent (Yang and Magnusdottir 2018). Second, data of a particular phenomenon are used to characterize its statistical properties for use in model improvements, for example, for sea ice ridging (Roberts et al. 2019). For both of these approaches, sufficiently large datasets are needed that take into account spatial and temporal autocorrelation of the observable quantity, and compatibility between observations and models.

Sea ice has many heterogeneous properties (Fig. 2a) that are important for sea ice melt, growth, and motion, and in turn impact climate. These properties occur at spatial scales below the size of a model grid cell, which is typically around 100 km for a coupled Earth system model, meaning they are not resolved and thus are in need of parameterization. Frequent observations of properties like ice thickness and freeboard, snow conditions, melt-ponds, and mass and energy fluxes over an intensely studied field area are essential for process understanding and for developing statistical aggregations of ridging, snow deposition, albedo, and ponding for use in model parameterizations. However, for some applications, more observations are not always better and autocorrelation and sample size are important when considering the design of an Arctic observing system. For example, simulated ice thickness is highly auto-correlated in space and time (Blanchard-Wrigglesworth and Bitz 2014); therefore, daily freeboard observations within close proximity yield little extra benefit compared to sparser weekly observations when assessing model skill on seasonal to decadal timescales. For this reason, the 91-day repeat orbits of the NASA Ice, Cloud, and land Elevation Satellite—ICESat and ICESat-2 (Markus et al. 2017)—are ideal for evaluating simulations (Fig. 2b), offering broad spatial coverage of the Arctic ice pack, seasonally separated in time, while yielding meaningful compatibility intervals and spatially distributed estimates of ice freeboard as a proxy for thickness. Such evaluations depend on an operational operator (e.g., Bench 2016) for converting modeled ice and snow thickness to satellite-equivalent freeboard.

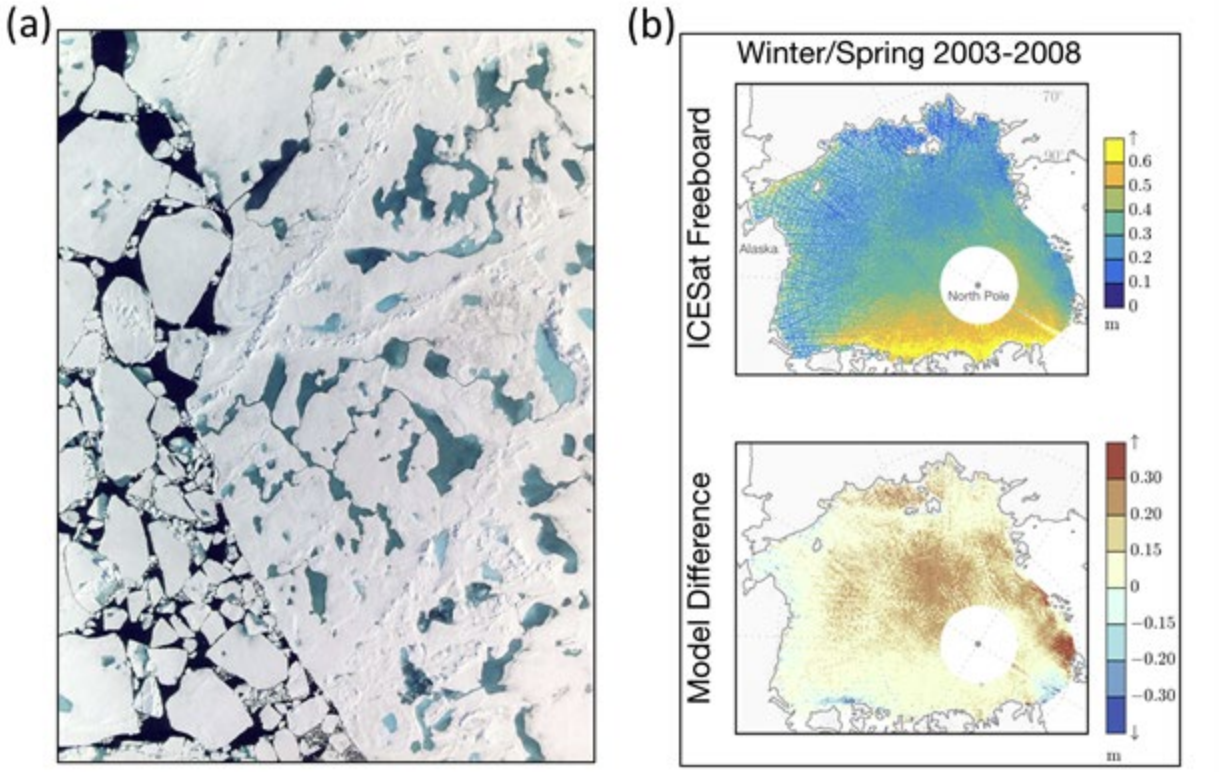

Fig. 2. The use of observations for model development. (a) Photo of Arctic sea ice indicating sub-gridscale quantities that need to be parameterized, including ice floes, melt ponds, snow cover, and ridges. Courtesy of D. Perovich. (b) ICESat freeboard (top) and the mean difference in freeboard along satellite laser tracks (model minus observation) from a Regional Arctic System Model simulation (bottom) using a satellite emulator following Bench (2016).

Using observations for initialized forecasts

The conditions today provide some ability to predict the future state of the system. Initialized forecasts rely on this "initial-value predictability" and thus require an accurate Earth system state as initial conditions. Obtaining this state for the Arctic is challenging given sparse, missing, and uncertain observations. The required accuracy of initial conditions needed to realize skillful forecasts is not clear and differs by variable, the property that is being forecasted (e.g., sea ice area), and the forecast lead time.

Data assimilation (DA) optimally combines observed data to estimate the system state. In recent work, sea ice DA has provided more accurate initial conditions with promise for improving forecasts (e.g., Massonnet et al. 2015). With the recent proliferation of satellite-based ice thickness data, which are important for seasonal ice area predictability (e.g., Day et al. 2014), there are new opportunities to use DA to improve initial conditions (e.g., Blockley and Peterson 2018). Reducing uncertainties in the satellite retrievals and extending them into the ice melt season (i.e., from early spring through the late summer when satellite retrievals of thickness are currently not possible) will allow for more accurate initial conditions, which is expected to substantially improve summer ice forecasts (Bushuk et al. 2020).

Integrating models with observations can help to quantify the value of existing or proposed observations for prediction. Observing systems experiments (OSEs) assess the influence of existing observations on forecast skill. For example, Bushuk et al. (2019) performed experiments that excluded certain observation types from a global DA system to diagnose the influence on Barents Sea ice predictions. They found that sea surface temperature (SST) observations (see essay *Sea Surface Temperature*) improved prediction skill on interannual scales, whereas deeper temperature observations improved trend forecasts and corrected the model's climatological bias (Fig. 3). This work demonstrated the value of ship-based conductivity-temperature-depth (CTD) measurements that are regularly collected in the Barents Sea along with satellite SST observations, emphasizing the need to sustain these crucial observing networks. Observing system simulation experiments (OSSEs) and quantitative network design (e.g., Kaminski et al. 2018) use similar methods to investigate the role of proposed observations for predictions, thereby informing the design of future observing systems.

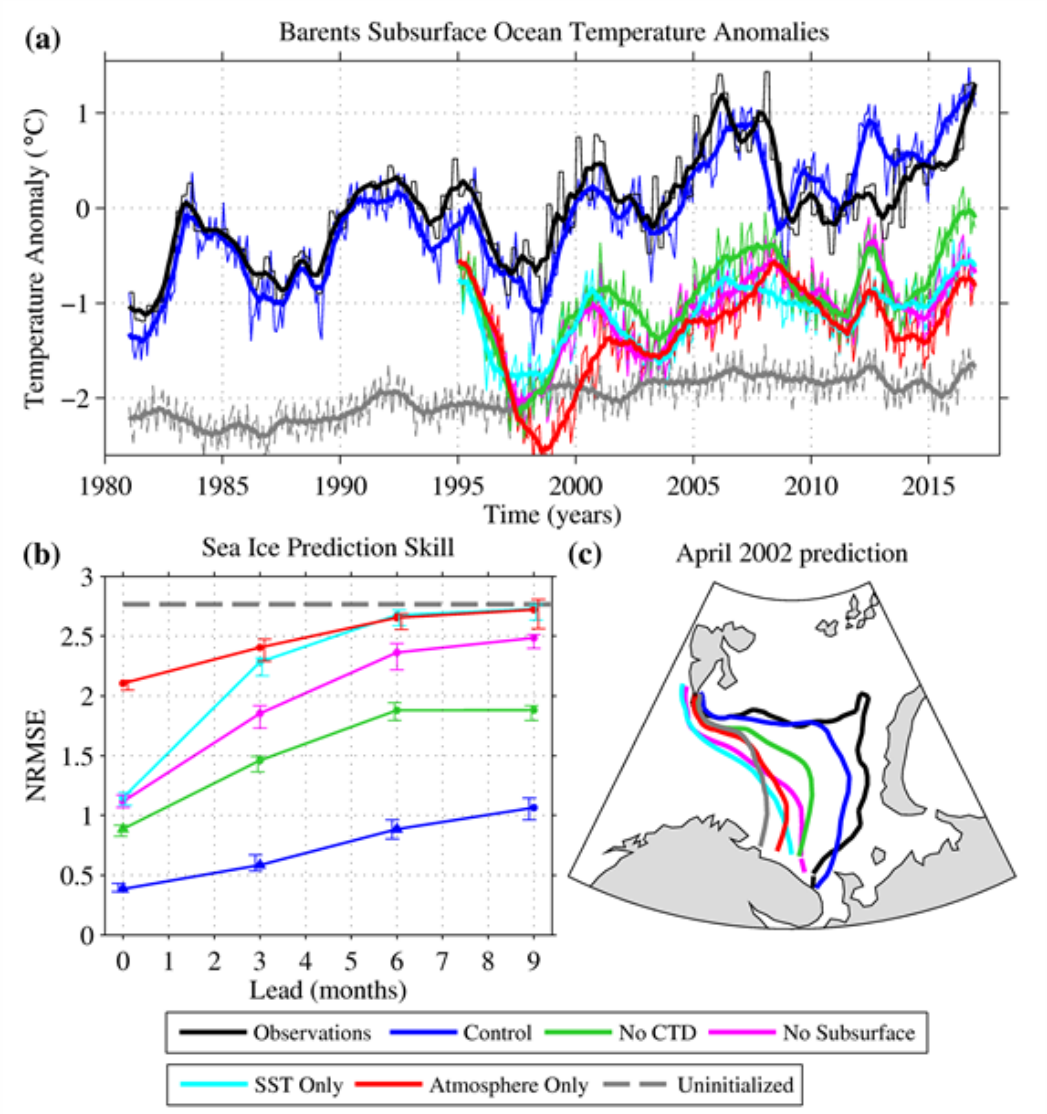

Fig. 3. Using observing systems experiments (OSEs) to assess observations for Barents Sea ice predictions. Barents Sea (a) 50-200 m temperature anomalies with monthly values in thin lines and a 12-month running mean in bold, (b) April ice extent prediction skill computed from the normalized root mean square error (NRMSE) with error estimates obtained using bootstrapping, and (c) 6-month predictions of the ice edge. The control experiment

(blue) assimilates ocean temperature and salinity profiles, satellite SST, and atmospheric temperature. OSEs (colors) exclude certain observations. Based on Bushuk et al. (2019).

Taken together, these advances in integrating models and observations have enabled better assessment of Arctic sea ice simulations, the development of improved sea ice models, and improved initialization of sea ice forecasts. This has increased the skill and utility of Arctic sea ice predictions across timescales from seasons to centuries. Collaborations between scientists taking measurements and those developing and utilizing models (e.g., Holland and Perovich 2017) have enabled these advances and will remain critical to continued innovations into the future.

References

Bench, K., 2016: Quantifying seasonal skill in coupled sea ice models using freeboard measurements from spaceborne laser altimeters. Naval Postgraduate School, Monterey, CA. Retrieved from http://hdl.handle.net/10945/49374.

Blanchard-Wrigglesworth, E., and C. M. Bitz, 2014: Characteristics of Arctic sea-ice thickness variability in GCMs. *J. Climate*, **27**(21), 8244-8258.

Blockley, E. W., and K. A. Peterson, 2018: Improving Met Office seasonal predictions of Arctic sea ice using assimilation of CryoSat-2 thickness. *Cryosphere*, **12**, 3419-3438, https://doi.org/10.5194/tc-12-3419-2018.

Bodas-Salcedo, A., and Coauthors, 2011: COSP: Satellite simulation software for model assessment. *Bull. Amer. Meteor. Soc.*, **92**, 1023-1043, https://doi.org/10.1175/2011BAMS2856.1.

Burgard, C., D. Notz, L. T. Pedersen, and R.T. Tonboe, 2020a: The Arctic Ocean observation operator for 6.9 GHz (ARC3O)-Part 1: How to obtain sea ice brightness temperatures at 6.9 GHz from climate model output. *Cryosphere*, **14**(7), 2369-2386, https://doi.org/10.5194/tc-14-2369-2020.

Burgard, C., D. Notz, L. T. Pedersen, R. T. Tonboe, 2020b: The Arctic Ocean observation operator for 6.9 GHz (ARC3O)-Part 2: Development and evaluation. *Cryosphere*, **14**, 2387-2407, https://doi.org/10.5194/tc-14-2387-2020.

Bushuk, M., M. Winton, D. B. Bonan, E. Blanchard-Wrigglesworth, and T. Delworth, 2020: A mechanism for the Arctic sea ice spring predictability barrier. *Geophys. Res. Lett.*, **47**, e2020GL088335, https://doi.org/10.1029/2020GL088335.

Bushuk, M., X. Yang, M. Winton, R. Msadek, M. Harrison, A. Rosati, and R. Gudgel, 2019: The value of sustained ocean observations for sea ice predictions in the Barents Sea. *J. Climate*, **32**(20), 7017-7035, https://doi.org/10.1175/JCLI-D-19-0179.1.

Day, J. J., E. Hawkins, and S. Tietsche, 2014: Will Arctic sea ice thickness initialization improve seasonal forecast skill? *Geophys. Res. Lett.*, **41**, 7566-7575, https://doi.org/10.1002/2014GL061694.

Deser, C., and Coauthors, 2020: Insights from Earth system model initial-condition large ensembles and future prospects. *Nat. Climate Change*, **10**, 277–286, https://doi.org/10.1038/s41558-020-0731-2.

Holland, M. M., and D. Perovich, 2017: Sea ice summer camp: Bringing together sea ice modelers and observers to advance polar science. *Bull. Amer. Meteor. Soc.*, **98**(10), 2057-2059, https://doi.org/10.1175/BAMS-D-16-0229.1.

Jahn, A., J. E. Kay, M. M. Holland, and D. M. Hall, 2016: How predictable is the timing of a summer ice-free Arctic? *Geophys. Res. Lett.*, **43**, 9113-9120, https://doi.org/10.1002/2016GL070067.

Kaminski, T., and Coauthors, 2018: Arctic mission benefit analysis: impact of sea ice thickness, freeboard, and snow depth products on sea ice forecast performance. *Cryosphere*, **12**, 2569-2594, https://doi.org/10.5194/tc-12-2569-2018.

Markus, T., and Coauthors, 2017: The Ice, Cloud, and land Elevation Satellite-2 (ICESat-2): science requirements, concept, and implementation. *Remote Sens. Environ.*, **190**, 260-273, https://doi.org/10.1016/j.rse.2016.12.029.

Massonnet, F., T. Fichefet, and H. Goosse, 2015: Prospects for improved seasonal Arctic sea ice predictions from multivariate data assimilation. *Ocean Model.*, **88**, 16-25, https://doi.org/10.1016/j.ocemod.2014.12.013.

Roberts, A. F., E. C. Hunke, S. Kamal, W. F. Lipscomb, C. Horvat, and W. Maslowski, 2019: A variational method for sea ice ridging in Earth System Models. *J. Adv. Model. Earth Sys.*, **11**, 771-805, https://doi.org/10.1029/2018MS001395.

Smith, A., A. Jahn, and M. Wang, 2020: Seasonal transition dates can reveal biases in Arctic sea ice simulations. *Cryosphere*, **14**, 2977-2997, https://doi.org/10.5194/tc-14-2977-2020.

Steele, M., A. Bliss, G. Peng, W. N. Meier, and S. Dickinson, 2019: Arctic sea ice seasonal change and melt/freeze climate indicators from satellite data, Version 1, Data subset: 1979-03-01 to 2017-02-28. Data accessed 2019-08-26, 2019.

Swart, N. C., J. C. Fyfe, E. Hawkins, J. E. Kay, and A. Jahn, 2015: Influence of internal variability on Arctic sea-ice trends. *Nat. Climate Change*, **5**, 86-89, https://doi.org/10.1038/nclimate2483.

Yang, W., and G. Magnusdottir, 2018: Year-to-year variability in Arctic minimum sea ice extent and its preconditions in observations and the CESM Large Ensemble simulations. *Sci. Rep.*, **8**(1), 9070, https://doi.org/10.1038/s41598-018-27149-y.

Yu, W., M. Doutriaux, G. Sèze, H. Le Treut, and M. Desbois, 1996: A methodology study of the validation of clouds in GCMs using ISCCP satellite observations. *Climate Dyn.*, **12**, 389-401, https://doi.org/10.1007/BF00211685.

November 12, 2020

New Arctic Research Facility Opens Door to Science Collaborations

DOI: 10.25923/24rn-c757

B. Vasel[1], C. Schultz[1], R. Schnell[1,2], D. Stanitski[1], and B. Thomas[1]

[1]Global Monitoring Laboratory, NOAA, Boulder, CO, USA
[2]Cooperative Institute for Research in Environmental Sciences, University of Colorado Boulder, Boulder, CO, USA

Highlights

- The Arctic climate is changing rapidly; long-term, in situ, well-supported atmospheric Arctic monitoring is critical to understanding current change and predicting future conditions.
- NOAA has completed construction of a large, modern Arctic research facility connected with a high-capacity fiber optic link.
- The Barrow Atmospheric Baseline Observatory (BRW), a pillar of the global Arctic research community for almost 50 years, encourages new interdisciplinary research and partnerships in Utqiaġvik.

For almost half a century, some of the most important observations of the changing Arctic climate have been captured in a temporary structure at the northernmost tip of the United States. NOAA's Barrow Atmospheric Baseline Observatory (BRW) is located 8 km northeast of the City of Utqiaġvik (formerly Barrow) and very near the northernmost point (71.325° N, 156.625° W) of the U.S. (Fig. 1). BRW was established by NOAA in January 1973, joining observatories on Mauna Loa, Hawaii, American Samoa, and at the South Pole as foundational atmospheric research observatories spanning the length of the Pacific Ocean. The observatory's mandate was, and still is today, "to measure the necessary parameters for establishing trends of trace constituents important to climate change and of those elements that can assist in apportioning the source of changes to natural or anthropogenic sources" (Miller 1974).

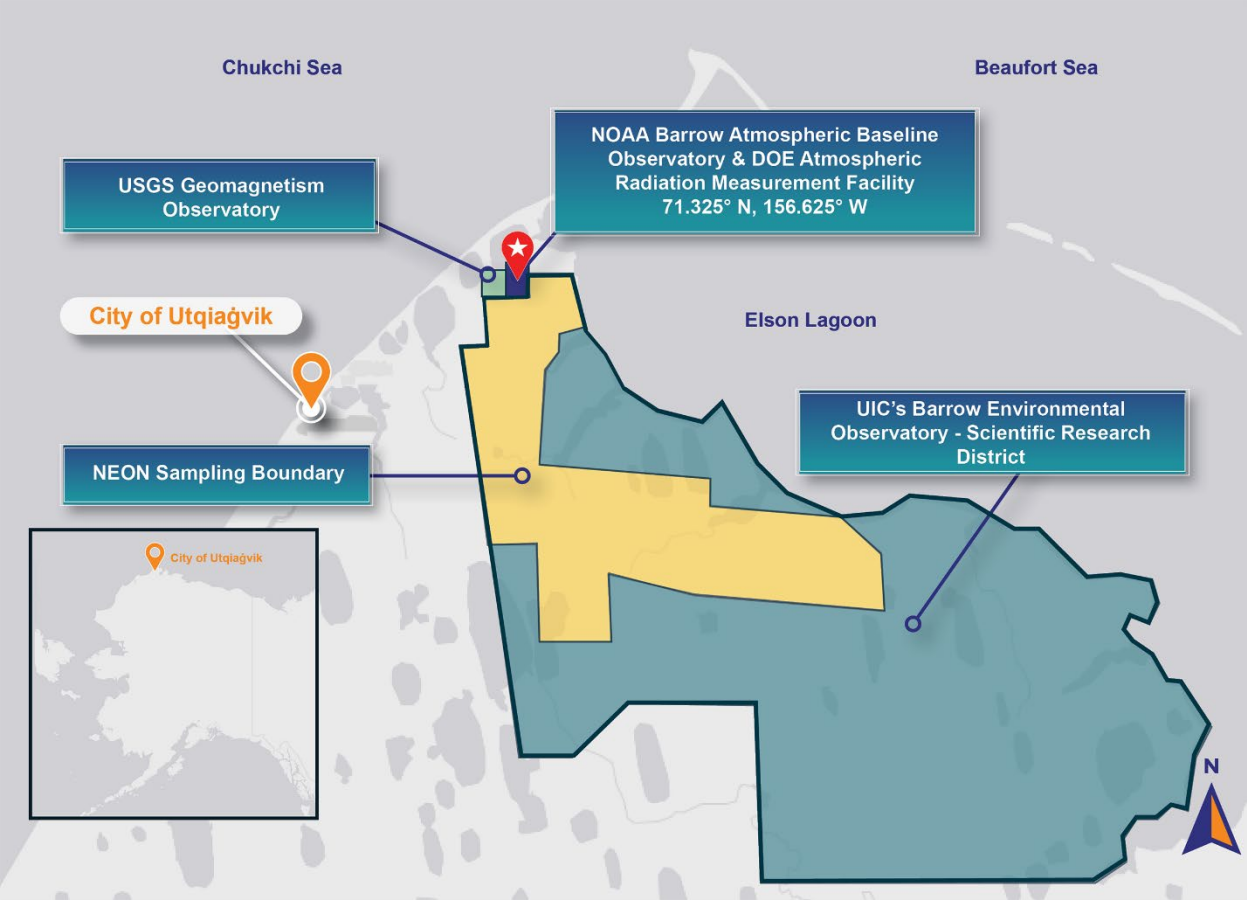

Fig. 1. NOAA Barrow Atmospheric Baseline Observatory (BRW) and surrounding partner research sites. All positions and boundaries are approximate. (Basemap provided by Esri)

Since its establishment, BRW has played an important role in Arctic research, providing long-term observations of atmospheric composition as it relates to climate change, ozone depletion, and air quality. With its unique location and ongoing, long-term data records, BRW is a critical member of multiple international observatory networks, including the World Meteorological Organization's (WMO) Global Atmospheric Watch (GAW) and the Global Cryosphere Watch (GCW) networks, that document change on a global scale. In addition, BRW is part of the International Arctic Systems for Observing the Atmosphere (IASOA), an effort to coordinate intensive long-term measurements collected across the Arctic (Uttal et al. 2016).

BRW has also hosted numerous interdisciplinary studies of the Arctic, supporting hundreds of cooperative science projects from researchers around the world. The observatory supports a NOAA Climate Reference Network (CRN) station and two NOAA/NESDIS polar-orbiting satellite antennas. In addition, NOAA has partnered with the U.S. Department of Energy (DOE) to operate an Atmospheric Radiation Measurement (ARM) facility on the observatory property, and BRW staff take regular measurements to support the U.S. Geological Survey (USGS) Magnetic Observatory nearby (Fig. 2). These projects are co-located at BRW for its access to undeveloped Arctic tundra.

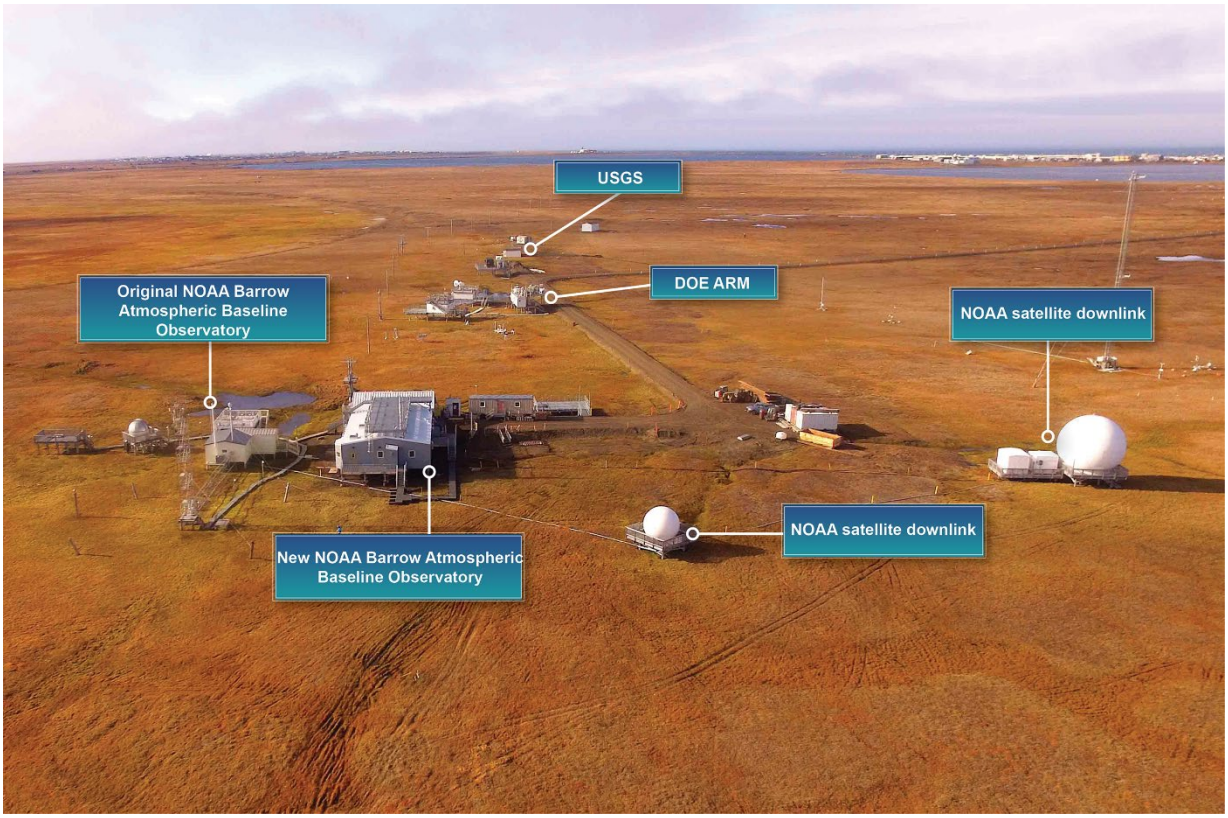

Fig. 2. Aerial view of the new BRW building alongside the original facility taken in September 2020. Also visible are the NOAA/NESDIS satellite downlink domes, the DOE ARM facilities, the USGS facilities, and the community of Utqiaġvik on the horizon. (Photo credit: NOAA)

The lengthy datasets developed from measurements captured at BRW are core elements of NOAA's responsibility for monitoring the state of, and changes in, the global atmosphere. The observatory is well-suited to sample air that is minimally influenced by local or regional air pollution sources when winds blow from the east-northeast "clean air sector", approximately half of the time. With an established "clean air sector," BRW can detect air from remote regions originating hundreds of kilometers upwind of the observatory. Situated on a land parcel over 40 hectares in size, BRW is also an ideal location to measure surface radiation over a natural landscape that will remain undisturbed in perpetuity.

The original 1973 BRW facility was just 74 m^2 and built, by the U.S. Navy, as a temporary structure for NOAA. Over the years, the number of scientific programs conducted at the BRW Observatory tripled in number until additional NOAA and cooperative programs could not be accommodated due to space, power, and safety constraints. As scientific interest in the Arctic has grown, the original observatory was simply inadequate to meet the research and monitoring needs required to improve understanding of the global climate system, and the drivers causing the Arctic to warm at a rate much faster than the lower latitudes. A National Science Foundation report examining U.S. investment in Arctic research determined that upgrading the BRW facility was the single most pressing and cost-effective means to enhance atmospheric research and monitoring within the United States Arctic (NSF 2002).

Now, 47 years after it was commissioned, the science has outgrown the original modest accommodations. The new, state-of-the-art research facility constructed on the NOAA site is poised to support the observatory's vital role furthering Arctic science for decades to come. In 2020, after years of

preparation and planning, a new 273 m^2 building to house the Barrow observatory is opening its doors to interdisciplinary scientific collaboration. The facility includes a new roof deck, a 30-meter instrument tower, a campaign science platform sized to hold two 6-m metal shipping containers, a dedicated computer server room, a high-speed fiber connection to the contiguous U.S., a plumbed bathroom and kitchenette, a garage remodel and expansion, and a permafrost temperature monitoring facility.

NOAA awarded the design/build contract to an Alaska Native Corporation, UIC Nappairit, LLC, a subsidiary of Ukpeaġvik Iñupiat Corporation (UIC). UIC designed the facility to qualify as a Leadership in Energy and Environmental Design (LEED)-certified building with the U.S. Green Building Council and has already achieved that mark. The building may still qualify for a higher level of LEED certification as the project is completed, continuing NOAA's commitment to environmental stewardship in the Arctic.

As an adaptation to the COVID-19 pandemic, NOAA worked closely with UIC to host a virtual completion inspection of the new facility; hosting this project milestone with remote participants was a first for NOAA. The BRW revitalization project also brings a fiber connection to the observatory; this new high-speed connection will enable faster data sharing and better communication with school and media outlets in exciting ways. The ability to stream live video and move large data sets out of the Arctic—from ship-borne missions, aircraft campaigns, buoys, and satellites—creates the potential to access the remote Arctic in novel ways.

Today, the BRW Observatory supports more than 200 measurements enabling critical research on changes in atmospheric composition and the Arctic region, including greenhouse gases, ozone-depleting chemicals such as chlorofluorocarbons, air pollution events from Eurasia known as Arctic Haze, stratospheric ozone depletion, and advancing snowmelt dates and lengthening of summers along Alaska's North Slope. Data acquired at BRW are available online: https://www.esrl.noaa.gov/gmd/dv/data/. Arctic modeling and satellite observations will benefit from the infrastructure and science available at BRW that allows in situ observations as part of a larger, integrated system. Increasing the number of diverse measurements at the new BRW facility will improve our knowledge of the complex Arctic environment, including the hydrology, glaciology, oceanography, terrestrial, and biological systems, as well as mechanisms related to the entire Arctic system.

The Arctic region is a vast and challenging place in which to operate. It undoubtedly still holds many keys to our collective understanding of Earth's climate, weather, and water systems. The new BRW observatory, in combination with other complementary international efforts and networks, will provide a state-of-the-art research platform where the global scientific community can gain fundamental insights into our changing Arctic.

NOAA strongly encourages cross-disciplinary science at BRW and new partnerships. Proposals for collaborative research projects hosted at the observatory may be submitted here: https://www.esrl.noaa.gov/gmd/obop.

References

Miller, J. M., Ed., 1974: Geophysical Monitoring for Climatic Change No. 1 Summary Report - 1972. U. S. Department of Commerce, National Oceanic and Atmospheric Administration, Environmental Research Laboratories, https://www.esrl.noaa.gov/gmd/publications/summary_reports/summary_report_1.pdf.

National Science Foundation (NSF) Office of Polar Programs, 2002: The Feasibility of a Barrow Arctic Research Center. https://www.esrl.noaa.gov/gmd/publications/historical/NSF Report_BARC Feasibility_Apr2002.pdf.

Uttal, T., and Coauthors, 2016: International Arctic Systems for Observing the Atmosphere: An International Polar Year Legacy Consortium. *Bull. Amer. Meteor. Soc.*, **97**, 1033-1056, https://doi.org/10.1175/BAMS-D-14-00145.1.

November 9, 2020

Authors and Affiliations

L. M. Andreassen, Section for Glaciers, Ice and Snow, Norwegian Water Resources and Energy Directorate, Oslo, Norway

T. J. Ballinger, International Arctic Research Center, University of Alaska Fairbanks, Fairbanks, AK, USA

A. Baranskaya, Faculty of Geography, Lomonosov Moscow State University, Moscow, Russia

N. Belova, Faculty of Geography, Lomonosov Moscow State University, Moscow, Russia

M. Bendixen, Institute of Arctic and Alpine Research, University of Colorado, Boulder, CO, USA

L. T. Berner, School of Informatics, Computing and Cyber Systems, Northern Arizona University, Flagstaff, AZ, USA

U. S. Bhatt, Department of Atmospheric Sciences, University of Alaska Fairbanks, Fairbanks, AK, USA; Geophysical Institute, University of Alaska Fairbanks, Fairbanks, AK, USA

J. W. Bjerke, Norwegian Institute for Nature Research, FRAM - High North Research Centre for Climate and the Environment, Tromsø, Norway

J. E. Box, Geological Survey of Denmark and Greenland, Copenhagen, Denmark

R. Brown, Climate Research Division, Environment and Climate Change Canada, Ottawa, ON, Canada

D. Burgess, Geological Survey of Canada, Ottawa, ON, Canada

M. Bushuk, Geophysical Fluid Dynamics Laboratory, NOAA, Princeton, NJ, USA

J. Cappelen, Danish Meteorological Institute, Copenhagen, Denmark

J. C. Comiso, Cryospheric Sciences Laboratory, Goddard Space Flight Center, NASA, Greenbelt, MD, USA

L. W. Cooper, Chesapeake Biological Laboratory, University of Maryland Center for Environmental Science, Solomons, MD, USA

E. Damm, Alfred Wegener Institute, Helmholtz Center for Polar and Marine Research, Bremerhaven, Germany

B. Decharme, Centre National de Recherches Météorologiques, Toulouse, France

C. Derksen, Climate Research Division, Environment and Climate Change Canada, Ottawa, ON, Canada

K. Dethloff, Alfred Wegener Institute, Helmholtz Center for Polar and Marine Research, Potsdam, Germany

D. Divine, Norwegian Polar Institute, Fram Centre, Tromsø, Norway

M. L. Druckenmiller, National Snow and Ice Data Center, University of Colorado Boulder, Boulder, CO, USA

A. Elias Chereque, Department of Physics, University of Toronto, Toronto, ON, Canada

H. E. Epstein, Department of Environmental Sciences, University of Virginia, Charlottesville, VA, USA

L. M. Farquharson, Geophysical Institute, University of Alaska Fairbanks, Fairbanks, AK, USA

S. Farrell, NOAA Earth System Science Interdisciplinary Center, University of Maryland, College Park, MD, USA

R. S. Fausto, Geological Survey of Denmark and Greenland, Copenhagen, Denmark

X. Fettweis, University of Liege, Liege, Belgium

A. A. Fong, Alfred Wegener Institute, Helmholtz Center for Polar and Marine Research, Bremerhaven, Germany

B. C. Forbes, Arctic Centre, University of Lapland, Rovaniemi, Finland

K. E. Frey, Graduate School of Geography, Clark University, Worcester, MA, USA

G. V. Frost, Alaska Biological Research, Inc., Fairbanks, AK, USA

E. Gargulinski, National Institute of Aerospace, Langley Research Center, NASA, Hampton, VA, USA

J. C. George, Department of Wildlife Management, North Slope Borough, Utqiaġvik, AK, USA

S. Gerland, Norwegian Polar Institute, Fram Centre, Tromsø, Norway

A. E. Gibbs, U.S. Geological Survey, Pacific Coastal and Marine Science Center, Santa Cruz, CA, USA

S. J. Goetz, School of Informatics, Computing and Cyber Systems, Northern Arizona University, Flagstaff, AZ, USA

Z. Grabinski, Alaska Fire Science Consortium, International Arctic Research Center, University of Alaska Fairbanks, Fairbanks, AK, USA

R. Gradinger, Department of Arctic and Marine Biology, University of Tromsø, Tromsø, Norway

J. M. Grebmeier, Chesapeake Biological Laboratory, University of Maryland Center for Environmental Science, Solomons, MD, USA

M. Grigoriev, Mel'nikov Permafrost Institute, Siberian Branch, Russian Academy of Sciences, Yakutsk, Russia

G. Grosse, Alfred Wegener Institute, Helmholtz Centre for Polar and Marine Research, Potsdam, Germany; Institute of Geosciences, University of Potsdam, Potsdam, Germany

C. Haas, Alfred Wegener Institute, Helmholtz Centre for Polar and Marine Research, Bremerhaven, Germany

E. Hanna, School of Geography and Lincoln Centre for Water and Planetary Health, University of Lincoln, Lincoln, UK

I. Hanssen-Bauer, Norwegian Meteorological Institute, Blindern, Oslo, Norway

S. Hendricks, Alfred Wegener Institute, Helmholtz Centre for Polar and Marine Research, Bremerhaven, Germany

C. Heuzé, Department of Earth Sciences, University of Gothenburg, Göteborg, Sweden

M. M. Holland, Climate and Global Dynamics Laboratory, National Center for Atmospheric Research, Boulder, CO, USA

A. M. Irrgang, Alfred Wegener Institute, Helmholtz Centre for Polar and Marine Research, Potsdam, Germany

A. Jahn, Department of Atmospheric and Oceanic Sciences and Institute of Arctic and Alpine Research, University of Colorado, Boulder, CO, USA

P. Jain, Natural Resources Canada, Canadian Forest Service, Northern Forestry Centre, Edmonton, Alberta, Canada

B. M. Jones, Institute of Northern Engineering, University of Alaska Fairbanks, Fairbanks, AK, USA

L. Kaleschke, Alfred Wegener Institute, Helmholtz Centre for Polar and Marine Research, Bremerhaven, Germany

J. T. Kerby, Aarhus Institute of Advanced Studies, Aarhus University, Aarhus, Denmark

S. -J. Kim, Korea Polar Research Institute, Incheon, Republic of Korea

J. Kohler, Norwegian Polar Institute, Tromsø, Norway

N. J. Korsgaard, Geological Survey of Denmark and Greenland, Copenhagen, Denmark

A. Kroon, Department of Geosciences and Natural Resource Management, University of Copenhagen, Copenhagen, Denmark

Z. Labe, Colorado State University, Fort Collins, CO, USA

H. Lantuit, Alfred Wegener Institute, Helmholtz Centre for Polar and Marine Research, Potsdam, Germany

B. Loomis, Goddard Space Flight Center, NASA, Greenbelt, MD, USA

B. Loose, Graduate School of Oceanography, University of Rhode Island, South Kingston, RI, USA

B. Luks, Institute of Geophysics, Polish Academy of Sciences, Warsaw, Poland

K. Luojus, Arctic Research Centre, Finnish Meteorological Institute, Helsinki, Finland

M. J. Macander, Alaska Biological Research, Inc., Fairbanks, AK, USA

C. Maio, Geography, University of Alaska Fairbanks, Fairbanks, AK, USA

A. Makarov, Arctic and Antarctic Research Institute, St. Petersburg, Russia

K. D. Mankoff, Geological Survey of Denmark and Greenland, Copenhagen, Denmark

A. Maslakov, Faculty of Geography, Lomonosov Moscow State University, Moscow, Russia

W. Maslowski, Department of Oceanography, Naval Postgraduate School, Monterey, CA, USA

W. Meier, Cooperative Institute for Research in Environmental Sciences, University of Colorado Boulder, Boulder, CO, USA; National Snow and Ice Data Center, Boulder, CO, USA

T. A. Moon, Cooperative Institute for Research in Environmental Sciences, University of Colorado Boulder, Boulder, CO, USA; National Snow and Ice Data Center, Boulder, CO, USA

S. E. Moore, Center for Ecosystem Sentinels, University of Washington, Seattle, WA, USA

T. Mote, Department of Geography, University of Georgia, Athens, GA, USA

L. Mudryk, Climate Research Division, Environment and Climate Change Canada, Ottawa, ON, Canada

I. Myers-Smith, School of GeoSciences, University of Edinburgh, Edinburgh, UK

M. Nicolaus, Alfred Wegener Institute, Helmholtz Center for Polar and Marine Research, Bremerhaven, Germany

I. Nitze, Alfred Wegener Institute, Helmholtz Centre for Polar and Marine Research, Potsdam, Germany

S. Ogorodov, Faculty of Geography, Lomonosov Moscow State University, Moscow, Russia

J. Overbeck, Alaska Division of Geological & Geophysical Surveys, Anchorage, AK, USA

P. Overduin, Alfred Wegener Institute, Helmholtz Centre for Polar and Marine Research, Potsdam, Germany

J. E. Overland, Pacific Marine Environmental Laboratory, NOAA, Seattle, WA, USA

T. Park, Ames Research Center, NASA, Mountain View, CA, USA; Bay Area Environmental Research Institute, Moffett Field, Mountain View, CA, USA

O. Pavlova, Norwegian Polar Institute, Fram Centre, Tromsø, Norway

D. Perovich, Thayer School of Engineering, Dartmouth College, Hanover, NH, USA

A. A. Petty, Goddard Space Flight Center, NASA, Greenbelt, MD, USA

G. K. Phoenix, Department of Animal and Plant Sciences, University of Sheffield, Sheffield, UK

B. Rabe, Alfred Wegener Institute, Helmholtz Center for Polar and Marine Research, Bremerhaven, Germany

M. K. Raynolds, Institute of Arctic Biology, University of Alaska Fairbanks, Fairbanks, AK, USA

C. H. Reijmer, Institute for Marine and Atmospheric Research Utrecht, Utrecht University, Utrecht, The Netherlands

M. Rex, Alfred Wegener Institute, Helmholtz Center for Polar and Marine Research, Potsdam, Germany

J. Richter-Menge, Institute of Northern Engineering, University of Alaska Fairbanks, Fairbanks, AK, USA

R. Ricker, Alfred Wegener Institute, Helmholtz Centre for Polar and Marine Research, Bremerhaven, Germany

A. Rinke, Alfred Wegener Institute, Helmholtz Center for Polar and Marine Research, Potsdam, Germany

A. Roberts, Theoretical Division, Los Alamos National Laboratory, Los Alamos, NM, USA

V. E. Romanovsky, Geophysical Institute, University of Alaska Fairbanks, Fairbanks, AK, USA

R. Schnell, Cooperative Institute for Research in Environmental Sciences, University of Colorado Boulder, Boulder, CO, USA; Global Monitoring Laboratory, NOAA, Boulder, CO, USA

C. Schultz, Global Monitoring Laboratory, NOAA, Boulder, CO, USA

H. Shapiro, Arctic Research Consortium of the United States, Fairbanks, AK, USA

M. Sharp, Department of Earth and Atmospheric Sciences, University of Alberta, Edmonton, AB, Canada

M. D. Shupe, Cooperative Institute for Research in Environmental Sciences, University of Colorado Boulder, Boulder, CO, USA; Physical Sciences Laboratory, NOAA, Boulder, CO, USA

A. Sinitsyn, SINTEF AS, SINTEF Community, Trondheim, Norway

C. J. P. P. Smeets, Department of Physical Geography, Utrecht University, Utrecht, The Netherlands

A. Soja, National Institute of Aerospace, Langley Research Center, NASA, Hampton, VA, USA

V. Sokolov, Arctic and Antarctic Research Institute, St. Petersburg, Russia

A. Sommerfeld, Alfred Wegener Institute, Helmholtz Center for Polar and Marine Research, Potsdam, Germany

D. Stanitski, Global Monitoring Laboratory, NOAA, Boulder, CO, USA

S. Starkweather, Cooperative Institute for Research in Environmental Sciences, University of Colorado Boulder, Boulder, CO, USA; Earth System Research Laboratory, NOAA, Boulder, CO, USA

L. V. Stock, Cryospheric Sciences Laboratory, Goddard Space Flight Center, NASA, Greenbelt, MD, USA

M. C. Strzelecki, Institute of Geography and Regional Development, University of Wroclaw, Wroclaw, Poland

M. Tedesco, Lamont Doherty Earth Observatory of Columbia University, Palisades, NY, USA; Goddard Institute of Space Studies, NASA, New York, NY, USA

J. G. M. Thewissen, Department of Anatomy and Neurobiology, Northeast Ohio Medical University, Rootstown, OH, USA

R. L. Thoman, Alaska Center for Climate Assessment and Policy, University of Alaska Fairbanks, Fairbanks, AK, USA; International Arctic Research Center, University of Alaska Fairbanks, Fairbanks, AK, USA

B. Thomas, Global Monitoring Laboratory, NOAA, Boulder, CO, USA

X. Tian-Kunze, Alfred Wegener Institute, Helmholtz Centre for Polar and Marine Research, Bremerhaven, Germany

M. -L. Timmermans, Yale University, New Haven, CT, USA

H. Tømmervik, Norwegian Institute for Nature Research, FRAM - High North Research Centre for Climate and the Environment, Tromsø, Norway

M. Tschudi, Aerospace Engineering Sciences, University of Colorado, Boulder, CO, USA

C. Tweedie, Department of Biology, University of Texas El Paso, El Paso, TX, USA

S. Vakhutinsky, National Snow and Ice Data Center, Boulder, CO, USA

D. van As, Geological Survey of Denmark and Greenland, Copenhagen, Denmark

R. S. W. van de Wal, Institute for Marine and Atmospheric Research Utrecht, Utrecht University, Utrecht, The Netherlands; Department of Physical Geography, Utrecht University, Utrecht, The Netherlands

B. Vasel, Global Monitoring Laboratory, NOAA, Boulder, CO, USA

G. Vieira, Centre of Geographical Studies, Institute of Geography and Spatial Planning, University of Lisbon, Portugal

D. A. Walker, Institute of Arctic Biology, University of Alaska Fairbanks, Fairbanks, AK, USA

J. E. Walsh, International Arctic Research Center, University of Alaska Fairbanks, Fairbanks, AK, USA

M. Wang, Pacific Marine Environmental Laboratory, NOAA, Seattle, WA, USA; Cooperative Institute for Climate, Ocean, and Ecosystem Studies, University of Washington, Seattle, WA, USA

M. Webster, Geophysical Institute, University of Alaska Fairbanks, Fairbanks, AK, USA

D. Whalen, Natural Resources Canada, Geological Survey of Canada-Atlantic, Dartmouth, Nova Scotia, Canada

G. J. Wolken, International Arctic Research Center, University of Alaska Fairbanks, Fairbanks, AK, USA; Alaska Division of Geological & Geophysical Surveys, Fairbanks, AK, USA

K. Wood, Cooperative Institute for Climate, Ocean, and Ecosystem Studies, University of Washington, Seattle, WA, USA; Pacific Marine Environmental Laboratory, NOAA, Seattle, WA, USA

B. Wouters, Institute for Marine and Atmospheric Research, Utrecht University, Utrecht, The Netherlands; Department of Geoscience & Remote Sensing, Delft University of Technology, Delft, The Netherlands

A. York, Alaska Fire Science Consortium, International Arctic Research Center, University of Alaska Fairbanks, Fairbanks, AK, USA

P. Zagórski, Institute of Earth and Environmental Sciences, Marie Curie Skłodowska University, Lublin, Poland

R. Ziel, Alaska Fire Science Consortium, International Arctic Research Center, University of Alaska Fairbanks, Fairbanks, AK, USA